Cost-Effective Optical Network Architecture – A Joint Optimization of Topology, Switching, Routing and Wavelength Assignment

by

Kyle Chi Guan

Submitted to the Department of Electrical Engineering and Computer Science
in partial fulfillment of the requirements for the degree of

Doctor of Philosophy

at the

MASSACHUSETTS INSTITUTE OF TECHNOLOGY

February 2007

Author .....
Department of Electrical Engineering and Computer Science
February, 2007

Certified by .....
Vincent W. S. Chan
Professor of Electrical Engineering and Computer Science
Thesis Supervisor

Accepted by .....
Arthur C. Smith
Chairman, Department Committee on Graduate Students

Cost-Effective Optical Network Architecture – A Joint Optimization of Topology, Switching, Routing and Wavelength Assignment

by

Kyle Chi Guan

Submitted to the Department of Electrical Engineering and Computer Science
on February, 2007, in partial fulfillment of the
requirements for the degree of
Doctor of Philosophy

Abstract

To provide end users with economic access to high bandwidth, the architecture of the next generation metropolitan area networks (MANs) needs to be judiciously designed from the cost perspective. In addition to a low initial capital investment, the ultimate goal is to design networks that exhibit excellent scalability – a decreasing cost-per-node-per-unit-traffic as user number and transaction size increase.

As an effort to achieve this goal, in this thesis we search for the scalable network architectures over the solution space that embodies the key aspects of optical networks: fiber connection topology, switching architecture selection and resource dimensioning, routing and wavelength assignment (RWA). Due to the inter-related nature of these design elements, we intended to solve the design problem jointly in the optimization process in order to achieve over-all good performance. To evaluate how the cost drives architectural tradeoffs, an analytical approach is taken in most parts of the thesis by first focusing on networks with symmetric and well defined structures (i.e., regular networks) and symmetric traffic patterns (i.e., all-to-all uniform traffic), which are fair representations that give us suggestions of trends, etc.

We starts with a examination of various measures of regular topologies. The average minimum hop distance plays a crucial role in evaluating the efficiency of network architecture. From the perspective of designing optical networks, the amount of switching resources used at nodes is proportional to the average minimum hop distance. Thus a smaller average minimum hop distance translates into a lower fraction of pass-through traffic and less switching resources required.

Next, a first-order cost model is set up and an optimization problem is formulated for the purpose of characterizing the tradeoffs between fiber and switching resources. Via convex optimization techniques, the joint optimization problem is solved analytically for (static) uniform traffic and symmetric networks. Two classes of regular graphs – Generalized Moore Graphs and Δ-nearest Neighbors Graphs – are identified to yield lower and upper cost bounds, respectively. The investigation of the cost

scalability further demonstrates the advantage of the Generalized Moore Graphs as benchmark topologies: with linear switching cost structure, the minimal normalized cost per unit traffic decreases with increasing network size for the Generalized Moore Graphs and their relatives. In comparison, for less efficient fiber topologies (e.g., Δ-nearest Neighbors) and switching cost structures (e.g., quadratic cost), the minimal normalized cost per unit traffic plateaus or even increases with increasing network size. The study also reveals other attractive properties of Generalized Moore Graphs in conjunction with minimum hop routing – the aggregate network load is evenly distributed over each fiber. Thus, Generalized Moore Graphs also require the minimum number of wavelengths to support a given uniform traffic demand.

Further more, the theoretical works on the Generalized Moore Graphs and their close relatives are extended to study more realistic design scenarios in two aspects. One aspect addresses the irregular topologies and (static) non-uniform traffic, for which the results of Generalized Moore networks are used to provide useful estimates of network cost, and are thus offering good references for cost-efficient optical networks. The other aspect deals with network design under random demands. Two optimization formulations that incorporate the traffic variability are presented. The results show that as physical architecture, Generalized Moore Graphs are most robust (in cost) to the demand uncertainties. Analytical results also provided design guidelines on how optimum dimensioning, network connectivity, and network costs vary as functions of risk aversion, service level requirements, and probability distributions of demands.

Thesis Supervisor: Vincent W. S. Chan
Title: Professor of Electrical Engineering and Computer Science

Acknowledgments

First and foremost, I would like to express my deepest gratitude to my thesis advisor Professor Vincent Chan. This thesis would not have been possible without his patience, guidance, and support. His emphasis on creative thinking, communication skills, and leadership is invaluable to my career development.

I would like to thank my thesis committee members, Eric Swanson and Professor Asuman Ozdaglar. Their advice and constructive criticism greatly improve the quality of this thesis.

I am grateful to DARPA and MIT for the financial support to this research.

My sincere thanks also go to my officemates Etty, Guy, Lillian, Lizzy, Nick, Patrick, Roop, and Yonggang, who make the life at 32-D678 truly enjoyable.

I cannot end without thanking my parents and my sister, on whose unrelenting love and constant encouragement I have relied throughout the ups and downs of my graduate study.

Contents

List of Figures

List of Tables

Chapter 1

Introduction

1.1 Thesis Motivation

As we move forward in the Information Age, the ravenous demands for bandwidth grow at an alarming rate with each passing decade. Despite significant cycles in the economy that supports digital demands, traffic volume is still expected to have exponential growth in the foreseeable future. This comes as more and more households are switching to broadband access and network operators are aggressively marketing advanced services, such as FiOS[1] and Triple/Quadruple Play[2]. In addition, consumers' ever growing appetite for bandwidth-devouring applications, such as IPTV, digital movie, and peer-to-peer file sharing, is driving the demand for high data rate infrastructure.

To keep up with the rising traffic volume, telecom carriers have drastically increased the capacity of long-haul networks with the deployment of wavelength division multiplexing (WDM) technology. WDM transmission systems can have capacity greater than 10 Tb/s (10^{13} b/s) over a single fiber, a feat achieved by multiplexing

[1]FiOS is an abbreviation of Fiber Optic Service, a fiber to the premises (FTTP) service offered by Verizon.

[2]Triple Play: a marketing term for offering three services over a single broadband connection: high-speed Internet, television (Video on Demand (VoD) or regular broadcast), and telephone service. Triple Play leads to the term Quadruple Play, where wireless communication is introduced as another way to deliver video, Internet, and voice content.

more than 200 channels at 40 Gb/s (4×10^{10} b/s) each [1]. At the same time, service providers are laying fiber cables with more than 100 fibers per cable, with a total capacity of 1 Pb/s (10^{15} b/s). This capacity allows 1 million user-pairs to transmit simultaneously, each at a data rate as high as 1 Gb/s.

While the deployment of capacity in backbone networks has been impressive, end-users' access to the broad array of services made available by this deployment is quite limited. The current data rates for most end-users are in the range of kilobits to a few megabits per second; and the access to higher data rates (in the range of hundreds megabits per second) is still considerably more expensive [2]. In these situations, because the access cost is so dominant, even if long haul transmission cost could be reduced to zero, the cost incurred to end-users would not come down significantly. End-users still pay heftily for high bandwidth usage. One can say that aggregation and access have become the new bottlenecks for the growth and the adoption of high bandwidth applications. As such, the full potential of optical network, which promises low-cost and high data rate access to the masses, has not yet been realized [2].

From an engineering perspective, the discrepancy between the bandwidth glut at the backbone and the high access cost for the end-users can be attributed to the following factors. The first factor, which is widely recognized among both industry and research communities, is related to the predominant routing and switching mechanism utilized by the current network. Though the WDM technology has been a huge success in providing high-capacity point-to-point transmissions, the routing and switching are exclusively carried out electronically in the current metro and access environment. Though this router-centric architecture is cost-effective in supporting low data rate traffic [3], the architecture does not scale well with increasing network size and traffic. The complexity of route computations at the network processing units of the routers grows with increasing network size. In addition, at high data rate the router port utilization needs to be kept low (less than 30% [4]) to ensure that the delay and packet loss meet the service level requirement. As such, the elec-

[3]For example, a data rate below 1 Gb/s for every source-destination pair for a 50-node network, according to the analysis in this thesis and [3].

tronic processing, which advances at a rate quantified by Moore's Law (the number of transistors on a chip doubles every 18 to 20 months), is both costly and slow in keeping up with future's surge of high capacity demand. As network traffic grows, router-centric networks will require increasingly higher capacity routers, yet there are clear limits to the footprint and speed of an electronic router in terms of space, power, and reliability. For carrier-grade networks, where scalability of growth is of paramount importance, these limitations start to cause problems. To provide relief, optical cross-connect based lightpath switching can be incorporated with electronic routing and switching in the metro networks.

The second factor is the optimization of network architectures. It is in most part overlooked, yet is crucial in our opinion. The architectures of metro and access networks have not been well thought-out, especially from the perspective of cost scalability. Most of the proposed WDM network architectures are direct adoption of those with electronic circuit and packet switching paradigms. There are still few guidelines on how to properly design various architectural elements of metro and access networks. Take the design of network fiber connection topology [4] as an example, traditionally ring configuration – the legacy topology for SONET (Synchronous Optical Network) based electronic switching – is chosen as the default topology for optical switching networks, without considering mesh topologies as viable alternatives [5] and [6]. Though recent years witness the migration to mesh networks from ring networks, the optimal topology as the tradeoff among various network resources and technologies has not been carefully considered to date. Since architectures optimized for optical switching paradigms will not be the same as the router-centric network architectures that are widely adopted for today's Internet, efficient optical network architectures that truly take the advantage of WDM technology need to be created.

In this thesis, our main focus is to address these challenges by proposing viable solutions. In regard to the scalability issue of a router-centric architecture, the consen-

[4] In this thesis, we distinguish the notions of network cable plant topology (also referred as physical topology in most of the research literatures) and fiber connection topology, as elaborated in Section 1.2.1.

sus is that the optical switching can be introduced to work in synergy with electonic routing and switching [5]. Compared with electronic switching, optical switching offers the following advantages:

- Transparency: each wavelength can carry data that are encoded and transmitted at different bit rate and use different formats and protocols. This allows the networks to interface with customers in need of a wide variety of services.

- Lower capital expenditure (CapEx) and operational expenditure (OpEx): in stead of handling the pass-through traffic at the packet level, well groomed lightpaths [5] can bypass costly router ports, reducing the route computation and forwarding load on the routers. In addition, network operators can implement end-to-end lightpath scheduling (e.g., optical flow switching [7]) and dynamic protection and restoration in the optical domain. With well considered designs, these advantages can translate into a reduction of capital investment and maintenance cost.

Optical cross-connect and other enabling technologies (such as tunable transceiver and wavelength converter, etc.), when judiciously integrated with current electronic-centric network infrastructure, provide us the technological foundations to build dynamically reconfigurable networks that offer end users with higher data rate services at lower cost-per-bit. To fully realize the potential of these enabling technologies, network architectures need to be carefully designed, in terms of cost and performance. That is, finding sensible architectures involves searching over a broad solution space of fiber connection topology, switching, routing and wavelength assignment (RWA), transport mechanism, transport protocol, as well as network management, which are allowable by the current and possible future technologies [2]. In addition to a low subscriber cost, the ultimate goal is to design networks that exhibit excellent scalability – a decreasing cost-per-node-per-unit-traffic as user number and transaction size increase.

[5] Traffics are aggregated and groomed electronically at the edge of the feeder network, as described in Section 2.3.2.

Obviously, solving this optimization problem entails a gigantic endeavor. Our approach is to decouple this optimization into more manageable tasks with the belief that by focusing on a less ambitious goal, we can still obtain insights into the intrinsic tradeoff that characterizes the global optimum. As such, in this thesis we study scalable optical network architecture by focusing on a solution *subspace* that includes fiber connection topology, switching, routing and wavelength assignment, with emphasis on analyzing the role of fiber connection topology design. The problem statement is provided in detail in the next section.

1.2 Problem Statement, Complexity, and Approaches

1.2.1 Problem Statement

The central theme of this thesis is searching for cost-effective network architectures over the solution space that embodies the key aspects of an optical network: fiber connection topologies, physical layer switching, routing and wavelength assignment (RWA), etc. In particular, the question we ask is, given the locations of network nodes and a traffic demand matrix (or a range of matrices), how we can minimize the total network cost (capital investment) over the following design elements:

- Network fiber connection topologies. While the cable plant topologies (also called as physical topology in most of the research literatures, as illustrated in Figure 1-1) are determined by factors such as speculated traffic and rights of way, how these fibers (inside the cables) are connected (via fiber patch panels) to form the fiber connection topologies (as illustrated in Figure 1-1), is a key design element that has significant leverage on the network cost. In this thesis, we optimize over two aspects of fiber connection topologies – node degree (connectivity) and connection rules (patterns).

- Dimensioning switching resources and selecting switching architectures. A lightpath that traverses multiple physical hops has to be switched at intermediate nodes. As such, sizing the switching resources to support the given traf-

fic demand (on a given fiber connection topology) is crucial. Also switching mechanism comes with different forms, such as optical-electrical-optical (OEO) switching or all-optical switching. With different switching technologies, the cost of an optical switch scales differently as a function of the port count. For example, for 3-dimensional (3-D) switching architecture (as shown in Figure 1-2 (a)), the cost, to the first order, can be modeled as approximately linear with the number of ports (e.g., $F_1(K_o) = \beta_1 K_o$, where K_o denotes the number of ports and β_1 denotes the corresponding cost per port). For 2-dimensional (2-D) switching architecture (as shown in Figure 1-2 (b)), the cost increases approximately quadratically with the number of ports (e.g., $F_3(K_o) = \beta_3 K_o^2$, where β_3 denotes the corresponding cost per port). In addition to the cost scalings, parameters such as cost per port β_1 and β_3, which depend highly on the technologies and manufacturing yields, play an equally important role in the switching cost [6]. from the perspective of designing a cost-effective optical network, properly dimensioning the switching resources and choosing a suitable switching mechanism is also important.

- Routing and wavelength assignment (RWA). In designing optical networks, the demands among node pairs are first mapped into a set of lightpaths. For a given network fiber connection topology, we need to decide how to establish these lightpaths through routing and assigning a wavelength for each lightpath. When wavelength continuity constraint (the same wavelength must be used on every fiber along the route of a lightpath) is enforced, RWA problem is quite difficult to solve, as will be explained in Section 1.2.2. Nonetheless, for Moore Graphs and uniform traffic, the RWA problem can be solved, as the results of symmetry and special constructions of Moore Graphs. This result is then used as bounds for other types of topologies.

Among these design elements, this thesis emphasizes the importance of designing fiber connection topologies, which is largely overlooked in current research. Using a

[6]The cost model will be described in detail in Chapter 5.

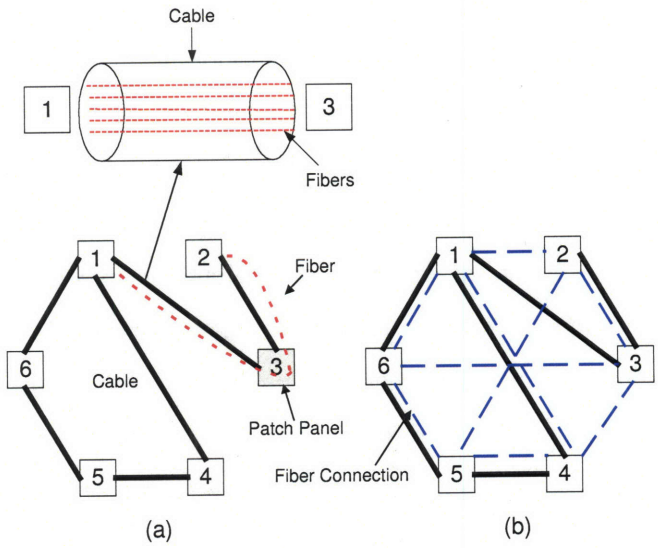

Figure 1-1: We can set up a fiber connection between two nodes that are not directly linked by a cable (e.g., node 1 and node 2), using fiber patch panels (at node 3). These fiber connections constitute network physical (fiber) topology.

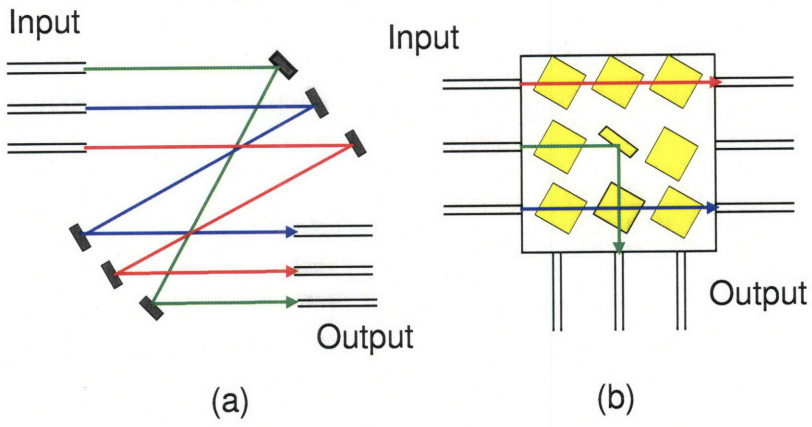

Figure 1-2: Optical switching architectures: (a) 3-D and (b) 2-D architectures.

50-node network as an example (the details of the analysis are presented in Chapter 4 to Chapter 6), Figure 1-3 plots the normalized network cost (cost per node) as a function of network node degree Δ to support a uniform traffic, for two types of topologies – Δ-nearest Neighbors and Generalized Moore Graphs [7]. As shown in the plot, the maximum normalized network cost (at $\Delta = 49$) is about 2.5 times of the minimum cost (at $\Delta = 8$). This shows that finding the optimal connectivity is essential. Also, finding the optimal connection rule is equally vital. For example, connecting the same set of 50 nodes via a Generalized Moore Graph will save about 40% in (minimum) normalized cost per unit traffic than connecting via a Δ-nearest Neighbors, as illustrated in Figure 1-3 and Figure 1-8 and discussed in detail in Section 1.3. From this example, we also note that the optimal node degree (at $\Delta = 4$)for the Generalized Moore Graphs is different from that for the Δ-nearest Neighbors (at $\Delta = 8$).

Since these design elements (fiber connection topology, switching resources dimensioning, routing and wavelength assignment) are inter-related, ideally they need to be considered *jointly* in the optimization process in order to achieve good performance [8]. Besides the network cost at the initial deployment, the ultimate goal is to design a network architecture (a combination of fiber connection topologies, RWA, and switching mechanisms) that has the best cost scalability – a decreasing cost per user per transaction with increasing number of users and data rates. Thus, in this thesis we call this problem as the Design of Scalable Optical Network Architectures.

1.2.2 Complexity

The Design of Scalable Optical Network Architectures belongs to a class of problems known as combinatorial optimization. Solving them involves selecting suitable combinations of discrete alternatives, i.e., where the solution is a set of integers or

[7] Δ-nearest Neighbors and Generalized Moore Graphs provide upper bounds and lower bounds on the average minimum hop distances and network costs for regular networks of the same size and connectivity, as to be presented in Chapter 4 to Chapter 6.

[8] In this thesis, we only solve the joint problem for Generalized Moore Graphs.

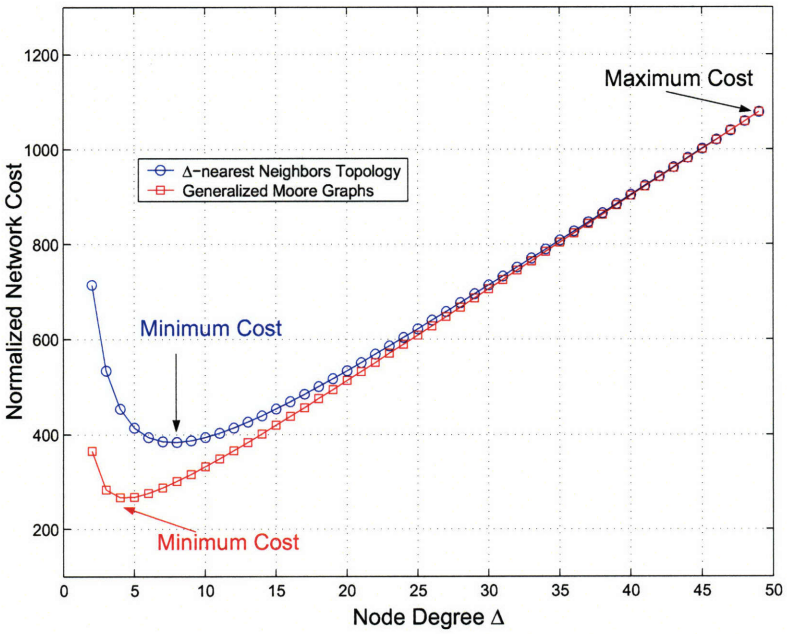

Figure 1-3: The normalized network cost (cost per node) as a function of network node degree Δ, with $N = 50$. Two types of topologies – Δ-nearest Neighbors and Generalized Moore Graphs are compared. The switching architecture is linear ($F_1(K_o) = \beta_1 K_o$). The elaborations of fiber topology and network cost models are deferred to Chapter 4, 5, and 6.

other discrete objects. In combinatorial optimization, the number of feasible solutions increases rapidly as the size of the input increases. Moreover, though it is usually easy to construct a feasible solution, finding an optimal solution remains extremely difficult.

To gauge the problem's complexity, we first look at the size of the solution space of a sub-problem – the designing of network physical topologies. As illustrated in Figure 1-3, finding the global optimal solution for a network of N nodes requires a consideration of every distinct subset of $N-1$ or more edges (at least $N-1$ edges are required to ensure that all nodes in the network are interconnected) out of $N(N-1)/2$ possible edges [9]. In other words, the complexity for a strictly optimal solution involves testing the following number of scenarios:

$$\sum_{i=N-1}^{N(N-1)/2} \binom{N(N-1)/2}{i}. \tag{1.1}$$

A simple manipulation in algebra shows that

$$\sum_{i=N-1}^{N(N-1)/2} \binom{N(N-1)/2}{i} \approx \sum_{i=0}^{N(N-1)/2} \binom{N(N-1)/2}{i} = 2^{N(N-1)/2}, \tag{1.2}$$

when N is large (e.g., $N \geq 20$). That is, the topology design problem has a complexity of $O(2^{N^2})$. For a design that involves 10 nodes, 3.518×10^{13} scenarios need to be tested. If, for the sake of argument, 10^6 cases could be tested in one second, an exhaustive search would still require 400 days!

Notice that to find the global optimal solution to the Design of Scalable Optical Network Architectures, we also need to solve the RWA for every topology (that is enumerated among $\sum_{i=N-1}^{N(N-1)/2} \binom{N(N-1)/2}{i}$ scenarios). For a given network topology and a given traffic matrix, the solution of the associated RWA can be found via solving an equivalent node-coloring problem [8]. Since node-coloring problems are NP-complete [9], finding solutions for a RWA is far from trivial. Even if a RWA can be approximately divided into routing only and wavelength assignment only, each of

[9] We consider an undirected topology. For a directed topology, we need to consider $N-1$ or more edges out of $N(N-1)$ possible edges.

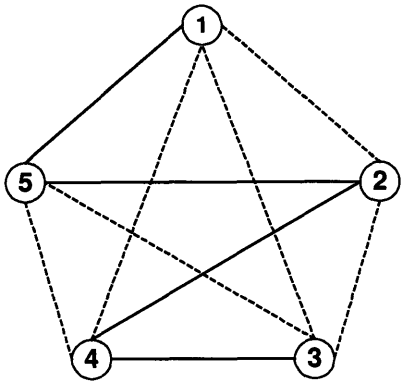

Figure 1-4: Finding the global optimal solution for a network of nodes requires a consideration of every distinct subset of $N-1$ or more edges (at least $N-1$ edges are required to ensure that all nodes in the network are interconnected) out of the $N(N-1)/2$ possible edges.

the sub-problem is still NP-complete [10]. Moreover, solving decoupled problems may not generate global optimum.

In addition to the topologies and RWA problems [10], we also need to consider the problem of selecting switching architectures and dimensioning switching resources. This will further increase the complexity. By now, we can easily see that, by brute force, the global optimum solution can be obtained only for very small networks (e.g., for $N \leq 8$) [4].

1.2.3 Approaches

Analytical Approach

As discussed in the previous section, when the size of a design problem becomes large, the required computation can be prohibitive and the notions of the dependencies among design parameters can be lost. In this thesis work, we are more interested in evaluating how the cost affects and drives architectural tradeoffs, rather than in

[10]We only solve the RWA problem for Generalized Moore Graphs in this thesis.

finding solutions for specific network design problems. Therefore, we take an analytical approach in most parts of the thesis by focusing on networks with symmetric and well-defined structures (i.e., regular networks) and symmetric traffic patterns (e.g., all-to-all uniform traffic). These are reasonable approximations for the metro environment. More practically, these assumptions and simplifications keep the analysis tractable. For quite a few classes of regular networks, we first derive or approximate the closed-form expressions for important parameters, such as average minimum hop distance, switch size, and network cost. We then set up and solve the corresponding optimization formulations. The analytical solutions obtained can show in concise form the relationships among key network design parameters, thus providing valuable references as points of departure for the final design. By analytically solving the Design of Scalable Optical Network Architectures over the space of fiber connection topologies, RWA, and switching architectures, this thesis offers insights and guidelines that numerical approaches cannot provide. Moreover, analytical results obtained under regular topology and uniform traffic assumptions can be extended to evaluate the performance of irregular networks under arbitrary traffic pattern (including random), for which analytical results are difficult to derive directly.

Numerical Approach

In reality, traffic is seldom symmetric, nor are networks regular or regularizable. Therefore we also study the design of irregular networks under non-uniform traffic. For these cases, it is difficult, most of the time impossible, to derive analytical expressions and solutions. We first formulate the corresponding designs as linear programming (LP), integer linear programming (ILP), or nonlinear programming (NLP) problems. We then obtain the solutions numerically, either by using solver packages or by developing heuristics. In this thesis, these numerical solutions are used mostly to evaluate the tightness of various analytical lower or upper bounds. We strive to find good analytical approximations in this thesis because we want to provide the system architecture a tractable view across a wide range of the solution space through simple analytical expressions.

1.3 Main Results and Related Works

1.3.1 Main Results

As stated in previous sections, we concentrate on illustrating the trends and the scaling of optimal architecture as functions of network parameters, traffic demands, and technologies via an analytical approach. For the sake of tractability, we first focus our attention to uniform all-to-all traffic and regular topologies, which are fair representations of realistic metro networks.

We start by examining various measures of regular topologies. Among these measures, the average minimum hop distance $H_{\min}$ plays a crucial role in evaluating the efficiencies of network architectures. From the perspective of designing optical networks, we show that the amount of switching resources used at nodes is proportional to $H_{\min}$. Thus a smaller $H_{\min}$ will translate into fewer expensive switching ports. We also demonstrate that topologies with smaller average minimum hop distance have a lower fraction of pass-through traffic and hence require less optical switches. This is especially important for both optical and electronic switching, since a scalable network architecture clearly wants to minimize the network resources that every transaction must use.

The average minimum hop distance is clearly a strong function of network size N and node degree Δ. For a fixed N, the larger the node degree, the shorter the $H_{\min}$. To illustrate how the $H_{\min}$ scales for different topologies, we plot $H_{\min}$ as a function of N, with Δ set to 3, as shown in Figure 1-4. It is evident that there are significant differences among network topologies for degree 3 networks. These differences can be as large as an order of magnitude. Generalized Moore Graphs (e.g., Petersen Graph, as shown in Figure 1-6) provide lower bounds (Moore Bound) on $H_{\min}$ (with a scaling of $\log_{\Delta} N$). Compared with Generalized Moore Graph, some topologies, such as (one-sided) Δ-nearest Neighbors (as shown in Figure 1-7) and Symmetric Hamilton Graphs, scale poorly as N increases (e.g., $N/2\Delta$ for Δ-nearest Neighbors topology). Other more complex topologies, such as the ShuffleNet and deBruijn Graphs, which come close to the Moore Bound, also scale favorably with

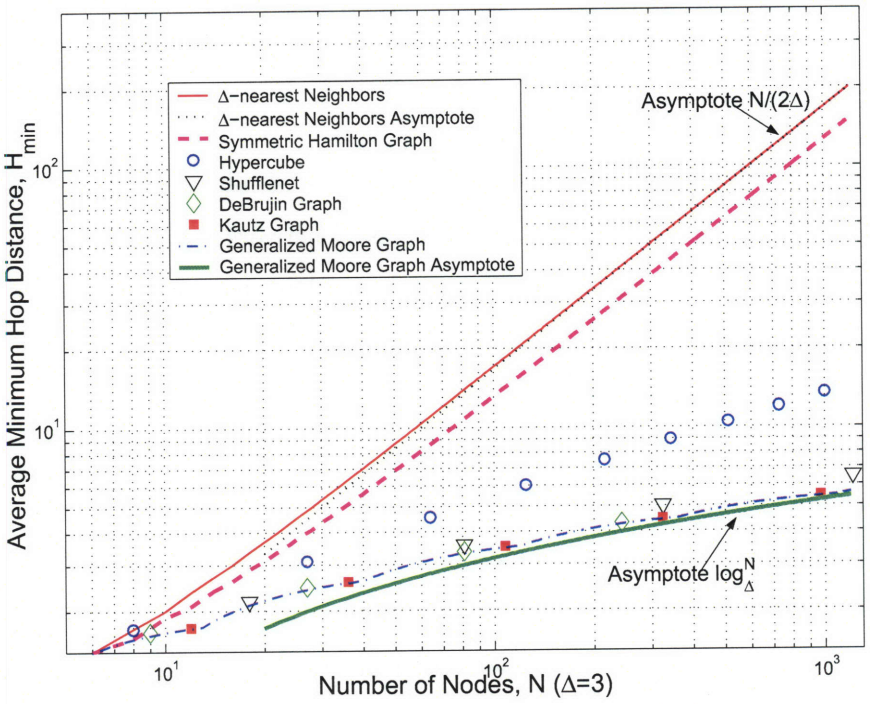

Figure 1-5: Average minimum hop distances $H_{\min}$ for different classes of symmetric regular physical topologies as a function of node number N. The node degree is set at $\Delta = 3$.

$\log_\Delta N$, thus keeping $H_{\min}$ short. Since the magnitude of difference in $H_{\min}$ means a similar magnitude of difference in switching cost of the corresponding networks, choosing a good topology is tremendously beneficial.

We next set up a first-order cost model and formulate a cost minimization problem (over choices of fiber topologies, switching architectures, and RWA)for the purpose of characterizing the tradeoffs between fiber and switching resources. Under uniform traffic and symmetric networks, the optimization problem can be solved analytically. An important result, given in Figure 1-8, depicts the minimum normalized cost per unit traffic with respect to network size, including both analytical asymptotes and exhaustive search results. These curves highlight the cost-optimality of Generalized Moore Graphs as network physical topologies: the minimal normalized cost per unit traffic decreases with increasing network size for Generalized Moore Graphs and their

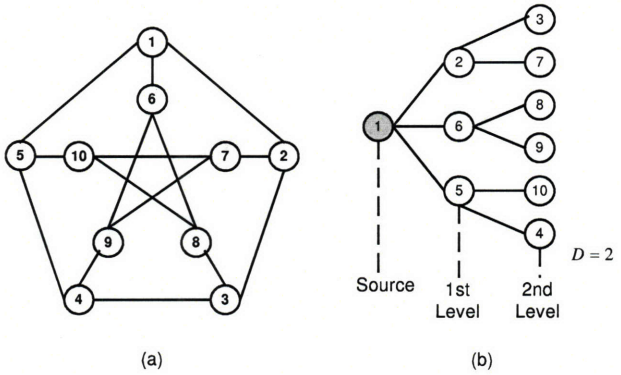

Figure 1-6: (a) An example of Generalized Moore Graphs – the Petersen Graph, with $N = 10$, $\Delta = 3$, and $D = 2$; (b) The routing spanning tree from node 1.

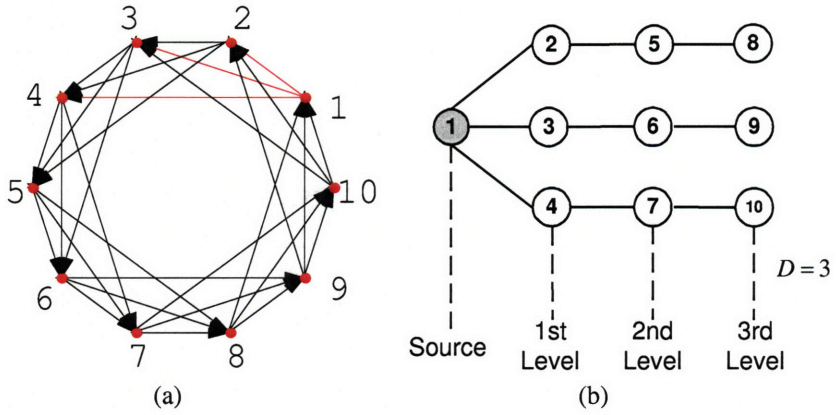

Figure 1-7: (a) (One-sided) Δ-nearest Neighbors topology with $N = 10$, $\Delta = 3$, and $D = 3$; (b) Routing spanning tree from node 1.

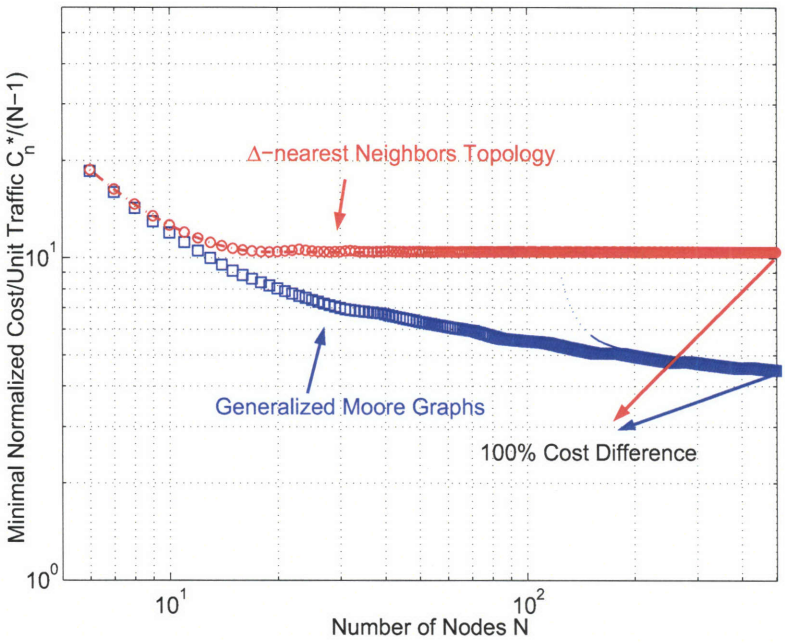

Figure 1-8: Minimal normalized network cost per unit traffic as a function of network size N for the Δ-nearest Neighbors (in red) and the Generalized Moore Graphs (in blue).

relatives; whereas the minimum normalized cost per unit traffic for Δ-nearest neighbors topologies stays constant with increasing network size. Our study also reveals other attractive properties of Generalized Moore Graphs in conjunction with minimum hop routing. When minimum hop routing is employed for uniform traffic in Generalized Moore Graphs, the aggregate network load is evenly distributed over each fiber. Thus, Generalized Moore Graphs require the minimum (or close to minimum) number of wavelengths to support a given uniform traffic demand.

In addition, we have taken steps in broadening the scope of this work to irregular network topologies and non-uniform traffic, which represent most existing networks. By investigating the implications of topology regularity, traffic uniformity, and switching cost scaling on the minimum hop routing (the results are summarized in Table 10.1 and Table 10.2), we show that if switching cost is linear with port count the minimum hop routing still optimal for arbitrary (regular and non-regular) traffic.

Table 1.1: Minimum hop routing for linear increasing switching cost.

Topology Traffic / Traffic	Uniform All-to-all	Non-uniform
Regular Topology	Optimal	Optimal
Irregular Topology	Optimal	Optimal

Table 1.2: Minimum hop routing for super-linear increasing switching cost.

Topology Traffic / Traffic	Uniform All-to-all	Non-uniform
Regular Topology	Optimal	Not necessarily optimal
Irregular Topology	Optimal	Not necessarily optimal

The results of Generalized Moore networks may be used to provide useful estimates for the cost of irregular networks under uniform or non-uniform demand, offering a benchmark for designing cost-efficient WDM optical networks.

Up until this point, we have focused on deterministic traffic, which is effective only when traffic volume and pattern are well known in advance. With more recent diversification of services, change in usage patterns, and data-dominated traffic, accurate forecasting of future demands for transport network planning has become increasingly complex. Thus designing networks that are robust to demand uncertainty is of great importance. In this thesis, we also present a framework to dimension optical networks incorporating uncertainties in demands. In this framework the interplay among topology design, switching resource provisioning, and routing are analyzed based on two optimization models. In one model, the weighted sum of network installation cost and expected penalty cost for unsatisfied traffic is minimized. In another model, the network installation cost is minimized subject to certain service level requirements (e.g., blocking probability). The optimization results enable us to identify the physical architectures that are most robust (in cost) to demand uncertainties. We also provide analytical references on how optimum dimensioning, network connectivity, and network costs change as functions of risk aversion, service level requirements,

and probability distributions of demands.

We conclude this section by commenting on the assumptions used in setting up the switching cost model. We use static all-to-all uniform model as an idealization of real world traffic, which is in general dynamic. We further assume that dynamic switching handles every wavelength of the pass-through and add-drop traffic, The main advantages of dynamic optical switching, besides protection and restoration switching, lies in its capability to adapt to traffic fluctuation and pattern change. More importantly, with dynamic switching wavelength resources are no longer reserved permanently – they can be efficiently shared among user pairs. Depending on the characteristic of the traffic, it may not be necessary to switch every wavelength dynamically. For example, when the network traffic is constant (e.g., the traffic has a very small variance to mean ratio), the lightpaths can be provisioned statically – they can be setup via "hard-wiring" using fixed routing and wavelength assignment. The main advantage of the static provisioning is that it can be implemented with the equipments such as fiber-patched panels, which incur much lower cost, compared with active switching equipment. In other words, the per port cost of quasi-static provisioning is smaller than that of dynamic switching. The downside of the static provisioning is the inefficient use of the network resources, especially for dynamic traffic. For dynamic traffic, it is practical to take a "hybrid" approach in network dimensioning. That is, low-cost switching equipments, such as fiber-patched panels, handle the static or quasi-static portions of the traffic, while more expensive dynamic switching equipments accommodate the fluctuating portions. *For this scenario, the parametric formulation of network cost optimization does include the patch panel case with lower cost per port.* The hybrid network dimensioning is a natural extension of this thesis. In addition to network cost, other design objectives, such as network blocking probability, throughput, network resource utilization, and the number of users supported, are also to be included. It is reasonable to expect that the optimal amount of static and dynamic provisioning is likely to be determined by the factors such as characteristics of traffic, the relative (per port) cost ratio between static and dynamic provisioning, fiber topology, and routing algorithm, etc. Correctly formulating and efficiently solving

such an optimization problem with multi-objectives is difficult, thus out of the scope of this thesis. Nonetheless, we comment of possible first steps and directions to study hybrid network dimensioning at the end of this thesis.

1.3.2 Related Works

The problems of designing cost-effective architectures for WDM networks have received considerable attention in the past decade. In most of these works, the concepts between cable plant topologies and fiber connection topologies are not differentiated. That is, the fiber connection topologies are assumed identical to the cable plant topologies, which are provided upfront. As such, with given network topologies and traffic demands, these studies mostly focus on solving the dimensioning or RWA problems.

There exists a significant amount of research in network dimensioning for given physical topologies. Some of these works take an analytical approach, such as [11] and [3]. [11] presents a set of equations that relate network size, average network node degree, traffic demand, and capacity. These results can be used to assess the characteristics of the topology required to support a given traffic matrix. However, in [11] a network cost model is not explicitly set up and the effects of different switching architectures are not considered. [3] follows a similar approach and goes a step further by constructing a detailed network cost model that considers switching architectures. [3] shows that for uniform demands, the parameters, such as network size, node degree, traffic between a node pair, and equipment cost structures, are sufficient to estimate the network cost. Since network fiber connection topology is given, the author does not address how the network costs are affected by different fiber connection topologies. Throughout this thesis, we show that there is a significant cost difference between an optimized topology and a casually designed one, as already illustrated in Figure 1-3 and Figure 1-8. Thus, the benefit of choosing a good topology is evident.

Other studies in network dimensioning of a given physical topology, such as [12], [13], [14], [15], and [16], focus on formulating ILP problems with the objective to minimize the total capital investment. These optimization problems, even with the

topology given, are shown to be NP-hard. As such, various heuristics and numerical techniques have been proposed for solving problems of realistic sizes. These results are drawn upon the case studies of existing national or regional networks, thus providing limited insights on how the optimal architectures scale and how they depend on critical design parameters. In comparison, the results presented in this thesis illustrate the analytical trends (e.g., Table 6.1, Table 6.2, and Table 6.3, etc.).

There are also a great deal of works that focus on RWA, from the early studies, such as [8], [9], [17], and [18], to the more recent ones, such as [10], [19], and [20]. Most of the RWA literatures to date use wavelength usage as the primary figure of merit. The typical objective in these studies is to minimize the maximum number of wavelengths required to support a set of lightpaths. Though these works provide various results on how to efficiently provision wavelength resources, they suffer from the following shortcomings:

- Using number of wavelengths as a figure of merit only makes sense when the cost is linear in the number of wavelengths. However, the cost is usually highly non-linear in reality. For example, for a line system of 64 wavelengths, the cost of using 50 and 55 wavelengths is almost the same. However, if 65 wavelengths are required and an additional fiber is unavailable, setting up a new fiber connection will substantially increase the cost.

- Some works, while minimizing the maximum number of wavelengths, force data to take much longer routes than the shortest path from source to destination, thus incurring higher switching cost. In addition, optical signals traveling via a longer path are more susceptible to attenuation and noise, thus more amplifiers are required and accumulated dispersion requires more expensive dispersion management hardware (in the form of specialty fiber, electronic dispersion compensation, and even regenerators).

There are a few works that study the design of network physical topologies. Among them, [21] represents an early foray into designing physical topologies at the infancy of WDM networks. At the time, routing and wavelength were usually statically pro-

visioned, this work focuses on hierarchically clustering stations and couplers, with the objective of minimizing the length of optical fibers. [5] addresses the topology design issue for the feeder of metropolitan area networks (MANs). However, the work considers the ring as the default topology, without considering mesh topologies as viable alternatives. [22] provides a cost-comparison analysis between mesh and multi-ring architectures. The results indicate that the average node degree has significant impact on network cost and upgradability. However, the comparisons are merely based on the analysis of several existing networks. [4] formulates the joint mesh topology design, routing, and spare capacity dimensioning as an ILP problem. Since the ILP problem can only be solved optimally for networks of small size, the work concentrates on developing heuristics to provide near-optimal solutions. Though some of the heuristic approaches share some similarities with the analytical approach adopted in this thesis (e.g., integer relaxation and rounding), the very nature of the ILP formulations predetermines that the results can only qualitatively reveal the dependencies of the optimal network connectivity (node degree) on the tradeoffs between the cost of fiber connection and the cost of routing and provisioning lightpaths. Moreover, the formulation does not take different switching architectures into account. The work does not address what kind of physical architectures exhibit good scalability.

In regard to network design with traffic demand uncertainties, most recent works, such as [23], [24], [25], [26], and [27], also assume that network physical topology is given (thus only dimensioning and routing sub-problems remain to be solved); the effects of traffic uncertainties on the network cost and its robustness are only evaluated and quantified with simulations or with stochastic programming techniques.

1.3.3 Summary

This thesis differs from the existing works in that it addresses the following important network design issues in detail via an analytical approach:

- Exploring the optimization of fiber connection topologies on top of a cable plant topology.

- Suggesting connection architectures that exhibit good scalability – a decreasing cost per node per unit traffic with increasing number of users and transcation size.
- Incorporating the switching architectures into the modeling.
- Gaining insights through analytically solution.

Most of the existing works related to this thesis inadvertently neglect one or more of the aspects mentioned above. Thus, the design principles derived from these works are incomplete, if not flawed. For example, in Section 9.2.2 we compare the costs of the network topologies used in some of these existing works with the costs of optimized network topologies. We show that a simple "rewiring" of the same set of nodes via a Generalized Moore Graph results in savings on the number of switching ports [11]. Through thoroughly tackling these design issues, this thesis gives more complete and creditable insights and benchmarks for designing cost-efficient WDM optical networks.

1.4 Thesis Outline

The thesis is organized as follows. Chapter 2, 3, 4, and 5 are preparatory parts of the thesis. Chapter 2 gives background on technological and architectural issues related to WDM networks. In Chapter 3, we model the traffic demand among access nodes. In Chapter 4, we take a graph theoretical approach to set up models for network physical architectures. Besides reviewing some important concepts in graph theory, we focus on presenting graph theoretical results derived for this work. In Chapter 5, we set up a parametric, first-order, and homogeneous network cost model in preparation for the analysis of optimal network architectures.

Chapter 6, 7, 8 and 9 are the core of the thesis. In Chapter 6, we formulate and solve analytically the joint optimization problem of physical topology, dimensioning

[11] In these examples, every improved network uses the same number of fiber connections as the original one does, as illustrated in Section 9.2.2

of network resources, and routing algorithms. In Chapter 7, we study the RWA for Generalized Moore Graph. In Chapter 8, we address the issues of dimensioning WDM networks under random traffic demand. In Chapter 9, we study how we can use the results for symmetric regular networks to evaluate the cost-efficiency of irregular networks under uniform or non-uniform traffic.

Chapter 10 concludes the thesis and suggests possible extensions of the work.

Chapter 2

Enabling Technologies and Architectures for WDM Networks

This chapter gives background on technological and architectural issues related to WDM networks, to provide a self-contained "setting of stage" for this thesis. The objectives here are: 1) to give a survey of the state-of-the-art of current photonic and optoelectronic technologies as they apply to optical networking; and more importantly, 2) to understand how the availability and the limitations of the enabling technologies affect a designer's choices of network architectures. As such, we first give brief descriptions of key building blocks of optical networks in Section 2.1. We then review the architectural evolutions of long-haul networks during the past decades in Section 2.2. Finally, in Section 2.3, we turn our attention to MAN by presenting a high-level architectural view of the next generation WDM-based MAN.

2.1 Key Building Blocks of WDM Networks

In this section, we present the basic features of representative devices and systems used in the implementation of optical networks [6], [28], and [29]. This area has experienced rapid developments and innovations with continuous upgrading and integration. By integration, multiple functionalities are joined into a single module or subsystem to provide higher performance and reliability, as well as to lower overall

cost. The component market is diverse, dynamic, and crowded, despite the industry downturn in late 1990s. It is common that several different products compete for a single area of application. To deal with the diversity, international committees have kept pushing out standards to define key performance parameters and interface specifications. Nevertheless, there are still differences in the secondary parameters. So it has been the carrier's choice, in the network design and upgrading, to select right combinations of technologies based on the system requirements in capacity, upgradeability/scalability, power consumption, environment condition, cost, etc., with the cost as the biggest driver.

2.1.1 DWDM and CWDM

Emerged in 1990s, the WDM technology was aimed to resolve bandwidth exhaustion and to enable multiple services over the same network. With a simultaneous transmission of 100 or more wavelength channels at a rate of 10Gb/s per channel in the same fiber link, WDM potentially allows an aggregate traffic of many terabits per second per fiber.

Depending on the number of optical channel (wavelength) specifications, a WDM system can be classified as dense WDM (DWDM) system, if many wavelengths are used (above 40 channels); or as coarse WDM (CWDM) system, if only a few wavelengths are used ($4 \sim 16$ channels). In this thesis, we use the terms WDM and DWDM indistinguishably.

- DWDM systems require precise standardization of the carrier frequencies. The International Telecommunications Union (ITU) recommended 81 wavelengths (channels) in the C-band (1528-1561 nm) of the fiber attenuation minimum with a line spacing of 50 GHz (or 0.39 nm). To maintain such high accuracy, light channels of DWDM systems must have extremely narrow line-widths and are usually under active feedback control for absolute center frequency stabilization to within 0.1 nm. Also, the powers of all channels need to be maintained at a relatively equal level. Driven by the competition among carriers to pro-

vide broadband service to the masses, metropolitan networks are now the fast growing segment for DWDM technology.

- CWDM systems, with ITU specified line spacing of 20 nm, are allowed to have a much broader spectral occupancy and looser center frequency stability. Also, in CWDM systems the issue of power equalization is in general not present. CWDMs are considered as low capacity and lower cost choice for access network which requires low channel count, short distance, but a wide variety of client interfaces. For this market, CWDM technology still faces challenges, such as cost reduction, small size, low insertion loss, and reliable performance in the temperature-uncontrolled environment.

2.1.2 Transmitter

In WDM systems, the main function of a transmitter is to send out a modulated optical signal complying with a set of specifications, such as bit error rate (BER) or signal-to-noise ratio (SNR). The important components of a transmitter include the light source and the modulator.

Light Source

In optical communication, light sources are required to be compact, monochromatic, stable, and long lasting. The background of the most popular light sources, *light-emitting diode* (LED) and *semiconductor laser*, along with *tunable laser* is given in the following.

- LED is a p-n semiconductor device. The light emission takes place when the excited electrons and holes are recombined at the junction. LEDs, though inexpensive, are slow devices and exhibit a relatively broad spectral range. Also, LEDs emit light with a relatively wide cone. Therefore, they are mostly used in multimode fiber communication links for short-distance and low-bit rate applications.

- Semiconductor laser is similar to LED, but with an additional active layer (with high index) sandwiched between n-type and p-type layers. The cleaved end surfaces of the chip serve as cavity mirrors. Semiconductor lasers transmit coherent light within a very narrow cone, and thus the beam can be more efficiently coupled to optical fibers. In addition, they can be directly modulated and thus are better suited for high bit rates and long fiber spans. Lasers for DWDM applications are required to have precise wavelengths of ITU grid, narrow spectrum width, high power output. Currently, there are different types of commercially available semiconductor lasers, such as Fabry-Perot (FP) laser, distributed Bragg reflector (DBR) laser, distributed feedback (DFB) laser, quantum well laser, and vertical-cavity surface-emitting laser (VCSEL), etc. The most commonly used lasers in communications are FP and DFB lasers. The DFB laser, with a built-in narrow-bandwidth filter in the laser cavity, is well suited for DWDM application. To deal with the wavelength drift by temperature (0.1 nm/ °C) or aging, a wavelength locker is used to provide an active feed back to stabilize the wavelength by adjusting the temperature via a thermal electric cooler (TEC).

- Tunable lasers can simplify network design and inventory management [31]. The advances in laser chip technology have enabled narrow-band and full C-band tunability. There are various technical approaches for the tunability. In the monolithic InP technology, the wavelength is selected by the thermal tuning to different peaks of the built-in grating. Another approach for rapid tunability is to use multi-wavelength laser arrays with wavelengths that span the desired tuning range. One or more lasers in an array can be activated to produce simultaneous transmission, or be selected by the external cavity structures, including tunable mirrors, tunable filters, etc. Although different technologies have to meet common specifications (ITU grid wavelength accuracy, stability, linewidth, etc.), they are different in tuning speed, size, cost, etc. Tunable laser has drawn significant attentions in the current market. Together with reconfig-

urable add/drop multiplexer (see Section 2.1.8), it enables extreme flexibility and cost reduction in the new generation of optical system.

Modulator

In optical communication, modulations come in two different forms: internal modulation and external modulation.

- For internal modulations, electrical signals representing a data stream directly modulate the light source. Directly modulated FP and DFB lasers have simple structures (thus lower cost). They are used for transmission distance up to 200-400 km and data rate up to 2.5 Gb/s.

- For external modulations, an external optical modulator is positioned in line with a continuous wave (CW) laser. Electrical signals act on the optical modulator, so the light that passes through is modulated. The major benefit of the external modulators is that they have negligible phase jitter, as compared with direct modulation. Thus external modulators are used in high data rate (above 2.5 Gb/s) applications. An external modulator can be based on a Mach-Zehnder interferometer structure fabricated on a $LiNbO_3$ substrate. Other types of optical modulators include semiconductor multiple quantum well (MQW) modulator and electro-refraction modulator.

Note that modulators are normally integrated with laser diodes to form modules, which contain also electronic circuitry, TEC and controller, semiconductor amplifier, and even electronic dispersion compensation, etc.

2.1.3 Receiver

The main function of a receiver is to detect a modulated photonic signal with a predetermined level of accuracy, which is measured in BER. Normally, a receiver consists of optical preamplifier (optional), polarization filter (optional), power equalizer, focusing lens, photodetector, electronic low-pass filter, and electronic circuits that extract

the clock from the incoming signal and determine the time and threshold level for sampling (in on-off keying demodulation).

The most crucial component in a receiver is the photodetector, which is required to have high power sensitivity, very fast response time (fast rise and fast fall time), and a spectral response that matches the range of transmitted wavelengths. The types of such photodetectors include the semiconductor *positive intrinsic negative* (PIN) photodiode and the *avalanche photodiode* (APD).

- PIN photodiode is a semiconductor device that consists of an intrinsic (lightly doped) region that is sandwiched between a p-type layer and a n-type layer. In the reversely biased PIN photodiodes, each absorbed photon produces one electron of photocurrent and thus the output current is proportional to the input optical power.

- APD has a more sophisticated structure than PIN photodiode. In the reversely biased APD, a strong electric field is formed in the junction, where the primary electrons are accelerated and acquire enough energy to excite new electron-hole pairs – an avalanche (multiplication) process arises. Because of the avalanche process one arriving photon can produce 10 to 100 or so photoelectrons.

In general, an APD photodetector has a much higher gain a PIN photodetector has. PINs, however, have a much faster switching speed, thus they have been largely deployed in high bit rate (e.g., 10Gb/s) detection.

For the applications in metropolitan and access networks, transmitter module and receiver module, along with drivers and other electronic circuitry are integrated to a compact transceiver. DWDM transceivers include also wavelength locker by active TEC control loop and protection circuit. The telecom carriers also seek for designs with small size, low power consumption, and plugability for high density and flexible deployment.

2.1.4 Regenerator and Optical Amplifier

An optical signal attenuates and becomes distorted as it travels in the fiber. To reach destinations that are hundreds of kilometers away, the power level of the optical signal must be periodically amplified and reconditioned, so that it can be detected with an expected BER at the receiver side. In optical communication networks, there are two distinct amplification devices: *regenerator* and *optical amplifier.*

- A regenerator transforms the optical signal to an electronic signal of the same bit rate, amplifies it, and then converts the electronic signal back to optical domain. Regenerators provide also additional functions, such as timing, error recovery, and pulse shaping. Regenerators are classified as 2R or 3R amplifiers – 2R, if they amplify and reshape; 3R, if they amplify, reshape, and retime. Prior to the introduction of DWDM, the regenerators incur very high cost and they are maintenance intensive, because for a multi-wavelength system an equal number of regenerators are needed. Considering the fact that a fiber contains multi-wavelengths and an optical link requires several stages of regenerations (typically spaced every 50 km), the cost of regeneration is significant.

- An optical amplifier is a device based on conventional laser principles. It receives one or more optical signals and simultaneously amplifies all wavelengths without OEO conversion. This is a significant advantage over regenerators, since only one device is required, instead of one for each wavelength. The key performance parameters of optical amplifiers are gain, gain flatness (all signals are amplified uniformly), noise level, and output power. There are different types of optical amplifiers, such as semiconductor optical amplifiers (SOA) and fiber-type amplifier: erbium-doped fiber amplifier (EDFA) or praseodymium-doped fiber amplifier (PDFA). In addition, there are other amplifying devices that are based on the nonlinear properties of optical materials, such as stimulated Raman scattering (SRS) and stimulated Brillouin scattering (SBS) amplifiers. Currently the most commonly used optical amplifiers are SOA and EDFA.

  - A SOA is based on the same technology as a Fabry-Perot diode laser. The

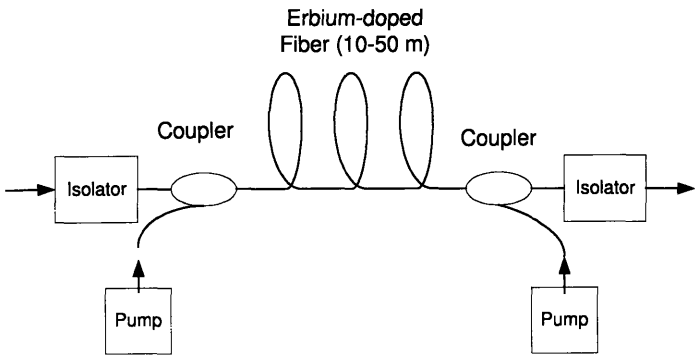

Figure 2-1: Schematics of a dual-pumped EDFA in-line with an optical path.

amplification is achieved by current injection of electrical pumping in its active layer.

- An EDFA, as shown in Figure 2-1 is based on the stimulated emission of erbium around 1550 nm, when the erbium doped in fiber is excited by optical pumping at 980 nm or 1480 nm. EDFA can have single-pump for shorter distance application or dual-pump for longer distance application. PDFA operates at 1300 nm.

Optical amplifiers are 1R amplifiers. That is, they only amplify the optical power. In practice, the signals can travel up to 120 km between amplifiers, but need regeneration after a distance of 600 to 1000 km.

2.1.5 Optical Multiplexer/Demultiplexer

An optical multiplexer receives several spatially separated wavelengths and form a single beam that consists of all these wavelengths; an optical demultiplexer performs the reverse functionality by spatially spliting the multi-wavelenght beam and coupling them into individual fibers. Demultiplexer can be passive or active in design. The passive demultiplexers are based on prisms, diffraction gratings, arrayed waveguide gratings (AWG), or spectral filters. Active demultiplexers are based on a combination of passive components and tunable filters. The two major technologies for DWDM

demultiplexer are thin film filter (TFF) and AWG, although a high-end bulk grating can have a comparable performance as the AWG.

- A TFF is a multi-layer dielectric filter that allows one wavelength to pass while reflects all other wavelengths. By cascading the filters in a substrate level integration, as shown in Figure 2-2, the wavelengths can be demultiplexed. TFFs are stable and low cost, but have higher insertion loss, thus are normally used in CWDM systems or DWDM systems with lower channel count.

- An AWG functions based on diffraction principle. It consists of an array of curved-channel waveguides with a fix difference in path length between adjacent channels. A lihgt beam with multiple wavelengths is launched into waveguides. At the output port the light beams with different phase delays are recombined and the interference among the beams diffracts different wavelengths to spatially separated output channels, as illustrated in Figure 2-3. AWGs are batch fabricated with planar lightwave circuits (PLC) technology by taking advantage of the mature semiconductor technology. This offers cost advantage at the chip level. Their insertion loss is independent of channel count, but their temperature sensitivity increases the packaging complexity. They are mostly used in high channel count applications (40 channels).

2.1.6 Optical Wavelength Converter

Wavelength converters are important devices that convert signal from one incoming wavelength to another outgoing wavelength. An intelligent deployment of wavelength conversion capability in an optical network can improve the utilization of the available wavelength resources and reduce the blocking of traffic. There are three basic ways to achieve wavelength conversion [6]: *opto-electronic converter*, *cross-gain modulation*, and *four-wave mixing*.

- Opto-electronic approach is the most practical method today to realize wavelength conversion – the input signal is converted to electronic form, regenerated, and then retransmitted using a laser at a different wavelength.

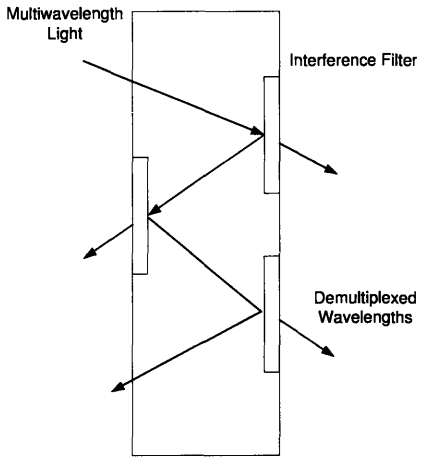

Figure 2-2: Schematics of cascaded TFF arrays as a wavelength demultiplexer.

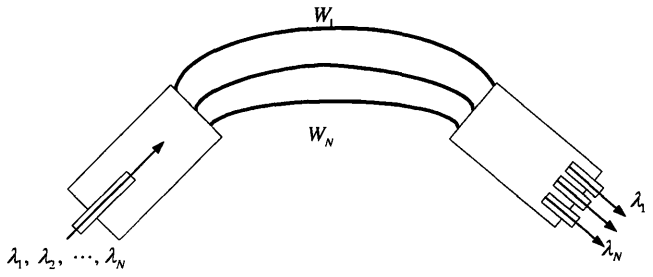

Figure 2-3: Schematics of arrayed waveguide grating.

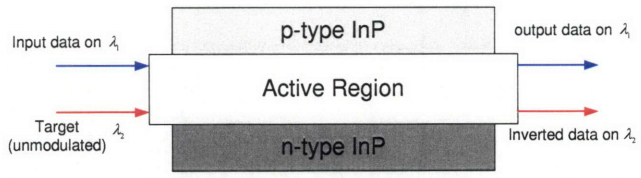

Figure 2-4: A Cross-gain modulating device transfers inverted data from one wavelength channel to another.

- Cross-gain modulation is based on the gain saturation in an optical amplifier. When high optical power is injected in the active region and the carrier concentration is depleted through stimulated emission, the optical gain is reduced. Based on this, consider two wavelengths injected in the active region of an optical amplifier. Wavelength λ_1 is modulated with binary data, and wavelength λ_2 is not modulated. When the input bit in λ_1 is a logic ONE (i.e., high power), depletion occurs and λ_2 is blocked. When the input bit in λ_1 is a logic ZERO (i.e., low power), depletion does not occur and λ_2 is at high power. Thus, a transfer of inverted data from λ_1 to λ_2 takes place, as illustrated in Figure 2-4.

- Four-wave mixing is a nonlinear optical phenomenon. Consider three closely spaced lightwave frequencies: f_1, f_2, and f_3. Due to the nonlinear interaction of the three, a fourth frequency is generated at $f_{\text{FWM}} = f_1 + f_2 - f_3$, as shown in Figure 2-5. If a modulated wavelength λ_1 is to be converted to another λ_{FWM}, one can select two more wavelengths, λ_2 and λ_3, in addition to λ_1, such that when all three are injected in the fiber device, a fourth wavelength λ_{FWM} is generated due to four-wave mixing. By inserting a pass-band filter in series with the fiber device, only the new wavelength λ_{FWM} is allowed to pass through and thus a wavelength conversion is realized.

We note that the latter two all-optical approaches are not yet mature enough for practical deployment.

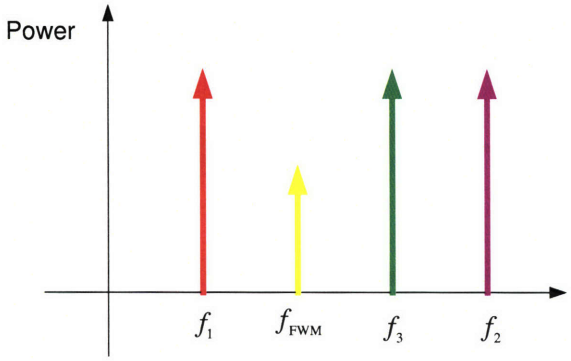

Figure 2-5: Principle of four-wave mixing.

2.1.7 Cross-Connect Fabrics

The cross-connection of communication channels is a key function in most communications systems. In electronic systems, the electronic cross-connecting fabric is constructed with massively integrated circuits and is capable of interconnecting thousands of inputs with thousands of outputs. The same interconnection functionality is also crucial in optical communication systems. In general, optical (channel) cross-connect can be accomplished in two ways:

- *Optical-electrical-optical* (OEO): the optical data streams are first converted into electronic data streams, then cross-connected in electronic domain, and converted back into optical data streams.

- *All optical switching*: the optical data streams are cross-connected within the optical domain.

The OEO approach is currently more popular in handling medium aggregate bandwidth due to the maturity in designing high-bandwidth and non-blocking electronic cross-connect fabrics. However, for high aggregate bandwidth on the order of several Tb/s, all-optical switching becomes more efficient and cost-effective. Currently, the optical switch size is from 2 to perhaps 64. Larger sizes up to 1000 are in experimental and planning phases. An economically feasible and reliable 1000×1000 all-photonic

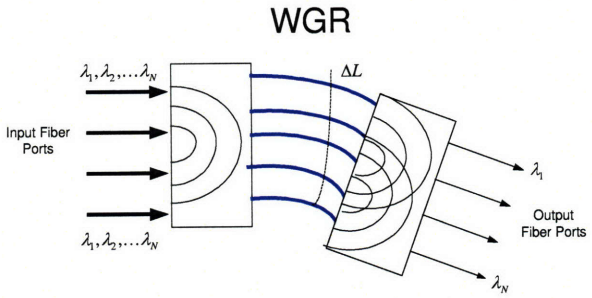

Figure 2-6: Free-space optical switching based on the generalized Mach-Zehnder waveguide grating router.

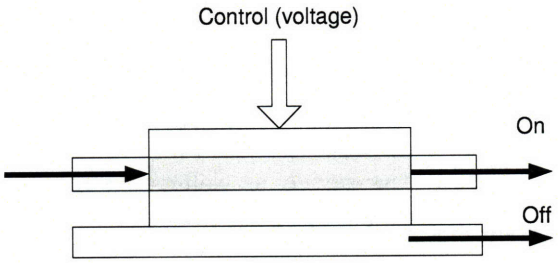

Figure 2-7: A solid-state optical cross-connect based on the principle of directional coupler.

non-blocking and dynamically reconfigurable switch, though promising, remains as a challenge.

All-optical cross-connect fabrics are based on at least three competing technologies: Mach-Zehnder waveguide grating router (WGR), solid-sate devices, and micro-electromechanical systems (MEMS). It is still too early to predict which technology will dominate, but the winner will likely offer network designer advantages of modularity, upgradeability, protection, and fault tolerance.

- Mach-Zehnder WGR: this is the most promising switch with many input ports and many output ports, as shown in Figure 2-6. In this device, a given wavelength at any input port appears at a specified output port, an input-to-output connectivity map is thus constructed. The functionality accomplished by this type of free-space optical switching is also known as wavelength routing.

- Solid-sate device: this device is essentially a semiconductor directional coupler, which can selectively change one of their optical properties on a path upon the application of a control signal, as shown in Figure 2-7. The optical property in consideration can be polarization, absorption, or index of refraction. Depending on the type of material, the optical property can be changed by applying heat, light, mechanical stress, electric current, or electric field (voltage). For example, electric field can be applied to modulate the index of refraction of ferroelectric $LiNbO_3$ crystals. Thin film heater can also be applied for the modulation. The material type, the controlling mechanism, and the controlled property impact the switching speed of the device, as well as the number of ports of the switch. For example, switches made with $LiNbO_3$ crystal exhibit switching speeds in the order of nanoseconds; whereas those made with SiO_2 on Si exhibit speeds in the order of microseconds. In practice a multi-port switch is constructed by using several 2×2 directional switches in multi-stage (Clos or Banyan) architecture, as illustrated in Figure 2-8.

- MEMS: this technology uses traditional semiconductor process to fabricate movable mirrors on a silicon substrate. These mirrors are placed vertically in the gap

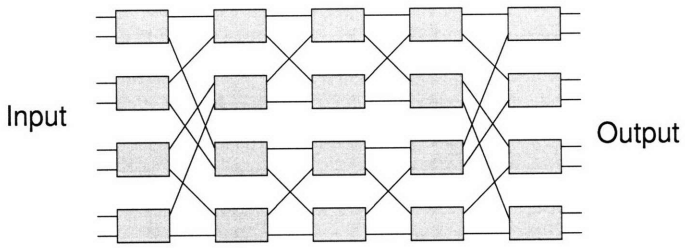

Figure 2-8: A multi-port switch is constructed by using many 2×2 solid-state directional switches in a multi-stage architecture.

of 3 intersecting optical paths and the mirrors' configurations can be electrically actuated, as shown in Figure 2-9. This arrangement constructs an optical switch whereby the mirror may either reflect a beam to different directions or block (or pass through) a beam, depending on the fabrication technology. For example, by rotating to two positions, a mirror directs a beam to one of two directions, as shown in Figure 2-9 (a). In another construction, a mirror may be pulled down (when a voltage is applied) or up (when no voltage), as shown in Figure 2-9 (b). There are in general two types of configurations of the micro switching elements for constructing an all-optical switching fabric: *two-dimensional* (2-D) switching fabrics and *three-dimensional* (3-D) switching fabrics (Figure 2-10). 2-D fabrics consist of two-dimensional arrays of micro switching elements that have one degree of freedom. 3-D fabrics are built using two arrays of micro switching elements, each of which has two degrees of freedom, allowing light to be directed from one input port to any output port.

2.1.8 Optical Add/Drop Multiplexer and Optical Cross-connect

Optical Add/Drop Multiplexer

An optical add/drop muiltiplexer (OADM) operates between demultiplexing and multiplexing points to drop certain wavelengths and add others, as schematically illus-

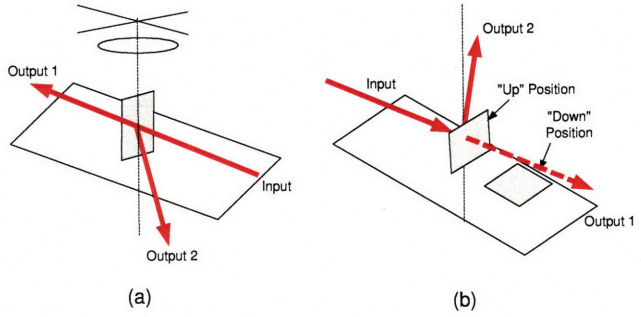

Figure 2-9: Micro-machined mirrors can be rotated (as in (a)) or pulled up/down (as in (b)) to construct optical switches.

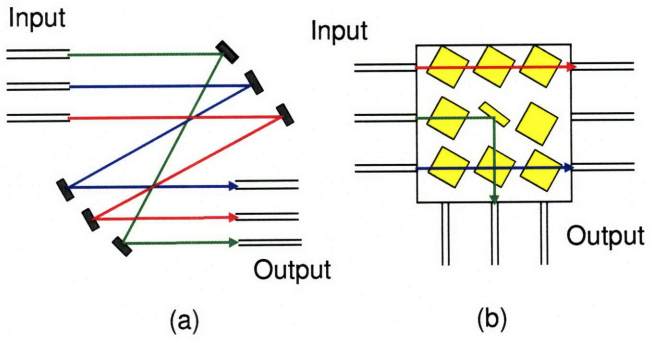

Figure 2-10: (a) 3-D MEMS configuration; (b) 2-D MEMS configuration.

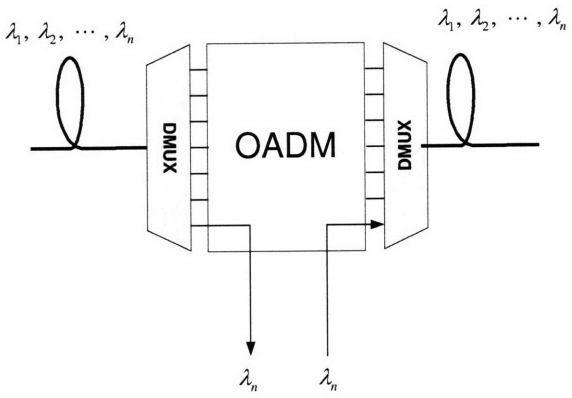

Figure 2-11: OADM or ROADM

trated in Figure 2-11. The first generation of OADM is a fixed one that is configured to drop and add predetermined wavelengths, so it works as a wavelength blocker. The new generation reconfigurable optical add/drop multiplexer (ROADM) works as wavelength-selective switch that can drop any wavelength to any fiber. ROADMs were first constructed for long haul DWDM networks. They started to move to the metro and regional networks in the past two years, driven by the increasing requirements in bandwidths and flexible service provisioning. ROADM is an optical subsystem with a high level integration of several critical functionalities: wavelength demultiplexing, switching, variable optical attenuator, and embedded control and circuitry. Various combinations of technologies and architectures have been applied in the design, e.g., diffractive grating or AWG for demultiplexing, MEMS mirrors or planar waveguides for switching, PLC technology for photonic integration, etc. The selection of specific types of OADMs depends on the targeted sector of networks. Fixed OADMs are used in a ring to reconfigure pass-through and add/drop wavelengths; Multi-degree ROADMs are for ring-to-ring interconnects and mesh networks. In fact, the migration of metro networks to mesh architectures is a secondary driver for ROADM deployment, next to cost.

Optical Cross-connect

Compared with OADM or ROADM, an optical cross-connect (OXC) usually has higher capacity and are more flexible in supporting different topological configurations. OADM or ROADM are normally used for ring or interconnected ring topologies; while an OXC can support an arbitrary mesh topology. In Section 2.2.2 and 2.2.3, we will give a detailed discussion of different functionalities and configurations of OXC in the context of the second and the third generation long-haul network architectures.

2.2 Architecture Evolution of Long-haul Networks

2.2.1 First Generation Architecture

In 1980s, the necessity of interconnecting telecom carriers' existing fiber networks throughout the world led to the *Synchronous Optical NETwork* (SONET) standard in North America and the *Synchronous Digital Hierarchy* (SDH) standard in Europe. Both SONET and SDH define a hierarchy of interface rates that allow data streams at different rates to be multiplexed in a network element (NE). Specific to SONET, the established optical carrier (OC) levels are from OC-1 (51.8 Mb/s) to OC-3072 (159.2 Gb/s)[1]. With these standard interfaces, the NEs convert the received signals, which are of different formats (such as DS1, DS3, and ATM), into SONET format.

The first generation of long-haul infrastructure is based on a traditional SONET/SDH ring topology, as illustrated in Figure 2-12. Point-to-point WDM links are terminated and interconnected using SONET add-drop multiplexer (ADM), and the rings are interconnected using digital cross-connect system (DCS). The ADMs also support standard SONET/SDH protection schemes, such as automatic protection switching (APS), unidirectional path-switched rings (UPSR), or bi-directional line-switched rings (BLSR). This architecture provided a reliable infrastructure, but suffered from a number of drawbacks:

- Artificial partitioning of meshes into rings (or interconnected rings): although

[1]As of 2006, OC-3072 is still a work in progress. It has not yet been manufactured.

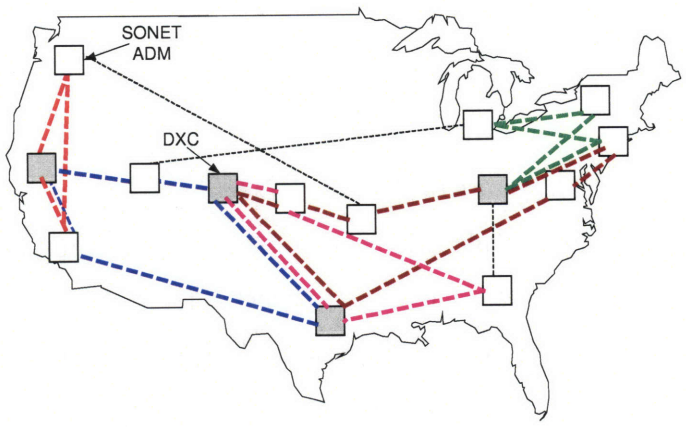

Figure 2-12: The first generation of long-haul infrastructure is based on a traditional SONET/SDH ring topology. Point-to-point WDM links are terminated and interconnected using SONET add-drop multiplexer (ADM), and the rings are interconnected using digital cross-connect (DCS).

the physical topologies of most long-haul networks are meshes, they are artificially partitioned into rings. This results in back-to-back line systems along many segments, which lead to inefficiencies in dimensioning network resources. Identifying the optimum ring partitioning and balancing the traffic loads on these rings are usually difficult, often resulting in increased bandwidth consumption and CapEx.

- Manual provisioning of services: new service request has to be manually provisioned, thus necessitating lengthy contracts, cumbersome provisioning sequences, and increased OpEx.

- Cumbersome scaling: stacking SONET rings to accommodate higher bandwidth does not scale gracefully, especially when rings need to be interconnected. This results in large increases in OpEx for real estate, power, and fiber management issues.

2.2.2 Second Generation Architecture

The second generation long-haul networks are built with intelligent OEO grooming switches that are connected by point-to-point WDM links in a mesh topology, as shown in Figure 2-13. Figure 2-14 shows a functional diagram of an OEO grooming switch. The central electronic switch core is essentially the same as that for a SONET DCS. The core operates at some standard synchronous rate and may be implemented in several stages, such as Clos non-blocking configuration [32]. Each individual incoming optical signal (wavelength) is converted to electronic signal, demodulated, and regenerated, so that the payload (carried by each incoming wavelength) is adapted to the format and the rate of the electronic switching fabric. The switching rate, which depends on the clock speed of electronic switching fabric, is called port (interface) rate. Electronic fabrics can "groom" several low-rate payloads to a port rate for a better utilization of switching resources. When the payloads are of higher rate than port rate, approaches such as parallel paths or inverse multiplexing [4] can be used to "break up" the high-rate payload into several port-rate payloads. Currently some commercially available switch fabrics can provide non-blocking switching capability of up to 512×512 OC-48 (2.5 Gb/s) signals. These switching fabrics can also support sub wavelength grooming at STS-1 granularity, as well as all standard SONET rates.

The OEO switches in long-haul networks are deployed in two phases. In the first phase, they serve as high capacity replacements for SONET ADMs and DCS. In this role, the OEO switches provide traditional ring termination and protection services like BLSR, UPSR, and APS. This phase allows a graceful upgrade for carriers, without obsolescing capital investments already made in line and terminal WDM equipment. In the second phase, these OEO switches are deployed in a mesh topology. Compared to a ring topology, the use of a mesh topology provides additional flexibility in terms of bandwidth allocation and shared protection / restoration schemes. Moreover, an intelligent network management system enables a number of advanced features that were not possible with traditional SONET/SDH systems, such as point and click

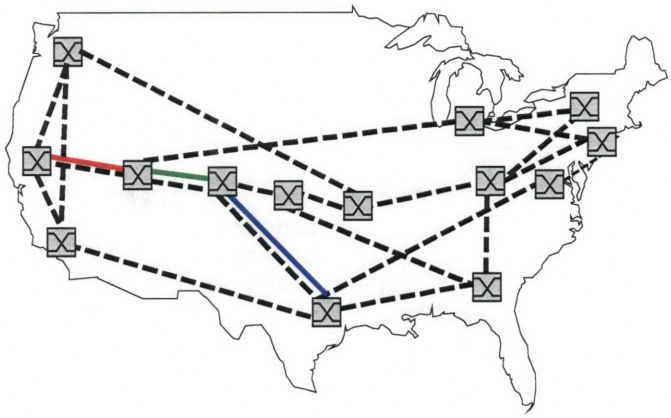

Figure 2-13: The second generation long-haul networks are built with intelligent OEO grooming switches that are connected by point-to-point WDM links in a mesh topology.

provisioning (or tearing down) of end-to-end services and advanced dynamic mesh restoration schemes.

One drawback of second-generation architecture lies in the all-electronic switching: OEO transponders and large electronic switching cores are installed at each node. They are expensive and power-consuming when operating at high data rates. As traffic rates increase, the pure-electronic switching approach becomes less feasible.

2.2.3 Third Generation Architecture

The third generation long-haul networks are built with optical OXC switches that are connected by point-to-point WDM links in a mesh topology, as shown in Figure 2-15. The third generation networks are often referred to as "all-optical" networks, since in contrary to the previous two generations, the switching for the third generation networks is carried out in optical domain. All-optical networking can take different forms, depending on how wavelength conversion and electronic processing are used in setting up lightpaths.

In the purest form of optical networking, each lightpath is assigned a dedicated

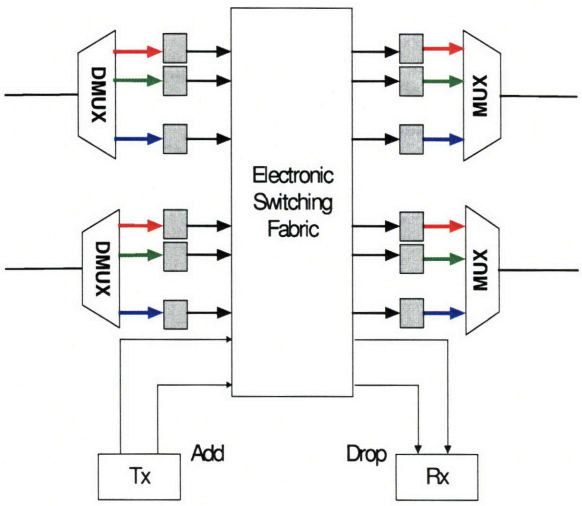

Figure 2-14: Functional diagram of an OEO grooming switch.

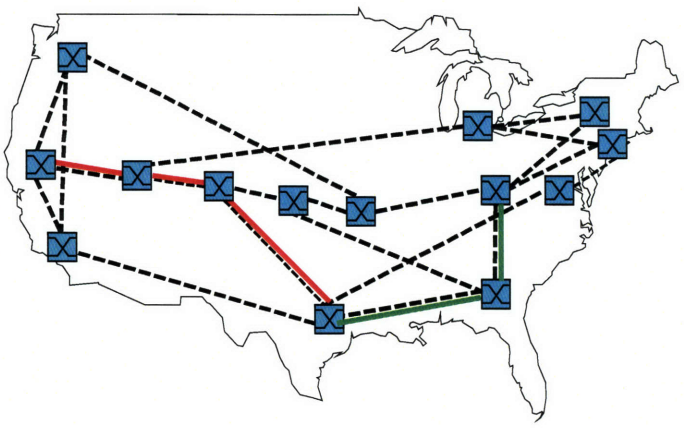

Figure 2-15: The third generation long-haul networks are built with OXC switches that are connected by point-to-point WDM links in a mesh topology.

wavelength and is routed from source to destination without any electronic processing at intermediate nodes. Under the circumstance, the intermediate nodes do not perform any wavelength conversion, and every path must have the same wavelength on each fiber. We call such a lightpath *transparent*, in the sense that the transmission of the signal is indifferent to the payload being in specific format in terms of framing, bit-rate, coding, etc. The respective OXC architecture is depicted in Figure 2-16. The wavelength channels on each incoming fiber are first demultiplexed into separated local jumper fibers. Then all copies of the same wavelength from each incoming fiber are directed to an optical switch module where they can be routed to any outgoing fiber and multiplexed with other wavelengths. Since wavelength channels are already separated when they are demultiplexed, the middle stage optical switches do not have to be wavelength selective; they need only to redirect the entire band of light from each incoming fiber to a specific outgoing fiber. For this reason, 3-D or 2-D MEMs switches are good candidates. The main advantage of a pure all-optical network is that the wavelength converters are not required and the lightpaths are transparent to payloads. Also, compared with OEO switches, OXCs have less power consumption [6]. However, there are also disadvantages:

- Wavelength assignment is much more complex, because a lightpath must use the same wavelength end-to-end. Routing and wavelength assignment can be a difficult problem, as already discussed in Section 1.2.2.

- To avoid wavelength blocking that a path cannot be routed because a single wavelength is not available on every span of any routing, more wavelength channels and OXC ports are required at fibers and nodes, respectively.

Current technological limitations and issues in network management and control make such all-optical networks difficult to implement. Performance assurance is especially an issue when the lightpaths are to carry a data rate at 10 Gb/s or 40 Gb/s. At high rates, the point-to-point transmission is so dependent on dispersion, noise, polarization, and nonlinearity of the fiber, etc., that the electronic regeneration at each OXC node is almost required to maintain the end-to-end BER performance.

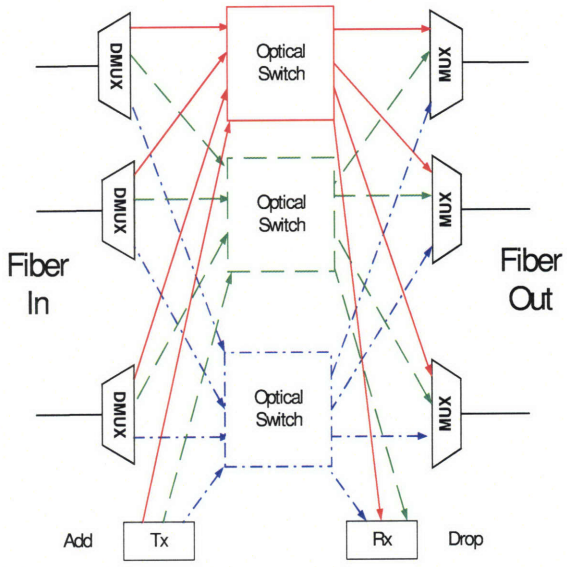

Figure 2-16: Functional diagram of a wavelength-selective optical switch in a transparent optical network.

In another form of optical networking, all the OXC nodes are capable of full regeneration and wavelength conversion. This type of networks is often called *opaque* optical networks. Figure 2-17 shows a representative architecture, in which the OXC use a single optical space-switch core. Any incoming lightpath can be transformed to any other wavelength on any outgoing fiber through conversion and remodulation. The practical advantage is that, once the signal is converted to electronic domain, monitoring and regeneration can be performed to maintain its quality. Also, wavelength blocking problem can be eliminated. The capacity design and routing problem are logically similar to that of traditional circuit switching network. The disadvantage is that every node requires a large number of expensive transponders.

A third form of all-optical network can strike a balance between transparency and opaqueness of the network. This type of network is often called *transluscent* optical network. A translucent optical network consists of OXC nodes that can perform a limited number of wavelength conversions using a shared pool of wavelength convert-

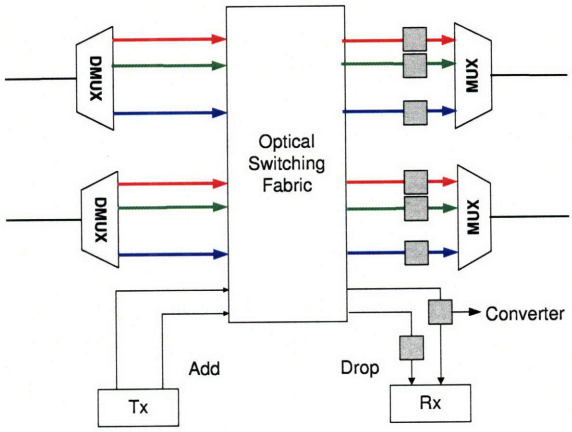

Figure 2-17: Functional diagram of an optical switch followed by separate wavelength converters in an opaque optical networks.

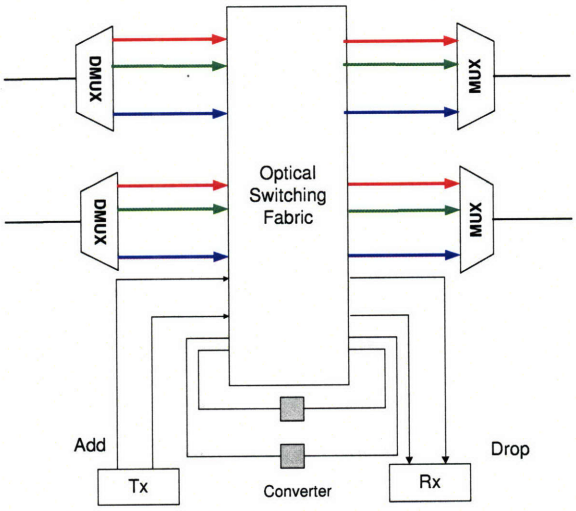

Figure 2-18: Functional diagram of an optical switch with a small pool of wavelength converters in a translucent optical network.

ers, as shown in Figure 2-18. If a lightpath does not require wavelength conversion, it is space-switched to an appropriate outgoing fiber. Otherwise, the lightpath can be locally switched to a free port in the pool of wavelength converters. From there, the output of the wavelength converter is space-switched again to the desired output fiber on its new wavelength. This architecture may be the most important and practical approach for optical networking in the near future, because the blocking performance is close to that of a network with full wavelength conversion at every node. That is, the wavelength blocking can be greatly reduced by provisioning a small number of wavelength converters.

2.3 Metropolitan Area Networks (MANs)

As mentioned in Chapter 1, while the growth of the capacity in long-haul network has been tremendous, an economical deployment of capacity in metro and access networks has been lagging behind. Aggregation and access have replaced capacity as the new bottleneck. As a result, end-users' access to this capacity is still expensive and limited to the data rates of kilobits and megabits per second. As such, seeking low-cost architecture becomes ever important to ensure the efficient utilization of the bandwidth glut. This is the motivation behind this thesis work. In this section, we illustrate the key physical architectures of the next generation MAN in preparation for the analysis in the chapters to follow.

Current access networks mostly operate in the electronic domain. The electronic-based switching can't keep up with the future surge of traffic demand, mainly due to the super-linear complexity increase (with respect to traffic) in route computation as the network processing units of the OEO switch [2]. We believe that the introduction of WDM technologies as both transport and switching mechanisms can significantly improve the capabilities of the access network and enhance the range and the quality of services. First, WDM technologies can increase the capacity that is critically needed in a metropolitan environment. Second, WDM can provide intelligent network functionality at the optical layer, as well as allows optical and electronic switching

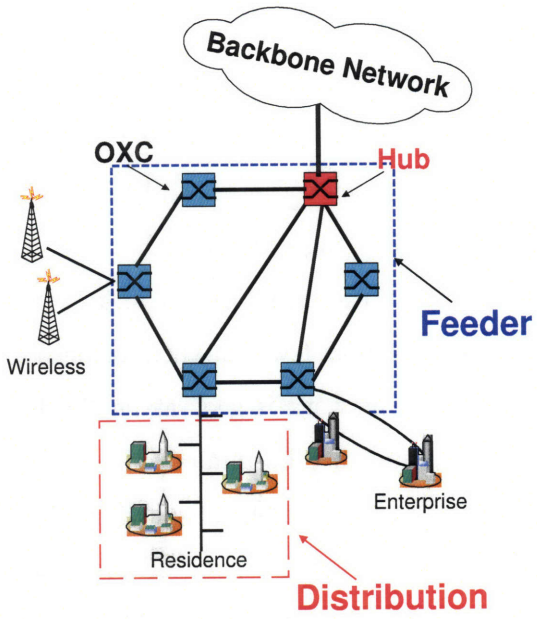

Figure 2-19: Physical architecture of an optical metropolitan access network.

layer to operate in synergy. Finally, WDM provides a degree of transparency – services can be carried by the network independent of data rate and format. This is very important in an access environment, as the carriers need to serve the customers with wide varieties of service demands.

The envisioned next generation MAN is divided hierarchically into a feeder network and multiple distribution networks. End users are locally connected to the distribution networks, which in turn are connected to the access nodes in the feeder network, as shown in Figure 2-19. In the following, we present a high-level view of the distribution and feeder portions of the MAN.

2.3.1 Distribution Networks

The distribution network directly interfaces with the customer premises and is responsible for collecting and delivering traffic. Extending from access nodes, the distribution networks use several types of topologies, including tree, bus, and ring, as shown

in Figure 2-19. The choices of a specific type of topology depend on the required redundancy and the geographical distribution of the customers. Also high-end user can directly connect to an access node by bypassing the distribution network. The distribution architecture is flexible with respect to the density and the allocation of wavelengths: in some cases, each end-user can have a dedicated wavelength; in other cases, many end users share a single wavelength.

An important feature of a distribution network is that it should be kept mostly passive, i.e., it should contain as few amplifiers or active switches as possible. The distribution portion of the network is geographically diverse, making it highly desirable that required maintenance be minimized. Since a significant percentage of network failures is due to power problems, deploying only passive components should greatly improve the reliability of the network. Also, a distribution network, and hence its cost, is shared among relatively fewer users. this is another motivation for using mostly low-cost, low-maintenance passive components.

2.3.2 Feeder Networks

The main functionalities of feeder networks include: aggregating traffic, delivering traffic to a hub (that interfaces with other MANs or long-haul networks), and transferring traffic from one distribution network to another. The feeder also supports the protection switching for high reliability, differentiated Quality of Service (QoS), and all network management and control functions of the access network. In short, a feeder network is no different from a long-haul network in functionality. Given the fact that there is significant traffic aggregation at the feeder, important core technology building blocks such as OXCs and tunable filters can be used.

A feeder network consists of a set of access nodes and hub nodes that are connected either in a ring or in a mesh topology (searching for the optimal topology is the central theme of this thesis). Access nodes, equipped with optical and electronic switches, serve as intermediary points between the feeder and the distribution portion of the network. As illustrated in Figure 2-20, demands from the distribution network enter the feeder at an access node via electronic switch where they

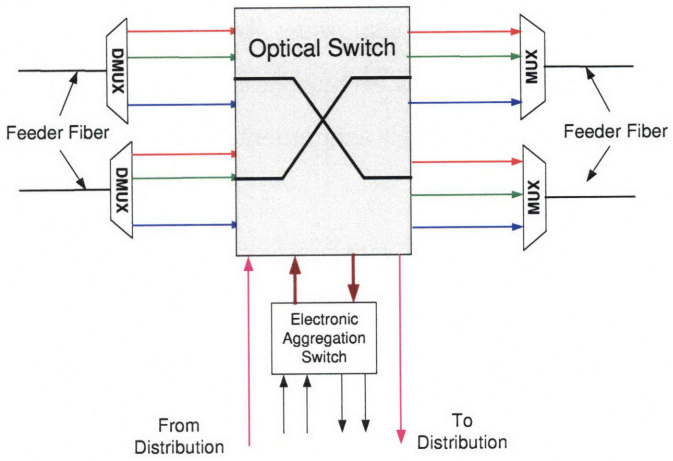

Figure 2-20: Functional diagram of an access node in the feeder of a MAN network.

are groomed (switched and multiplexed) into the fundamental units of inter-nodal bandwidth. The groomed output channels from the electronic switch then enter the optical switch, where they are directed to appropriate fiber of the feeder according to a routing scheme determined by either a centralized or a distributed management system. Note that a high-end user can bypass the distribution network and electronic aggregation via a dedicated wavelength that is directly added/dropped at the access node. Configurability in the access nodes provides efficient utilization of resources while accommodating dynamic traffic patterns. By allowing resources to be shared, it enables a given blocking probability to be achieved with fewer deployed switching ports and wavelengths. Configurability can be provided at the wavelength level (shown in Figure 2-20), waveband level (not shown in Figure 2-20), or even fiber level (not shown in Figure 2-20). Hub nodes serve as the interface between the access network and a backbone network or another access network. Therefore a hub node is equipped with optical and electronic switches of much higher capacities. A node can serve as both an access and a hub node. At a feeder network, a fiber can carry 10 to 100 wavelength channels, each at a data rate of 2.5 Gb/s (OC-48), 10 Gb/s (OC-192), and potentially higher. Since a feeder network can support a large number of users,

it allows more expensive equipments to be used; and at the same time, it makes the scalability of network cost a crucial issue. As such, in this thesis, we concentrate on finding a scalable feeder network architecture via the joint optimization over physical topology, routing and wavelength assignment, and dimensioning switching resources.

Chapter 3

Traffic Model

As discussed in Chapter 2, access nodes serve as intermediary points between the feeder and the distribution portion of the network. The key functionalities of an access node are to aggregate and to deliver the traffics from and to the end users of the distribution networks based on their common destinations, as illustrated in Figure 3-1. The aggregation of flows between each pair of access nodes constitutes the traffic demand of the feeder network. From the perspective of designing an optical feeder network, the traffic demand is normally specified in terms of the number of lightpaths to be set up between each node pair. Each of theses lightpaths carry data streams in an application-specific format and at a certain data rate.

In general, a network with limited resources cannot be designed to meet arbitrary traffic demand, thus we need certain models that reflect different modes of operations. In this chapter, we establish models to simulate the characteristics of the traffic demand among access nodes. Each of these models has its pros and cons, and none of them can provide an entirely complete and realistic account of network traffic demand. Different models can lead to substantially different performance criteria. Therefore, an understanding of the nature of the traffic in the target network and a selection of an appropriate traffic model are critical to the success of identifying optimal network architectures.

Based on different aspects of the network operation, past literatures on network design and planning gave a variety of classifications on traffic models. We summarize

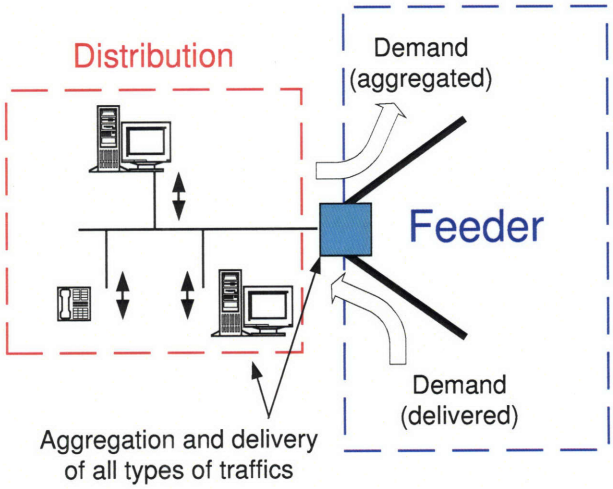

Figure 3-1: An access node aggregates/delivers traffic from/to the end users of the distribution network.

these classifications here to facilitate the discussions.

- *Offline* and *online* model [33][34]: in the offline model, an entire set of lightpaths is given upfront; while in the online model, the demand for lightpaths arises one at a time, and each lightpath must be provisioned on demand without waiting for future demand to become known. Specifically, in the online model, existing lightpaths cannot be rerouted to accommodate new lightpath requests. An offline model normally concentrates on long-term network operations and aggregated traffic demands; while an online model focuses on instantaneous network states and individual connections.

- *Static* (*deterministic*) and *random* model[4][33]: in a static model, the number of lighpaths between a node pair is given as a fixed value; while in a random traffic model, the amount of traffic between a node pair is treated as a random variable.

- *Blocking* and *non-blocking* model [4][33]: in a blocking model, the network is allowed to block some lightpaths; while in a non-blocking model the network must

support all lightpaths. For example, the traditional voice network is designed to support the majority of call requests. Some call requests may be blocked due to insufficient capacity in the network. With the blocking model, the goal is to design the network to keep the blocking probability within an acceptable limit.

In the following, we provide detailed descriptions of the traffic models employed in this thesis. In the process we also discuss the relative pros and cons of each model.

3.1 Deterministic (Static) Traffic Model

For the deterministic traffic model, the entire traffic demand is provided a priori. The set of lightpaths to be set up is given in the form of a traffic matrix $T = [t_{i,j}]$, where $t_{i,j}$, a deterministic value, represents the number of lightpaths between node i and j. With the deterministic traffic model, the network is designed to support all the lightpath requests. In other words, this is an offline, static, and non-blocking model.

We note that sometimes the demand of lightpaths is also called logical links to highlight the relationship to and the distinction from the physical links (edges) [4][33]. If a lightpath is set up between node i and j, there is a corresponding logical link (edge) that connects node i to node j. More precisely, the set of lightpath requests forms a logical topology.

A deterministic traffic model can have an arbitrary demand pattern $T = [t_{i,j}]$. Researches in network design and planning use two patterns extensively: *all-to-all uniform* traffic and *all-to-one* traffic [4][35]. Each of these two demand patterns captures the reality of the network traffic to certain degree, and, more importantly, using them can keep the analysis tractable.

- All-to-all uniform traffic: each node sends exactly t lightpaths of traffic to each of other nodes in the network. That is, in the traffic matrix $T = [t_{i,j}]$, we have $t_{i,j} = t$, for $i \neq j$. In other words, the lightpaths constitute a fully connected (complete) logical topology, as shown in Figure 3-2 (a). This type of demand pattern occurs in dense metropolitan area networks where the communities of

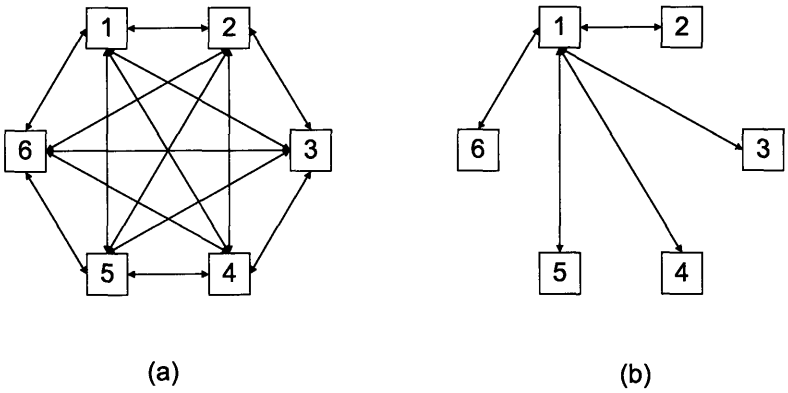

Figure 3-2: (a) Lightpaths in an all-to-all uniform traffic model constitute a fully connected logical topology; (b) lightpaths in an all-to-one traffic model constitute a star logical topology.

interest among all nodes are almost equal. Callers and other forms of communications from each node are as likely to go to one node as any other nodes in the rest of the network.

- All-to-one traffic: in this case, one node in the network is designated as a hub. Each of other nodes sends and receives t lightpaths of traffic to and from the hub. For example, let node k be the hub. In the traffic matrix $T = [t_{i,j}]$, we have $t_{i,k} = t_{k,i} = t$ and $t_{i,j} = 0$, for $i, j \neq k$. In other words, the lightpaths constitute a star logical topology, as shown in Figure 3-2 (b). The hub traffic pattern often characterizes metro or regional networks involving hub sites.

3.2 Random Traffic Model

The deterministic traffic model is effective when the traffic volumes and patterns are reasonably well known in advance, such as voice-dominated traffic. But with recent diversification of services, changing usage patterns, and data-dominated traffic, an accurate forecast of future demand volumes and patterns for transport network planning has become difficult. This is especially true in today's metro environment,

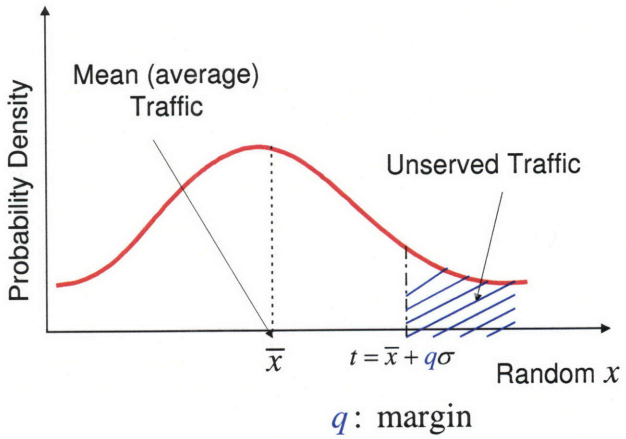

Figure 3-3: In random traffic model, traffic between a node pair is treated as a random variable.

in which the traffic demands among end users become more volatile [34], and the uncertainties of the traffic forecast increase. For these scenarios, the deterministic model becomes inadequate; we need a random model to account for the variability associated with the traffic.

In the random traffic model, the demand between a node pair is characterized by a random variable x, specified by its probability density function (PDF) $f(x)$, as shown in Figure 3-3. The mean $\bar{x}$ represents the mean (expected) value of the traffic demand; while the standard deviation σ measures the level of volatility of the demand forecast.

Based on the information obtained from market analysis and business models, a network designer can choose a suitable PDF that reflects the "best guess" of the demand. When such information is unavailable, various known theoretical distributions are employed to gauge the impact of the demand uncertainties [23]. Table 3.1 lists the theoretical distributions and their corresponding PDFs used in this work. For fair comparisons, the PDFs are all expressed with independently adjustable mean $\bar{x}$ and standard deviation σ. For example, the uniform distribution, which corresponds to the case that only the maximum and the minimum of the demand (denoted as $t_{\max}$

Table 3.1: Probability distributions expressed with independently adjustable mean and standard deviation.

Distributions	PDF with Independently Adjustable Mean $\bar{x}$ and Standard Deviation σ
Uniform	$f(x) = \begin{cases} \frac{1}{2\sqrt{3}\sigma}, & \text{if } \bar{x} - \sqrt{3}\sigma \le x \le \bar{x} + \sqrt{3}\sigma; \\ 0, & \text{otherwise.} \end{cases}$
Exponential	$f(x) = \begin{cases} \frac{1}{\sigma} e^{\frac{\bar{x}-\sigma-x}{\sigma}}, & \text{if } x \ge \bar{x} - \sigma; \\ 0, & \text{otherwise.} \end{cases}$
Half Normal	$f(x) = \begin{cases} \frac{1}{B}\sqrt{2\pi} e^{-\frac{(x-A)^2}{2B^2}} & \text{if } x \ge A; \\ 0, & \text{otherwise.} \end{cases}$ $A = \bar{x} - (\pi/2 - 1)^{-\frac{1}{2}}\sigma$ $B = (1 - 2/\pi)^{-\frac{1}{2}}\sigma$
Upper Bound	$f(x) = \begin{cases} p, & \text{if } x = \bar{x} + \sqrt{\frac{1-p}{p}}\sigma; \\ 1-p, & \text{if } x = \bar{x} - \sqrt{\frac{p}{1-p}}\sigma. \end{cases}$

and $t_{\min}$, respectively) are known, is normally specified by

$$f(x) = \begin{cases} \frac{1}{t_{\max} - t_{\min}}, & \text{if } t_{\min} \le x \le t_{\max}; \\ 0, & \text{otherwise.} \end{cases} \tag{3.1}$$

The definition given by (3.1) can be expressed with independently adjustable $\bar{x}$ and standard σ,

$$f(x) = \begin{cases} \frac{1}{2\sqrt{3}\sigma}, & \text{if } \bar{x} - \sqrt{3}\sigma \le x \le \bar{x} + \sqrt{3}\sigma; \\ 0, & \text{otherwise,} \end{cases} \tag{3.2}$$

where $\bar{x} = (t_{\max} + t_{\min})/2$ and $\sigma^2 = (t_{\max} - t_{\min})^2/12$. Since a demand x is non-negative, for a given mean $\bar{x}$, the maximal possible standard deviation for the uniform distribution is $\sigma = \bar{x}/\sqrt{3}$.

For a practical network provisioning under random traffic, it is often not necessary

(or impossible) to achieve totally non-blocking operation – it suffices if the blocking probability is sufficiently low. In this thesis, we are primarily concerned with a special blocking event that we call *overflow*. An overflow event occurs when the capacity provisioned cannot accommodate the traffic demand. We call the probability of this event as the *overflow probability*, denoted as p. For a random demand x and its associated probability density function $f(x)$, if t units of bandwidth are provisioned, the overflow probability p is defined by

$$p = \int_t^{\infty} f(x)dx. \tag{3.3}$$

With the meaning of the fraction of unserved traffic, the overflow probability p is usually used as a Quality of Service (QoS) parameter in the network provisioning and is also called as shortage probability requirement. Given a fixed low value of p (e.g., $p = 10^{-6}$), the network designer needs to determine the minimum bandwidth t to meet the targeted overflow requirement.

For the convenience of analysis, we write t as $t = \bar{x} + q\sigma$, with q being a constant to be determined. In this thesis, we call the constant q as the *margin* with the meaning of extra dimensioning required. A larger q means that more bandwidth is to be provisioned and the network cost will increase accordingly.

Among all PDFs with the same mean $\bar{x}$ and standard deviation σ, we prove that there exists one probability distribution that requires the maximum (worst case) margin $q = (t - \bar{x})/\sigma$,

$$f(x) = \begin{cases} p, & \text{if } x = \bar{x} + \sqrt{\frac{1-p}{p}}\sigma; \\ 1-p, & \text{if } x = \bar{x} - \sqrt{\frac{p}{1-p}}\sigma. \end{cases} \tag{3.4}$$

We term this distribution as the "Upper Bound" distribution and list it also in Table 3.1. We note that, in addition to being specified by a $\bar{x}$ and a σ, the "Upper Bound" distribution is also parameterized by an overflow probability p. In Chapter 8, we use this distribution as an upper bound in comparing the results from different PDFs that model the random demand. The proof of (3.4) is deferred to Appendix 8.5.3. For the analysis in Chapter 8, we assume also that the network traffic between node pairs

is independent and identically distributed (i.i.d.). That is, traffic demands between each node pair have the same PDF $f(x)$, and they are independent from each other. In summary, here we characterize the demand variability with an offline, random, and blocking model.

3.3 Stochastic Traffic Model

The stochastic traffic model is used to depict the bursty traffic from the end-users, by focusing on the instantaneous state of lightpath arrival and departure process, as illustrated in Figure 3-4. In this model, theoretical distributions are usually used to describe the process of lightpath establishment and release. For example, the requests for lightpaths between each node pair may be assumed to form a Poisson process with a known rate. The holding time (the time between establishment and release of a lightpath) has an exponential distribution with a known rate. This kind of stochastic model has traditionally been used in the design of voice network. For optical data networks, it is difficult to predict the statistics of the lightpath arrivals and holding times. This limits the validity of this model. Most of the current researches using this model assume a Poisson traffic, although there have been some recent works on non-Poisson traffic [36]. To summarize, this is usually an online and blocking model.

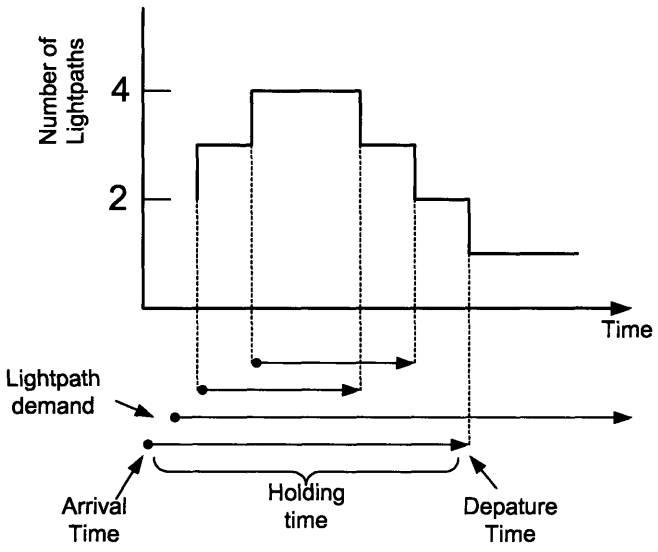

Figure 3-4: The stochastic traffic model focuses on the instantaneous state of the lightpath arrival and departure process.

Chapter 4

Network Model

Having established various traffic models in Chapter 3, in this chapter, we take a graph theoretical approach to set up models for network physical architectures. Besides reviewing some important concepts in graph theory, we focus on presenting graph theoretical results derived in this thesis work, especially the results of the Generalized Moore Graphs and other relevant regular topologies. Based on theses results, we also provide close estimates for irregular topologies, for which analytical solutions are difficult to obtain. The concepts and results in this chapter will serve as foundations for the in-depth analysis of scalable network architectures in Chapter 5 through Chapter 9.

4.1 Regular Topologies

On first order, the physical architecture of an optical network consists of cable plants, with each cable containing numerous fibers, and optical switches that are interconnected by the cables, as illustrated in Figure 4-1. Such a cable plant layout is called the cable plant topology, which is determined by speculated traffic and target of opportunities for affordable rights of way, as well as other factors, such as bi-lateral agreements between the carriers. How the fibers within the cables are connected is called the physical (fiber) topology, which is a key design element that has a significant leverage and is largely up to the network designer, as illustrated in Figure 4-2. In

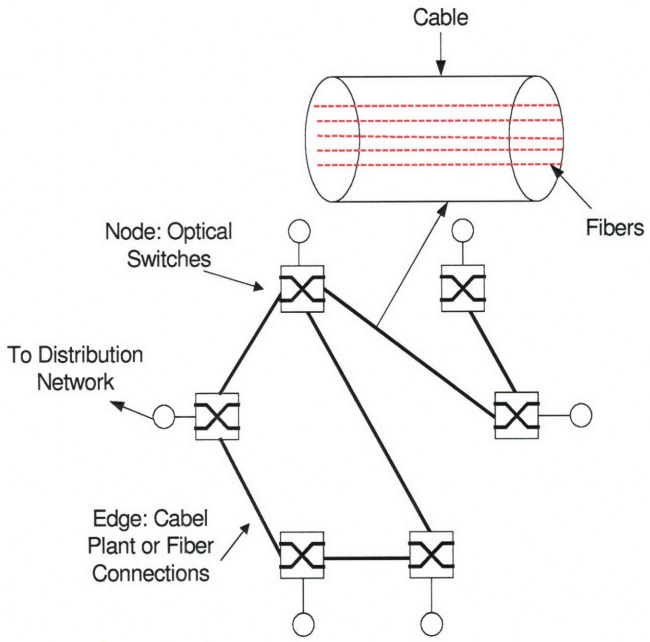

Figure 4-1: On first order, the physical architecture of an optical network consists of cable plants and optical switches that interconnect the fiber plants. Each cable contains numerous fibers.

this thesis, we follow the practice of representing a WDM mesh network as a (directed or undirected) graph $G(V, E)$. Vertices V (or nodes) represent the optical switches, and (directed or undirected) edges E represent the fiber connections. A path from a source node to a destination node consists of several edges. We call the number of edges of a path as the number of hops.

The network physical topologies can be broadly classified into two categories: regular and irregular (arbitrary). In this work we mostly focus on networks with regular topologies, since with their symmetric and well-defined connectivity pattern, they are analytically more tractable than irregular ones. Regular topologies are good approximations for MANs and local area networks (LANs), and can also be used as guidelines for wide area networks (WANs). For an irregular cable plant topology, a regular fiber connection topology can be constructed on top of it by connecting fibers

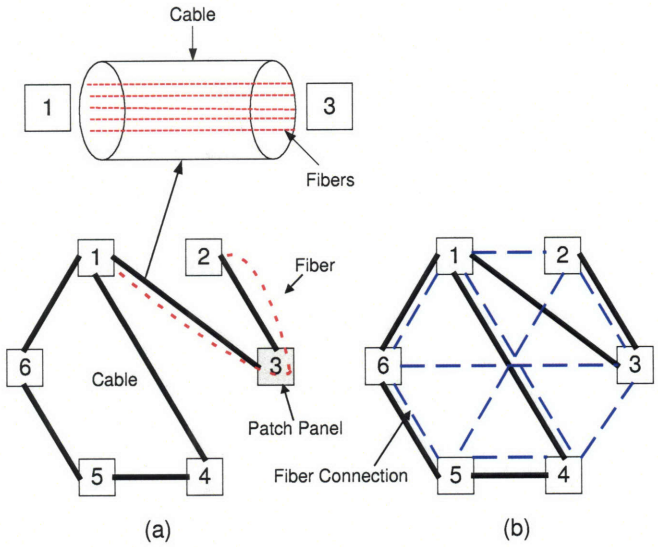

Figure 4-2: A regular fiber connection topology (shown in dashed line in (b)) can be constructed on an irregular cable plant topology (shown in solid line in (a) and (b)) by connecting fibers at nodes via static patch panel. For example, fiber connection between node 1 and node 2 can be implemented by patching fibers in the cable $1 \rightarrow 3$ and $3 \rightarrow 2$ at node 3.

via static patch panel, as illustrated in Figure 4-2. The analysis of such constructed regular topologies can provide estimates for the irregular ones. A detailed study of the irregular topologies by this method will be presented in Chapter 9.

In graph theory literatures, regular topology is defined differently in various contexts. In this thesis, we provide our definition of regular topology to cover a broad class of topologies that exhibit symmetric and well-defined structures. We say that a topology is regular of node degree Δ, when it satisfies the following conditions:

- There are Δ outgoing edges from and Δ incoming edges to each of its nodes.
- Each node links to Δ other nodes following the same set of (predefined) connectivity rules. In other words, the regular topologies studied in this work have nodal symmetry.

- A topology needs to be Δ-connected. That is, $n(i) \geq \Delta$, $1 \leq i \leq D-1$, as defined in [37]. In this definition, $n(i)$ denotes the number of nodes that are i hops away from a node via minimum hop routing; D denotes the diameter of a topology – the maximum distance among all possible node pairs via minimum hop routing.

Besides node degree, diameter, and connectivity rule, some other parameters are used to characterize a regular topology:

- The average minimum hop distance $H_{\min}$ between node pairs is an important quality measure for a network. For a regular topology of N nodes, $H_{\min}$ can be expressed as

$$H_{\min} = \frac{1}{N-1} \sum_{i=1}^{D} i n(i). \tag{4.1}$$

  $H_{\min}$ is usually used as an indicator of the propagation delay performance of a network [29] [33]. In this thesis, we will show that it can also be interpreted as a measure for the switching and wavelength resources required for supporting uniform all-to-all traffic. As such, $H_{\min}$ serves as a fundamental parameter and has an ultra importance in our work.

- The load of an edge is defined as the number of source and destination pairs using this edge. Obviously, for a given network and traffic demand, the load depends on the routing strategies. Assume that minimum hop routing is used and there is one unit of traffic for each source-destination pair ($t = 1$), the total (aggregated) load on the network, denoted as L, is related to the average minimum hop distance $H_{\min}$ in a simple way,

$$\begin{aligned} L(N,\Delta) &= N \sum_{i=1}^{D} i n(i) \\ &= N(N-1) H_{\min}(N,\Delta). \end{aligned} \tag{4.2}$$

  The average load on each edge L_{avg} for a network of size N and node degree Δ is

$$L_{\text{avg}}(N,\Delta) = \frac{L}{N\Delta} = \frac{(N-1) H_{\min}(N,\Delta)}{\Delta}. \tag{4.3}$$

Next we define L_i, $L_{\max}$, and $L_{\min}$ as the load on the edge i ($i \in E$), the maximum load (also called congestion), and the minimum load, respectively, all under minimum hop routing algorithms. To achieve a minimum congestion, the best we can do is to distribute the total load evenly over each fiber. That is, if $L_i = L_{\text{avg}}$ for every $i \in E$, we have an evenly distributed load.

4.2 Moore Graph and Generalized Moore Graph

4.2.1 Moore Graph

As to be presented in the subsequent chapters, Moore Graphs are a class of graphs that have great importance in this thesis. The Moore Graph concept stems from the problem of finding an upper bound on the number of vertices in a graph, given a diameter D and a maximum node degree $\Delta_{\max}$. Such a bound, which was established by E. F. Moore, exists for both directed and undirected graphs. For a directed graph, the maximum number of nodes that can be supported is

$$\begin{aligned} N_{\max}(\Delta_{\max}, D) &\leq 1 + \sum_{i=1}^{D} (\Delta_{\max})^i \\ &= \frac{{\Delta_{\max}}^{D+1} - 1}{\Delta_{\max} - 1}. \end{aligned} \tag{4.4}$$

For an undirected graph, the maximum number of nodes that can be supported is

$$\begin{aligned} N_{\max}(\Delta_{\max}, D) &\leq 1 + \Delta_{\max} \sum_{i=0}^{D-1} (\Delta_{\max} - 1)^i \\ &= 1 + \Delta_{\max} \frac{(\Delta_{\max} - 1)^D - 1}{\Delta_{\max} - 2}. \end{aligned} \tag{4.5}$$

For a regular graph of node degree Δ, we have $\Delta_{\max} = \Delta$. We call the class of regular graphs for which $N(\Delta, D) = N_{\max}(\Delta, D)$ as Moore Graphs. In other words, a Moore Graph is an ideal (not necessarily realizable) regular topology, in which each node reaches every other node in a fully populated Δ-ary minimum hop routing spanning tree. (A spanning tree is a connected subgraph that includes all the nodes and has

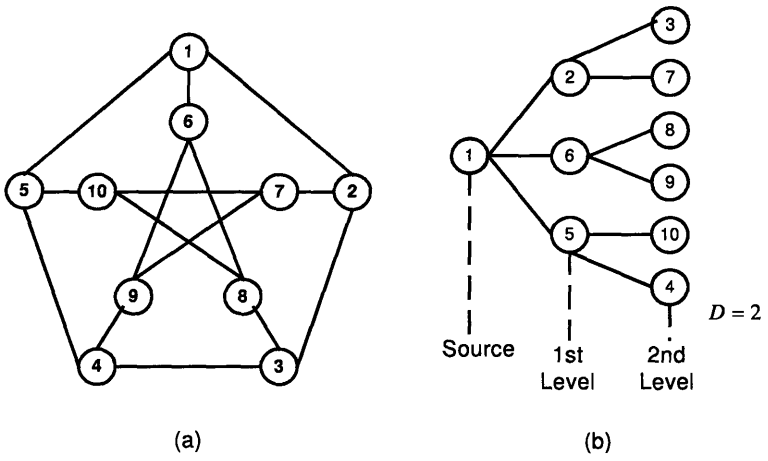

Figure 4-3: (a) The Petersen Graph, $N = 10$, $\Delta = 3$, and $D = 2$; (b) The routing spanning tree from node 1.

no cycles). As an example, Figure 4-3 shows the Petersen Graph – one of the existing Moore Graphs – and the routing spanning tree from node 1.

To our interests, the most important property of a Moore Graph is that, among regular topologies with the same node number and node degree, a Moore Graph provides the lower bound on the average minimum hop distance. For given D and Δ, the lower bound on the average minimum hop distances, denoted as $H^{o}_{\min}(\Delta, D)$, is given by

$$H^{o}_{\min}(\Delta, D) = \frac{D\Delta^{D}}{\Delta^{D} - 1} - \frac{1}{\Delta - 1}, \tag{4.6}$$

for a directed Moore Graph; or is given by

$$H^{o}_{\min}(\Delta, D) = \frac{D(\Delta - 1)^{D}}{(\Delta - 1)^{D} - 1} - \frac{1}{\Delta - 2}, \tag{4.7}$$

for an undirected Moore Graph.

Directed Moore Graphs exist only for trivial cases where $\Delta = 1$ or $D = 1$ [38]. Undirected Moore Graphs also exist, though there are only few of them. For $D = 1$ (of any value), we have Moore Graphs that are full (complete) graphs; and for $\Delta = 2$,

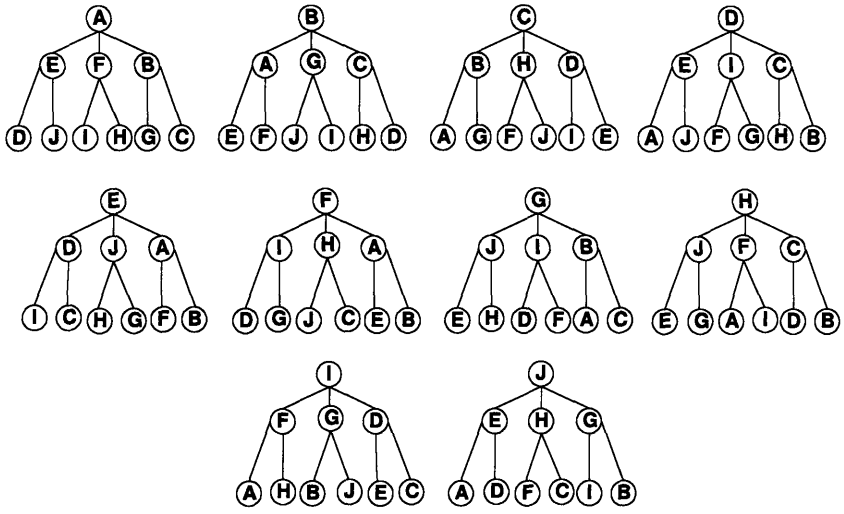

Figure 4-4: The minimum hop routing spanning trees of the Petersen Graph.

we have Moore Graphs that are rings (with odd number of nodes). The Petersen Graph, show in 4-3, is with $N = 10$, $\Delta = 3$, and $D = 2$. The Hoffman-Singleton Graph, with $N = 50$, $\Delta = 7$, and $D = 2$, is also an existing Moore Graphs [39]. A Moore Graph with $\Delta = 57$ and $D = 2$ may exist, though its construction has not been realized yet [39]. It has been shown that a (undirected) Moore Graph with $D \geq 3$ does not exist [39].

Next we use the Petersen Graph to show some important properties of Moore Graphs. To facilitate the discussion, we relabel node 1 to node 10 as node A to node J. By enumerating the routing spanning trees of all nodes, as shown in Figure 4-4, we make the following observations and generalizations. First, the minimum hop routing spanning tree from each node of the Petersen Graph is unique. For instance, source node A can reach nodes E, F, and B on the first level of its routing spanning tree. Also node A can reach D and J only through E; reach I and H only through F; and reach G and C only through B. Every source-destination pair has a unique minimum hop path in the Petersen Graph. For example, A can only reach D via the minimum hop path $\mathsf{A} \rightarrow \mathsf{E} \rightarrow \mathsf{D}$. The observation can be generalized as in Theorem 1. A detailed

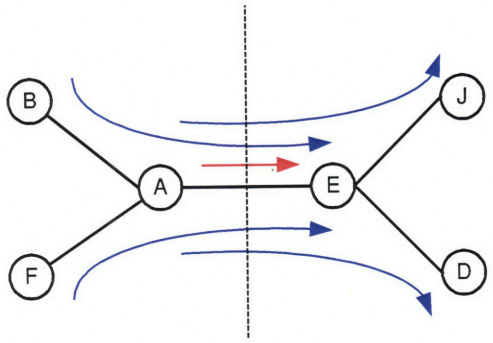

Figure 4-5: The load generated on edge AE by uniform all-to-all traffic.

proof is provided in Appendix 4.5.1.

Theorem 1 *Each node of a Moore Graph has a unique minimum hop routing spanning tree. Thus, every source destination pair of a Moore Graph has a unique minimum hop path.*

Second, the minimum hop routing perfectly distributes the load on every edge of the Petersen Graph. As illustrated in Figure 4-4, edge AE is used as the 1st hop by lightpaths $A \rightarrow E$, $A \rightarrow E \rightarrow D$, and $A \rightarrow E \rightarrow J$; it is also used as the 2nd hop by $B \rightarrow A \rightarrow E$ and $F \rightarrow A \rightarrow E$. In total, 5 source-destination pairs use the edge AE, generating a load of 5, as shown in Figure 4-5. It is easy to verify that every edge has the exact load of 5. As provided in Appendix 4.5.2, the same result holds for other Moore Graphs, as summarized in Theorem 2.

Theorem 2 *For a Moore Graph of degree Δ and diameter D, balanced load distribution can be achieved for the static uniform all-to-all traffic, with each edge having a load of $\sum_{i=1}^{D}(\Delta-1)^{i-1}$.*

4.2.2 Generalized Moore Graph

A Generalized Moore Graph refers to a regular (directed or undirected) graph, which does not achieve the upper bound on the number of nodes (as given in (4.4) and

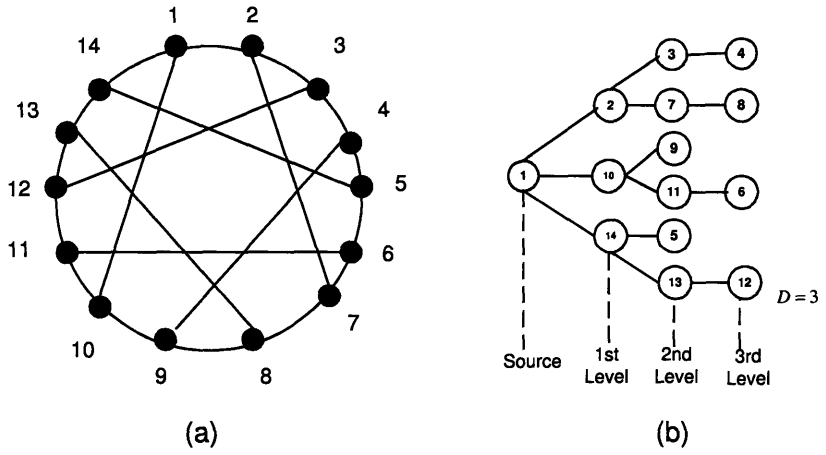

Figure 4-6: (a) The Heawood Graph with $N = 14$, $\Delta = 3$, and $D = 3$; (b) The routing spanning tree of node 1.

(4.5)), but achieves the lower bound on the average minimum hop distance [?][40]. In other words, Moore Graphs belong to a special subset of Generalized Moore Graphs. In a Generalized Moore Graph, the routing spanning tree has all the levels that are full, except possibly the last level. Figure 4-6 shows an example of Generalized Moore Graphs – Heawood Graph ($N = 14$, $\Delta = 3$, $D = 3$) and the routing spanning tree from node 1.

For a directed Generalized Moore Graph with size N and node degree Δ, the diameter is

$$D(N, \Delta) = \lceil \log_{\Delta} (1 + N(\Delta - 1)) \rceil - 1, \tag{4.8}$$

and the average minimum hop distance is

$$H^{\mathrm{M}}_{\min}(N, \Delta) = \frac{\Delta - \Delta^{D+1} + ND(\Delta - 1)^2 + D(\Delta - 1)}{(N - 1)(\Delta - 1)^2}. \tag{4.9}$$

The average minimum hop distance can be approximated as

$$H^{\mathrm{M}}_{\min}(N, \Delta) \approx \log_{\Delta} [1 + N(\Delta - 1)] - 1. \tag{4.10}$$

As $N \to \infty$, we have the asymptotic scaling of the average minimum hop distance

$$H^{\mathrm{M}}_{\mathrm{asym}}(N, \Delta) \to \log_{\Delta} N = \frac{\ln N}{\ln \Delta}. \tag{4.11}$$

The derivation of (4.11) is provided in Appendix 4.5.3.

For an undirected Generalized Moore Graph with size N and node degree Δ, the diameter is

$$D(N, \Delta) = \left\lceil \log_{\Delta-1} \frac{N(\Delta-2)+2}{\Delta} \right\rceil, \tag{4.12}$$

and the average minimum hop distance is

$$H^{\mathrm{M}}_{\mathrm{min}}(N, \Delta) = \frac{\Delta\left[1-(\Delta-1)^{D}\right] + ND(\Delta-2)^2 + 2D(\Delta-2)}{(N-1)(\Delta-2)^2}. \tag{4.13}$$

This average minimum hop distance can be approximated as

$$H^{\mathrm{M}}_{\mathrm{min}}(N, \Delta) \approx \log_{\Delta-1} \left\lceil \frac{N(\Delta-2)+2}{\Delta} \right\rceil. \tag{4.14}$$

As $N \to \infty$, we have the asymptotic scaling of the average minimum hop distance

$$H^{\mathrm{M}}_{\mathrm{asym}}(\Delta, N) \to \log_{\Delta-1} N = \frac{\ln N}{\ln(\Delta-1)}. \tag{4.15}$$

Compared with Moore Graphs, the routing spanning tree of a Generalized Moore Graph is not unique, as shown in Figure 4-7 using the example of the Heawood Graph. In general, there are multiple minimum-hop paths between a source-destination pair. As a result, minimum hop routing does not necessarily distribute the load evenly on every edge, even under a uniform traffic. Routing and load distribution of a Generalized Moore Graph will be discussed in detail in Chapter 7 in the context of solving RWA problems.

In contrast to Moore Graphs, there exists a richer class of directed [40] and undirected [40] Generalized Moore Graphs. For example, in [41] directed Generalized Moore Graphs with size up to a 100 are constructed for $\Delta = 3$, $\Delta = 4$, and $\Delta = 5$.

4.3 Other Important Regular Topologies

In this section, we provide descriptions of some other important regular network topologies and a comparative study of their various performance metrics, e.g., average

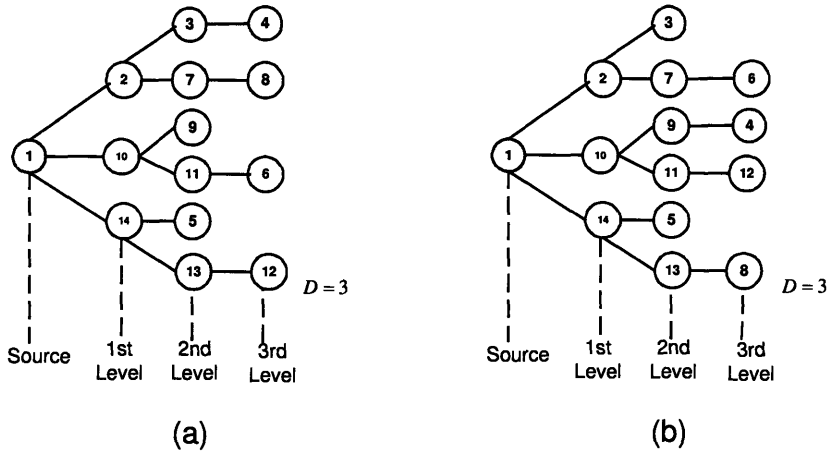

Figure 4-7: Two different routing spanning trees from node 1 for the Heawood Graph.

minimum hop distance, routing complexity, and scalability. These topologies, which will be used as examples in facilitating the analysis in the subsequent chapters, include (one-sided) Δ-nearest Neighbors, Symmetric Hamilton Graph, ShuffleNets, de Bruijn Graph, Kautz Graph, GEMNet, Manhattan Street Network (MSN), and (binary) Hypercube. Among these topologies, (one-sided) Δ-nearest Neighbors and Symmetric Hamilton Graph are constructed and analyzed first time in this thesis work, to the best of our knowledge. As such, these two classes of topologies will be described in detail in the following. The rest of the topologies have been well studied in various literatures, thus we give only a brief summary of the properties that are relevant to this work.

4.3.1 (One-Sided) Δ-Nearest Neighbors Topology

Figure 4-8 depicts a 6-node (one-sided) Δ-nearest Neighbors, in which each node connects to its 3 closest (one-sided) neighbors in a cyclic fashion. For succinctness, we refer (one-sided) Δ-nearest Neighbors simply as Δ-nearest Neighbors in the rest of the thesis. In a general way, for each node i, there are Δ directed connections from node i to node $|i+1|_N$, $|i+2|_N$, ..., $|i+\Delta|_N$, where $|x|_N$ denotes x module over N.

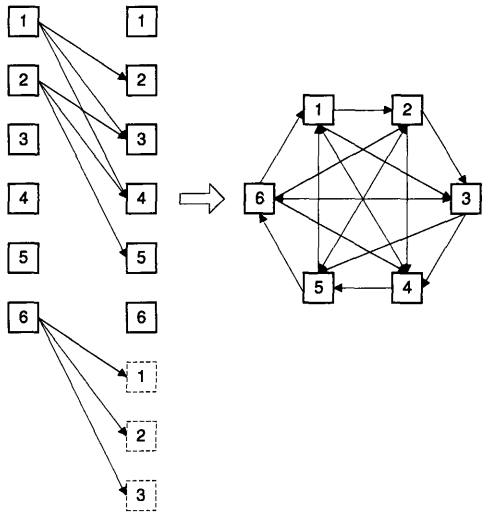

Figure 4-8: (One-sided) Δ-nearest Neighbors topology ($N = 6$, $\Delta = 3$, and $D = 2$).

For a Δ-nearest Neighbor topology, the network diameter D is given by

$$D = \left\lceil \frac{N-1}{\Delta} \right\rceil. \tag{4.16}$$

The average minimum hop distance is given by

$$H_{\min}^{\mathrm{N}} = \left(1 + \frac{\Delta}{2(N-1)}\right) \left\lceil \frac{N-1}{\Delta} \right\rceil - \frac{\Delta}{2(N-1)} \left(\left\lceil \frac{N-1}{\Delta} \right\rceil \right)^2, \tag{4.17}$$

if N can not be evenly divided by Δ; and

$$H_{\min}^{\mathrm{N}} = \frac{1}{2} + \frac{N-1}{2\Delta}, \tag{4.18}$$

if N can be evenly divided by Δ. The derivations of (4.17) and (4.18) are provided in Appendix 4.5.4.

Compared with the Generalized Moore Graphs, a Δ-nearest Neighbors topology provides the upper bound on the average minimum hop distance among all regular topologies with the same node number and node degree, as summarized in the following theorem.

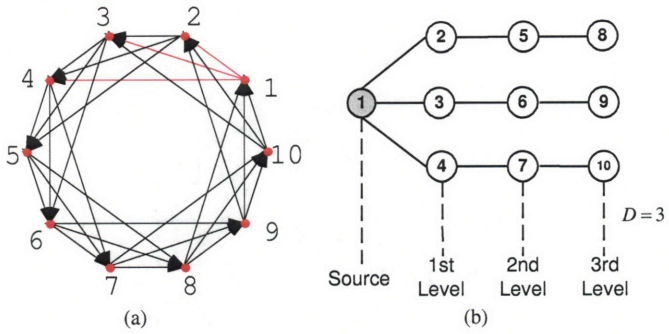

Figure 4-9: (a) (One-sided) Δ-nearest Neighbors topology ($N = 10$, $\Delta = 3$, and $D = 3$); (b) Routing spanning tree from node 1.

Theorem 3 *A Δ-nearest Neighbors Topology provides the upper bound on the average minimum hop distance among all regular topologies with the same node number N and node degree Δ.*

A rigorous substantiation is provided in Appendix 4.5.5. The intuition is illustrated in Figure 4-9, using a Δ-nearest Neighbors topology with $N = 10$, $\Delta = 3$, and $D = 3$ as an example. From the point of view of a routing spanning tree, each of its level is packed with Δ nodes – the minimum number of nodes required to maintain the connectivity (compared with Δ^i nodes at ith level, with $1 \leq i \leq D-1$, for a directed Generalized Moore Graph).

This class of topologies also exhibits some desired properties in terms of modularity:

- Since each node connects to its Δ closest neighbors in a cyclic fashion, a Δ-nearest Neighbors topology allows us to construct a N-node network with any node degree from 1 to $N-1$. This good property provides us flexibility for the analysis in Chapter 5 through Chapter 9.

- For the same network size N, a topology of degree $\Delta+i$ ($i = 1, 2, \ldots, N-1-\Delta$) can be built on top of a topology of degree Δ, without tearing down the existing fiber connections (edges), as shown in Figure 4-10.

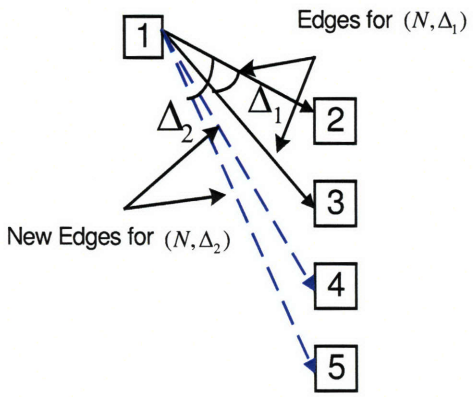

Figure 4-10: For the same network size N, a $\Delta+i$-nearest Neighbors of degree $\Delta+i$ ($i=1,2,\ldots,N-1-\Delta$) can be built on top of a Δ-nearest Neighbors of degree Δ, without tearing down the existing edges.

4.3.2 Symmetric Hamilton Graph

This class of graphs belongs to a subset of Hamilton Graph (a graph containing a cycle that connects all the nodes and passes through each node exactly once). Their specific constructions are introduced first time in this thesis work. In a Symmetric Hamilton Graph of node degree Δ, each node connects to other Δ nodes with an even "spacing" between nodes in a cyclic fashion, as shown in Figure 4-11. That is, denote an integer s as the spacing parameter, there are directed edges from each node i to nodes $|i+1|_N$, $|i+1+s|_N$, $|i+1+2s|_N$, ..., $|i+1+ks|_N$, ..., $|i+N-1|_N$, where k is an integer satisfying $k \leq \Delta-1$ and $|x|_N$ denotes x module over N. The size of a Symmetric Hamilton Graph is determined by both s and Δ, that is, $N=(\Delta-1)s+2$. Figure 4-12 shows some other examples of the Symmetric Hamilton Graphs.

The diameter of a Symmetric Hamilton Graph is given by

$$D = \begin{cases} \frac{s+1}{2}, & \text{if } s \text{ is odd;} \\ \lceil \frac{s+1}{2} \rceil, & \text{if } s \text{ is even.} \end{cases} \tag{4.19}$$

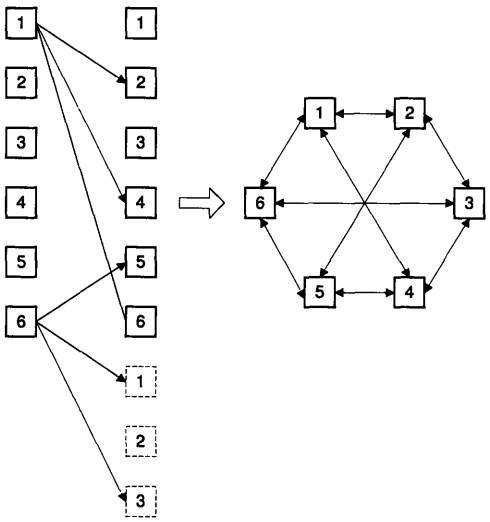

Figure 4-11: A Symmetric Hamilton Graph with $N = 6$, $\Delta = 3$, $s = 2$, and $D = 2$.

The expression for average minimum hop distance as a function of N, Δ, and s can be derived as

$$H_{\min} = \begin{cases} \frac{\Delta}{N-1} + \frac{(N-\Delta-1)(N+5\Delta-7)}{4(N-1)(\Delta-1)}, & \text{if } s \text{ is odd;} \\ \frac{\Delta}{N-1} + \frac{(N-2)^2+4(N-2)(\Delta-1)-4(\Delta-1)}{4(N-1)(\Delta-1)}, & \text{if } s \text{ is even.} \end{cases} \tag{4.20}$$

The derivations of (4.19) and (4.20) are provided in Appendix 4.5.6.

It is worthy to point out that when $\Delta = 2$, a Symmetric Hamilton Graph is simply a (undirected) ring topology. By substituting $\Delta = 2$ into (4.20), we have the following expression:

$$H_{\min} = \begin{cases} \frac{N+1}{4}, & \text{if } N \text{ is odd;} \\ \frac{N+1}{4} + \frac{1}{4(N-1)}, & \text{if } N \text{ is even,} \end{cases} \tag{4.21}$$

which agrees with the expression for the average minimum hop distance of a ring network [33].

For a Symmetric Hamilton Graph, $H_{\min}$ can be approximated by (the approximation is denoted as $H^{\mathrm{a}}_{\min}$):

$$H^{\mathrm{a}}_{\min} = \frac{3}{4} + \frac{N-2}{4(\Delta-1)}, \tag{4.22}$$

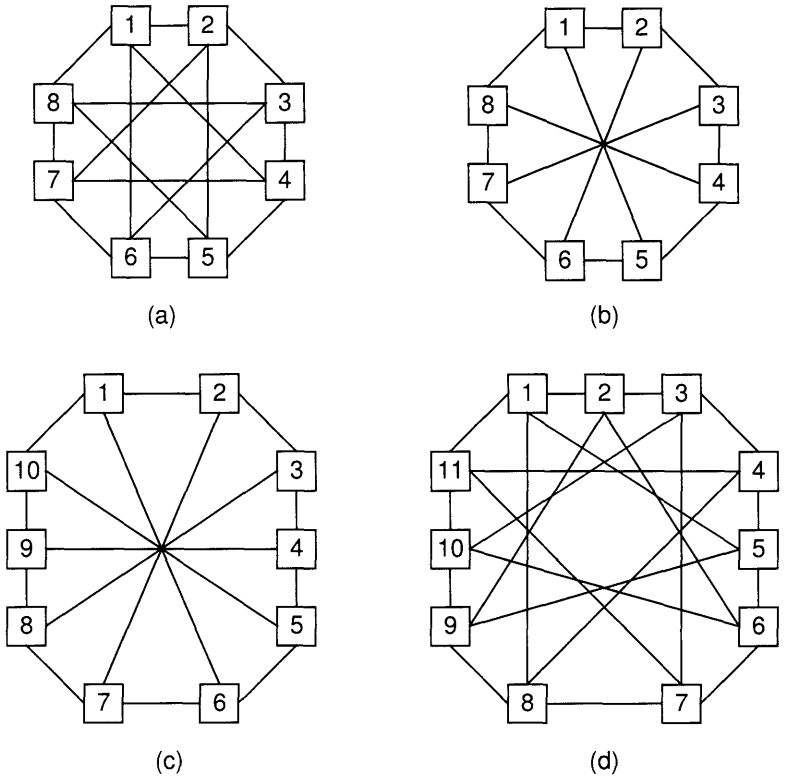

Figure 4-12: Examples of Symmetric Hamilton Graphs: (a) $N = 8$, $\Delta = 4$, $s = 2$, and $D = 2$; (b) $N = 8$, $\Delta = 3$, $s = 3$, and $D = 2$; (c) $N = 10$, $\Delta = 3$, $s = 4$, and $D = 2$; (d) $N = 11$, $\Delta = 4$, $s = 3$, and $D = 2$.

which is convex in Δ. When $\Delta \ll N$, we have the asymptotic average hop distance

$$H_{\text{asym}} = \frac{N}{4(\Delta - 1)}. \tag{4.23}$$

It is interesting to note that the class of Symmetric Hamilton Graph includes some instances of Generalized Moore Graphs. For example, Symmetric Hamilton Graphs shown in 4-12 (a), (b), and (d) are Generalized Moore Graphs.

Unlike a Δ-nearest Neighbors topology, the construction of a N-node Symmetric Hamilton Graph has fewer choices on node degree, owing to the restriction of $N = (\Delta - 1)s + 2$. However, we still have more options on node degree, especially when N is large, compared with other types of topologies (e.g., ShuffleNet, De Bruijn Graphs, and Kautz Graphs). As an illustrative example, a ShuffleNet with $N = 18$ can only have a node degree 3; while a Symmetric Hamilton Graph of the same size can have node degrees of 2, 3, 5, 9, or 17.

4.3.3 ShuffleNet

In a ShuffleNet the nodes are arranged in columns. Given a node degree Δ and a column number k, a ShuffleNet, denoted as SN(Δ, k), consists of k columns of nodes. With each column having Δ^k nodes, the total number of nodes is given by $N = k\Delta^k$ (k = 1, 2, 3 ...). The kth column connects to the first column, as if the topology is wrapped around a cylinder. In general, in a SN(Δ, k), a node (r, c) on row r and column c is connected to nodes ($|\Delta \cdot r|_{\Delta^k}$, $|c+1|_k$), ($|\Delta \cdot r|_{\Delta^k} + 1$, $|c+1|_k$), ..., ($|\Delta \cdot r|_{\Delta^k} + \Delta - 1$, $|c+1|_k$), where $|x|_y$ denotes x module over y. That is, the structure of a ShuffleNet can be viewed as a spanning tree rooted at each node, as shown by the nodes and edges that are highlighted in red in Figure 4-13. The diameter of a ShuffleNet is given by [42]

$$D = 2k - 1. \tag{4.24}$$

The average minimum hop distance is given by [42]

$$H_{\min}(\Delta, k) = \frac{k\Delta^k(\Delta - 1)(3k - 1) - 2k(\Delta^k - 1)}{2(\Delta - 1)(k\Delta^k - 1)}. \tag{4.25}$$

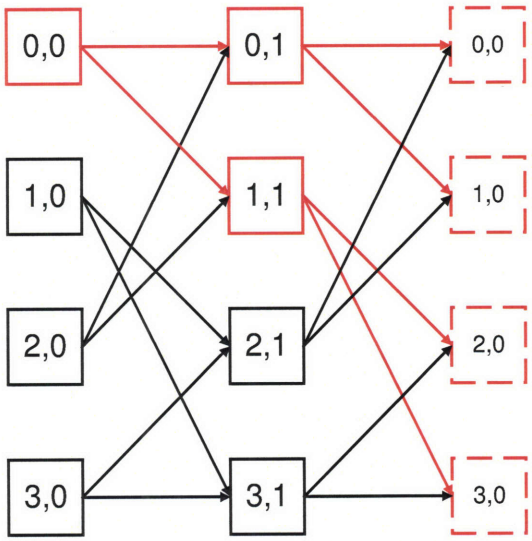

Figure 4-13: The ShuffleNet SN(2,2) with $N = 8$, $\Delta = 2$, $k = 2$, and $D = 2k - 1 = 3$.

Next, we describe a simple addressing and (fixed) routing scheme for the ShuffleNet [42]. We first assign a node (r, c) in a SN(Δ, k) an address $(r_{k-1}r_{k-2}\cdots r_1r_0, c)$. That is, we write every r in terms of base-Δ digits and every c in decimal digits. The routing algorithm involves comparing the address of every node $(\hat{r}, \hat{c})$ on the route (starting with the source node) with the address of the destination node (r^d, c^d). If $(\hat{r}, \hat{c})$=(r^d, c^d), the destination node is reached. If $(\hat{r}, \hat{c}) \neq (r^d, c^d)$, we need to first calculate the distance between $(\hat{r}, \hat{c})$ and (r^d, c^d), which is denoted as X and is given as following:

$$X = \begin{cases} k + c^d - \hat{c}, & \text{if } c^d \neq \hat{c}; \\ k, & \text{if } c^d = \hat{c}. \end{cases} \tag{4.26}$$

The address of the next node on the route follows $(r_{k-2}r_{k-3}\cdots r_1r_0r^d_{X-1}, |c+1|_k)$. That is, out of the Δ nodes in the next column to which node $(\hat{r}, \hat{c})$ may route traffic to, we choose the node whose coordinate r has r^d_{X-1} as the least significant digit. As an example, for a SN(2,2), the minimum hop path from (0,0) to (1,0) follows

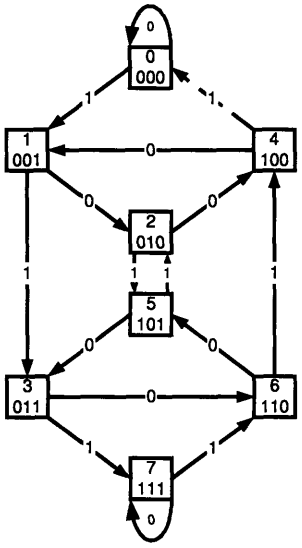

Figure 4-14: The de Bruijn Graph B(2,3) with $N = 8$, $\Delta = 2$, and $D = 3$.

$(0,0) \rightarrow (0,1) \rightarrow (1,0)$, as shown in Figure 4-13.

For minimum hop routing and uniform traffic demand, the total network load cannot be evenly distributed – some of the links are more congested than others.

4.3.4 De Bruijn Graph

Given a node degree Δ ($\Delta \geq 2$) and a diameter D ($D \geq 1$), a de Bruijn Graph, denoted by B(Δ, D), is a regular directed graph having $N = \Delta^D$ nodes [43]. Each node in a de Bruijn Graph is represented by a string of D digits, each of which takes values from $\{0, 1, 2, \cdots, D-1\}$. There is a directed edge from node $(a_1, a_2, \ldots, a_D)$ to node $(b_1, b_2, \ldots, b_D)$, if and only if $b_i = a_{i+1}$ for $1 \leq i \leq D-1$. In other words, there is one-to-one correspondence between all possible states of a Δ-shift register of length D and the connectivity from node i to node j. For example, in the de Bruijn Graph B(2,3), shown in Figure 4-14, there are direct edges from node 001 to node 010 and to node 011, since one (left) shift operation on string 001 yields string 010 and string 011. Note that for a de Bruijn Graph , there are D nodes that have self-loops,

which are presented in the graph (such as node 0 (000) and node 7 (111) in a B(2,3), as shown in Figure 4-14), but will not be presented in the actual network.

Next we illustrate the routing algorithm for a de Bruijn Graph [43]. From the shift register analogy, an edge from node A to node B can be represented by a string of $D+1$ digits, with the first D digits representing node A and the last D digits representing node B. Similarly, any path of k hops can be represented by a string of $D+k$ digits. For better explaining the routing algorithm, we also need to define two operations on strings:

- $shift{-}match(i, \mathsf{A}, \mathsf{B})$ operates on two strings $(a_1, a_2, \ldots, a_D)$ and $(b_1, b_2, \ldots, b_D)$. The operation yields true, if and only if $(b_1, b_2, \ldots, b_{D-i}) = (a_{i+1}, a_{i+2}, \ldots, a_D)$ for $0 \leq i \leq D$; otherwise, the operation yields false.

- $merge(i, \mathsf{A}, \mathsf{B})$ combines two strings $(a_1, a_2, \ldots, a_D)$ and $(b_1, b_2, \ldots, b_D)$ into a new string of length $D+i$, in the form of $(a_1, a_2, \ldots, a_D, b_{D-i+1}, b_{D-i+2}, \ldots, b_D)$.

The minimum hop path routing algorithm from a node $\mathsf{A} = (a_1, a_2, \ldots, a_D)$ to a node $\mathsf{B} = (b_1, b_2, \ldots, b_D)$ can then be described as follows:

$$
\boxed{
\begin{array}{c}
i = 0; \\
\text{while } shift - match(i, \mathsf{A}, \mathsf{B}) \text{ is false} \\
i = i + 1; \\
\text{end while} \\
\text{min-hop-path} = merge(i, \mathsf{A}, \mathsf{B}).
\end{array}
}
$$

Using B(2,3) as an example, the minimum hop path from node 001 to node 101 follows 001 $\rightarrow$ 010 $\rightarrow$ 101. We also note that the minimum hop path between a source-destination pair is unique.

There is no closed form expression for the average minimum hop distance of a de Bruijn Graph. In [43], a lower and an upper bound on the average minimum hop distance are presented as:

$$
\begin{aligned}
(\log_\Delta N)\frac{N}{N-1} - \frac{\Delta}{(\Delta-1)^2} + \frac{\log_\Delta N}{(N-1)(\Delta-1)} &\leq H_{\min}(N, \Delta) \\
&\leq (\log_\Delta N)\frac{N}{N-1} - \frac{1}{(\Delta-1)}, \quad (4.27)
\end{aligned}
$$

for $\Delta \geq 2$ and $D \geq 1$.

We next determine the edge loading of the minimum hop routing. The number of edges in the network is $N\Delta - \Delta$, after excluding the edges from a node to itself. Under the uniform traffic ($t = 1$), the average load on each edge is given by

$$L_{\text{avg}} = \frac{H_{\min}(N, \Delta)N(N-1)}{N\Delta - \Delta} = H_{\min}(N, \Delta)\Delta^{D-1}. \tag{4.28}$$

In a de Brujin Graph, even for uniform traffic, the minimum hop routing algorithm can not distribute the load evenly on each edge, due to the graph's inherent asymmetry (some nodes have self-loops). Other routing algorithms, such as maximum hop routing, can mitigate the discrepancies of loadings on the edges, albeit at an expense of increasing the total load on the network [43].

4.3.5 Kautz Graph

Given a node degree Δ and a diameter D, a Kautz Graph, denoted by Ka(Δ,D), satisfies $N = \Delta^D + \Delta^{D-1}$. Similar to a de Brujin Graph, the nodes of a Kautz Graph are also represented by all possible strings of length D, with each symbol of the string taking the values from the set $\{0, 1, 2, \ldots, \Delta\}$. Compared with a de Brujin Graph, these strings have the restrictions that two consecutive symbols are always different. Thus it is simple to see that there are $N = (\Delta + 1)\Delta^{D-1} = \Delta^D + \Delta^{D-1}$ such strings, since the first symbol of such a string can be chosen in $\Delta + 1$ possible ways and all subsequent ones in Δ possible ways. Two nodes (strings) A and B will have an edge from A to B, if B is a shifted version of A. That is, there is an edge from $\mathsf{A} = (a_1, a_2, \ldots, a_D)$ to a node $\mathsf{B} = (a_2, a_3, \ldots, a_D, b_1)$ with $a_i \neq a_{i+1}$, $1 \leq i \leq D-1$, and $b_1 \neq a_D$. Compared with de Bruijn graphs, none of the nodes in a Kautz Graph has a self-loop, since two consecutive symbols in a string always differ. An example of Kautz Graph is shown in Figure 4-15.

The minimum hop routing algorithm from a source node to a destination node in a Kautz Graph is similar to that in a de Brujin Graph. The algorithm also utilizes the string representation of the nodes and the two string operations – *shift-match*(i, A, B) and *merge*(i, A, B). Using Ka(2,3) as an example, the minimum hop path from node

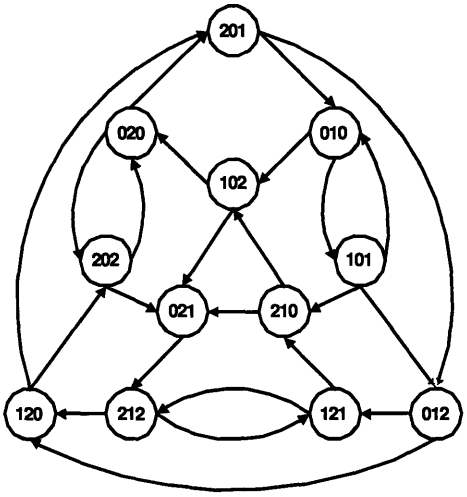

Figure 4-15: The Kautz Graph Ka(2,3)with $N = 12$, $\Delta = 2$, and $D = 3$.

201 to node 212 is 201 $\rightarrow$ 012 $\rightarrow$ 121 $\rightarrow$ 212. The minimum hop path for a source-destination pair is also unique in a Kautz Graph. There is no closed form expression for average minimum hop distance. In [44], a recursive upper bound on the minimum hop distance is given as:

$$H_{\min}(\Delta, D+1) \leq 1 + \frac{N\Delta - \Delta}{N\Delta - 1} H_{\min}(\Delta, D) - \frac{D+1}{2(N\Delta - 1)}. \tag{4.29}$$

In a Kautz Graph, even for uniform traffic, the minimum hop routing algorithm can not distribute the load evenly on each link. Other routing algorithms, such as maximum hop routing, can also be applied to make the load more evenly distributed, albeit at an expense of increasing the total load on the network [44].

4.3.6 GEMNet

Generalized Shuffle Exchange Multihop NETwork (GEMNET)[45] is a generalization of shuffle-exchange network and it can represent a family of network structures (including ShuffleNet and de Bruijn Graph as special cases) for an arbitrary number of nodes. For a network of N nodes, if N is evenly divisible by an integer k,

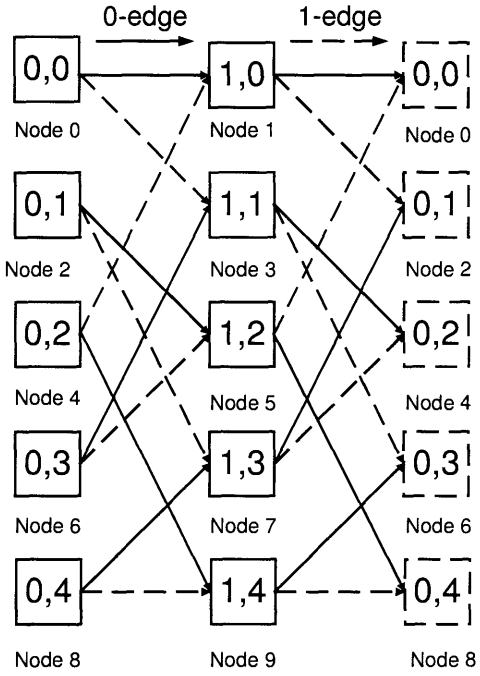

Figure 4-16: The GEMNet with $N = 12$, $\Delta = 2$, and $D = 3$.

there is a GEMNet with k columns. In the corresponding (k, m, Δ) GEMNet, the $N = k \times m$ nodes are arranged in k columns ($k \geq 1$) and m rows ($m \geq 1$) with each node having a degree Δ. Node a ($a = 0, 1, 2, \ldots, N-1$) is located at column c ($c = 0, 1, 2, \ldots, k-1$) and row r ($r = 0, 1, 2, \ldots, m-1$), where and $c = |a|_k$, $r = \lfloor a/k \rfloor$, and $|x|_y$ denotes x module over y. The Δ edges emanating out of a node are referred to as i-edge, $i = 0, 1, 2, \ldots, \Delta - 1$. The i-edge from the node (c, r) is connected to node $(\hat{c}, \hat{r})$ for $i = 0, 1, 2, \ldots, \Delta - 1$, where $\hat{c} = |c+1|_k$ and $\hat{r} = [r \times \Delta]$. Figure 4-16 shows a 10-Node GEMNet with $k = 2$, $m = 5$, and $\Delta = 2$.

The minimum hop routing algorithm is given as follows. Let (c_s, r_s) and (c_d, r_d) be the locations of the source and destination node, respectively. The column distance, δ, from the source node to the destination node is given by

$$\delta = 1 + |[(k-1) + (c_d - c_s)]|_k. \tag{4.30}$$

The hop distance from the source node to the destination node is given by the smallest integer h of the form $\delta + ik$ with $i = 0, 1, \ldots$, satisfying the following expression:

$$R = |[M + r_d - |(r_s \Delta^h)|_M]|_M < \Delta^h. \tag{4.31}$$

R, called as the route code, specifies the shortest route from the source to the destination, when it is expressed as a sequence of h base-Δ digits. For example, for the route from source node (0,0) to destination node (1,4), we have $c_s = 0$, $c_d = 1$, $r_s = 0$, and $r_d = 4$. With (4.30) we have $\delta = 1$. Thus we have

$$R = |[5 + 4 - |(0 \cdot 2^h)|_5]|_5 < 2^h.$$

Solving this inequality yields $h = 3$ and $R = (100)_{\text{base-2}}$. Thus minimum hop path from node (0,0) to node (1,4) is $(0,0) \rightarrow (1,1) \rightarrow (0,2) \rightarrow (1,4)$.

There is no closed form expression for the average minimum hop distance in GEMNet. However, tight upper and lower bounds of the average minimum hop distance are obtained in [45] as

$$H_{\text{upper}}(m, k, \Delta) = \frac{mk(D + \frac{1}{2} - \frac{1}{2}k) - k(\frac{\Delta^{D-k+1}-1}{\Delta-1})}{mk - 1} \tag{4.32}$$

and

$$H_{\text{lower}}(m,k,\Delta) = \sum_{i=0}^{S} i\Delta^i + \sum_{i=S+1}^{S+k} i(M - \Delta^{|i|_k} \sum_{j=0}^{\lfloor i/k \rfloor} \Delta^{kj}). \tag{4.33}$$

In (4.33) S is given by

$$S = \begin{cases} D-k, & \text{if } \Delta^{|D-k|_k} \frac{(\Delta^k)^{F+1}-1}{\Delta-1} \leq M; \\ D-k-1, & \text{otherwise,} \end{cases}$$

and F is given by

$$F = \left\lfloor \frac{D-k}{k} \right\rfloor.$$

4.3.7 Manhattan Street Network (MSN)

Developed by Maxemchuk in 1985, MSN (also called as a Two dimensional Torus) is a directed and two connected network that resembles the geographical topology of the streets and avenues of Manhattan, as shown in Figure 4-17. For a N-node MSN with m rows and k columns, the average minimum hop distance can be computed as

$$H_{\min} = \begin{cases} \frac{N/4(m+k+4)-k-4}{N-1}, & \text{if } m/2 \text{ is even, } k/2 \text{ is odd;} \\ \frac{N/4(m+k+4)-m-4}{N-1}, & \text{if } m/2 \text{ is odd, } k/2 \text{ is even;} \\ \frac{N/4(m+k+4)-k}{N-1}, & \text{if } m/2 \text{ is even, } k/2 \text{ is even;} \\ \frac{N/4(m+k+4)-m-k-4}{N-1}, & \text{if } m/2 \text{ is odd, } k/2 \text{ is odd.} \end{cases} \tag{4.34}$$

For large N and $m = k$, we have $H_{\min} \approx \sqrt{N}$ [29]. [29] shows that if both m and k are divisible by 4, a minimum hop routing can distribute the load evenly on each edge (fiber), under the uniform all-to-all traffic.

4.3.8 Binary Hypercube

A Δ-cube graph [46] is a degree Δ undirected graph consisting of $N = 2^{\Delta}$ nodes that are labeled from 0 to $2^{\Delta-1}$ in base-2 numbers. There is an edge between any two

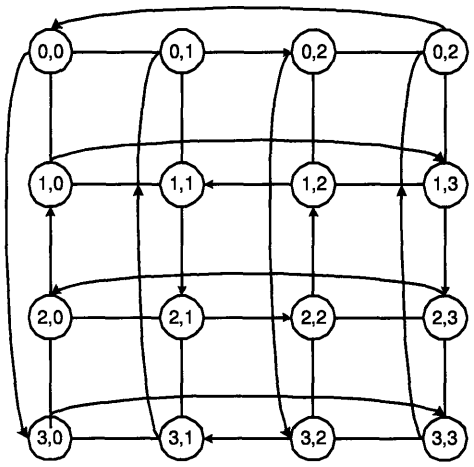

Figure 4-17: A 16-node (4 × 4)Manhattan Street Network.

vertices, if and only if the binary representations of their labels differ by only one bit. As an example, Figure 4-18 shows an 8-node 3-cube ($N = 2^3 = 8$).

The minimum hop routing in a binary hypercube is quite simple. Let $x_1x_2x_3 \ldots x_\Delta$ and $y_1y_2y_3 \ldots y_\Delta$ be the base-2 representations of node x and y, respectively. The minimum hop path between these two nodes $x_1x_2x_3 \ldots x_\Delta$ and $y_1y_2y_3 \ldots y_\Delta$ in a Δ-dimensional binary hypercube corresponds to correcting the first different bit in x and y, then the second, and so on to the last bit different in x and y. For convenience but without losing generality, we assume that A and B differ in their first bits. Then the minimum hop path from x to y is given as the following:

$$\begin{aligned} x &= \text{node A} = x_1x_2x_3 \ldots x_ix_{i+1} \ldots x_\Delta; \\ &= y_1x_2x_3 \ldots x_ix_{i+1} \ldots x_\Delta; \\ &= y_1y_2x_3 \ldots x_ix_{i+1} \ldots x_\Delta; \\ &\ldots \\ y &= \text{node B} = y_1y_2y_3 \ldots y_ix_{i+1} \ldots x_\Delta. \end{aligned} \tag{4.35}$$

For example, in a 3-cube the minimum hop path between node 010 and 101 follows $010 \rightarrow 110 \rightarrow 100 \rightarrow 101$, as shown in Figure 4-18.

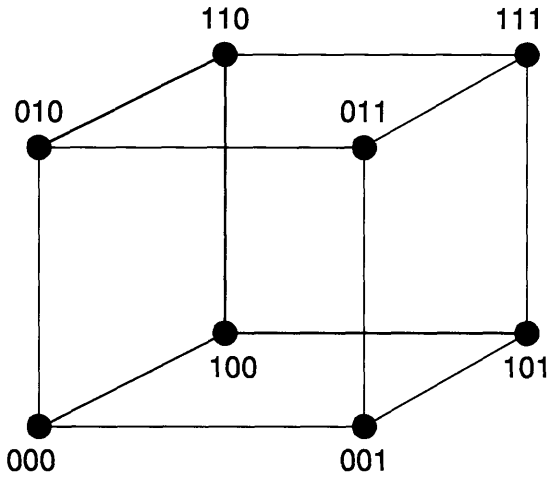

Figure 4-18: A 3-cube with $\Delta = 3$ and $N = 2^3 = 8$. The highlighted nodes and edges illustrate a minimum hop path from node (010) to node (101).

It is easy to see that a Δ-cube is a graph of diameter Δ. The average minimum hop distance between node A and node B is equal to the number of bits that differ between A and B, i.e., the Hamming distance H_{ham} [46]. The average minimum hop distance as a function of N and D is given by

$$\begin{aligned} H_{\min}(N,\Delta) &= \frac{\sum_{i=1}^{\Delta}\binom{\Delta}{i}i}{N-1} \\ &= \frac{\Delta \cdot 2^{\Delta-1}}{2^{\Delta}} \\ &= \frac{\Delta}{2} \\ &= \frac{\log_2 N}{2}. \end{aligned} \tag{4.36}$$

Another important property of the Δ-cube is that it can be constructed recursively from lower dimensional cubes. Consider two identical Δ-cubes whose nodes are numbered likewise from 0 to $2^{\Delta-1}-1$. By joining every node of the first $\Delta-1$-cubes with the node of the same number in the second cube, we obtain a Δ-cube. Figure 4-19 shows how a 4-cube is constructed from two 3-cubes.

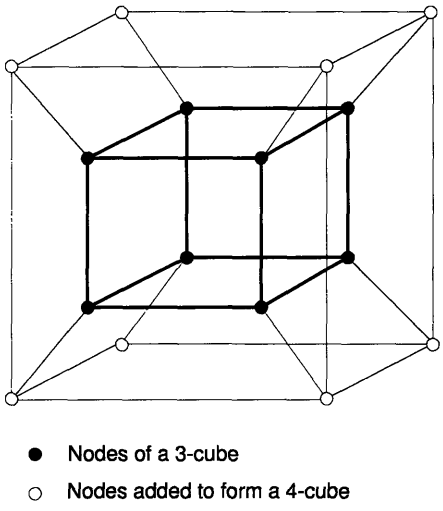

Figure 4-19: A 4-cube constructed from two 3-cubes.

4.3.9 Summary of Regular Topologies

Table 4.1 summarizes the important measures of the regular topologies surveyed in Sections 4.2 and 4.3. These measures include network diameter, average minimum hop distance, routing complexity, modularity, and symmetry. Among these measures, the performance of average minimum hop distance plays a crucial role in evaluating the efficiencies of physical architectures. The average minimum hop distance (as well as the network diameter) is clearly a strong function of node degree Δ. The larger the node degree, the shorter the average minimum hop distance (as well as the network diameter). To illustrate how the average minimum hop distances for different topologies scale, we plot the average minimum hop distance between all node pairs as a function of network size N, all with node degree set at 3, as shown in Figure 4-20. It is evident that there are significant differences between good and pedestrian network topologies for degree 3 networks. These differences can be over an order of magnitude. Generalized Moore Graphs provide lower bound (Moore Bound) on the average minimum hop distance (with a scaling of $\log_{\Delta} N$). Some topologies, such as Δ-nearest Neighbors and Symmetric Hamilton Graphs, scale poorly (with a scaling

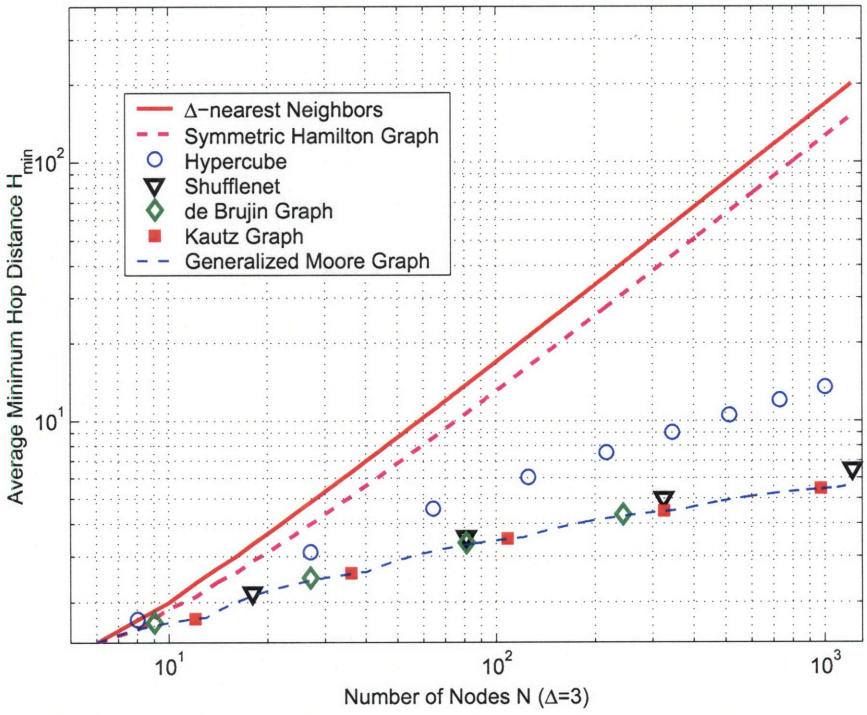

Figure 4-20: Average minimum hop distances $H_{\min}$ for different classes of symmetric regular physical topologies as a function of number of nodes N. The node degree is set at $\Delta = 3$.

of N/Δ) with the number of nodes N in the network. Other more sophisticated topologies, such as the ShuffleNet and deBruijn graphs, which come close to the Moore Bound, scale favorably as $\log_\Delta N$, thus keeping the minimum average hop distance between a node pair short.

From the perspective of designing optical network, we show in Chapter 5 that the amount of switching resources used at nodes is proportional to the average minimum hop distance $H_{\min}$ of a regular topology. Thus a smaller $H_{\min}$ will translate into fewer number of expensive optical switch ports. This is especially crucial for optical switching, since minimizing the network resources is desirable for a good network architecture. In this sense, the order of magnitude difference in average minimum hop distance most likely means a similar difference in cost of the corresponding networks, owing to the usage of optical switching ports at the nodes. In Chapter 5, we also

Table 4.1: Comparisons of the important measures of the regular topologies.

	Number of Nodes N	Diameter D	Avg. Min. Hop Dist. $H_{\min}$	Routing Complexity	Modularity	Symmetry
Moore Graph	$\sum_{i=0}^{D}(\Delta-1)^i$	D	$\log_\Delta N$	Low	Very poor	Perfect symmetry
Shuffle-Net	$k\Delta^k$	$2k-1$	$\log_\Delta N$	Medium	Poor	Perfect symmetry
De Bruijn Graph	Δ^D	D	$\log_\Delta N$	Low	Poor	Good
Kautz Graph	$\Delta^D+\Delta^{D-1}$	D	$\log_\Delta N$	Low	Poor	Perfect symmetry
GEMNet	$k\times m$	$\lceil\log_\Delta m\rceil$ $+k-1$	$\log_\Delta N$	Medium	Good	Perfect symmetry
Hyper-cube	2^Δ	$\log_2 N$	$\frac{\log_2 N}{2}$	Low	Poor	Perfect symmetry
MSN	$m\times k$	$\sqrt{N}$	$\sqrt{N}$	Medium	Good	Good
Δ-Nearest Neighbors	Any N	$\lceil\frac{N-1}{\Delta}\rceil$	$\frac{N}{2\Delta}$	Medium	Excellent	Perfect symmetry
Symmetric Hamilton Graph	$2(\Delta-1)+s$	$(s+1)/2$	$\frac{N}{4(\Delta-1)}$	Medium	Good	Perfect symmetry

demonstrate that topologies with smaller average minimum hop distance have a lower fraction of pass-through traffic and hence require small optical switches. This provides another way to appreciate the fact that a good topology is crucial from the aspect of switching cost at the nodes.

As discussed in Section 4.2.1, the existence of Moore Graphs is rare, due to the stringent requirement for their constructions (e.g., a fully populated routing spanning tree from every node). However, there exists a very rich class of Generalized Moore Graphs. And also, regular graphs such as ShuffleNets, de Brujin Graphs, and Kautz Graphs are known as close relatives to Generalized Moore Graphs in the sense that they have average minimum hop distances that are very close to those of Generalized Moore Graphs. In summary, Generalized Moore Graphs and their close relatives provide sufficient instances that could serve as starting points for the final design of networks. To illustrate this, in Figure 4-20 we plot a map of the existing Generalized Moore Graphs and their close relatives. In this plot, the network size is in the range from 4 to 100 nodes, which are typical sizes for most metropolitan area networks.

4.4 Irregular Topologies

In reality, traffic is seldom symmetric, nor are networks regular or regularizable, thus we also study the design of irregular network. We can characterize an irregular topology by the following parameters:

- The number of nodes N;
- The maximum node degree $\Delta_{\max}$;
- The minimum node degree $\Delta_{\min}$;
- The average node degree $\bar{\Delta}$, $\bar{\Delta} = \frac{1}{N}\sum_{i=1}^{N}\Delta_i$, where Δ_i is the degree of node i.

For the convenience of discussion, we denote an irregular topology as $(N, \Delta_{\max}, \Delta_{\min}, \bar{\Delta})$.

In studying the irregular topologies, it is hard to derive analytical expressions and solutions. However, we can apply the results of symmetric regular networks to

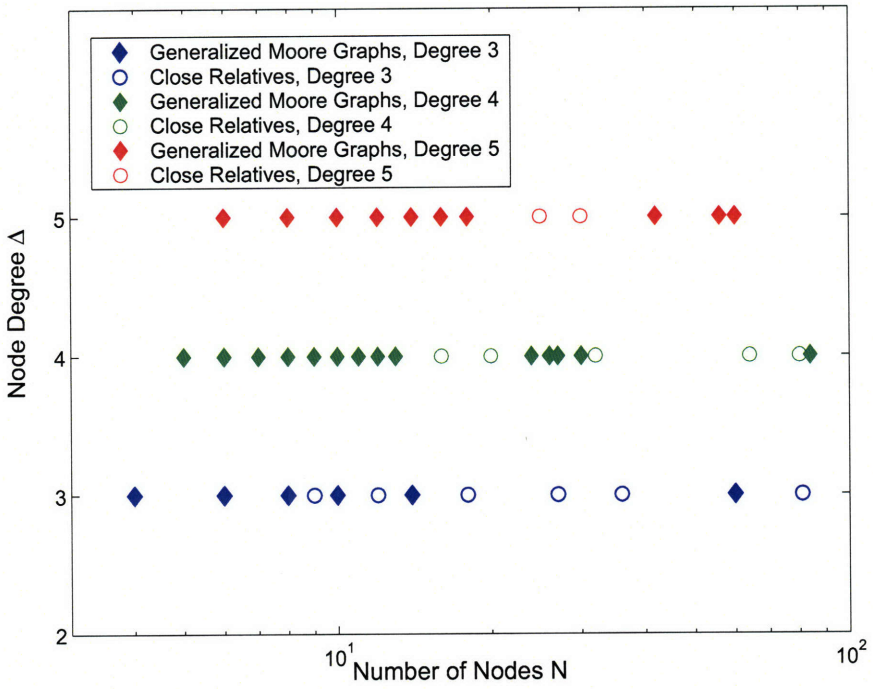

Figure 4-21: The density of Generalzied Moore Graphs and their close relatives for $N \leq 100$, Δ =3, 4, and 5.

provide estimates for irregular networks. Under this guideline, we concentrate on the following two approaches to study the irregular topologies. The first approach is to use the results of average minimum hop distances for Generalized Moore Graphs and Δ-nearest Neighbors to gauge the average minimum hop distance of an irregular topology $(N, \Delta_{\max}, \Delta_{\min}, \bar{\Delta})$. The Theorems 4 and 5 summarize our findings. The proofs are provided in Chapter Appendix 4.5.7 and 4.5.8, respectively.

Theorem 4 *The average minimum hop distance of an irregular topology* $(N, \Delta_{\max}, \Delta_{\min}, \bar{\Delta})$ *is lower bounded by the average minimum hop distance of a Generalized Moore Graph of* N *nodes and node degree* $\Delta_{\max}$. *That is,*

$$H_{\min}(N, \Delta_{\max}, \Delta_{\min}, \bar{\Delta}) \geq H^{\mathrm{M}}_{\min}(N, \Delta_{\max}). \tag{4.37}$$

Theorem 5 *The average minimum hop distance of an irregular topology* $(N, \Delta_{\max}, \Delta_{\min}, \bar{\Delta})$ *is upper bounded by the average minimum hop distance of a* Δ*-nearest Neighbors Topology of* N *nodes and node degree* $\Delta_{\min}$. *That is*

$$H_{\min}(N, \Delta_{\max}, \Delta_{\min}, \bar{\Delta}) \leq H^{\mathrm{N}}_{\min}(N, \Delta_{\min}). \tag{4.38}$$

The second approach is to "embed" an irregular topology into a regular one. That is, by adding nodes and edges, we can construct a $\Delta_{\max}$-regular topology from an irregular one$(N, \Delta_{\max}, \Delta_{\min}, \bar{\Delta})$. Reference [47] gives the upper bound on the additional nodes required to regularize an irregular topology. This property is summarized in the following theorem.

Theorem 6 *Let* $G = (V, E)$ *be a graph with maximum degree* $\Delta_{\max}$. *If* $\Delta_{\max}$ *is odd, the* G *is a subgraph of a* $\Delta_{\max}$ *regular graph* $G' = (V', E')$ *with*

$$|V' - V| \leq \Delta_{\max} + 2; \tag{4.39}$$

if $\Delta_{\max}$ *is even, the* G *is a subgraph of a* $\Delta_{\max}$ *regular graph* $G' = (V', E')$ *with*

$$|V' - V| \leq \Delta_{\max} + 1. \tag{4.40}$$

4.5 Chapter Appendix

In this section, we provide the proofs of the theorems and other results presented in this chapter.

4.5.1 Proof for Theorem 1

Proof: We first show that the minimum hop routing spanning tree is unique. For an arbitrary Moore Graph of degree Δ and diameter D, we note that, by definition, each of the nodes appears only once in each routing spanning tree. Every source node has Δ edges to Δ 1st level nodes; every 1st level node then has $\Delta - 1$ edges to $\Delta - 1$ 2nd level nodes. None of the 2nd level nodes can be reached from the source node in one hop. Generally, every node at the ith level ($1 \leq i \leq N-1$) can reach $\Delta - 1$ nodes at the $(i+1)$th level. None of the nodes at the $(i+1)$th level can be reached from the source node in less than $i+1$ hops. More importantly, there are no edge connecting two nodes that are of both i hops away from the source node, for $1 \leq i \leq D-1$ [39]. With such a construction, if a source node could reach every other nodes in more than one minimum hop routing spanning tree (non-uniqueness), there would exist at least one node whose node degree is larger than D. This violates the regularity required by a Moore Graph. Thus the construction and regularity of a Moore Graph ensure the uniqueness of the minimum hop routing spanning tree of each node.

Next, we show that every source destination pair has a unique minimum hop path. For an arbitrary Moore Graph of degree Δ and diameter D, suppose that there exist two minimum hop paths from a source node $\mathsf{S_0}$ to a destination node $\mathsf{D_0}$, as illustrated in Figure 4-22. Without loss of generality, let $\mathsf{D_0}$ be at the bottom level of the minimum hop routing spanning tree. One minimum hop path from $\mathsf{S_0}$ to $\mathsf{D_0}$ traverses along the path of $\mathsf{S_0} \rightarrow \mathsf{S_1} \ldots \rightarrow A \rightarrow \mathsf{D_0}$, another traverses along the path of $\mathsf{S_0} \rightarrow \mathsf{S_2} \ldots \rightarrow B \rightarrow \mathsf{D_0}$. Due to the uniqueness of the minimum hop routing spanning tree of Moore Graphs, node B has $\Delta - 1$ directed edges to the $\Delta - 1$ nodes at the bottom level and one directed edge to a node one level up. All these nodes are distinct from node $\mathsf{D_0}$. As a result, there are at least $\Delta + 1$ outgoing edges from

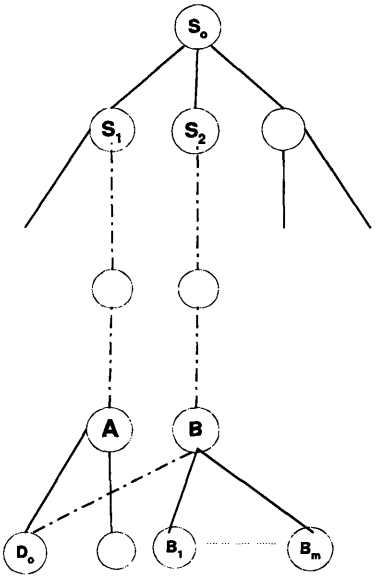

Figure 4-22: The uniqueness of the minimum hop path of a Moore Graph.

node B. This violates the regularity required by Moore Graphs. Thus the minimum hop path between the node pairs must be unique.

4.5.2 Proof for Theorem 2

Proof: To prove this result, we count how many times a given edge is traversed as the ith ($i = 1, \ldots D$) hop and then sum over all possible i from 1 to D. The times that a given edge is used by lightpaths equal to the load on this edge.

From the enumerations of the routing spanning trees of an arbitrary full Moore Graph, we note that every edge in the graph is enumerated exactly once as the 1st hop. Let l_1 denote the load on a given edge generated by lightpaths using this edge as their 1st hops,

$$l_1 = \sum_{i=0}^{D-1} (\Delta - 1)^i. \tag{4.41}$$

Similarly, at the ith level of all the routing spanning trees with $i < D$, each edge is

enumerated exactly $(\Delta-1)^{i-1}$ times. Let l_i denote the load on a given edge generated by lightpaths using this edge as their ith hops,

$$l_i = \sum_{j=i-1}^{D-1} (\Delta-1)^j. \tag{4.42}$$

Finally, at the Dth level of all routing spanning trees, each edge is enumerated exactly $(\Delta-1)^{D-1}$ times. We have

$$l_D = (\Delta-1)^{D-1}. \tag{4.43}$$

By summing up the load l_i over $i = 1$ to D, we have the total load on a given edge,

$$\begin{aligned} \sum_{i=1}^{D} l_i &= 1 + 2(\Delta-1) + 3(\Delta-1)^2 + \ldots + D(\Delta-1)^{D-1} \\ &= \sum_{i=1}^{D} i(\Delta-1)^{i-1}. \end{aligned} \tag{4.44}$$

The actual load on a given edge equals to the average load for a Moore Graph. Thus we conclude that a balanced load distribution can be achieved.

4.5.3 Derivation of Asymptotic Average Minimum Hop Distance for Generalized Moore Graphs

We first make an assumption that each node has a full routing spanning tree, so the number of nodes N satisfies

$$\begin{aligned} N &= \sum_{i=0}^{D} \Delta^i \\ &= \frac{1-\Delta^{D+1}}{1-\Delta}. \end{aligned} \tag{4.45}$$

We next assume that $\Delta \approx \Delta - 1$ and $N \gg \Delta$. Then, the network diameter D can be further approximated as

$$D(\Delta, N) = \lceil \log_\Delta (1 + N(\Delta-1)) \rceil - 1 \approx \log_\Delta N. \tag{4.46}$$

We proceed to obtain the asymptotic average minimum hop distance of a Generalized Moore Graph as a function of N and Δ, as stated in (4.11),

$$\begin{aligned} H^{\mathrm{M}}_{\min}(N,\Delta) &= \frac{\sum_{i=1}^{D} in(i)}{N-1} \\ &= \frac{\sum_{i=1} i\Delta^i}{\sum_{i=0}^{D}\Delta^i - 1} \\ &= \frac{\frac{(D+1)(\Delta-1)\Delta^{D+1}-\Delta(\Delta^{D+1}-1)}{(\Delta-1)^2}}{\frac{\Delta^{D+1}-1}{\Delta-1}-1} \\ &\approx D+1-\frac{\Delta}{\Delta-1} \\ &\approx D \\ &\approx \log_{\Delta} N. \end{aligned} \tag{4.47}$$

Note that the function $\log_{\Delta} N$ is strictly convex in Δ.

4.5.4 Derivation of Average Minimum Hop Distance for Δ-Nearest Neighbors Topology

In a Δ-nearest Neighbors topology of size N, for every node i, there are directed connections (from node i) to node $|i+1|_N$, $|i+2|_N$, ..., $|i+D|_N$, where $|x|_N$ denotes x module over N. For a Δ-nearest Neighbors topology, the network diameter D is given by

$$D = \left\lceil \frac{N-1}{\Delta} \right\rceil. \tag{4.48}$$

For an arbitrary node j, let $n_j(i)$ denote the number of nodes that can be reached (from node j) in i hops. With the symmetry of Δ-nearest Neighbors topology, $n_j(i) = n_k(i) = n(i)$ for any node j and k. To obtain the path length distribution $n(i)$ for a Δ-nearest Neighbors topology, we need to consider two cases:

- Case 1: $N-1$ cannot be divided evenly by Δ. For $1 \le i \le D-1$, $n(i)$ is given by

$$n(i) = \begin{cases} \Delta, & \text{if } 1 \le i \le D-1; \\ N-1-\lfloor \frac{N-1}{\Delta} \rfloor, & \text{if } i = D. \end{cases} \tag{4.49}$$

With the path length distribution $n(i)$, we can evaluate the average minimum hop distance of a Δ-nearest Neighbors topology of size N, as stated in (4.17),

$$\begin{aligned} H^{\mathrm{N}}_{\min}(N,\Delta) &= \frac{1}{N-1}\sum_{i=1}^{D} i n(i) \\ &= \left(1+\frac{\Delta}{2(N-1)}\right)\left\lceil\frac{N-1}{\Delta}\right\rceil - \frac{\Delta}{2(N-1)}\left(\left\lceil\frac{N-1}{\Delta}\right\rceil\right)^2 \end{aligned} \quad (4.50)$$

- Case 2: $N-1$ can be divided evenly by Δ. For $1 \le i \le D$, $n(i)$ is given by

$$n(i) = \Delta. \quad (4.51)$$

The expression for the average minimum hop distance takes the form, as state in (4.18),

$$H^{\mathrm{N}}_{\min}(N,\Delta) = \frac{1}{2} + \frac{N-1}{2\Delta}. \quad (4.52)$$

4.5.5 Proof of Theorem 3

In this section, we provide the substantiation that a Δ-nearest Neighbors topology provides the upper bound on the average minimum hop distance among all regular topologies with the same network size N and node degree Δ, as summarized in Theorem 3.

To prove this, we first show that Δ-nearest Neighbors topology has the maximum diameter among all regular topologies with the same network size N and node degree Δ. As in the derivation in Section 4.5.4, the diameter of a Δ-nearest Neighbor topology is given as $\lceil (N-1)/\Delta \rceil$, which is exactly the maximum diameter for a Δ-connected graph, according to a theorem in [37]. Note that the definition of regular topologies in this thesis includes Δ-connectivity.

Next, we look at the $n(i)$ for a Δ-nearest Neighbors topology. As shown in the derivation in Section 4.5.4, we have $n(i) = \Delta$ (for $1 \le i \le D-1$), which meets the minimum requirement to maintain the Δ-connectivity. (Note that Δ-connectivity requires that $n(i) \ge \Delta$, $1 \le i \le D-1$, as defined in [37]).

By combining these two results and use the the definition of average minimum hop distance, we can easily see that a Δ-nearest Neighbors topology has the maximum

average minimum hop distance among all regular topologies with the same network size N and node degree Δ.

4.5.6 Derivation of Average Minimum Hop Distance for Symmetric Hamilton Graph

In a Symmetric Hamilton Graph with degree Δ, each node connects to Δ other nodes with even "spacing" between nodes in a symmetric and cyclic fashion. Denote an integer s as the spacing parameter, there are directed connections from each node i to nodes $|i+1|_N$, $|i+1+s|_N$, $|i+1+2s|_N$, ..., $|i+1+ks|_N$, ..., $|i+N-1|_N$, where k is an integer satisfying $k \leq D-1$. The size of a Symmetric Hamilton Graph is determined by s and Δ. That is, $N = (\Delta-1)s+2$. To obtain the path length distribution $n(i)$, we need to consider the following two cases:

- Case 1: the spacing parameter s is odd. For an odd s, the network diameter D is given by

$$D = \frac{s+1}{2}. \tag{4.53}$$

  From node i, there are:

  - Δ nodes that can be reached in 1 hop, i.e., $n(1) = D$;
  - $2(\Delta-1)$ nodes that can be reached in i hops, i.e., $n(i) = 2(\Delta-1)$, for $2 \leq i \leq D$.

  By using the path length distribution $n(i)$, the average minimum hop distance, as a function of N, Δ, and s, can be expressed as

$$\begin{aligned} H_{\min}(N,\Delta,s) &= \frac{1}{N-1}\sum_{i=1}^{D} in(i) \\ &= \frac{1}{N-1}\left[\Delta + 2(\Delta-1)\sum_{i=2}^{D} i\right] \\ &= \frac{1}{N-1}\left[\Delta + 2(\Delta-1)(\frac{D^2+D-2}{2})\right]. \end{aligned} \tag{4.54}$$

With $s = \frac{N-2}{\Delta-1}$, $H_{\min}$ can also be expressed as a function of N and Δ only, as stated in

$$H_{\min}(N, \Delta) = \frac{\Delta}{N-1} + \frac{(N-\Delta-1)(N+5\Delta-7)}{4(N-1)(\Delta-1)}. \tag{4.55}$$

Taking the second derivative of $H_{\min}(N, \Delta)$ in regard to Δ, we have

$$\frac{\partial^2 H_{\min}(N, \Delta)}{\partial \Delta^2} = \frac{(N-2)^2}{2(N-1)(\Delta-1)^3}. \tag{4.56}$$

For any $N \geq 3$ and $D \geq 2$, we have

$$\frac{\partial^2 H_{\min}(N, \Delta)}{\partial \Delta^2} > 0. \tag{4.57}$$

$H_{\min}(N, \Delta)$ is strictly convex in Δ.

- Case 2: the spacing parameter s is even. For an even s, the network diameter D is given by

$$D = \left\lceil \frac{s+1}{2} \right\rceil. \tag{4.58}$$

From node i, there are:

  - Δ nodes that can be reached in 1 hop, i.e., $n(1) = D$;
  - $2(D-1)$ nodes that can be reached in i hops, i.e., $n(i) = 2(D-1)$, for $2 \leq i \leq D-1$;
  - $\Delta - 1$ nodes that can be reached in D hops, i.e., $n(D) = \Delta - 1$.

By using the path length distribution $n(i)$, the average minimum hop distance, as a function of N, Δ, and s, can be expressed as

$$\begin{aligned} H_{\min}(N, \Delta, s) &= \frac{1}{N-1} \sum_{i=1}^{D} i n(i) \\ &= \frac{1}{N-1} [\Delta + 2(\Delta-1) \sum_{i=2}^{D-1} i + (\Delta-1)D] \\ &= \frac{1}{N-1} [\Delta + (\Delta-1)(D^2-2)]. \end{aligned} \tag{4.59}$$

With $s = \frac{N-2}{\Delta-1}$, $H_{\min}$ can also be expressed as a function of N and Δ only, as stated in

$$H_{\min}(N,\Delta) = \frac{\Delta}{N-1} + \frac{(N-2)^2 + 4(N-2)(\Delta-1) - 4(\Delta-1)}{4(N-1)(\Delta-1)}. \quad (4.60)$$

Taking the second derivative of $H_{\min}(N,\Delta)$ in regard to Δ, we have

$$\frac{\partial^2 H_{\min}(N,\Delta)}{\partial \Delta^2} = \frac{(N-2)^2}{2(N-1)(\Delta-1)^3}. \quad (4.61)$$

For any $N \geq 3$ and $D \geq 2$, we have

$$\frac{\partial^2 H_{\min}(N,\Delta)}{\partial \Delta^2} > 0. \quad (4.62)$$

$H_{\min}(N,\Delta)$ is strictly convex in Δ.

For Symmetric Hamilton graph, when $N \approx N-1$, $H_{\min}$ can be approximated by $H^{\mathrm{a}}_{\min}$, which is also convex in Δ,

$$H^{\mathrm{a}}_{\min} = \frac{3}{4} + \frac{N-2}{4(\Delta-1)}. \quad (4.63)$$

When $\Delta \ll N$, we have the asymptotic minimum hop distance as

$$H_{\mathrm{asym}} = \frac{N}{4(\Delta-1)}. \quad (4.64)$$

4.5.7 Proof for Theorem 4

We compare the average minimum hop distances of a Generalized Moore Graph (with N nodes and degree $\Delta_{\max}$) and that of an irregular topology specified by $(N, \Delta_{\max}, \Delta_{\min}, \bar{\Delta})$. Let D_{M} and D_{G} denote the network diameters for a Generalized Moore Graph and an irregular topology, respectively. For a Generalized Moore Graph, let $n_{\mathrm{M}}(i)$ denote the number of nodes that are i hops away from every node; for an irregular topology, let $n^j_{\mathrm{G}}(i)$ denote the number of nodes that are i hops away from node j. This proof hinges on the following properties of a Generalized Moore Graph:

$$D_{\mathrm{M}} \leq D_{\mathrm{G}} \quad (4.65)$$

and

$$n_{\mathrm{M}}(i) \geq n_{\mathrm{G}}^{j}(i),\ 1 \leq i \leq D_{\mathrm{M}} - 1,\ \forall j \in N. \tag{4.66}$$

In the following derivation, we drop the superscript in the notation of $n_G^j(i)$ for the clarity of presentation. First, with a simple manipulation, we have

$$\begin{aligned} n_{\mathrm{M}}(1) &= n_{\mathrm{G}}(1) + [n_{\mathrm{M}}(1) - n_{\mathrm{G}}(1)] \\ &\leq n_{\mathrm{G}}(1) + 2[n_{\mathrm{M}}(1) - n_{\mathrm{G}}(1)] \\ &= n_{\mathrm{G}}(1) + 2\Delta n(1), \end{aligned} \tag{4.67}$$

where $\Delta n(1) = n_{\mathrm{M}}(1) - n_{\mathrm{G}}(1)$.

Next, we have

$$\begin{aligned} 2n_{\mathrm{M}}(2) &\leq 2n_{\mathrm{G}}(2) + 3[n_{\mathrm{M}}(2) - n_{\mathrm{G}}(2)] \\ &\leq 2n_{\mathrm{G}}(2) + 3\Delta n(2) + \Delta n(1) \\ &= 2[n_{\mathrm{G}}(2) - \Delta n(1)] + 3[\Delta n(2) + \Delta n(1)], \end{aligned} \tag{4.68}$$

where $\Delta n(2) = n_{\mathrm{M}}(2) - n_{\mathrm{G}}(2)$.

Similarly, for $2 \leq i \leq D_{\mathrm{M}} - 1$, we have

$$in_{\mathrm{M}}(i) \leq i[n_{\mathrm{G}}(i) - \sum_{j=1}^{i-1} \Delta n(j)] + (i+1)[\sum_{j=1}^{i} \Delta n(j)], \tag{4.69}$$

where $\Delta n(i) = n_{\mathrm{M}}(i) - n_{\mathrm{G}}(i)$. We also need this trivially held relation,

$$D_{\mathrm{M}} n_{\mathrm{M}}(D_{\mathrm{M}}) \leq D_{\mathrm{M}} n_{\mathrm{M}}(D_{\mathrm{M}}). \tag{4.70}$$

By adding both sides of equations (4.67) to (4.70), we have

$$\begin{aligned} \sum_{i=1}^{D_{\mathrm{M}}} in_{\mathrm{M}}(i) &\leq \sum_{i=1}^{D_{\mathrm{M}}-1} in_{\mathrm{G}}(i) + D_{\mathrm{M}}[\sum_{i=D_{\mathrm{M}}}^{D_{\mathrm{G}}} n_{\mathrm{G}}(j)] \\ &\leq \sum_{i=1}^{D_{\mathrm{G}}} in_{\mathrm{G}}(i). \end{aligned} \tag{4.71}$$

Dividing (4.71) by $N-1$, we have, as stated in Theorem 4,

$$\begin{aligned} H^{\mathrm{M}}_{\min}(N, \Delta_{\max}) &= \sum_{i=1}^{D_{\mathrm{M}}} \frac{i n_{\mathrm{M}}(i)}{N-1} \\ &\leq \frac{1}{N-1} \sum_{i=1}^{D_{\mathrm{G}}} i n_{\mathrm{G}}(i) \\ &\leq \frac{1}{N(N-1)} \sum_{j=1}^{N} \sum_{i=1}^{D_{\mathrm{G}}} i n^{j}_{\mathrm{G}}(i) \\ &= H_{\min}(N, \Delta_{\max}, \Delta_{\min}, \bar{\Delta}). \end{aligned} \tag{4.72}$$

4.5.8 Proof for Theorem 5

We compare the average minimum hop distances of a Δ-nearest Neighbors topology (with N nodes and degree $\Delta_{\min}$) and that of an irregular topology specified by $(N, \Delta_{\max}, \Delta_{\min}, \bar{\Delta})$. Let D_{N} and D_{G} denote the network diameters for a Δ-nearest Neighbors topology and for an irregular topology, respectively. For a Δ-nearest Neighbors topology, let $n_{\mathrm{N}}(i)$ denote the number of nodes that are i hops away from every node; for an irregular topology, let $n^{j}_{\mathrm{G}}(i)$ denote the number of nodes that are i hops away from node j. This proof hinges on the following properties of a Δ-nearest Neighbors topology:

$$D_{\mathrm{G}} \leq D_{\mathrm{N}} \tag{4.73}$$

and

$$n^{j}_{\mathrm{G}}(i) \geq n_{\mathrm{N}}(i), 1 \leq i \leq D_{\mathrm{N}} - 1, \forall j \in N. \tag{4.74}$$

In the following derivation, we drop the superscript in the notation of $n^{j}_{\mathrm{G}}(i)$ for the clarity of presentation. First, with a simple manipulation, we have

$$\begin{aligned} n_{\mathrm{G}}(1) &= n_{\mathrm{N}}(1) + [n_{\mathrm{G}}(1) - n_{\mathrm{N}}(1)] \\ &\leq n_{\mathrm{N}}(1) + 2[n_{\mathrm{G}}(1) - n_{\mathrm{N}}(1)] \\ &= n_{\mathrm{N}}(1) + 2\Delta n'(1), \end{aligned} \tag{4.75}$$

where $\Delta n'(1) = n_{\mathrm{G}}(1) - n_{\mathrm{N}}(1)$.

Similarly, for $2 \leq i \leq D_{\mathrm{G}} - 1$, we have

$$in_{\mathrm{G}}(i) \leq i[n_{\mathrm{N}}(i) - \sum_{j}^{i-1} \Delta n'(j)] + (i+1)[\sum_{j}^{i} \Delta n'(j)], \tag{4.76}$$

where $\Delta n'(i) = n_{\mathrm{G}}(i) - n_{\mathrm{N}}(i)$. We also need this trivially held relation,

$$D_{\mathrm{G}} n_{\mathrm{G}}(D_{\mathrm{G}}) \leq D_{\mathrm{G}} n_{\mathrm{G}}(D_{\mathrm{G}}). \tag{4.77}$$

By adding both sides of equations (4.75) to (4.77), we have

$$\begin{aligned} \sum_{i=1}^{D_{\mathrm{G}}} in_{\mathrm{G}}(i) &\leq \sum_{i=1}^{D_{\mathrm{G}}-1} in_{\mathrm{N}}(i) + D_{\mathrm{G}}[\sum_{i=D_{\mathrm{G}}}^{D_{\mathrm{N}}} n_{\mathrm{N}}(j)] \\ &\leq \sum_{i=1}^{D_{\mathrm{N}}} in_{\mathrm{N}}(i). \end{aligned} \tag{4.78}$$

Dividing (4.78) by $N-1$, we have, as stated in Theorem 5,

$$\begin{aligned} \frac{1}{N-1} \sum_{i=1}^{D_{\mathrm{G}}} in_{\mathrm{G}}(i) &\leq \frac{1}{N(N-1)} \sum_{j=1}^{N} \sum_{i=1}^{D_{\mathrm{G}}} in_{\mathrm{G}}^{j}(i) \\ &= H_{\min}(N, \Delta_{\max}, \Delta_{\min}, \bar{\Delta}) \\ &\leq \sum_{i=1}^{D_{\mathrm{N}}} \frac{in_N(i)}{N-1} \\ &= H_{\min}^{N}(N, \Delta_{\min}). \end{aligned} \tag{4.79}$$

Chapter 5

Parametric, First-Order, and Homogeneous Network Cost Model

In this section, we set up network cost model in preparation for the analysis of optimal network architectures in the following chapters. In the process of establishing the model, we seek a balance between the analytical tractability and a good representation of today's network. As such, the cost model is parametric, first-order, and homogeneous.

We establish a *parametric* model, since cost estimates for some key network components, such as for OXC ports, could vary by $50\% - 200\%$ according to different market researches. With a parametric model the dependencies of network architecture on the key design parameters can be easily analyzed when these parameters vary over a realistic range of values. Our cost model is also *first-order* in the sense that the parameters and metrics are estimated and represented by their first moments (e.g., the arithmetic mean) rather than by their distributions over time or space. In this thesis, we mostly restrict our attention to regular fiber topology with nodal symmetry and uniform all-to-all traffic. We thus dimension the network *homogeneously*. This means that each fiber connection has the same cost and the switches installed at nodes are of the same type and size (port count).

In our model, the network cost consists of three parts: the transmitter/receiver cost, the fiber connection cost, and the switching (optical cross-connect or OEO

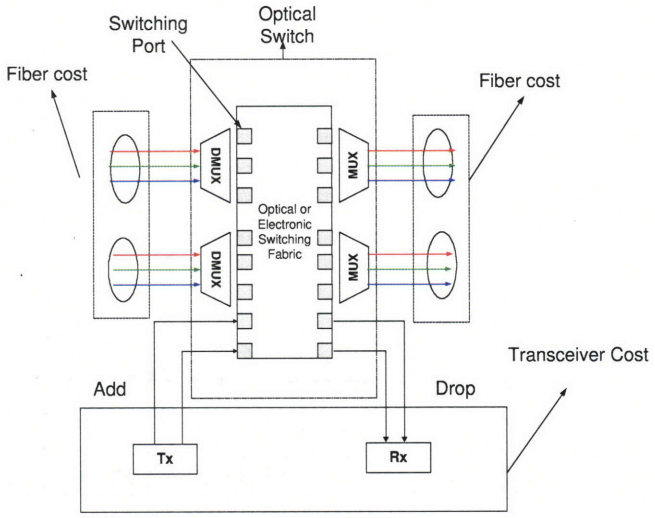

Figure 5-1: Three constituent parts of network cost – transmitter/receiver cost, fiber connection cost, and switching cost.

switch) cost, as shown from a perspective near a node in Figure 5-1. They are described in detail in the following.

5.1 Transmitter/Receiver Cost

To support a uniform traffic demand of a unit traffic ($t = 1$) , each node needs $N - 1$ transmitters/receivers to send/receive traffic to/from every other $N - 1$ nodes in the network. For a network of size N, we need $N(N - 1)$ transmitters/receivers. Once N is given, the cost associated with transmitters/receivers does not change with the node degree Δ. Thus the transmitter/receiver cost can be considered as a constant offset and will not be included in the following cost analysis.

5.2 Fiber Connection Cost

As mentioned in Chapter 4, by using fiber patch panels we can set up a fiber connection between two nodes that are not directly linked by a cable, as shown in Figure 5-2.

In a metro environment, a fiber connection spans much shorter distance than that in a wide-area network, thus amplifiers, which dominate the long haul fiber connection costs, are not required in general. As such, we can assume that all fiber connections have approximately the same cost. In other words, when modeling the fiber connection cost, the dependency of cost on distance can be suppressed. Let C_{f} denote the cost associated with fiber connections in the network, we have C_{f} as a linear function of N and Δ,

$$C_{\mathrm{f}} = \alpha N \Delta, \tag{5.1}$$

where the proportional coefficient α is denoted as the marginal cost of a new fiber connection. Note that depending on whether the cable plants pre-exist or not, we assign the marginal cost of a fiber connection differently. For green-field scenarios, network operators need to install the complete network by digging all the ducts and laying all the cables. As a result, the cost for digging and laying is included in the fiber cost usually by dividing this cost over all fibers installed in a single duct. On the contrary, when the cable plants have already existed, the cost of digging the ducts and laying the cable is usually not included in the fiber cost. Various technical researches and market analyses provide references on the cost of fiber connection in the long haul or metro environments [48]. For a MAN, the cost for a fiber connection is estimated in the range of \$2K-\$25K/km. A typical fiber in MAN is 5 to 20km in length; α in (5.1) is in the range of \$10K -\$500K/fiber.

5.3 Switching Cost

One of the key attributes of optical switches is the port count K, which depends on the network traffic demand and the network physical topology, etc. In this chapter and Chapter 6, we assume that the network traffic is uniform all-to-all, i.e., each node sends exactly t wavelengths of traffic to every other node, with each wavelength modulated at a data rate of r (Gb/s). We first use this deterministic traffic model to approximate the mean of the random traffic and to dimension the capacities of the

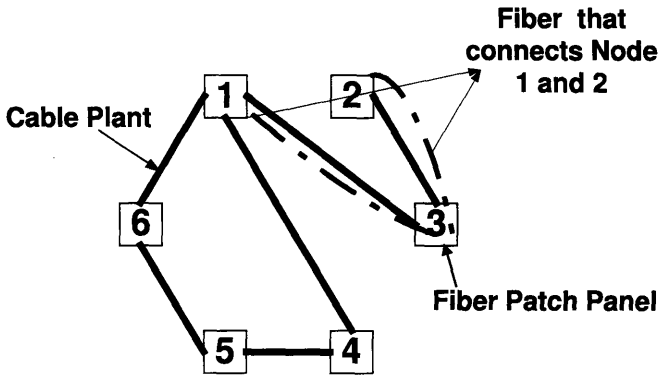

Figure 5-2: By using fiber patch panels, a fiber connection can be established between two nodes that are not directly linked by a cable.

fibers and nodes accordingly. We leave the analysis of network dimensioning under random traffic in Chapter 8. For the time being, we also assume that dynamic switching handles all the pass-through and add-drop traffic. This assumption is realistic - even static traffic requires active protection switching for network reliability [1].

5.3.1 Number of Ports and Size of an Optical Switch

The number of ports on an optical switch in a mesh network can be determined by counting the number of ports that each lightpath occupies as it traverses through the network, tallying the number of ports for all the demands, and then dividing the sum by the number of cross-connects. In our analysis, an optical switch is placed at each node of the network to manage transport bandwidth, thus the number of switches is given by the number of nodes N.

[1]To be economical, low-cost switching equipment, such as fiber-patched panels, can handle the static or quasi-static portion of the traffic with fixed routing and quasi-static switching; while more expensive dynamic switching equipment accommodate the fluctuating/stochastic portions. In Chapter 10, we provide comments on the issue of "mixed" switching and lightpath dimensioning.

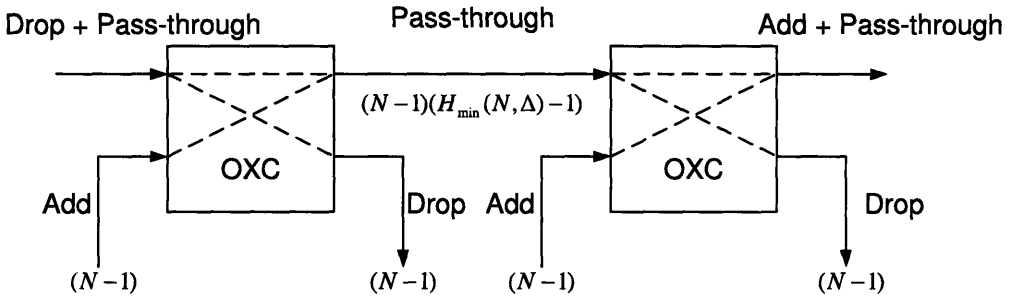

Figure 5-3: Lightpaths and cross-connect ports. The figure serves as a guideline to count the number of cross-connect ports occupied by a lightpath as it traverses through the network. The relationship among the local add, drop, and pass-through channels are also illustrated. Here, the number of add and drop traffic, $N-1$ each, corresponds to the all-to-all uniform traffic demand ($t = 1$).

Sizing the Pass-Through and Add/Drop Traffic

Lightpaths of more than one hop have to be switched at the intermediate nodes, thus they generate pass-through traffic, as depicted in Figure 5-3. We first size up the amount of the pass-through traffic (in terms of number of wavelengths) at each node under uniform traffic, by looking at the case of $t = 1$, i.e., each node sends 1 wavelength of traffic to every other node. Referring to Figure 5-3, a lightpath of j hops is switched $j-1$ times at the intermediate nodes, thus generating $j-1$ wavelengths of pass-through traffic. Let q_i denote the pass-through traffic generated by the traffic from node i. With minimum hop routing, q_i satisfies

$$q_i = \sum_{j=1}^{D} n_i(j)(j-1), \tag{5.2}$$

where $n_i(j)$ denotes the number of nodes whose minimum hop path from node i consists of j hops. Let Q denote the average pass-through traffic (in the number of wavelengths) at each node of the network, we have

$$Q = \frac{1}{N}\sum_{i=1}^{N}\sum_{j=1}^{D} n_i(j)(j-1). \tag{5.3}$$

By exploiting the symmetry of a regular topology ($n_i(j) = n(j)$) and using (4.1), we can further simplify Q as follows:

$$\begin{aligned} Q &= \frac{1}{N}[N\sum_{i=1}^{D} n(i)(i-1)] \\ &= (H_{\min}-1)(N-1). \end{aligned} \tag{5.4}$$

Since $H_{\min} \leq D$ for a regular topology, we can have an upper bound on Q,

$$Q \leq (D-1)(N-1). \tag{5.5}$$

The add-drop traffic at each node, denoted as A, is $N-1$ for uniform traffic. Thus the ratio between the average pass-through and the add-drop traffic is given by

$$\frac{Q}{A} = \frac{(H_{\min}-1)(N-1)}{(N-1)} = H_{\min}-1. \tag{5.6}$$

Next we look at the general case of $t > 1$. With derivations similar to those for $t = 1$, we have the average pass-through traffic at each node $Q(t)$ as

$$\begin{aligned} Q(t) &= \frac{1}{N}[N\sum_{i=1}^{D} n(i)(i-1)t] \\ &= (H_{\min}-1)(N-1)t. \end{aligned} \tag{5.7}$$

Since the add-drop traffic also scales proportionally with t, the ratio between the pass-through and the add-drop traffic stays the same as $H_{\min}-1$.

The insight provided by (5.7) is revealing: the ratio between the pass-through and the add-drop traffic under uniform traffic can be tied to a fundamental parameter of the regular topology – the average minimum hop distance $H_{\min}$.

- When node degree Δ is fixed, $H_{\min}$ increases as the network size N grows, according to previous results summarized in Table 4.1. Thus pass-through traffic tends to dominate add-drop traffic for large network size N.

- When network size N is fixed, $H_{\min}$ decreases, as node degree Δ increases, thus there is less pass-through traffic at each node. For maximal $\Delta = N-1$, the case of a fully connected network with each node reaching every other node in

one hop, i.e., $H_{\min} = 1$. From (5.7) the pass-through traffic is eliminated. This agrees with a simple fact that when the network's connectivity allows each node to reach every other node in one hop, then there is no pass-through traffic on each node. This validates the correctness of (5.7).

To illustrate this trend, for $N = 50$, we plot in Figure 5-4 the ratio between pass-through and add-drop traffic with respect to node degree Δ for three types of topologies: Δ-nearest Neighbors, Symmetric Hamilton Graphs, and Generalized Moore Graphs. We can see that when the node degree is small, a Δ-nearest Neighbors topology has the highest ratio of pass-through traffic vs. add-drop traffic; while a Generalized Moore Graphs has the lowest. As Δ increases, the difference of the ratios among the three topologies diminishes. Since more switch ports are needed to handle more pass-through traffic, one can already see that Generalized Moore Graphs have superior performances in terms of switch size, especially when the node degree Δ is small.

The Size of an OXC Switch

On the first order, the capacity of an OXC is independent of the actual data rate r of each wavelength. Referring to Figure 5-3, consider a directed demand that is added to the network via the switch at the node on the left. Adding the demand requires one input port. Eventually, this demand exits the network, by entering and exiting the switch at the destination node, such as the node on the right. Thus dropping the demand also requires one output port. Consequently, the size of a switch K_{o}, which equals to the sum of the number of lightpaths that pass-through and add-drop at each node, can be obtained as

$$\begin{aligned} K_{\mathrm{o}}(N, \Delta, t) &= (N-1)t[H_{\min}(N, \Delta) - 1] + 2(N-1)t \\ &= (N-1)t[H_{\min}(N, \Delta) + 1]. \end{aligned} \tag{5.8}$$

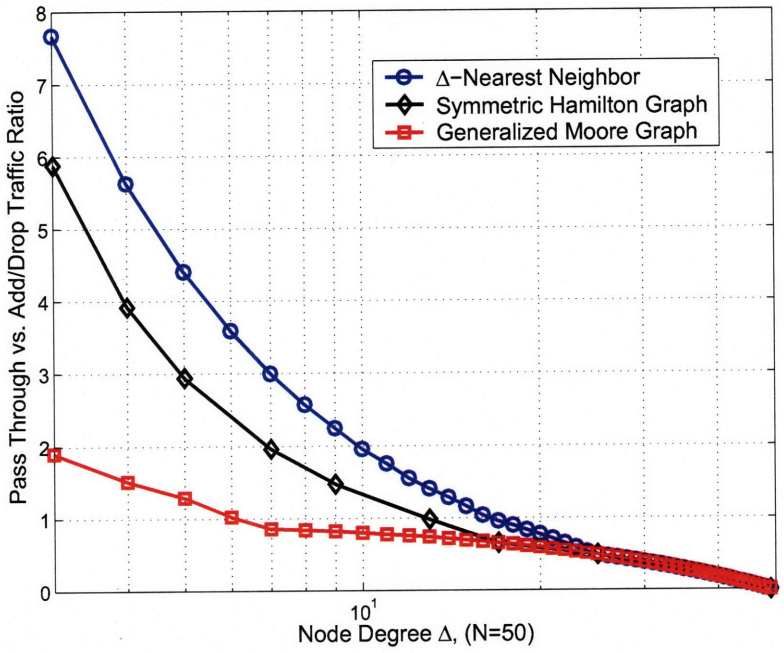

Figure 5-4: Pass-through vs. add-drop traffic ratio as a function of the node degree Δ, $N = 50$.

The Size of an OEO Switch

From (5.8), we note that if a wavelength carries a r Gb/s data rate, the total traffic switched at each node, in the unit of Gb/s, is $t(N-1)r[H_{\min}(N,\Delta)+1]$. Compared with that of an OXC switch, the port count of an OEO switch depends on the data rate per wavelength r. With the port (interface) rate R and the port utilization η, the number of OEO switching port K_e is given by

$$K_e(N,\Delta,t,r,R,\eta) = \frac{t(N-1)r[H_{\min}(N,\Delta)+1]}{R\eta}. \tag{5.9}$$

5.3.2 Modeling the Cost of an OXC

In this section we model the cost of an OXC as a function of the number of switching ports required. Since the traffic is all-to-all and the topologies are regular, we can assume that the size of OXC at each node is the same. If there are K_o lightpaths to be switched, added, and dropped at a node, the OXC needs at least K_o input ports and K_o output ports. For simplicity of analysis, we assume that OXCs have strictly non-blocking switching fabrics. We also suppress the wavelength continuity constraint by assuming that

- Either there are enough numbers of wavelengths available. This assumption is realistic at least in the foreseeable future, given the abundance of wavelengths in the metropolitan environment.

- Or the optical switches allow a full wavelength conversion, i.e., any wavelength channel on an input port can be switched to any wavelength channel on an output port. In general OXCs with wavelength conversions have higher cost per port. As a result, WDM networks equipped with such OXCs have higher optimal connectivity and higher network cost (as will be explained in detail in Chapter 6 and Chapter 7).

With wavelength continuity constraint suppressed, K_o ports are enough to switch lightpaths without causing any blocking on the network. In this thesis work, we focus

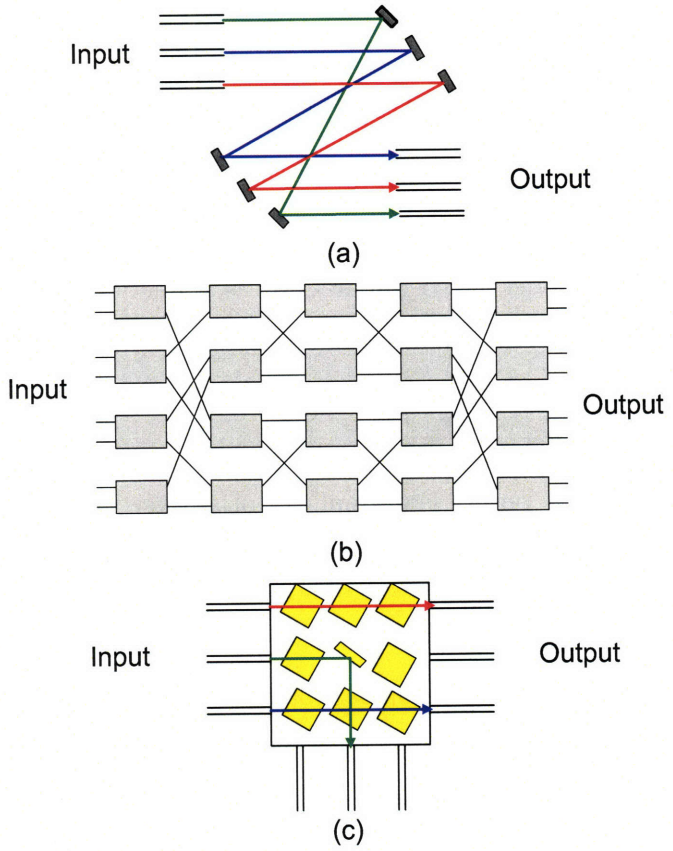

Figure 5-5: Switching architectures: (a) 3-D, (b) multi-stage, and (c) 2-D architectures.

Table 5.1: Cost of OXC switching architecture as functions of the number of ports K_o.

Switching Architecture	Cost Function
3-D	$F_1(K_o) = \beta_1 K_o^{1+\zeta}$
Multi-stage	$F_2(K_o) = \beta_2 K_o^{1+\theta} \log_2 K_o$
2-D	$F_3(K_o) = \beta_3 K_o^{2+\delta}$

on three most representative optical switching architectures: 3-D, multi-stage, and 2-D OXC, as depicted in 5-5. As described in Section 2.1.7, 3-D architectures, shown in 5-5 (a), are built using two arrays of micro switching elements, each of which has two degrees of freedom, allowing light to be directed from one input port to any output port. Multi-stage architectures, shown in 5-5 (b), refer to rearrangeable architectures, such as Clos or Banyan architectures. 2-D architectures, shown in 5-5 (c), consist of two-dimensional arrays of micro switching elements that have one degree of freedom. The cost of OXC scales differently for different types of switching architectures. Table 5.1 lists the first-order cost functions corresponding to these switching fabrics. In this table, ζ $(0 < \zeta < 1)$, θ $(0 < \theta < 1)$, and δ $(0 < \delta < 1)$ are coefficients associated with reliability and yield issues in the manufacturing of 3-D, multi-stage, and 2-D OXC switches, respectively. Notice that in modeling the cost of the multi-stage switching architecture, we assume that the basic switching element is of the size 2×2.

As stated in (5.8), K_o is a function of network size N, node degree Δ, and wavelengths of traffic t between node pairs. Let C_s^o denote the cost of OXC, C_s^o is given by

$$\begin{aligned} C_s^o &= NF_i[K_o(N, \Delta, t)] \\ &= NF_i[(N-1)t(H_{\min}+1)], i \in \{1, 2, 3\}, \end{aligned} \tag{5.10}$$

where i indexes the switch type and therefore β_1, β_2, and β_3 are scaling factors (cost per port) for 3-D, multi-stage, and 2-D switching fabrics, respectively. The ratios between β_1, β_2, and β_3 can be evaluated by using a cost crossover point K_c for

different switching fabrics, based on the status of the current technologies. Suppose the costs for 3-D, multi-stage, and 2-D switching fabrics are the same for a size of $K_c \times K_c$, then the ratios between β_1, β_2, and β_3 are

$$\beta_1 = \beta_2 \log K_c = \beta_3 K_c. \tag{5.11}$$

We estimate β_1 at \$10k/port for 8×8 OXC of 3-D fabrics; realistic α/β_1 ratio can be in the range from 1 to 50.

5.3.3 Modeling the Cost of an OEO Switch

We model the cost of an OEO switch as a linear function of the number of OEO switching ports K_e:

$$\begin{aligned} C_s^e &= \beta_e K_e(N, \Delta, t, r, \eta) \\ &= \beta_e \frac{t(N-1)r}{R\eta}[H_{\min}(N, \Delta) + 1], \end{aligned} \tag{5.12}$$

where β_e is the per port cost of an OEO switch. We set β_e at \$40k/port for a 2.5 Gb/s interface and \$80k/port for a 10 Gb/s interface, respectively, based on the estimate in [14].

It is worthy to point out that the the cost model for switches is general enough to include the static (patch panel) and dynamic switching. In other words, in addition to β_1, β_2, β_3, and β_e, we assign β_p as per port cost for patch panel switching.

5.4 Network Cost

For a network equipped with OXC, according to (5.1) and (5.10), the total network cost C is

$$\begin{aligned} C &= C_f + C_s^o \\ &= N\{\alpha\Delta + F_i[K_o(N, \Delta, t)]\},\ i \in \{1, 2, 3\}. \end{aligned} \tag{5.13}$$

The total cost can be further normalized as cost per node – *normalized network cost*

$$C_n = \frac{C}{N} = \{\alpha\Delta + F_i[K_o(N, \Delta, t)]\},\ i \in \{1, 2, 3\}, \tag{5.14}$$

and cost per node per unit traffic – *normalized network cost per unit traffic*

$$C_{\mathrm{n}/t} = \frac{C_{\mathrm{n}}}{t} = \frac{\{\alpha\Delta + F_i[K_{\mathrm{o}}(N,\Delta,t)]\}}{t},\ i \in \{1,2,3\}. \tag{5.15}$$

Similarly, for a network equipped with OEO switches, according to (5.1) and (5.12), the total network cost C is

$$\begin{aligned} C &= C_{\mathrm{f}} + C_{\mathrm{s}}^{\mathrm{e}} \\ &= N\{\alpha\Delta + \beta_{\mathrm{e}} K_{\mathrm{e}}(N,\Delta,t,r,\eta)\}. \end{aligned} \tag{5.16}$$

The corresponding normalized network cost is

$$C_{\mathrm{n}} = \frac{C}{N} = \alpha\Delta + \beta_{\mathrm{e}} K_{\mathrm{e}}(N,\Delta,t,r,\eta), \tag{5.17}$$

and the normalized network cost per unit traffic is

$$C_{\mathrm{n}/t} = \frac{C_{\mathrm{n}}}{t} = \frac{\{\alpha\Delta + \beta_{\mathrm{e}} K_{\mathrm{e}}(N,\Delta,t,r,\eta)\}}{t}. \tag{5.18}$$

We note that the normalized cost C_{n} also depends on the type of regular topologies through the expression of $H_{\min}$. For a given class of regular topologies, once we have the $H_{\min}$ as a function of network size and node degree, we can analyze the optimal node degree Δ^* that achieves the minimal cost.

Chapter 6

Optimal Network Architecture Under Deterministic Traffic

With models for network traffic, physical architectures, and cost set up in place, we are to formulate and solve the joint optimization problem of physical topology, dimensioning of network resources, and routing algorithms. By solving the joint problems analytically, we can obtain fundamental cost bounds as benchmarks for proposed architectures. More importantly, these results provide insights into what constitutes scalable network architectures.

As a first step in approaching the joint optimization problem, we give a qualitative appraisal of the key tradeoffs that influence the optimal network architectures. After examining and discussing these push-pull effects from a qualitative point of view, we rigorously set up the joint network optimization problem and quantitatively analyze the dependencies of the optimal network architectures on key design parameters.

When the locations of nodes (Figure 6-1 (a)) are given, there can be different underlying physical topologies to serve the same (deterministic) traffic demand, albeit at very different costs. In this thesis work, we approach the finding of a cost-effective physical topology by setting up a first-order network cost model and then analyzing the tradeoffs among key network resources. As described in Chapter 5, in our first-order cost model, the costs for fiber connections and switching resources vary with network connectivity. We note that lightpaths of more than one hop have to

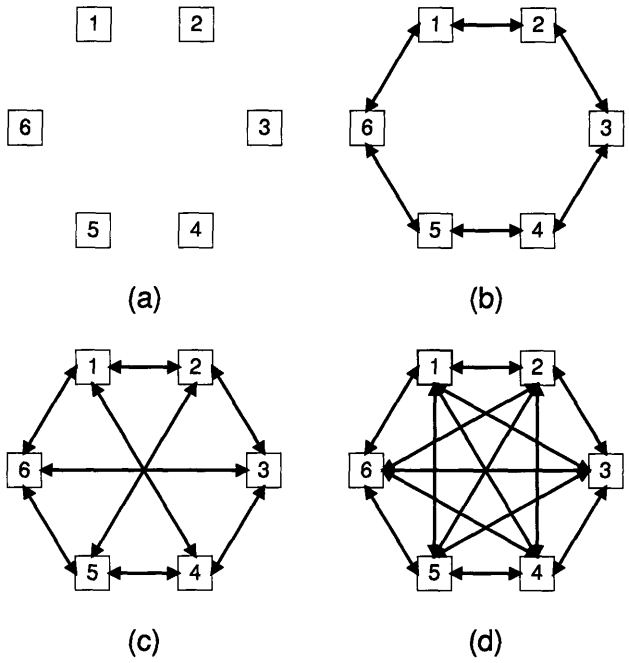

Figure 6-1: (a) Locations of the nodes; (b) Ring topology (sparsely connected); (c) Degree 3 topology; (d) Fully connected topology.

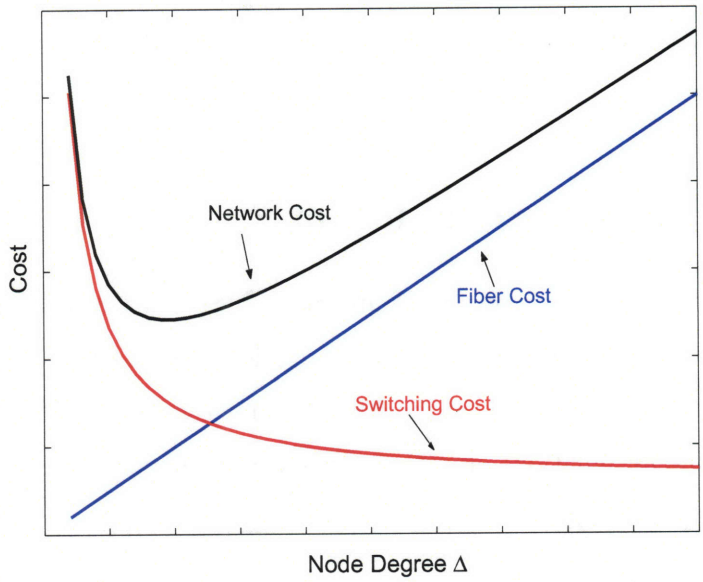

Figure 6-2: Tradeoff between the cost of fiber and the cost of switching.

be switched at intermediate nodes, thus taking up a certain amount of switching resources. A network with higher connectivity requires more fiber connections, but the lightpath traverses on average fewer hops and intermediate nodes, requiring less switching resources, albeit at the expense of more fiber costs. To better understand the tradeoffs, we consider two extreme cases and their implications on optimal network topologies: 1) if the cost of fiber plants dominates the cost of switches, the optimal network topology should be as sparsely connected as possible (Figure 6-1(b)); 2) if the cost of switches dominates the cost of fiber plants, the optimal network should be as fully connected as possible (Figure 6-1(d)). Realistic cost ratios between the fiber plants and the switching resources are in between these two extremes. Thus a tradeoff between fiber and switching resources will lead to an optimal network connectivity that is in between these two extreme cases, as shown conceptually in Figure 6-1(c). Figure 6-2 illustrates how the choice of network connectivity (topology) drives the fiber cost in one direction, and simultaneously, drives the switching cost in a counteracting direction. At an optimal connectivity or an optimal node degree, the minimal

network cost is achieved, as the result of optimal tradeoff between fiber connection cost and switching cost. Solving for the optimal node degree is the center of this chapter.

6.1 Problem Formulation

Using the network cost model in Chapter 5, we are now ready to formulate the physical topology design problem as an optimization over the type of symmetric regular topology (denoted as "tpl." in the formulation), the routing algorithms (denoted as "r.a." in the formulation), and the network node degree Δ. The formulation has a general form as follows:

$$\begin{aligned} \min_{\{\text{tpl.}\},\{\text{r.a.}\},\Delta} \quad & C_{\text{n}}(N,\Delta,t) \\ \text{s.t.} \quad & 2 \leq \Delta \leq N-1; \\ & \Delta \in \mathrm{Z}^{+}; \\ & N \text{ and } t \text{ are given.} \end{aligned} \tag{6.1}$$

In this optimization formulation, the inputs are:

- The number of nodes (network size) N;
- The traffic demand between a source-destination pair t (note that we assume a uniform all-to-all traffic);
- The type of optical switches and the corresponding parameters, as described in Section 5.3:
  - For OXC switching architecture, the inputs include the cost scaling function $F_i(K_{\text{o}})$, where K_{o} is the number of OXC ports, and the corresponding per port cost (cf. Table 5.1);
  - For OEO switching architecture, the inputs include the port (interface) rate R, data rate per wavelength r, port utilization η, and per port cost β_{e};

- The cost per fiber connection α.

The objective is to minimize the normalized network cost over:

- The type of symmetric regular topology;
- The type of routing algorithm;
- The node degree of the symmetric regular topology.

In the formulation (6.1), the constraint $\Delta \leq N-1$ imposes an upper limit to the possible values of the optimal node degree Δ^* for a topology of N nodes; while the constraint $\Delta \geq 2$ ensures that the optimal topology meets the reliability requirement of more than one connected. Since Δ represents the node degree, the optimal node degree Δ^* should be a positive integer.

Note that to maintain the tractability of the analysis and to shed light on the key properties of optimal network architecture, in our formulation we temporarily suppress some practical issues of network design:

- We take an "infinite capacity" approach in formulating the network optimization problem by assuming that a fiber can support as many wavelengths as needed. In other words, we don't impose the upper limit on the number of wavelengths that a fiber can carry.
- We consider a "capacity only" problem – we temporarily omit the details of wavelength assignment. The reason is that in a long-term context, costs and architecture efficiencies do not depend on the detailed channel assignment, as long as suitable channel assignment is feasible under the capacity available [4]. The wavelengths assignment problem will be discussed in detail in Chapter 7.
- We dimension the network for working capacity only – the extra fiber connections and switching ports that are required for network survivability are not included in our cost model and thus in the formulation (6.1).

In Chapter 10, we will extend the network optimization framework (6.1) to address some of these issues.

6.2 Optimal Routing Algorithm and Optimal Regular Topology

Though the optimization in (6.1) is carried out over all possible classes of routing algorithms and regular topologies, an exhaustive enumeration approach would be difficult and unnecessary. A close examination of the cost model reveals that only the switching costs depend on the routing algorithm and the type of the topology. In regard to the routing algorithm, we note that shorter lightpaths pass through fewer intermediate nodes, thus requiring fewer switching ports. Following this observation, we can prove that minimum hop routing is optimal for any given regular network, as long as the switch cost is a non-decreasing function of switch size (K_o or K_e). As for the optimal class of topology, existing classes of graphs – Generalized Moore Graphs – are known to achieve the lower bounds on the average minimum hop distance among regular topologies with the same node number and node degree. By making connections between this important property and the switching cost model, we identify that Generalized Moore Graphs yield cost lower bounds.

In this section, we show that for all classes of regular topologies and uniform traffic, we can rigorously solve the problem jointly and optimally. To proceed the analysis, we use a simple yet important concept – we refer to this as "dominated function" technique, as summarized in the following lemma. Since this lemma trivially holds, we omit the proof.

Lemma 1 *Consider two bounded functions on a closed and bounded set* X, $f_1(x)$ *and* $f_2(x)$. *Suppose for any* $x \in \mathrm{X}$, $f_1(x) \leq f_2(x)$, *then we have* $\min_x f_1(x) \leq \min_x f_2(x)$.

6.2.1 Optimization Over Routing Algorithms

In regard to the optimal routing algorithm, we have the following result:

Theorem 7 *Under uniform all-to-all traffic, minimum hop routing is optimal for any given regular network with a non-decreasing switch cost function.*

To see why minimum hop routing is optimal, we compare the cost incurred by a minimum hop routing algorithm with that by other (non minimum hop) routing algorithms for a given regular network of size N and node degree Δ. For simplicity we only consider networks equipped with OXC switches; yet the following substantiations also hold for networks equipped with OEO switches. Denote the average minimum hop distance of a regular topology as $H_{\min}$ and the average hop distance with another routing algorithm for the same topology as H'. By definition,

$$H_{\min}(N, \Delta) \leq H'(N, \Delta). \tag{6.2}$$

For the minimum hop routing algorithm, according to (5.14), the incurred normalized network cost, denoted by $C_{\mathrm{n}}^{\mathrm{m}}$, is

$$\begin{aligned} C_{\mathrm{n}}^{\mathrm{m}} &= \alpha\Delta + F_i(K_{\mathrm{o}}) \\ &= \alpha\Delta + F_i[(N-1)(H_{\min}(N, \Delta) + 1)],\ i \in \{1, 2, 3\}. \end{aligned} \tag{6.3}$$

For any other routing algorithm, the normalized network cost, denoted by C_{n}, is obtained as

$$\begin{aligned} C_{\mathrm{n}} &= \alpha\Delta + F_i(K'_{\mathrm{o}}) \\ &= \alpha\Delta + F_i[(N-1)(H'(N, \Delta) + 1)],\ i \in \{1, 2, 3\}. \end{aligned} \tag{6.4}$$

Since the switch size K_{o} and K'_{o} are linear in average minimum hop distance $H_{\min}$ and average hop distance H', respectively, and $F_i(K)$is non-decreasing in K, for a regular topology with size N and node degree Δ, the minimum hop routing achieves the minimal cost. That is,

$$C_{\mathrm{n}}^{\mathrm{m}}(N, \Delta) \leq C_{\mathrm{n}}(N, \Delta), \tag{6.5}$$

for any Δ ($1 \leq \Delta \leq N-1$). Using Lemma 1 (note that the set $\{\Delta \,|2 \leq \Delta \leq N-1 \text{ and } \Delta \in Z^+\}$ is closed and bounded), we have

$$\min_{\Delta} C_{\mathrm{n}}^{\mathrm{m}}(N, \Delta) \leq \min_{\Delta} C_{\mathrm{n}}(N, \Delta). \tag{6.6}$$

Thus we conclude that minimum hop routing is optimal for any given regular network with a non-decreasing switch cost function.

6.2.2 Optimization Over Different Types of Topologies

In regard to the optimal type of physical topology, we have the following result:

Theorem 8 *With minimum hop routing, among all classes of regular topologies, Generalized Moore Graphs provide the lower bound on the network cost under uniform traffic.*

To see why the Generalized Moore Graphs are optimal, we compare the costs of networks of the same size, but of different types of topologies. Here all the networks use minimum hop routing. For simplicity we again only consider networks equipped with OXC switches; yet the following substantiations also hold for networks equipped with OEO switches. As discussed in Section 4.2, for any regular topology with size N and node degree D, a Generalized Moore Graph achieves the lower bound on the average minimum hop distance. Denote the average minimum hop distance of a Generalized Moore Graph as $H_{\min}^{\mathrm{M}}$ and that of a general regular topology as $H_{\min}^{\mathrm{G}}$, we have

$$H_{\min}^{\mathrm{M}}(N,\Delta) \leq H_{\min}^{\mathrm{G}}(N,\Delta). \tag{6.7}$$

Following the same reasoning that leads to (6.5), for any regular topology of the same size N and node degree Δ, Generalized Moore Graphs achieve the minimal cost. That is,

$$C_{\mathrm{n}}^{\mathrm{M}}(N,\Delta) \leq C_{\mathrm{n}}^{\mathrm{G}}(N,\Delta), \tag{6.8}$$

for any Δ $(1 \leq \Delta \leq N-1)$, where $C_{\mathrm{n}}^{\mathrm{M}}$ and $C_{\mathrm{n}}^{\mathrm{G}}$ are the normalize network cost of a Generalized Moore Graph and a general regular topology, respectively.

Using the dominated function technique (Lemma 1) again, for a given N, we have

$$\min_{\Delta} C_{\mathrm{n}}^{\mathrm{M}}(N,\Delta) \leq \min_{\Delta} C_{\mathrm{n}}^{\mathrm{G}}(N,\Delta). \tag{6.9}$$

Thus, with minimum hop routing, among all classes of regular topologies, General Moore Graphs achieve the lower bound on the network cost under uniform traffic.

6.2.3 Network Topologies that Provide Upper (Worst Case) Bounds on Network Cost

As a natural extension, it is of interest to find a class of regular topologies that provides upper (worst case) bounds on network cost. We have already shown in Chapter 4.3.1 that a Δ-nearest Neighbors topology, in which each node connects to its Δ closest neighbors in a cyclic fashion, achieves upper bound on the average minimum hop distance among all the regular topologies of the same node number N and node degree Δ. By making connections between their properties of average minimum hop distance and switching cost model, we identify that Δ-nearest Neighbors yield a cost upper bounds. We summarize this result and provide a formal substantiation in the following:

Theorem 9 *A Δ-nearest Neighbors topology provides an upper bound on the average minimum hop distance among all regular topologies with the same node number and node degree. Moreover, Δ-nearest Neighbors topologies also achieve the upper bounds on the network cost under uniform traffic.*

As discussed in Section 4.3.1, for any regular topology with size N and node degree Δ, a Δ-nearest Neighbors Graph achieves the upper bound on the average minimum hop distance. Denote the average minimum hop distance of a Δ-nearest Neighbors topology as $H_{\min}^{\mathrm{N}}$ and that of a general regular topology as $H_{\min}^{\mathrm{G}}$, we have

$$H_{\min}^{\mathrm{N}}(N,\Delta) \geq H_{\min}^{\mathrm{G}}(N,\Delta). \tag{6.10}$$

Following the same reasoning that leads to (6.5), for any regular topology of the same size N and node degree Δ, a Δ-nearest Neighbors topology achieves the maximum cost. That is,

$$C_{\mathrm{n}}^{\mathrm{N}}(N,\Delta) \geq C_{\mathrm{n}}^{\mathrm{G}}(N,\Delta), \tag{6.11}$$

for any Δ $(1 \leq \Delta \leq N-1)$, where $C_{\mathrm{n}}^{\mathrm{N}}$ and $C_{\mathrm{n}}^{\mathrm{G}}$ are the normalized network costs of a Δ-nearest Neighbors Graph and a general regular topology, respectively.

Using the dominated function technique (Lemma 1) again, for a given N, we have

$$\min_{\Delta} C_{\mathrm{n}}^{\mathrm{N}}(N,\Delta) \geq \min_{\Delta} C_{\mathrm{n}}^{\mathrm{G}}(N,\Delta). \tag{6.12}$$

Thus, with minimum hop routing, among all classes of regular topologies, Δ-nearest Neighbors topologies achieve the upper bound on the network cost under uniform traffic.

6.3 Minimal Cost and Optimal Node Degree for Given Classes of Topologies

In this section, we obtain the optimal node degree Δ^* and minimal normalized network cost C_{n}^* in the formulation (6.1) for several classes of candidate topologies, all using minimum hop routing.

6.3.1 The Convexity of the Network Cost Functions

Before solving the optimization problem, we discuss the convexity of the network cost functions. We first relax Δ as a continuous variable and later round the result back to integer. In 6.4.1 we confirm that this approximation is very good. With a continuous Δ, the normalized cost C_{n} is also continuous and differentiable over Δ, according to (5.14). For a given N, the average minimum hop distance of the topologies studied in this work is (or can be approximated as) a convex function of Δ (cf. (4.11),(4.18), and (4.22)). Directly from (5.8) and (5.9), the number of OXC ports K_{o} and the number of OEO ports K_{e} are given by

$$K_{\mathrm{o}}(N,\Delta,t) = (N-1)t(H_{\min}(N,\Delta)+1) \tag{6.13}$$

and

$$K_{\mathrm{e}}(N,\Delta,t,r,R,\eta) = \frac{t(N-1)r(H_{\min}(N,\Delta)+1)}{R\eta}, \tag{6.14}$$

respectively. Thus both K_{o} and K_{e} are also convex in Δ. Further more, any OXC cost function $F_i(K_{\mathrm{o}})$ listed in Table 5.1 is convex and monotonically non-decreasing in K_{o},

therefore is convex in Δ, according to the theorem of convexity under composition [49]. Similarly, an OEO cost function is linear with Δ, thus also convex in Δ. As such, the normalized network cost C_{n} is convex in Δ and thus a local optimal Δ^* is also a global optimum, as illustrated in Figure 6-2.

6.3.2 Minimal Cost and Optimal Node Degree for a Given Class of Topologies

In this subsection, we proceed to find the optimal node degree as a function of N for three classes of topologies: Δ-nearest Neighbors, Symmetric Hamilton Graphs, and Generalized Moore Graphs. For each class of topologies, we analyze their optimal node degrees for three different types of OXC switching fabrics – 3-D, multi-stage, and 2-D switching fabrics, as well as for OEO switching fabrics. The analytical and asymptotic results are summarized in Table 6.1, Table 6.2, and Table 6.3. As an example, here we provide the analysis of Δ-nearest Neighbors topology equipped with 3-D OXC in the following. With some simplifications, the derivations for the rest of the combinations of topologies and switching fabrics (both OXC and OEO) are provided in Chapter Appendix 6.5.

From Section 4.3.1, the average minimum hop distance of the Δ-nearest Neighbors topology is given by

$$H_{\min}^{\mathrm{N}} = (1 + \frac{\Delta}{2(N-1)}) \left\lceil \frac{N-1}{\Delta} \right\rceil - \frac{\Delta}{2(N-1)} (\left\lceil \frac{N-1}{\Delta} \right\rceil)^2, \tag{6.15}$$

if N can not be evenly divided by Δ; and

$$H_{\min}^{\mathrm{N}} = \frac{1}{2} + \frac{N-1}{2\Delta}, \tag{6.16}$$

if N can be evenly divided by Δ. The average minimum hop distance can be approximated using (6.16). This approximated average minimum hop distance is a convex function of node degree Δ.

For 3-D OXC switching fabrics, we have $F_1(K_{\mathrm{o}}) = \beta_1 K_{\mathrm{o}}$ (for simplicity we let $\zeta = 0$, cf. Table 5.1), then the normalized network cost (cf. (5.8) and (5.14)) is

$$\alpha\Delta + \beta_1 t(N-1)(\frac{3}{2} + \frac{N-1}{2\Delta}). \tag{6.17}$$

. We have the following optimization problem with two inequality constraints,

$$\begin{aligned} \min_{\Delta} \quad & \alpha\Delta + \beta_1 t(N-1)(\frac{3}{2} + \frac{N-1}{2\Delta}) \\ \text{s.t.} \quad & g_1(\Delta) = \Delta - N + 1 \leq 0; \\ & g_2(\Delta) = -\Delta + 2 \leq 0. \end{aligned} \tag{6.18}$$

For an optimal Δ^* and its associated Lagrange multipliers μ_1^* and μ_2^*, the Karush-Kuhn-Tucker (KKT) necessary conditions [50] yield

$$\begin{aligned} \alpha - \beta_1 t\frac{(N-1)^2}{2\Delta^{*2}} + \mu_1^* - \mu_2^* &= 0; \\ \mu_1^*(\Delta^* - N + 1) &= 0; \\ \mu_2^*(-\Delta^* + 2) &= 0; \\ \mu_1^* \geq 0; \mu_2^* &\geq 0. \end{aligned} \tag{6.19}$$

There are two possible cases:

- Case 1: the above constraints are inactive,

$$2 < \Delta^* < N - 1. \tag{6.20}$$

  For this case we have $\mu_1^* = 0$ and $\mu_2^* = 0$. Then, we obtain

$$\Delta^* = \left(\frac{\beta_1 t}{2\alpha}\right)^{\frac{1}{2}}(N-1). \tag{6.21}$$

  Note that the inactivity of the constraint requires the fiber-to-switching cost ratio to satisfy

$$\frac{2}{N-1} \leq \left(\frac{\beta_1 t}{2\alpha}\right)^{\frac{1}{2}} \leq 1. \tag{6.22}$$

- Case 2: one constraint is active. We have either

$$\Delta^* = N - 1, \tag{6.23}$$

  in which case $\mu_1^* = \beta_1/2 - \alpha$ and $\mu_2^* = 0$; or

$$\Delta^* = 2, \tag{6.24}$$

Table 6.1: Optimal node degree Δ^* and minimal normalized network cost C_{n}^* for Δ-nearest Neighbors.

Switch Architecture	Optimal Node Degree Δ^*	Minimal Normalized Cost C_{n}^*
3-D	$(\frac{\beta_1 t}{2\alpha})^{\frac{1}{2}}(N-1)$	$(\sqrt{2\alpha\beta_1 t}+\frac{3\beta_1 t}{2})(N-1)$
Multi-stage	Transcendental optimal equation Numerical exact solution	Numerical exact solution
2-D	$\frac{1}{2^{\frac{1}{3}}}\left(\frac{\beta_3 t^2}{\alpha}\right)^{\frac{2}{3}}(N-1)^{\frac{4}{3}}\left\{1+\left[1-\left(\frac{2\beta_3 t^2}{\alpha}\right)(N-1)\right]^{\frac{1}{2}}\right\}^{\frac{1}{3}}$ $+\frac{1}{2^{\frac{2}{3}}}\left(\frac{\beta_3 t^2}{\alpha}\right)^{\frac{1}{3}}(N-1)^{\frac{5}{3}}\left\{1+\left[1-\left(\frac{2\beta_3 t^2}{\alpha}\right)(N-1)\right]^{\frac{1}{2}}\right\}^{\frac{-1}{3}}$ $\propto c_1 t^{\frac{2}{3}}N^{\frac{4}{3}}+c_2 t^{\frac{4}{3}}N^{\frac{5}{3}}$	$\alpha\Delta^*+\beta_3\left[t(N-1)\left(\frac{3}{2}+\frac{N-1}{2\Delta^*}\right)\right]^2$ $\propto (tN)^2$
OEO	$\frac{1}{\sqrt{2}}\left(\frac{\beta_e tr}{\alpha\eta R}\right)^{\frac{1}{2}}(N-1)$	$\left(\sqrt{\frac{2\alpha\beta_e rt}{R\eta}}+\frac{3\beta_e rt}{2R\eta}\right)(N-1)$

in which case $\mu_1^*=0$ and $\mu_2^*=\frac{\beta_1}{4}(N-1)^2-\alpha$. As in the [50], μ_1^* and μ_2^* both can be viewed as the rate of change of minimal cost when the level of constraints changes. Since we are more interested in finding the optimal node degree Δ^* as a function of N for a given type of topology with certain type of OXC switching fabrics, we focus on the Case 1, in which $\mu_1^*=\mu_2^*=0$. Substituting (6.21) into (6.17), we have the minimal normalized network cost

$$C_{\mathrm{n}}^*=\left(\sqrt{2\alpha\beta_1 t}+\frac{3\beta_1 t}{2}\right)(N-1). \tag{6.25}$$

6.4 Results and Discussions

Having obtained the analytical and asymptotic results in the previous section (as summarized in Table 6.1, Table 6.2, and Table 6.3), in this section we plot the analytical results or numerical solutions for various design examples to illustrate the effects of various design parameters on the optimal WDM network architecture. From Section 6.4.1 to Section 6.4.4, we focus on the OXC-switched WDM networks. In Section

Table 6.2: Optimal node degree Δ^* and minimal normalized network cost C_n^* for Symmetric Hamilton Graph.

Switch type	Optimal Node Degree Δ^*	Minimal Normalized Cost C_n^*
3-D	$\frac{1}{2}\left(\frac{\beta_1 t}{\alpha}\right)^{\frac{1}{2}}\sqrt{(N-1)(N-2)}+1$ $\approx \frac{1}{2}\left(\frac{\beta_1 t}{\alpha}\right)^{\frac{1}{2}}(N-1)+1$	$(\sqrt{\alpha\beta_1 t}+\frac{7\beta_1 t}{4})\sqrt{(N-1)(N-2)}+\alpha$ $\approx (\sqrt{\alpha\beta_1 t}+\frac{7\beta_1 t}{4})(N-1)+\alpha$
multi stage	Transcendental optimal equation Numerical exact solution	Numerical exact solution
2-D	$\frac{1}{4}\left(\frac{\beta_3 t^2}{\alpha}\right)^{\frac{1}{3}}(N-1)^{\frac{4}{3}}\left\{4+\frac{2}{9}\left[2^2 3^3-6\cdot 7^3\left(\frac{\beta_3 t^2}{\alpha}\right)(N-1)\right]^{\frac{1}{2}}\right\}^{\frac{1}{3}}+$ $14\left(\frac{\beta_3 t^2}{\alpha}\right)^{\frac{2}{3}}(N-1)^{\frac{5}{3}}\left\{4+\frac{2}{9}\left[2^2 3^3-6\cdot 7^3\left(\frac{\beta_3 t^2}{\alpha}\right)(N-1)\right]^{\frac{1}{2}}\right\}^{-\frac{1}{3}}+1$ $\propto c_3 t^{\frac{2}{3}}N^{\frac{4}{3}}+c_4 t^{\frac{4}{3}}N^{\frac{5}{3}}$	$\alpha\Delta^*+\beta_3\left[t(N-1)\left(\frac{7}{4}+\frac{N-2}{4(\Delta^*-1)}\right)\right]^2$ $\propto (tN)^2$
OEO	$\frac{1}{2}\left(\frac{\beta_e t r}{\alpha\eta R}\right)^{\frac{1}{2}}\sqrt{(N-1)(N-2)}+1$ $\approx \frac{1}{2}\left(\frac{\beta_e t r}{\alpha\eta R}\right)^{\frac{1}{2}}(N-1)+1$	$\left(\sqrt{\frac{\alpha\beta_e rt}{R\eta}}+\frac{7\beta_e rt}{4R\eta}\right)\sqrt{(N-1)(N-2)}+\alpha$ $\approx \left(\sqrt{\frac{\alpha\beta_e rt}{R\eta}}+\frac{7\beta_e rt}{4R\eta}\right)(N-1)+\alpha$

Table 6.3: Optimal node degree Δ^* and minimal normalized network cost C_n^* for Generalized Moore Graphs.

Switch type	Optimal Node Degree Δ^*	Minimal Normalized Cost C_n^*
3-D	$\frac{1}{4}\left(\frac{\beta_1 t}{\alpha}\right)\frac{(N-1)\ln N}{\left\{W\left(\frac{\sqrt{(\beta_1 t/\alpha)(N-1)\ln N}}{2}\right)\right\}^2}$ $\propto \frac{\beta_1 tN}{\alpha\ln N}$	$\alpha\Delta^*+\beta_1 t(N-1)(\frac{\ln N}{\ln\Delta^*}+1)$ $\propto tN\left(1+\frac{1}{\ln(tN)}\right)$
multi stage	Transcendental optimal equation Numerical exact solution	Numerical exact solution
2-D	$\frac{2}{27}\left(\frac{\beta_3 t^2}{\alpha}\right)\frac{(N-1)^2(\ln N)^2}{\left\{W\left(\frac{2^{\frac{1}{3}}}{3}\left[\left(\frac{\beta_3 t^2}{\alpha}\right)(N-1)^2(\ln N)^2\right]^{\frac{1}{3}}\right)\right\}^3}$ $\propto \frac{\beta_3 t^2 N^2}{\alpha\ln N}$	$\alpha\Delta^*+\beta_3\left[t(N-1)\left(\frac{\ln N}{\ln\Delta^*}+1\right)\right]^2$ $\propto (tN)^2\left[1+\frac{1}{\ln(tN)}\right]$
OEO	$\frac{1}{4}\left(\frac{\beta_e rt}{\alpha R\eta}\right)(N-1)\frac{\ln N}{\left\{W\left(\frac{\sqrt{(\beta_e rt/\alpha R\eta)(N-1)\ln N}}{2}\right)\right\}^2}$ $\propto \frac{\beta_e rtN}{\alpha R\eta\ln N}$	$\alpha\Delta^*+\frac{\beta_e rt}{R\eta}(N-1)(\frac{\ln N}{\ln\Delta^*}+1)$ $\propto tN\left(1+\frac{1}{\ln(tN)}\right)$

6.4.5, we turn our attention to the OEO-switched WDM networks. In Section 6.4.6 we provide a summary.

6.4.1 Dependencies of Optimal Network Connectivity on the Type of Topology and the Type of OXC Switching Fabric

In Section 6.3 and Chapter Appendix 6.5, we solve for the optimal node degrees and the minimal costs of different types of topologies and switching fabrics. As presented in Table 6.1 to Table 6.3, the optimal node degree depends on the network size, the fiber-to-switching cost ratio, as well as the number of wavelengths of traffic between each node pairs, etc. To illustrate these dependencies, we plot the normalized optimal node degree as a function of network size N in Figure 6-3. Here, we define the normalized optimal node degree as $\Delta^*/(N-1)$. For a fully connected network, the normalized node degree is one. In Figure 6-3, the traffic demand between each node pair is set at $t = 1$. We also let the cost crossover point equals to 32, thus the ratios between β_1, β_2, and β_3 are $\beta_1 = 5\beta_2 = 32\beta_3$. Based on the estimates of the realistic cost ratio between fiber and switch in metropolitan area networks, we set $\beta_1 = 1$, $\alpha = 40$, thus $\alpha/\beta_1 = 40$. For comparison, we also plot the normalized node degrees of rings and fully connected mesh networks. We have the following observations:

- For a metropolitan area network of moderate size (a few tens to a hundred nodes), neither rings nor fully connected mesh networks is optimal physical topologies. The optimal network connectivity is in the range of $0.03N$ to $0.1N$ (the optimal node degrees are in the range of $0.03N$ to $0.1N$ for Generalized Moore Graphs of 50 -100 nodes).

- When we compare the optimal connectivity among different topologies that use the same type of OXC switching fabrics, we notice that a Δ-nearest Neighbors topology generally has the highest optimal node degree, while a Generalized Moore Graph has the lowest. When the network size N is fixed and the node

degree Δ is variable or vice versa, among the three types of topologies studied, a Δ-nearest Neighbors topology always has the largest average minimum hop distance, while a Generalized Moore Graph has the least. By correlating the optimal connectivity with the average minimum hop distance, we conclude that for the same network size, a topology with smaller average minimum hop distance generally has lower optimal connectivity.

- When we compare the optimal connectivity of a particular topology with different types of OXC switching fabrics, we note that a network with 3-D switching fabrics has the smallest optimal node degrees; while that with 2-D switching fabrics has the largest optimal node degrees. For 2-D switching fabrics the optimal node degree (as a solution of the optimality equation) grows approximately as polynomials of N (for all three classes of the topologies studied, cf. Table 6.1 to Table 6.3). As such, the normalized optimal node degree ($\Delta^*/(N-1)$) increases as N increases. With this trend, as N is large enough, the solutions of the optimality equations will eventually surpass $N-1$, violating the constraint $\Delta \leq N-1$. When this happens, the constraint $\Delta \leq N-1$ becomes active – the optimal node degree Δ^* equals to $N-1$. In other words, the optimal network has to be fully connected so that the dominant switching cost can be minimized. It is also worth noticing that for the Δ-nearest Neighbors and Symmetric Hamilton Graph with 3-D switching fabrics, the normalized optimal node degrees are asymptotically independent of network size. They are determined only by the fiber-to-switching cost ratio α/β_1.

- In the process of finding the optimal node degree, Δ is relaxed as a positive real number. As a result, Δ^*, obtained by solving the optimality equation, may not be an integer. We then round Δ^* to an integer – we compare the network cost at $\lceil \Delta^* \rceil$ and $\lfloor \Delta^* \rfloor$, and choose the one with lower network cost. To evaluate the accuracy of the approximations, we compare the rounded analytical results with the results of exhaustive searches – we look for the node degree (an integer) for which the network achieves the minimal cost. In Figure 6-4, we plot both

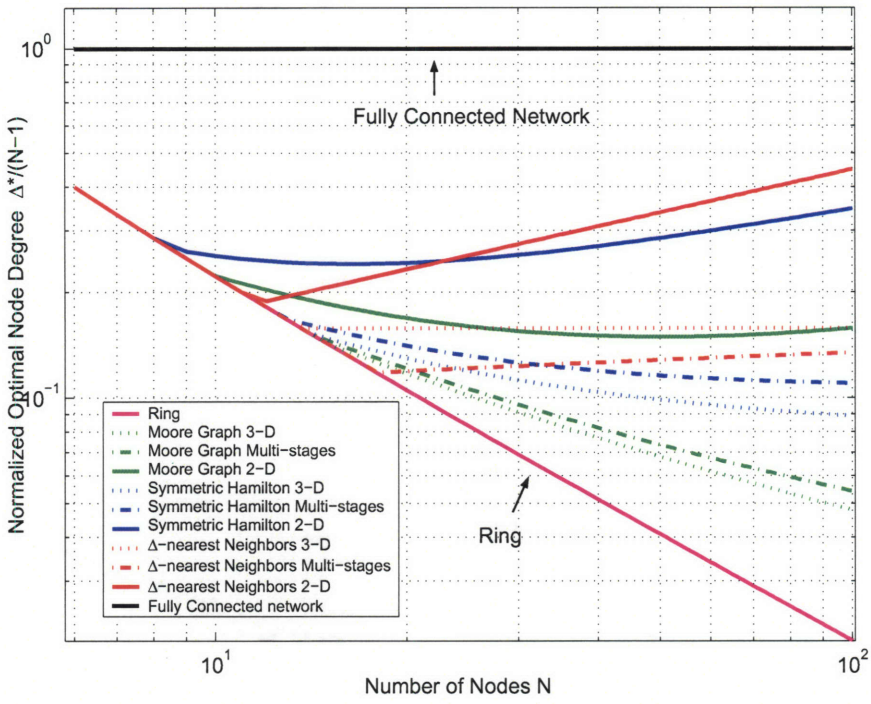

Figure 6-3: Normalized optimal node degree $\Delta^*/(N-1)$ as a function of network size N for Δ-nearest Neighbors, Symmetric Hamilton Graphs, and Generalized Moore Graphs. The fiber and switching cost parameters are: $\beta_1 = 1$, $\alpha/\beta_1 = 40$, and $\beta_1 = 5\beta_2 = 32\beta_3$.

analytical and exhaustive search results of normalized optimal node degree with respect to network size for the Δ-nearest Neighbors topology. It shows that the analytical solutions fit well with the exhaustive search results when the network size N is larger than 20. The "ripple" effect shown in the exhaustive search results reflects the discontinuity of the average minimum hop distance as a function of integers N and Δ, especially for smaller N. After running tests of this rounding algorithm, the results show that the maximum rounding error is within 1 node degree. The agreement between the analytical results and the exhaustive searches is also provided in Figures 6-5, 6-6, and 6-8.

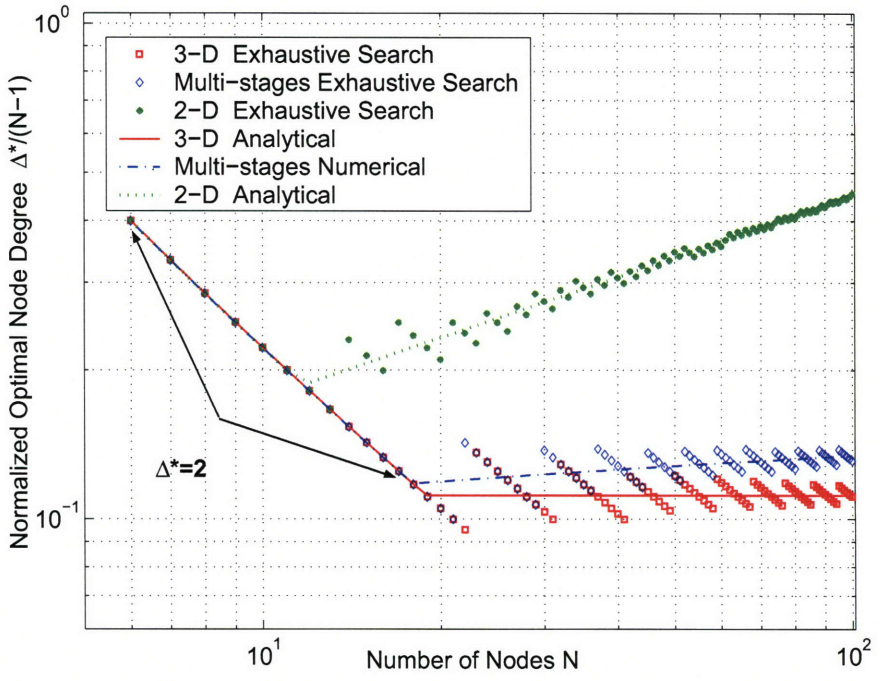

Figure 6-4: Normalized optimal node degree $\Delta^*/(N-1)$ as a function of network size N for Δ-nearest Neighbors topology. The lines represent the analytical results; while the points represent the results of extensive search. The fiber and switching cost parameters are: $\beta_1 = 1$, $\alpha/\beta_1 = 40$, and $\beta_1 = 5\beta_2 = 32\beta_3$.

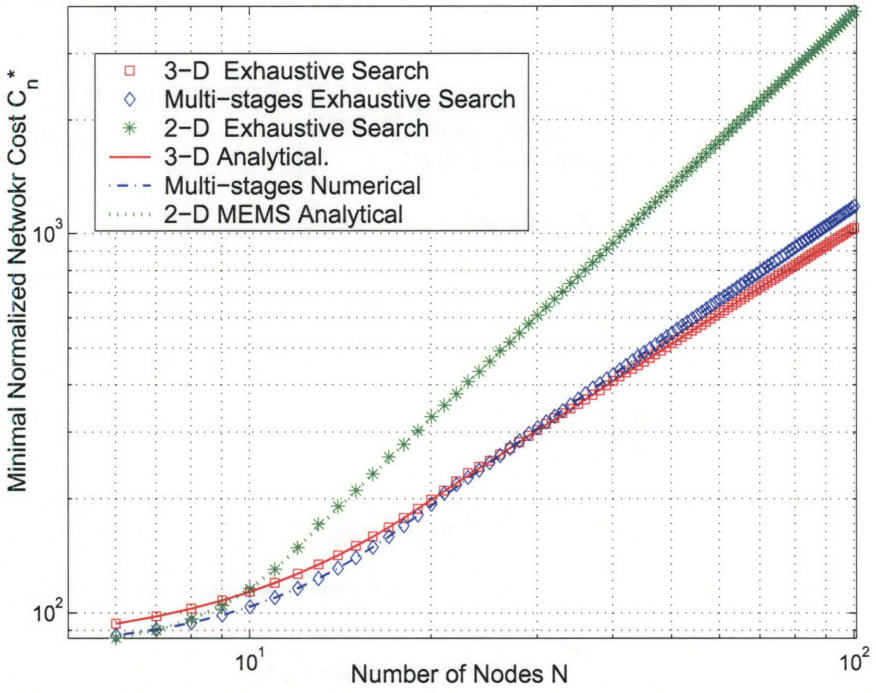

Figure 6-5: Normalized minimal network cost C_{n}^{*} as a function of network size N for Δ-nearest Neighbors topology. The lines represent the analytical results; while the points represent the results of exhaustive search. The fiber and switching cost parameters are: $\beta_1 = 1$, $\alpha/\beta_1 = 40$, and $\beta_1 = 5\beta_2 = 32\beta_3$.

6.4.2 Minimal Cost as a Function of Topology and OXC Switching Fabrics

Based on Table 6.1 to 6.3, we can demonstrate how well the minimal network cost scales with different types of topologies and technologies. For this purpose, we plot from Figure 6-5 to Figure 6-9 the minimal normalized cost and minimal normalized cost per unit traffic, for different topologies and switching fabrics. Figure 6-5 compares the minimal normalized network cost C_{n}^{*} of Δ-nearest Neighbors topology for three different types of switching fabrics. It is evident that, for small size networks (a few up to 10 nodes), it is more economical to use 2-D or multi-stage switching fabrics. As networks size increases, the differences in cost of various switching fabrics become

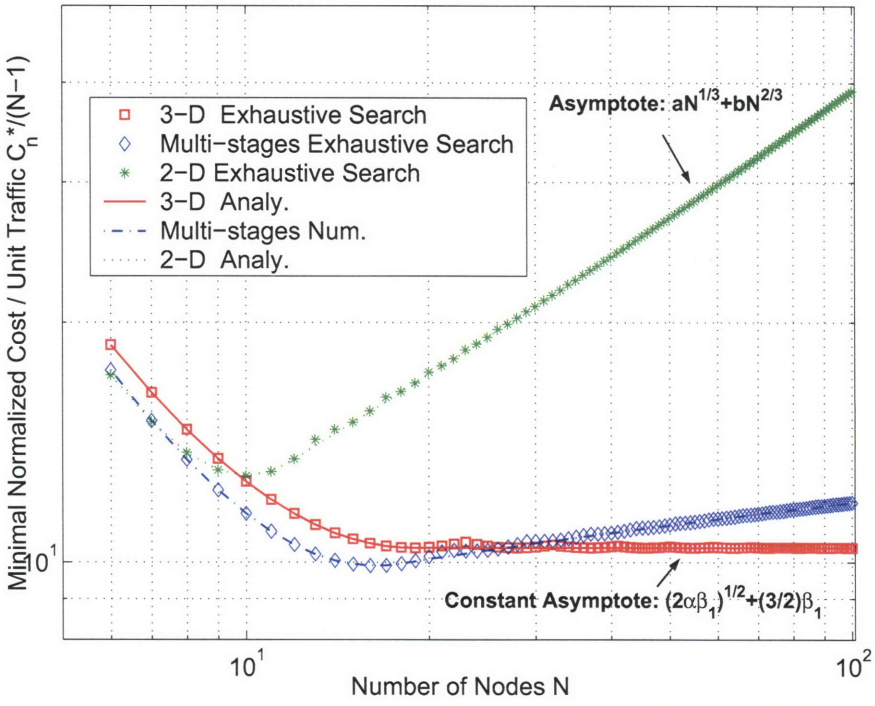

Figure 6-6: Normalized minimal network cost per unit traffic $C_{\mathrm{n}}^*/(N-1)$ as a function of network size N for Δ-nearest Neighbors topology. The lines represent the analytical results; while the points represent the results of exhaustive search. The fiber and switching cost parameters are: $\beta_1 = 1$, $\alpha/\beta_1 = 40$, and $\beta_1 = 5\beta_2 = 32\beta_3$.

more evident, mostly due to the scaling of the OXC cost $F_i(K_{\mathrm{o}})$ ($i \in \{1,2,3\}$, cf. Table 5.1). It is thus cost effective to use 3-D switching fabrics in a network of moderate size (a few tens to a hundred nodes).

Under uniform all-to-all traffic, the add-drop traffic at each node grows linearly with the network size. Figure 6-6 takes this factor into account. It plots the minimal normalized cost per unit traffic $C_{\mathrm{n}}^*/(N-1)$ with respect to network size N for three different types of switching fabrics. Both the plot and the analytical asymptote in this figure indicate the cost effectiveness of using 3-D switching fabrics as the size of the network increases: the minimal normalized cost per unit traffic stays constant with respect to N for 3-D fabrics, while it grows as the polynomials of N for 2-D fabrics.

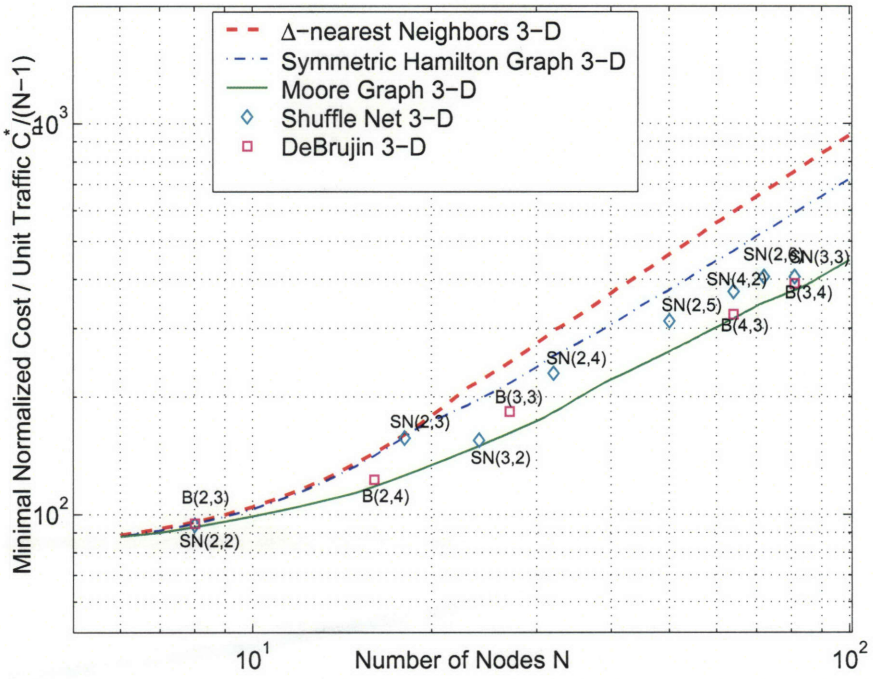

Figure 6-7: Minimal normalized network cost C_{n}^{*} as a function of network size N. The switching fabric is 3-D with $F_1(K_{\mathrm{o}}) = \beta_1 K_{\mathrm{o}}$. Results of ShuffleNets and de Brujin Graph are labeled as $\mathrm{SN}(\Delta, k)$ and $\mathrm{B}(\Delta, D)$, respectively. The fiber and switching cost parameters are: $\beta_1 = 1$, $\alpha/\beta_1 = 40$, and $\beta_1 = 5\beta_2 = 32\beta_3$.

Figure 6-7 compares the minimal normalized network cost for different classes of topologies all with 3-D OXC switching fabrics. The results for ShuffleNets and de Brujin Graph are also presented. We note that some ShuffleNets and de Brujin Graphs have costs that are close to that of Generalized Moore Graphs, thus from a cost perspective they are potential candidates for physical topologies of networks of certain sizes.

Figure 6-8 depicts the minimal normalized network cost per unit traffic with respect to network size N, with both analytical asymptotes and exhaustive search results. Both the plot and the analytical asymptote again show the cost effectiveness of Generalized Moore Graphs as network physical topologies: the minimal normalized cost per unit traffic decreases with respect to N for Generalized Moore Graphs;

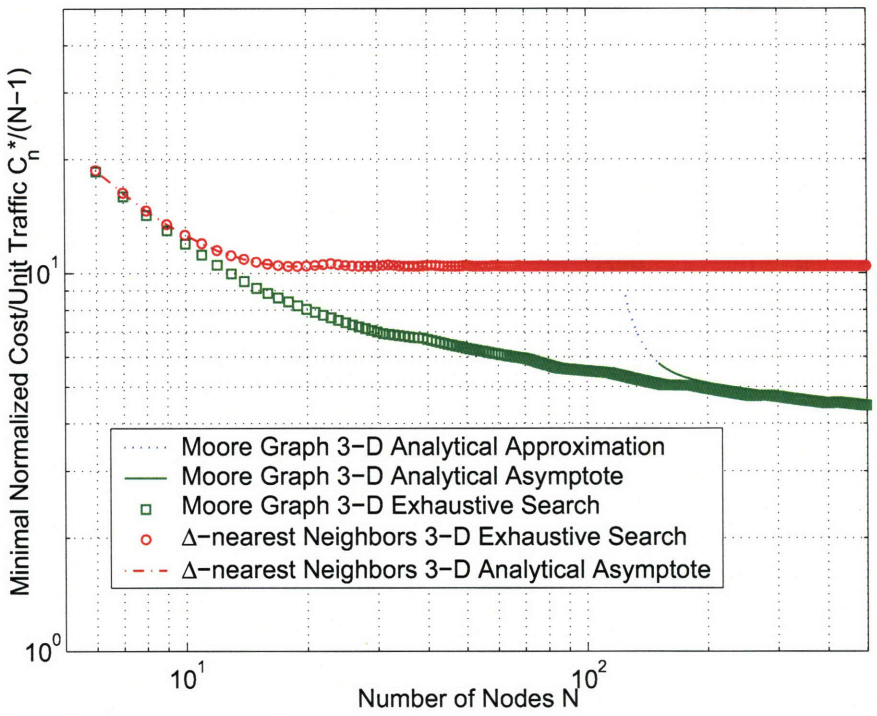

Figure 6-8: Minimal normalized cost per unit traffic $C_{\mathrm{n}}^*/(N-1)$ as a function of network size N for the Δ-nearest Neighbors and the Moore Graphs. The points represent the results of exhaustive searches; while the lines represent the analytical asymptotes. The switching fabric is 3-D with $F_1(K_{\mathrm{o}}) = \beta_1 K_{\mathrm{o}}$. The fiber and switching cost parameters are: $\beta_1 = 1$, $\alpha/\beta_1 = 40$, and $\beta_1 = 32\beta_3$.

while it stays constant (with the asymptote of $(2\alpha\beta_1)^{\frac{1}{2}}$) with respect to N for Δ-nearest-neighbor topologies. The analytical asymptote for Moore Graphs is given by ($a = \beta_1/\alpha$):

$$\frac{C_n^a(N)}{N-1} \approx \frac{\beta_1}{4} \frac{\ln(N)}{\left\{\frac{1}{2}\ln[\frac{a}{4}(N-1)\ln(N)] - \ln[\frac{1}{2}\ln[\frac{a}{4}(N-1)\ln(N)]] + \frac{\ln[\frac{1}{2}\ln[\frac{a}{4}(N-1)\ln(N)]]}{\frac{1}{2}\ln[\frac{a}{4}(N-1)\ln(N)]}\right\}^2}$$

$$+ \frac{\beta_1 \ln N}{\ln\left\{\frac{\frac{a}{4}(N-1)\ln(N)}{\left\{\frac{1}{2}\ln[\frac{a}{4}(N-1)\ln(N)] - \ln[\frac{1}{2}\ln[\frac{a}{4}(N-1)\ln(N)]] + \frac{\ln[\frac{1}{2}\ln[\frac{a}{4}(N-1)\ln(N)]]}{\frac{1}{2}\ln[\frac{a}{4}(N-1)\ln(N)]}\right\}^2}\right\}}. \quad (6.26)$$

The trends depicted in the above figures are what we expected. From the viewpoint of physical topology designs, Generalized Moore Graphs are very "efficient", in the sense that as their sizes increase, their diameter and average minimum hop distance scale favorably as $\log_\Delta N$, compared to Δ-nearest Neighbors or Symmetric Hamilton Graphs, whose diameter and average minimum hop distance scale as N/Δ. These efficiencies are further manifested when we consider the dimensioning of switching resource as traffic per node increases.

To stress the importance in choosing both physical topologies and OXC architectures that have good scalability, in Figure 6-9 we plot the minimal normalized network cost per unit traffic with respect to network size N, for combinations of two different classes of topologies (Δ-nearest Neighbors and Moore Graphs) and two types of OXCs (3-D and 2-D architectures). As shown in Figure 6-9, even with Generalized Moore Graphs as physical topology, which exhibit excellent scalability in average minimum hop distance, if 2-D OXCs, instead of 3-D OXCs, are deployed, the per node cost to support unit traffic still increases, as the network size increases. In other words, this particular choice of architecture (physical topology and switching technology) does not scale well.

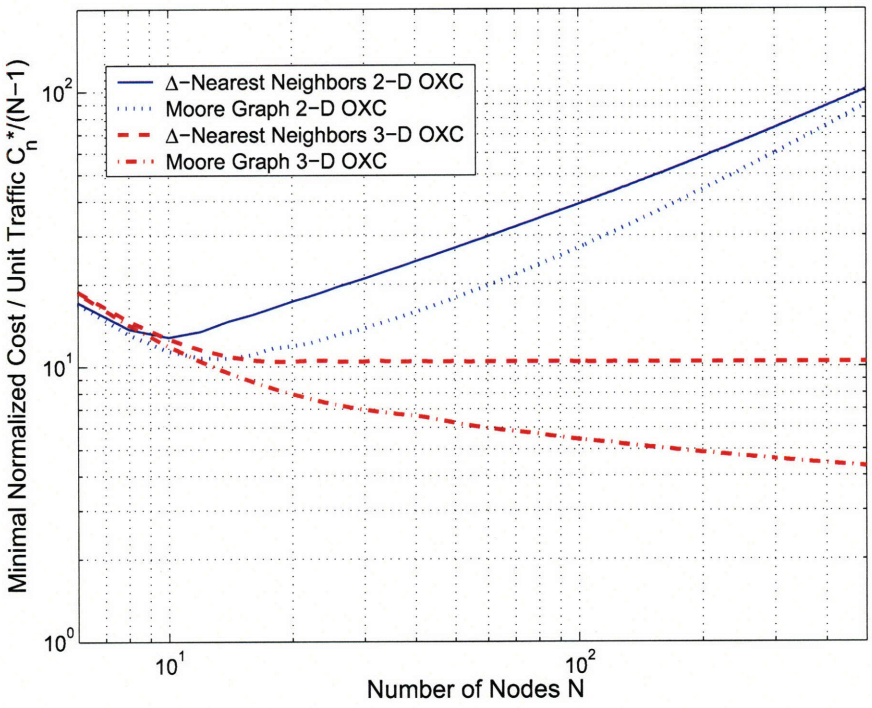

Figure 6-9: Minimal normalized cost per unit traffic $C_{\mathrm{n}}^{*}/(N-1)$ as a function of network size N for combinations of two different classes of topologies (Δ-nearest Neighbors and Generalized Moore Graphs) and two types of OXCs (3-D and 2-D fabrics). The fiber and switching cost parameters are : $\beta = 1$, $\alpha/\beta_1 = 40$, and $\beta_1 = 32\beta_3$.

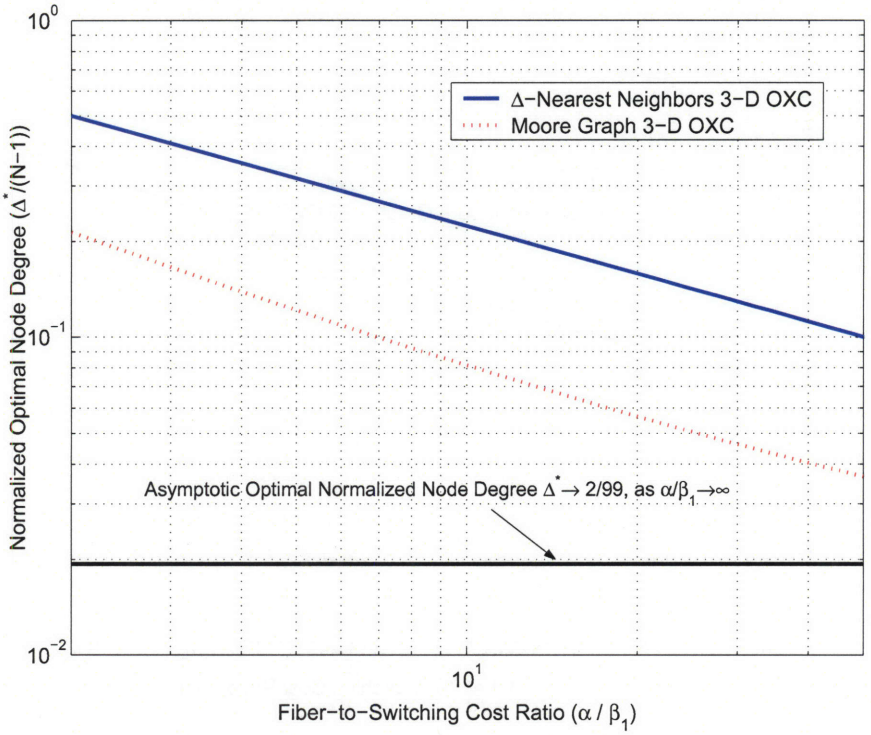

Figure 6-10: Normalized optimal node degree as a function of fiber-to-switching cost ratio α/β_1 for 3-D OXC. The network size is set as $N = 100$.

6.4.3 Optimal Network Connectivity and Minimal Cost as Functions of Fiber-to-Switching Cost Ratio

Using Δ-nearest Neighbors and Generalized Moore Graphs as examples, Figure 6-10 and Figure 6-11 illustrate how the optimal network connectivity and minimal normalized network cost vary as functions of fiber-to-switching cost ratio. For both figures, the network size is set as $N = 100$ and the OXC type is 3-D, i.e., $F_1(K_o) = \beta_1 K_o$. The fiber-to-switching cost ratio varies from 2 to 50, which are realistic estimates of current technologies. The trends depicted in both figures confirm our intuitions: a low α/β_1 ratio translates to a relatively small cost for a fiber connection, thus the optimal networks tend to have higher normalized optimal node degree (a densely connected network); a high α/β_1 ratio translates to a relatively large cost for a fiber connection,

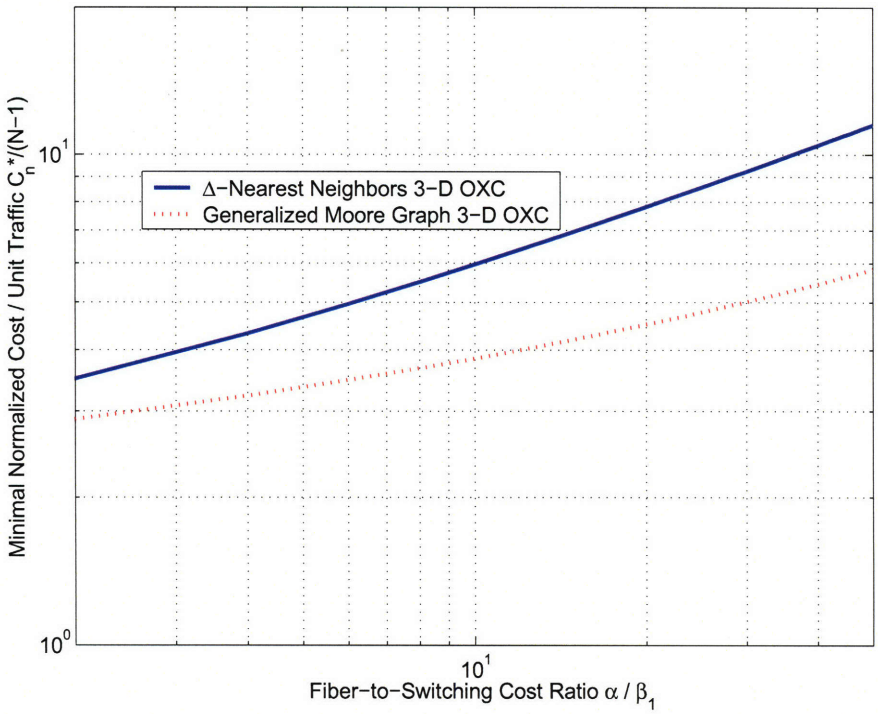

Figure 6-11: Normalized optimal node degree as a function of fiber-to-switching cost ratio α/β_1 for 3-D OXC. The network size is set as $N = 100$.

thus the optimal networks tend to be sparsely connected. We also note that per node cost increases monotonically with the ratio, as shown in Figure 6-11. To explain this trend, we plot in Figure 6-12 how the optimal fiber cost and optimal switching cost (both normalized to per node per unit traffic) change with ratio. Figure 6-12 shows that as per fiber connection cost α becomes more expensive relative to per port switching cost β_1, the optimal connectivity tends to decrease – the optimal physical topology uses less fibers. However, the actual fiber cost (the product of the optimal node degree Δ^* and the cost per fiber connection α) still increases. Moreover, as the result of a sparser network, a lightpath on average travels through more hops, increasing the number of ports, thus the cost of switching.

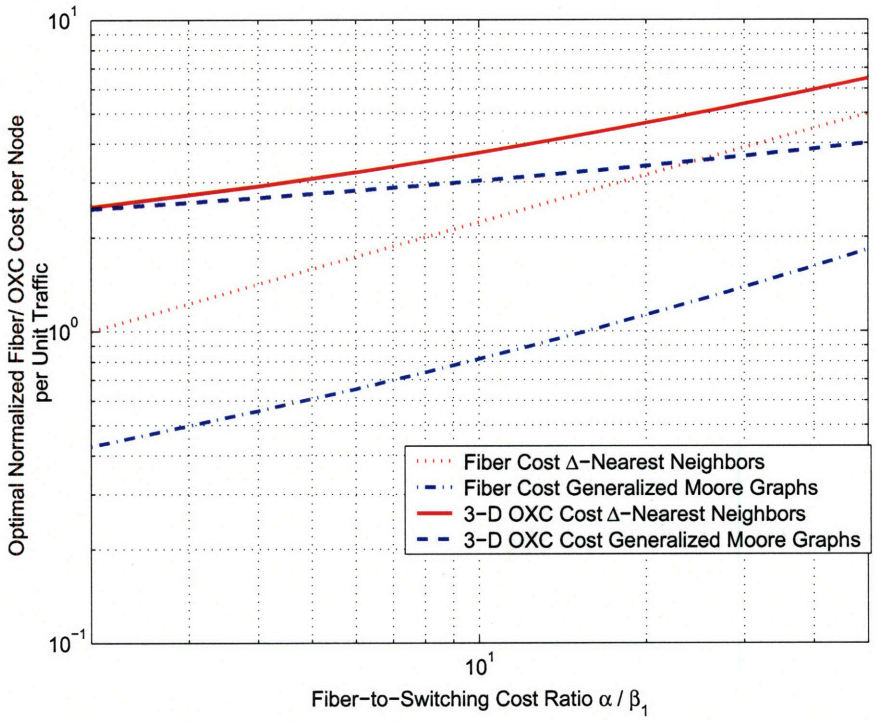

Figure 6-12: Optimal normalized fiber cost and optimal normalized 3-D OXC cost as functions of fiber-to-switching cost ratio α/β_1. The network size is set as $N = 100$.

6.4.4 Network Scalability as Traffic Increase

Our analytical results in Table 6.1 to Table 6.3 show that the optimal network node degree is also a function of wavelengths of traffic t between node pairs. The normalized optimal node degree $\Delta^*/(N-1)$ versus t is shown in Figure 6-13 for combinations of two classes of topologies and three types of OXC switching fabrics. The dependencies for fully connected mesh networks and ring topologies are also plotted for reference. It is shown in this figure that the Moore Graphs maintain smaller optimal connectivity than the Δ-nearest Neighbors topologies do for every type of OXC switching fabrics. In other words, Moore Graphs have better scalability. The impact of switching technologies is shown again in Figure 6-13 – networks with 3-D switching fabrics have the best scalability, while networks with 2-D switching fabrics do not scale well, in the sense that networks tend to be fully connected when the traffic between node pairs exceeds a certain value. In Figure 6-14, we plot the corresponding minimal normalized network cost per unit traffic with respect to t. The plot illustrates the trend that as the traffic between node pair increases, the minimal normalized cost per unit traffic actually decreases for networks using 3-D or multi-stage switching fabrics; while it increases for that using 2-D switching fabrics.

6.4.5 Comparisons of OXC and OEO Switches

In this section we turn our attention to OEO-switched WDM networks. The focus is to compare the relative cost benefits of deploying OXC or OEO switches in the network. As stated in Section 5.3.3, the cost of an OEO switch depends also on the port rate R and data rate per wavelength r; while the cost of an OXC switch can be considered as rate independent. Based on Table 6.1 and Table 6.3, in Figure 6-15 we plot the minimal normalized network cost C_{n}^* as a function of data rate per wavelength for two classes of network topologies (Δ-nearest Neighbors and Moore Graphs) in conjunction with two types of switching fabrics (OEO switch and 3-D OXC). The network size, fiber connection cost, OEO per port cost, and 3-D OXC per port cost are set as $N = 50$, $\alpha = 20$, $\beta_e = 7.5$, and $\beta_1 = 1$, respectively. We also assume that there is one

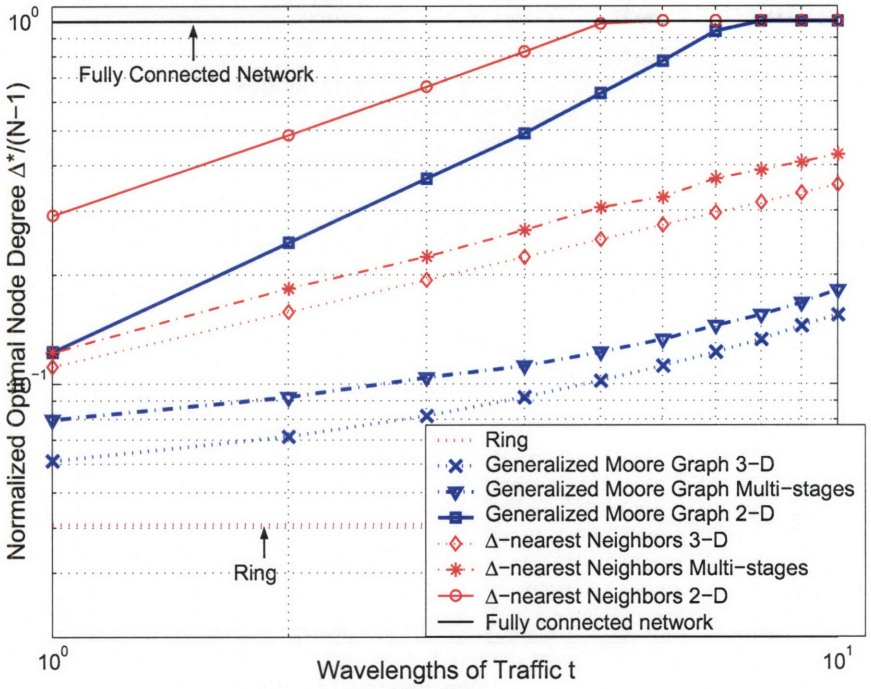

Figure 6-13: Normalized optimal node degree $\Delta^*/(N-1)$ as a function of the wavelengths of traffic between a source-destination pair, under uniform traffic. The size of the network is fixed at $N = 50$. The fiber and switching cost parameters are: $\beta_1 = 1$, $\alpha/\beta_1 = 40$, and $\beta_1 = 5\beta_2 = 32\beta_3$.

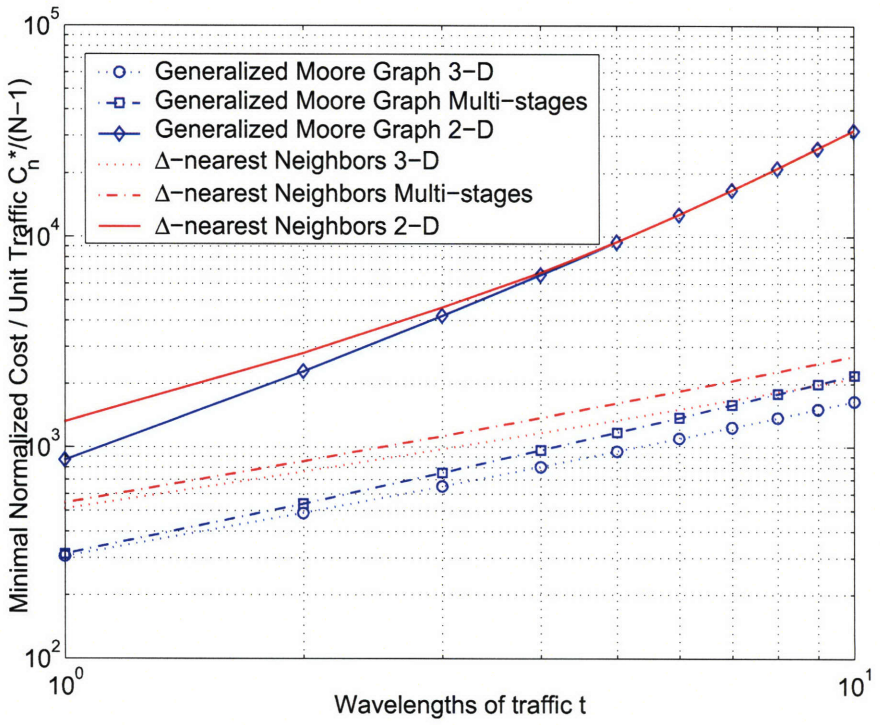

Figure 6-14: Minimal normalized cost per unit traffic $C_{\mathrm{n}}^{*}/(N-1)$ as a function of the wavelengths of traffic between a source-destination pair, under uniform traffic. The size of the network is fixed at $N = 50$. The fiber and switching cost parameters are: $\beta_1 = 1$, $\alpha/\beta_1 = 40$, and $\beta_1 = 5\beta_2 = 32\beta_3$.

wavelength of traffic between each node pair, i.e., $t = 1$. Figure 6-15 shows that the minimal normalized cost of a network with OXC switches does not depend on the data rate carried by each wavelength; while the normalized minimal cost for a network with OEO switches increases as the per wavelength data rate increase. At low data rate, it is economical to use OEO switches; as the per wavelength data rate increases, using 3-D OXC becomes more favorable. Figure 6-16 plots the minimal normalized network cost per unit traffic per data rate C_{n}^{*}/r as a function of data rate per wavelength for combinations of two classes of network topologies (Δ-nearest Neighbors and Moore Graphs) and two types of switching fabrics (OEO switch and 3-D OXC). This plot demonstrates that at high data rate (>10 Gb/s), networks with 3D-OXC exhibit much better scalability in terms of minimal normalized network cost per data rate, primarily due to the fact that the cost of OXC switches are intrinsically independent of data rate. In Figures 6-17, we plot minimal normalized network cost per data rate $C_{\mathrm{n}}^{*}/[(N-1)r]$ as a function of network size N, for the same combinations of two classes of network topologies and two types of switching fabrics, with per wavelength data rate set at 0.625 Gb/s (an OC-12 connection). In 6-18 we plot the same dependency with per wavelength data rate of 2.5 Gb/s (an OC-48 connection). From these plots, we again come to the conclusion that at a low data rate, it is economical to use OEO switches; at a high data rate, it is more cost-advantageous to use OXC switches.

6.4.6 Section Summary

In this thesis, we adopt an analytical approach to find cost-effective physical topologies and to select scalable switching technologies. We have so far focus on regular networks and static uniform traffic model. By setting up a first order cost model and analyzing the tradeoff between fiber and switching resources, we have found that for regular networks and uniform traffic, the joint design problems of physical topology, dimensioning, and routing can be solved optimally and analytically. We prove that with minimum hop routing, Generalized Moore Graphs achieve the lower bound on network cost and are good reference topologies. We also show that topologies with structures close to those of Generalized Moore Graphs can achieve near-optimal cost.

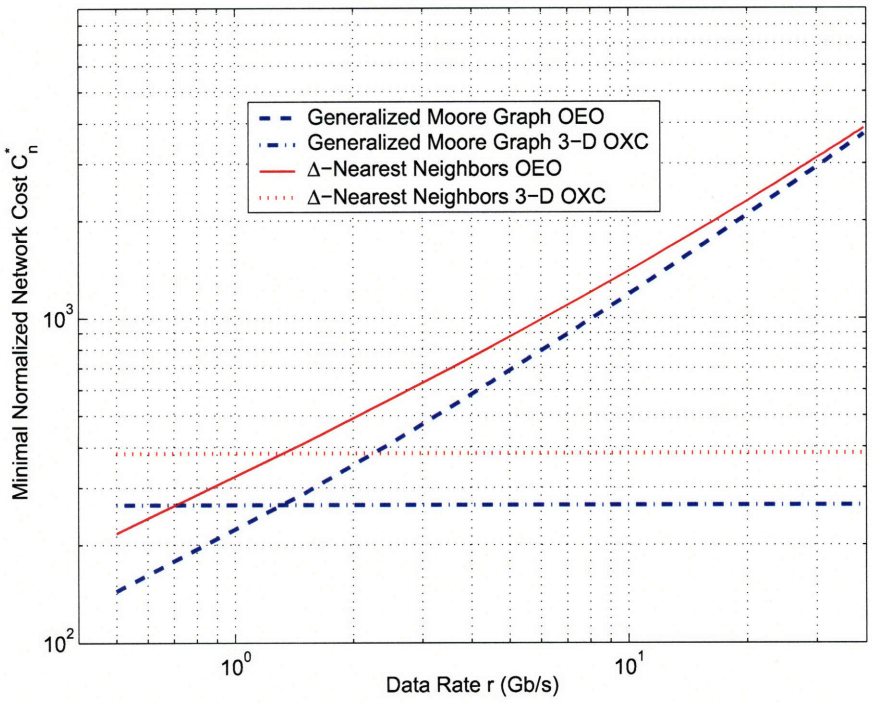

Figure 6-15: Minimal normalized network cost as a function of data rate per wavelength for combinations of two classes of network topologies (Δ-Nearest Neighbors and Generalized Moore Graphs) and two types of switching fabrics (OEO switch and 3-D OXC). $N = 50$, $\alpha = 20$, $\beta_1 = 1$, and $\beta_e = 7.5$.

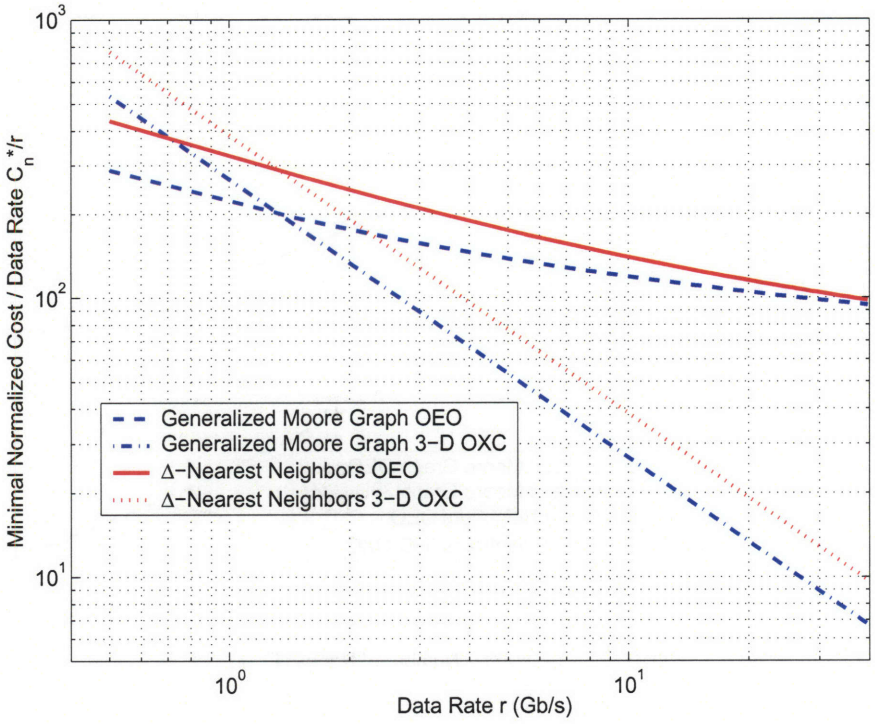

Figure 6-16: Minimal normalized network cost per data rate C_{n}^*/r as a function of data rate per wavelength for combinations of two classes of network topologies (Δ-Nearest Neighbors and Generalized Moore Graphs) and two types of switching fabrics (OEO switch and 3-D OXC). $N = 50$, $\alpha = 20$, $\beta_1 = 1$, and $\beta_{\mathrm{e}} = 7.5$.

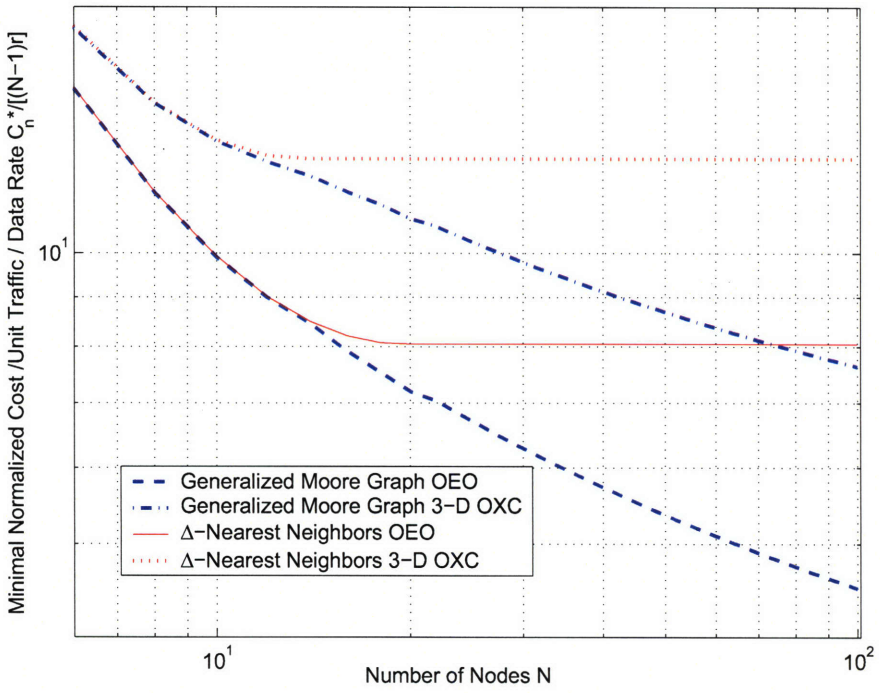

Figure 6-17: Minimal normalized network cost per unit traffic per data rate $C_{\mathrm{n}}^{*}/[(N-1)r]$ as a function of network size N, for combinations of two classes of network topologies (Δ-nearest Neighbors and Generalized Moore Graphs) and two types of switching fabrics (OEO switch and 3-D OXC), $r = 0.625$Gb/s, $\alpha = 20$, $\beta_1 = 1$, and $\beta_{\mathrm{e}} = 7.5$.

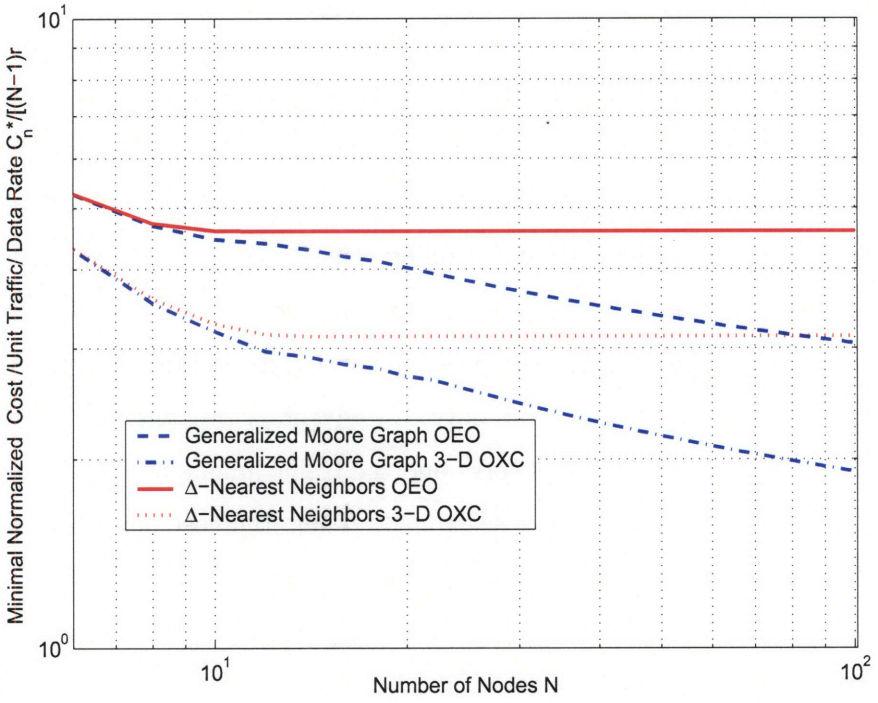

Figure 6-18: Minimal normalized network cost per unit traffic per data rate $C_{\mathrm{n}}^*/[(N-1)r]$ as a function of network size N, for combinations of two classes of network topologies (Δ-nearest Neighbors and Generalized Moore Graphs) and two types of switching fabrics (OEO switch and 3-D OXC), $r = 2.5$Gb/s, $\alpha = 20$, $\beta_1 = 1$, and $\beta_{\mathrm{e}} = 7.5$.

With simple network cost structures, closed-form solutions of the optimal degree and cost as functions of various network design parameters (such as network size and wavelengths of traffic between node pairs) are obtained. These results show that for a metropolitan area network of moderate size (a few tens to a few hundred nodes), neither rings nor fully connected mesh networks are optimal topologies. The optimal network connectivity is in the range of $0.03N$ to $0.1N$. The advantages of analytical approaches are self-evident: they provide valuable references on how the optimal network connectivity scales as the design parameters change. More importantly, the results demonstrate that switching technologies have a tremendous impact on the final topological architectures. The optimal topologies connecting the same set of nodes can differ significantly when different switching fabrics are used, even when these topologies are designed to serve the same traffic demand. Among all-optical technologies currently available, for smaller networks (a few to a dozen nodes) and light traffic, 2-D switching fabrics have cost advantage over the 3-D switching fabrics. However, as the size of the networks and the traffic among node pairs increases, 3-D switching fabrics have the best scalability. Thus, the cost benefit of deploying the latter type of technology for the future becomes apparent. Moreover, a comparison of the cost benefit between OXC and OEO switches shows that at a low data rate, it is economical to use OEO switches; at a high data rate, it is more cost-advantageous to use OXC switches.

The results presented in this section demonstrate the importance of making the right choices on both physical topologies and switching technologies in the network design process. At this stage, we shall also caution that the plots presented in this chapter serve primarily to illustrate the trends and the scaling of optimal topologies as functions of network parameters, traffic demands, and technologies, rather than to make a definitive recommendation based on the exact values in the plots.

6.5 Chapter Appendix

As shown in Section 6.3.1, the normalized network cost C_n is convex in Δ for the three classes of topologies: Δ-nearest Neighbors, Symmetric Hamilton Graphs, and Moore Graphs. We now proceed to find the optimal node degree as a function of N for these topologies in combination with different types of switching fabric: 3-D, multi-stage, 2-D, and electronic (OEO).

6.5.1 Δ-Nearest Neighbors Topoloy

The average minimum hop distance can be approximated using (6.16). This approximated average minimum hop distance is a convex function of node degree Δ.

3-D Switching Fabrics

The derivation of optimal node degree for Δ-nearest Neighbors networks with 3-D OXC switching fabrics is already presented in Section 6.3.2 and is thereby omitted here.

Multi-Stage Switching Fabrics

For multi-stage switching fabrics the OXC cost function has the form of $F_2(K_o) = \beta_2 K_o^{1+\theta} \log_2 K_o$. In the following θ is set to 0 for simplicity. The optimal node degree Δ^* shall satisfy

$$\alpha\Delta^{*2} - \beta_2 t\frac{(N-1)^2}{2\ln 2}\ln[\frac{3t(N-1)}{2} + \frac{t(N-1)^2}{2\Delta^*}] - \beta_2 t\frac{(N-1)^2}{2\ln 2} = 0. \qquad (6.27)$$

This optimality condition is a transcendental equation that can be solved numerically with given α, β_2, and N.

2-D Switching Fabrics

For 2-D switching fabrics, the switch cost function has the form of $F_3(K_o) = \beta_3 K_o^{2+\delta}$. In the following δ is set to 0 for simplicity. When the constraint is inactive, the

optimality condition for Δ^* is

$$\alpha\Delta^{*3} - \beta_3 t^2 \frac{3(N-1)^3}{2}\Delta^* - \beta_3 t^2 \frac{(N-1)^4}{2} = 0. \tag{6.28}$$

Solving for optimal node degree Δ^*, we have the only real and positive solution

$$\begin{aligned}\Delta^* &= \frac{1}{2^{\frac{1}{3}}}\left(\frac{\beta_3 t^2}{\alpha}\right)^{\frac{1}{3}}(N-1)^{\frac{4}{3}}\left\{1+\left[1-\left(\frac{2\beta_3 t^2}{\alpha}\right)(N-1)\right]^{\frac{1}{2}}\right\}^{\frac{1}{3}} \\ &+ \frac{1}{2^{\frac{2}{3}}}\left(\frac{\beta_3 t^2}{\alpha}\right)^{\frac{2}{3}}(N-1)^{\frac{5}{3}}\left\{1+\left[1-\left(\frac{2\beta_3 t^2}{\alpha}\right)(N-1)\right]^{\frac{1}{2}}\right\}^{\frac{-1}{3}}.\end{aligned} \tag{6.29}$$

In the case of 2-D switching fabrics, optimal node degree Δ^* grows with the linear combination of N polynomials,

$$\Delta^* \propto c_1 t^{\frac{2}{3}} N^{\frac{4}{3}} + c_2 t^{\frac{4}{3}} N^{\frac{5}{3}}, \tag{6.30}$$

where c_1 and c_2 are constants. When Δ^* becomes larger than $N-1$, the constraint $2 \leq \Delta \leq N-1$ becomes active. Hence, $\Delta^* = N-1$, i.e., the optimal topology is fully connected.

OEO Switching Fabrics

The derivation of optimal node degree for OEO switching fabrics is similar to that for 3-D OXC. The optimality condition leads to

$$\alpha - \frac{\beta_e t r}{R\eta}\frac{(N-1)^2}{2\Delta^{*2}} = 0. \tag{6.31}$$

Solving Δ^* yields

$$\Delta^* = \frac{1}{\sqrt{2}}\left(\frac{\beta_e t r}{\alpha\eta R}\right)^{\frac{1}{2}}(N-1). \tag{6.32}$$

6.5.2 Symmetric Hamilton Graph

As presented in Section 4.3.2, we can approximate the average minimum hop distance of a Symmetric Hamilton Graph as

$$H_{\min} = \frac{3}{4} + \frac{N-2}{4(\Delta-1)}. \tag{6.33}$$

This approximated average minimum hop distance is convex in Δ.

3-D Switching Fabrics

With 3-D switching fabrics, the optimality condition leads to

$$\alpha - \beta_1 \frac{(N-1)(N-2)}{4(\Delta^*-1)^2} = 0. \tag{6.34}$$

Solving for Δ^* yields

$$\Delta^* = \frac{1}{2}\left(\frac{\beta_1 t}{\alpha}\right)^{\frac{1}{2}} \sqrt{(N-1)(N-2)} + 1. \tag{6.35}$$

Multi-Stage Switching Fabrics

For multi-stage switching fabrics, the optimal node degree Δ^* satisfies:

$$\begin{aligned} \alpha(\Delta^*-1)^2 &- \beta t \frac{(N-1)(N-2)}{4\ln 2} \ln\left[\frac{7t(N-1)}{4} + \frac{t(N-1)(N-2)}{4(\Delta^*-1)}\right] \\ &- \beta_2 t \frac{(N-1)(N-2)}{4\ln 2} = 0. \end{aligned} \tag{6.36}$$

The optimality condition is a transcendental equation that can be solved numerically with given α, β_2, and N.

2-D Switching Fabrics

Similarly, for 2-D OXC switching fabrics we have the optimality equation

$$\alpha(\Delta^*-1)^3 - \beta_3 t^2 \frac{7(N-1)^2(N-2)}{8}(\Delta^*-1) - \beta_3 t^2 \frac{(N-1)^2(N-2)^2}{8} = 0. \tag{6.37}$$

For large N, solving for Δ^* yields

$$\begin{aligned} \Delta^* \approx\ & \frac{1}{4}\left(\frac{\beta_3 t^2}{\alpha}\right)^{\frac{1}{3}} (N-1)^{\frac{4}{3}} \left\{4 + \frac{2}{9}\left[2^2\cdot 3^3 - 6\cdot 7^3\left(\frac{\beta_3 t^2}{\alpha}\right)(N-1)\right]^{\frac{1}{2}}\right\}^{\frac{1}{3}} \\ &+ 14\left(\frac{\beta_3 t^2}{\alpha}\right)^{\frac{2}{3}} (N-1)^{\frac{5}{3}} \left\{4 + \frac{2}{9}\left[2^2\cdot 3^3 - 6\cdot 7^3\left(\frac{\beta_3 t^2}{\alpha}\right)(N-1)\right]^{\frac{1}{2}}\right\}^{-\frac{1}{3}} \end{aligned} \tag{6.38}$$

The optimal node degree of a Symmetric Hamilton Graph is also a linear combination of N polynomials,

$$\Delta^* \propto c_3 t^{\frac{2}{3}} N^{\frac{4}{3}} + c_4 t^{\frac{4}{3}} N^{\frac{5}{3}}, \tag{6.39}$$

where c_3 and c_4 are constants.

OEO Switching Fabric

The derivation of optimal node degree for OEO switching fabric is similar to that for 3-D OXC. One can simply replace β_1 with $\beta_e r/R\eta$, thus the optimal node degree Δ^* is

$$\Delta^* = \frac{1}{2}\left(\frac{\beta_e tr}{\alpha\eta R}\right)^{\frac{1}{2}}\sqrt{(N-1)(N-2)}+1, \tag{6.40}$$

which can be approximated as

$$\Delta^* \approx \frac{1}{2}\left(\frac{\beta_e tr}{\alpha\eta R}\right)^{\frac{1}{2}}(N-1)+1, \tag{6.41}$$

when N is large.

6.5.3 Generalized Moore Graphs

The exact expression of average minimum hop distance for a Generalized Moore Graph in (4.9) is not only cumbersome but also discontinuous due to the ceiling function in the expression. Our purpose here is to gain some insight into the asymptotic behavior of optimal node degree for a Generalized Moore Graph. As derived in Section 4.5.3, by assuming $\Delta \approx \Delta - 1$ and $N \gg \Delta$, we can approximate the average minimum hop distance $H_{\min}$ for a Moore Graph of size N and degree Δ as

$$H_{\min}(N,\Delta) = \log_\Delta N. \tag{6.42}$$

3-D Switching Fabrics

For 3-D OXC switching fabrics, the optimality condition leads to

$$\Delta^*(\ln\Delta^*)^2 = \frac{\beta_1 t}{\alpha}(N-1)\ln N. \tag{6.43}$$

Solving for Δ^* yields

$$\Delta^*(N) = \frac{1}{4}\left(\frac{\beta_1 t}{\alpha}\right)(N-1)\frac{\ln N}{\left\{W\left(\frac{\sqrt{(\beta_1 t/\alpha)(N-1)\ln N}}{2}\right)\right\}^2}, \tag{6.44}$$

where $W(x)$ denotes the Lambert function. Lambert function is the inverse of the function $f(W) = We^W$. When $x > 3$, $W(x)$ can be well approximated as

$$W(x) \approx \ln x - \ln[\ln x] + \frac{\ln[\ln x]}{\ln x}. \tag{6.45}$$

Let $a = \beta_1 t/\alpha$, for large N (e.g., $N > 100$ and $a = 1/40$), Δ^* can be approximated as

$$\frac{a}{4} \frac{\ln N}{\left\{\frac{1}{2}\ln[\frac{a}{4}(N-1)\ln N] - \ln[\frac{1}{2}\ln[\frac{a}{4}(N-1)\ln N]] + \frac{\ln[\frac{1}{2}\ln[\frac{a}{4}(N-1)\ln N]]}{\frac{1}{2}\ln[\frac{a}{4}(N-1)\ln N]}\right\}^2}. \tag{6.46}$$

Multi-Stage Switching Fabrics

For Multi-stage switching fabric, the optimality condition leads to

$$\begin{aligned} \alpha &- \beta_2 t \frac{(N-1)\ln N \ln[t(N-1)]}{\Delta^*(\ln\Delta^*)^2 \ln 2} \\ &- \beta_2 t \frac{(N-1)\ln N \ln(\log_{\Delta^*} N + 1)}{\Delta^*(\ln\Delta^*)^2 \ln 2} \\ &- \beta_2 t \frac{(N-1)\ln N}{\Delta^*(\ln\Delta^*)^2 \ln 2} = 0. \end{aligned} \tag{6.47}$$

The optimality condition is a transcendental equation, which can be solved numerically with given α, β_2, and N.

2-D Switching Fabrics

For 2-D switching fabrics, the optimality condition leads to

$$\alpha - 2\beta_3 t^2 (N-1)^2 \frac{[\ln N]^2}{(\ln\Delta^*)^3 \Delta^*} = 0. \tag{6.48}$$

Solving for Δ^* yields

$$\Delta^*(N) = \frac{2}{27}\left(\frac{\beta_3 t^2}{\alpha}\right)(N-1)^2 \frac{(\ln N)^2}{\left\{W\left(\frac{2^{\frac{1}{3}}}{3}\left[\left(\frac{\beta_3 t^2}{\alpha}\right)(N-1)^2(\ln N)^2\right]^{\frac{1}{3}}\right)\right\}^3}, \tag{6.49}$$

where $W(x)$ denotes the Lambert function. Let $a = \beta_3 t^2/\alpha$, for large N (e.g., $N > 100$ and $a = 1/40$), Δ^* can be well approximated as

$$\Delta^*(N) \approx \frac{2a}{27} \frac{(N-1)^2(\ln N)^2}{\left\{\frac{1}{3}\ln[\frac{2a}{27}(N-1)\ln N] - \ln[\frac{1}{3}\ln[\frac{2a}{27}(N-1)\ln N]] + \frac{\ln[\frac{1}{3}\ln[\frac{2a}{27}(N-1)\ln N]]}{\frac{1}{3}\ln[\frac{2a}{27}(N-1)\ln N]}\right\}^3}. \tag{6.50}$$

OEO Switching Fabric

The derivation of optimal node degree for OEO switching fabric is similar to that for 3-D OXC. One can simply replace the β_1 with $\beta_e r/R\eta$, thus the optimal node degree Δ^* is

$$\Delta^*(N) = \frac{1}{4}\left(\frac{\beta_e rt}{\alpha R\eta}\right)(N-1)\frac{\ln N}{\left\{W\left(\frac{\sqrt{(\beta_e rt/\alpha R\eta)(N-1)\ln N}}{2}\right)\right\}^2}. \tag{6.51}$$

Chapter 7

Routing and Wavelength Assignment (RWA) for Generalized Moore Graphs

When we addressed the OXC cost in Chapter 5 and 6, we implicitly suppressed the wavelength continuity constraints by assuming that either there are infinite number of wavelengths or a full wavelength conversion is available. As such, K_o ports are enough to switch K_o lightpaths, without causing wavelength blocking. The first assumption is realistic, given the abundance of wavelengths in the metropolitan environment. The second assumption is less realistic, given the fact that the current price of converters is still high. This motivates us to expand the scope of this thesis by exploring whether minimum hop routing algorithm, which minimizes the network switching cost, also minimizes the number of wavelengths required to establish all-to-all uniform lightpath connections for Moore Graphs, especially when wavelength conversion is not available. Our approach is to construct upper and lower bounds on the minimal number of wavelengths required: if the differences between the upper bound and lower bound are small, then we can conclude that Moore Graphs exhibit good efficiency in wavelength dimensioning.

7.1 Definition and General Solving Approaches of RWA Problems

We define the RWA problem as follows: given a network fiber topology and a set of end-to-end lightpath requests, we are to determine routes and assign wavelengths that require the minimal possible number of wavelengths. If the routing is already provided, we only need to deal with the wavelength assignment (WA) problem. In solving a WA problem, the following constraints, usually referred to as *wavelength continuity constraints*, must be obeyed:

- Any two different lightpaths must be assigned with different wavelengths on a given fiber.
- If wavelength conversion is not available, a lightpath must be assigned with the same wavelength on all the fibers of its route.

There are in general two approaches to solve a WA problem for a set of lightpaths and a given fiber topology. The first approach involves setting up the WA problem in the form of mathematical programming and solving it by using techniques such as linear programming (LP) or nonlinear programming (NLP)[4][9]. The second approach involves first constructing either a *node equivalence graph* or an *edge equivalence graph* and then solving the related problems of *node coloring* or *edge coloring*. In this thesis, we concentrate on the second approach, since this approach usually allows us to exploit good properties that are intrinsic to certain lightpath patterns (logical topologies) and fiber topologies. A comparison of node coloring and edge coloring approaches are summarized in Table 7.1. Next we provide detailed descriptions of the "graph coloring" approach [33].

First, we consider node coloring approach – constructing a node equivalence graph and solving the corresponding node coloring problem. For clarity, we again denote a given fiber topology as G and a set of lightpaths as P. We construct a node equivalence graph, denoted as G_N, as follows: each node in G_N corresponds to a lightpath in P and two nodes in G_N are connected by an (undirected) edge, if the two

Table 7.1: Comparison of node coloring and edge coloring approaches for solving RWA problems

	Node Coloring	Edge Coloring
Limitation on the length of a lightpath	No limitations	≤ 2 hops
Node of the equivalence graph	Represents a lightpath	Represents an edge of the fiber topology
Edge of the equivalence graph	If two lightpaths share at least one node	If two edges are used in one lightpath
Minimum number of wavelength required	Node chromatic number	Edge chromatic number

corresponding lightpaths in P share a common fiber. Once G_N is constructed, solving the WA problem is then equivalent to solving the classical node coloring problem in G_N. That is, we find an assignment of colors to nodes of G_N in such a way that adjacent nodes have distinct colors and the minimal number of colors is used. The minimal number of colors needed to color the nodes in this manner is called the *node chromatic number* of the graph G_N, denoted as $\chi(G_N)$. These colors correspond to wavelengths used on G. Thus the minimal number of wavelengths required for the WA problem equals to $\chi(G_N)$. There is a known result that provides an upper bound on the node chromatic number for a connected graph with maximal node degree [51], as summarized in the following:

Theorem 10 *Let G_N be a connected graph with maximal degree $\Delta_{\max}$. Suppose G_N is neither a complete graph nor an odd cycle, then $\chi(G) \leq \Delta_{\max}$.*

Next we consider the edge coloring approach – constructing an edge equivalent graph and solving the associated edge coloring problem. Unlike the node coloring approach, which has no limitation on the length (in the number of hops) of a lightpath request, the edge coloring approach can only apply to special cases in which all

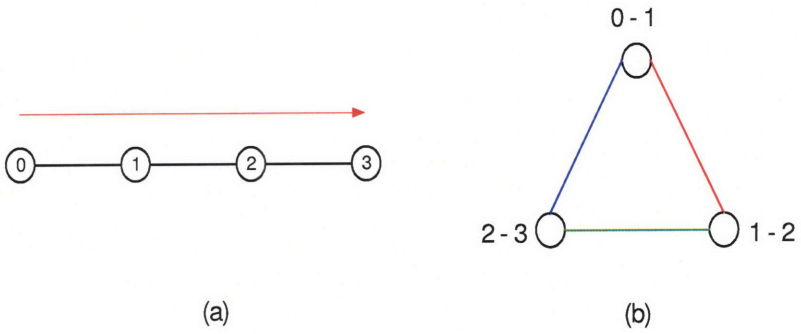

Figure 7-1: (a) A line topology and a lightpath request of 3 hops; (b) The WA result when edge coloring approach is used. This figure illustrates why the edge coloring approach can only be applied to solve WA for lightpaths of no more than 2 hops. In this example, it is trivial to see that one wavelength is enough to support this lightpath of three hops. However, if we used the edge equivalence graph approach, the constructed edge equivalence graph would be a 3-node ring, for which 3 colors (wavelengths) are required to ensure that all edges incident on a node are shaded with different colors.

lighpaths have at most two hops. The edge equivalent graph, denoted as G_L, is constructed as follows: for every edge $e \in E$ of the original fiber topology, we introduce a node ν_e in G_L. For a lightpath that uses both the edges e_1 and e_2, $e_1 \neq e_2$, we add an (undirected) edge that connects ν_{e_1} and ν_{e_2}. Once G_L is constructed, solving the WA problem is then equivalent to solving the edge coloring problem of G_L. That is, we are to find the *edge chromatic number* $\Lambda_e(G_L)$ of G_L – the minimal number of colors to be assigned to the edges of G_L, such that all edges incident on a node in G_L have different colors. These colors correspond to wavelengths used in the original fiber network G.

To illustrate why edge coloring approach can only be applied to solve RWA for lightpaths of no more than two hops, we provide a simple example, as shown in Figure 7-1. We set up a lightpath of 3 hops on a line topology. It is trivial to see

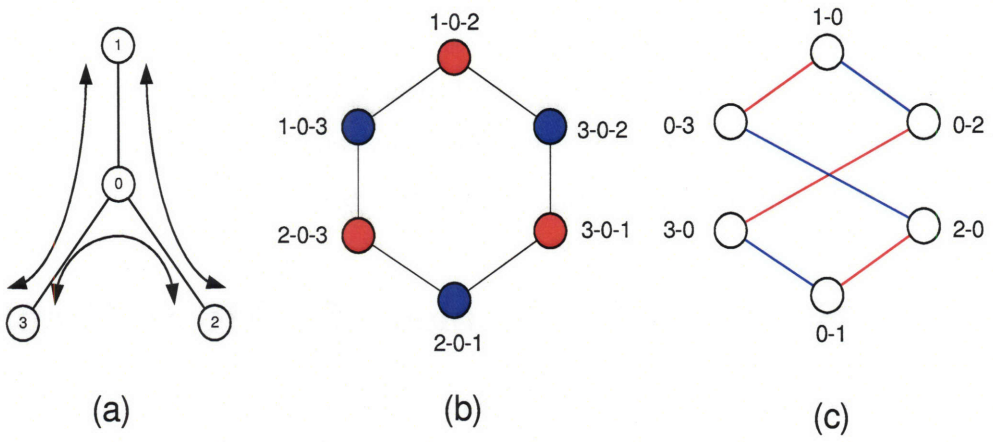

Figure 7-2: (a) End-to-end lightpath requests on a star topology: $1 \rightarrow 2$, $2 \rightarrow 1$, $1 \rightarrow 3$, $3 \rightarrow 1$, $2 \rightarrow 3$, and $3 \rightarrow 2$; (b) The node equivalence graph and the corresponding node coloring; (c) The edge equivalence graph and the corresponding edge coloring.

that 1 wavelength is enough to support this lightpath. However, if we used the edge equivalence graph approach, the constructed edge equivalence graph would be a 3-node ring, for which 3 colors are required to ensure that all edges incident on a node have different colors. In other words, an edge chromatic number of 3 would indicate that 3 wavelengths are required for setting up the lightpath. Obviously this is not true.

There is also a known result that provides an upper bound on the edge chromatic number for a connected graph with maximal node degree $\Delta_{\max}$[52][53], as summarized in the following:

Theorem 11 *For a connected graph G_L with a maximal node degree $\Delta_{\max}$, the edge chromatic number $\Lambda_e(G_L)$ is either $\Delta_{\max}$ or $\Delta_{\max} + 1$.*

To show how we can use both node equivalence graph and edge equivalence graph approaches to solve RWA problems, we provide a simple example. As shown in Figure 7-2 (a), we setup all-to-all uniform lightpath requests on a star network of 4 nodes. Figure 7-2 (b) and (c) show the constructed node and edge equivalence

graphs, respectively. Note that since there is a unique minimum path between any pair of nodes in a star topology, both the node-equivalence and the edge-equivalence graphs are unique. It is straightforward to show that both node chromatic and edge chromatic numbers are 2. We thus reach the conclusion that two wavelengths are required to support the uniform lightpath requests.

7.2 Solving RWA Problems for Moore Graphs

In this section, we study whether minimum hop routing algorithm, which minimizes the network cost, also minimizes the number of wavelengths required to establish all-to-all uniform lightpath connections for Moore Graphs. In Theorem 2 of Chapter 4, we showed that, for Moore Graphs, with minimum hop routing, the total network load generated by uniform all-to-all traffic can be evenly distributed on every fiber. In this section, we rely on this property to solve the RWA problem for a Moore Graph. For clarity, we again summarize the result of balanced load distribution.

Theorem 12 *(Theorem 2) For a Moore Graph of degree Δ and diameter D, balanced load distribution can be achieved for the static uniform all-to-all traffic, with each edge having a load of $\sum_{i=1}^{D} i(\Delta-1)^{i-1}$.*

We first consider the case when wavelength conversion is available, then the WDM network is logically identical to the traditional circuit-switched networks. With wavelength conversion, the joint RWA problem is simplified to a routing problem with the objective of minimizing the maximum load on each fiber. A direct application of balanced load distribution result (Theorem 12) leads to a conclusion that the minimum hop routing does minimize the number of wavelengths for uniform traffic. In other words, any other routing algorithms require at least the same number of wavelengths to support the same traffic demand.

We next consider the case when wavelength conversion is not available. For this case, RWA becomes rather complicated because of the wavelength continuity constraints. Since no two lightpaths that share a common fiber can use the same wavelength, the balanced load result (Theorem 12) can only be used to construct a lower

Table 7.2: RWA results for Moore Graphs

Graph	Node number Node degree, and diameter	Min. no. of wavelengths with conversion	Min. no. of wavlengths without conversion
Fully connected graphs	$\Delta = N - 1$ $D = 1$	1	1
Rings (with odd no. of nodes)	N is odd $\Delta = 2$	$\frac{N^2-1}{8}$	$\frac{N^2-1}{8}$
Petersen Graph	$N = 10$, $\Delta = 3$, and $D = 2$	5	5
Hoffman-Singleton Graph	$N = 50$, $\Delta = 7$ and $D = 2$	13	≤ 14
Possible $N = 3250$ $\Delta = 57$, and $D = 2$	$N = 3250$ $\Delta = 57$, and $D = 2$	113	≤ 114

bound on the number of wavelengths required. As such, we first solve the RWA problem for each instance of Moore Graphs and later extrapolate the solutions to a general result. RWA results for all the instances of Moore Graphs are summarized in Table 7.2.

We start with a fully connected (complete) graph, which can be treated as a (trivial) Moore Graph. In a complete graph, each node reaches every other node in exactly one hop. It is trivial that such a graph requires exactly one wavelength with or without wavelength conversion.

We next consider ring topologies (with odd number of nodes). A known result [33] shows that it requires the same (minimal) number of wavelengths, indifferent to the wavelength conversion capabilities of the network. The minimal number of wavelength required is $(N^2 - 1)/8$.

The rest instances of the existing Moore Graphs all have diameters of 2, that is, the longest lightpath has 2 hops. Using this property, we can transform a RWA

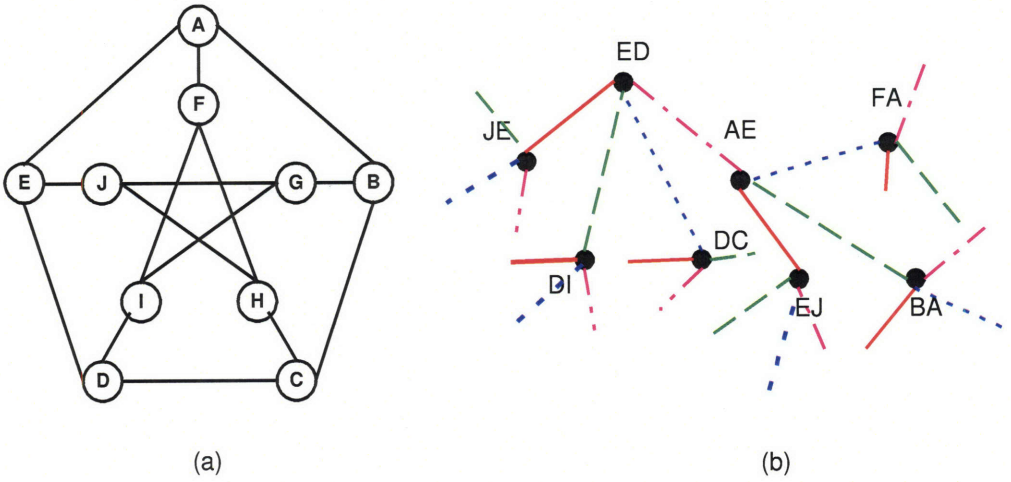

Figure 7-3: (a) Petersen Graph; (b) Part of the edge equivalence graph G_L and the edge coloring of the Petersen Graph.

problem into an edge coloring problem of an equivalence graph G_L and obtain a tight upper bound on the minimal number of wavelengths. In other words, for a Moore Graph (of diameter 2), finding the minimal number of wavelengths to support a given set of lightpath requests is the same as finding the edge chromatic number of the corresponding G_L. An example of constructing edge equivalence graph of the Petersen Graph is shown in Figure 7-3.

For solving a RWA, lightpaths using only a single fiber (edge) can always be assigned a wavelength independently from other lightpaths (using more than one fiber). Thus we only need to consider lightpaths of two hops. As shown in the proof for Theorem 12 (cf. Section 4.5.2), for a Moore Graph under uniform all-to-all traffic, each fiber is used as a first hop (of a two-hop path) for $\sum_{i=1}^{D-1}(\Delta-1)^i$ times ($D=2$); each fiber is used as a second hop (of a two-hop path) for $(\Delta-1)^{D-1}$ times ($D=2$).

In other words, the equivalence graph is regular with a node degree

$$\begin{aligned}\Delta(G_L) &= (\Delta-1)^{2-1} + \sum_{i=1}^{2-1}(\Delta-1)^i \\ &= \sum_{i=1}^{D=2} i(\Delta-1)^{i-1} - 1. \end{aligned} \tag{7.1}$$

According to Theorem 11, the minimal number of wavelengths to support all the lightpaths of two hops is at most

$$\Delta(G_L) + 1 = \sum_{i=1}^{D=2} i(\Delta-1)^{i-1}. \tag{7.2}$$

Adding one additional wavelength that is used for the lightpath of one hop, we can have an upper bound on the minimal number of wavelength W_{M} as

$$W_{\mathrm{M}} \leq 1 + \sum_{i=1}^{D=2} i(\Delta-1)^{i-1}. \tag{7.3}$$

In summary, Theorem 12 provides a lower bound on the minimal number of wavelengths required for a Moore Graph. For complete graphs and rings, it requires the same (minimal) number of wavelengths with or without wavelength conversions. An upper bound on the minimal number of wavelengths is given in (7.3). By combining these results, we extrapolate to the following general conclusion on the minimal number of wavelengths used to support all-to-all uniform traffic:

Theorem 13 *For a Moore Graph of degree Δ and diameter D, a minimal number of wavelengths required to support all-to-all uniform traffic with or without wavelength conversions satisfies*

$$\sum_{i=1}^{D} i(\Delta-1)^{i-1} \leq W_M \leq 1 + \sum_{i=1}^{D} i(\Delta-1)^{i-1}. \tag{7.4}$$

Note that the difference of the upper and lower bound is 1. In other words, for a Moore Graph, at most one additional wavelength is required in the absence of wavelength conversion. As for the Petersen Graph, using minimum hop routing and a simple wavelength assignment heuristic, a minimal 5 wavelengths are required to support the all-to-all uniform traffic. The heuristic is a combination of "First-fit" and

"Last-fit" RWA algorithm [10]. The details of the heuristic and the assignment result are provided in the Appendix 7.4. Theorem 13 shows that Moore Graphs are also efficient in regard to the wavelength usage, in the sense that wavelength conversions do not provide significant advantages.

7.3 Solving RWA Problems for Generalized Moore Graphs

The balanced load distribution property of a Moore Graph arises from its symmetric construction – each of its nodes has a fully populated routing spanning tree. For a Generalized Moore Graph, multiple minimum hop paths may exist for some source-destination pairs. As a result, the minimum hop routing may or may not balance the load or minimize the congestion even under uniform traffic. To illustrate this, we first use an example of a (undirected) Generalized Moore Graph with $N = 7$ and $\Delta = 3$, as shown in Figure 7-4 (a). In this example, with the minimum hop routing illustrated in Figure 7-4 (b), a load of 2 can be evenly distributed on each edge. We further show that 2 wavelengths are enough to support uniform all-to-all traffic without any wavelength conversion. We next consider another example – a Symmetric Hamilton Graph of 6 nodes and degree 3, shown in Figure 7-5 (a). This Symmetric Hamilton Graph can be also considered as a complete $K_{3,3}$ bipartite graph (a set of graph vertices can be decomposed into two disjoint sets, such that there are no two vertices within the same set are adjacent, but every pair of vertices in the two sets are adjacent). For the clarity of discussion, we redraw the same Symmetric Hamilton Graph in the bipartite $K_{3,3}$ form in Figure 7-5 (b). For this graph, the minimum hop routing algorithm is not unique. Table 7.3 lists two different minimum hop routing algorithms. We note that neither of the algorithms can distribute the load evenly over each fiber. Routing algorithm 1 incurs a maximum load of 4; while routing algorithm 2 minimizes the maximum load to 3. It is also straightforward to show that using routing algorithm 2, a minimum of 3 wavelengths are enough to

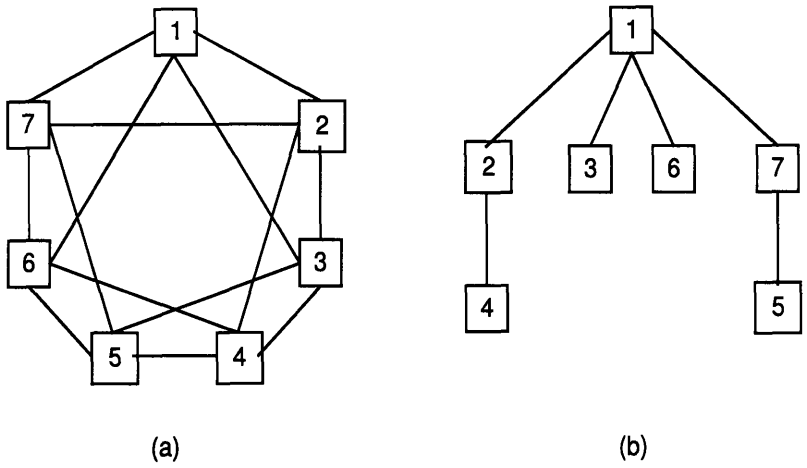

Figure 7-4: (a) A Generalized Moore Graph with $N = 7$ and $\Delta = 4$; (b) A routing spanning tree from node 1.

support a uniform demand ($t = 1$), even in the absence of wavelength conversion.

Using node coloring approaches, we investigate the wavelength assignments for Generalized Moore Graphs with $\Delta = 3$, 4 and $D = 2$, 3. The results are listed in Table 4. It is seen that the wavelength conversion does not reduce the minimal number of wavelengths required. We thus conclude that the wavelengths can also be efficiently provisioned for these Generalized Moore Graphs.

7.4 Chapter Appendix

In this appendix, we present the wavelength assignment algorithm and the result for the Petersen Graph. The following summarizes a RWA heuristic for the Petersen Graph. Table 5 summarizes RWA results for the Petersen Graph.

1. Number the 5 wavelengths from 1 to 5.

2. Start the assignment first for the two-hop paths, in the order: from source A to destination B, ..., J; from source B to destination C, ..., J; ..., from source I

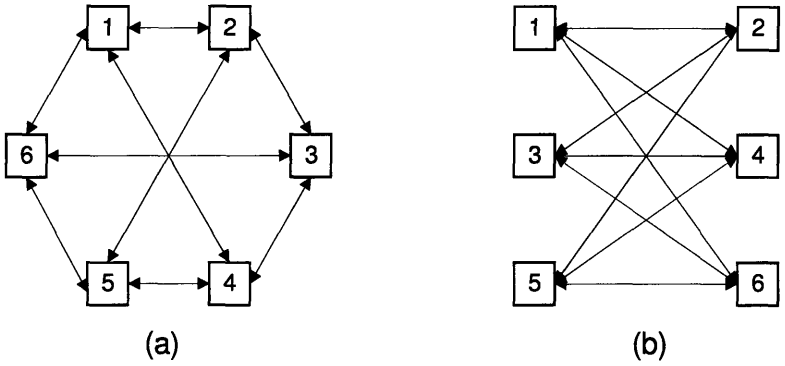

Figure 7-5: (a) A Symmetric Hamilton Graph with $N = 6$ and $\Delta = 3$; (b) The same graph is redrawn as a $K_{3,3}$ complete bipartite graph.

Table 7.3: The minimum hop routing algorithms for a Symmetric Hamilton Graph with $N = 6$ and $\Delta = 3$.

Routing algorithm	Algorithm 1	Algorithm 2
Node i	$\|i\|_6 \rightarrow \|i+1\|_6$, $\|i\|_6 \rightarrow \|i+1\|_6 \rightarrow \|i+2\|_6$ $\|i\|_6 \rightarrow \|i+3\|_6$, $\|i\|_6 \rightarrow \|i+3\|_6 \rightarrow \|i+4\|_6$ $\|i\|_6 \rightarrow \|i+5\|_6$	$\|i\|_6 \rightarrow \|i+1\|_6$, $\|i\|_6 \rightarrow \|i+3\|_6 \rightarrow \|i+2\|_6$ $\|i\|_6 \rightarrow \|i+3\|_6$, $\|i\|_6 \rightarrow \|i+3\|_6 \rightarrow \|i+4\|_6$ $\|i\|_6 \rightarrow \|i+5\|_6$
Max load	4	3

Table 7.4: RWA results for Generalized Moore Graphs with $\Delta = 3, 4$ and $D = 2, 3$.

Generalized Moore Graphs	Min. no. of wavelengths with conversions	Min. no. of wavelengths without conversions
$N = 6, \Delta = 3, D = 2$	3	3
$N = 8, \Delta = 3, D = 2$	4	4
$N = 14, \Delta = 3, D = 3$	10	10
$N = 6, \Delta = 4, D = 2$	2	2
$N = 7, \Delta = 4, D = 2$	2	2
$N = 8, \Delta = 4, D = 2$	3	3
$N = 9, \Delta = 4, D = 2$	3	3
$N = 10, \Delta = 4, D = 2$	4	4
$N = 11, \Delta = 4, D = 2$	4	4
$N = 12, \Delta = 4, D = 2$	5	5
$N = 13, \Delta = 4, D = 2$	5	5

Table 7.5: RWA result for the Petersen Graph.

	A	B	C	D	E	F	G	H	I	J
A	-	5	1	1	4	5	2	1	2	2
B	1	-	4	2	3	4	5	3	1	3
C	5	1	-	5	1	1	4	5	3	2
D	5	3	2	-	4	1	2	4	5	3
E	1	4	5	2	-	3	1	4	4	5
F	1	3	5	5	5	-	1	2	4	3
G	2	1	5	4	5	5	-	1	2	2
H	4	2	1	4	4	2	5	-	3	1
I	2	3	1	3	2	3	5	4	-	4
J	2	4	3	3	1	5	2	2	3	-

to destination J.

3. Assign to each two-hop path the lowest numbered wavelength that is previously unused by both fibers of the path.

4. Assign the wavelength for the two-hop path, in the order from source B to destination A; from source C to destination B, A; ..., from source J to destination I, ..., A.

5. Assign to each two-hop path the highest numbered wavelength that is previously unused.

6. Assign the unused wavelengths to all the one-hop paths.

Chapter 8

Network Dimensioning Under Demand Uncertainty

In this chapter, we address the issues of dimensioning WDM networks under random traffic demand. We still focus on the small-scale networks that support both WDM and OXC-based or OEO-based lightpath switching, such as next generation MAN and SAN. As already discussed in Chapter 6, in a green field design scenario, when the locations of nodes are known, a designer needs to determine the network physical topology (e.g., the fiber connections among network nodes), dimension the necessary switching resources (e.g., the size of optical switch at each node), and design routing algorithms. In Chapter 5, 6, and 7, the joint optimization over topology, switching resource dimensioning, and RWA is carried out based on a static traffic model, i.e., the traffic demand between a node pair is given as a fixed quantity (e.g., the average or the maximum possible traffic). This approach is effective when the traffic patterns are reasonably well known in advance, but it is insufficient in today's metro environment, where, as traffic demands among end users become more volatile [56], the uncertainties of the traffic forecast increase. As such, it is more difficult to choose an appropriate network topology and to provision the resources so that the actual demand can be closely matched. On one hand, insufficient provisioning causes a loss of revenue and a penalty cost for unsatisfied service level agreements (SLA); on the other hand, over-provisioning will result in under-utilized network resources, hence a delay in

the recovery of capital investment. Thus designing networks that are robust with respect to demand uncertainties poses a key challenge, especially in today's telecom environment where low cost and scalable solutions must be sought.

To achieve good performance, the design of the physical topology, as in the case for static traffic, should be carried out jointly with the dimensioning of network resources and the design of associated routing algorithm. Most prior works on network planning under demand uncertainties [23]- [27] have been undertaken in the context that network physical topologies are given (thus only dimensioning and routing subproblems remain to be solved). These works assess and quantify the effects of traffic uncertainties on the network cost either via simulations or via stochastic programming techniques. As discussed in Chapters 1,4, and 6, network physical topology is a crucial design element that has significant influence on the network cost. Thus the physical topology design should be addressed simultaneously with network resource dimensioning and routing algorithm design. The works presented in this chapter represent an attempt to gain analytical insight into the impact of demand variability on this joint (topology, dimensioning, and routing algorithm) design for WDM networks.

This chapter is organized as follows: in Section 8.1, we review the random traffic model, which was introduced in Chapter 3. In Section 8.2, we introduce two approaches to include the traffic variability in the network optimization model and then formulate the network topology design problems with random traffic demand. In Section 8.3, we first show that with a minimum hop routing algorithm, networks with physical architectures of Generalized Moore Graphs exhibit the best robustness (in cost) to demand uncertainties. We then give closed-form solutions of optimal degree, traffic provisioned, and effective system cost as functions of various network design parameters. In Section 8.4, we use results from various design examples to understand the fundamental behaviors of networks under demand uncertainties and to provide guidelines on designing optical networks in such dynamic environments.

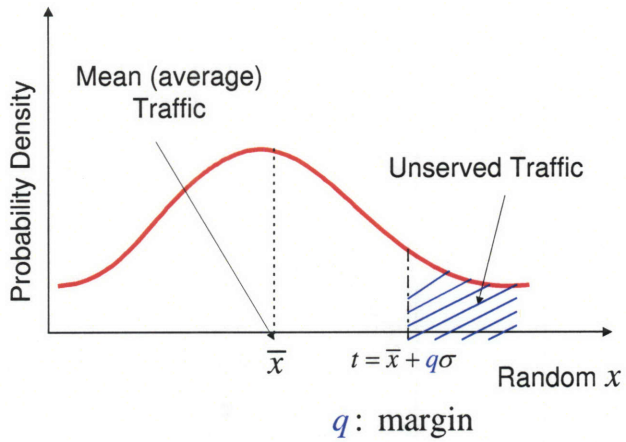

Figure 8-1: In random traffic model, traffic between a node pair is treated as a random variable.

8.1 Modelling the Uncertain Demand

As discussed in Chapter 3, the random demand between a node pair is characterized by a random variable x, specified by its probability density function (PDF) $f(x)$, as shown in Figure 8-1 (same as Figure 3-3). In this thesis work, we focus on using various known theoretical distributions to appraise the impact of the demand uncertainties on optimal network architecture. For fair comparisons, the PDFs are expressed with independently adjustable mean $\bar{x}$ and standard deviation σ – the mean $\bar{x}$ represents the magnitude of the expected demand; while the standard deviation σ measures the level of volatility of the forecast. The theoretical distributions used in this thesis are listed in Table 3.1 and are plotted in Figure 8-2. To maintain the tractability of the analysis, we further assume that traffic demands between node pairs are all-to-all uniform and i.i.d.

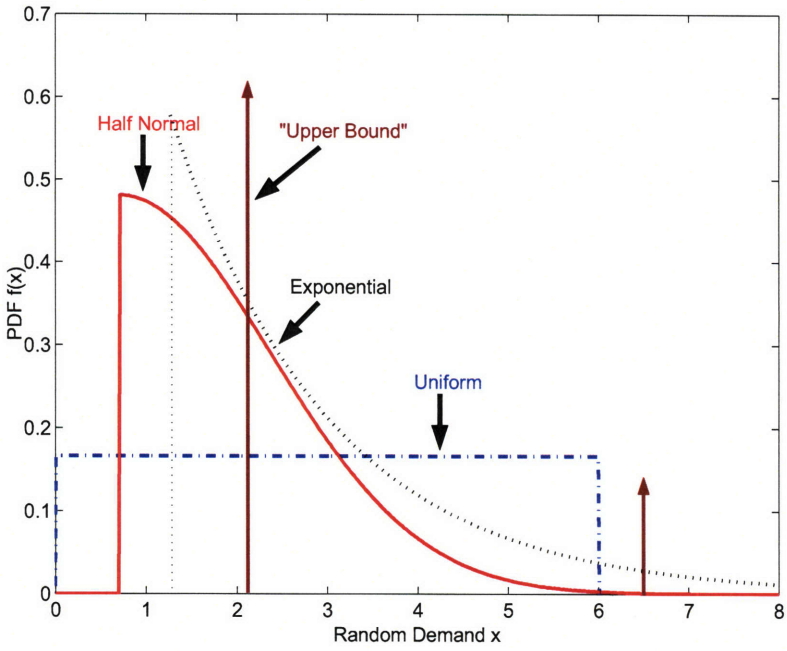

Figure 8-2: Distributions of random demand with $\bar{x} = 3$ and $\sigma = \sqrt{3}$.

8.2 Optimization Models for Network Design Under Demand Uncertainty

As mentioned previously, we assume that the network designer has a reasonable knowledge of the traffic demand, albeit with some uncertainties, and the demand between a node pair is characterized by a random variable. Thus, compared with the deterministic network design problems, for which traffic demand between a node pair is given as a fixed quantity, here we need to consider further how much bandwidth t to be provisioned. To include traffic variability in the optimization models, we use two approaches. The first approach is based on the *bi-objective optimization* technique; while the second one *–service level requirement approach–* is based on the idea of setting a service level requirement as a constraint in the optimization model.

8.2.1 Bi-Objective Optimization Approach

For bi-objective optimization, there are two objective functions, Y_1 and Y_2. A solution is said to be optimal if any further improvement in one objective necessarily results in a degradation of the other objective [49]. Such an optimal solution is call Pareto-optimal [49].

To use the method of bi-objective optimization, we first introduce a penalty cost associated with the unserved demand, which represents opportunity loss and also quantifies the risk of a competitor entering the market. In our model, we assume the penalty cost varies linearly with the expected unsatisfied demand. That is, when the real demand x exceeds the provisioned bandwidth t, a penalty of $\gamma(x-t)$ will be incurred. Here γ is a coefficient representing per unit cost for unsatisfied traffic. Since the traffic demands between node pairs are all-to-all uniform and i.i.d., the expected penalty cost per node takes the form

$$E[C_{\mathrm{p}}(x,t)] = (N-1)\gamma \int_t^{\infty} (x-t) f(x) dx, \tag{8.1}$$

where $E[\cdot]$ denotes the expectation function.

With the penalty cost for unserved traffic introduced, we note that there are clearly two conflicting objectives to be optimized – network installation cost and penalty cost. Under-provisioning the network saves on installation cost, but incurs more penalty cost; over-provisioning the network can reduce penalty cost for unsatisfied traffic, but increases the installation cost.

One common way to solve a bi-objective optimization problem is to form a weighted sum of two counteracting objectives. We define such a weighted sum of normalized network cost and expected penalty cost as the effective system cost, which is denoted as $C_{\mathrm{eff}}(N, \Delta, t)$. That is we have

$$\begin{aligned} C_{\mathrm{eff}}(N,\Delta,t) &= C_{\mathrm{n}}(N,\Delta,t) + E_x[C_{\mathrm{p}}(x,t)] \\ &= C_{\mathrm{n}}(N,\Delta,t) + \gamma(N-1)\int_t^{\infty} (x-t) f(x) dx. \end{aligned} \tag{8.2}$$

In (8.2), γ can be interpreted as the relative weight of the objective of minimizing the under-provisioning penalty cost, compared to the objective of minimizing the

network installation cost. It is worth pointing out that besides presenting the revenue loss for per unit of unsatisfied traffic, γ can also be interpreted as a risk index reflecting levels of risk aversion. A high γ value indicates the network designer's willingness to increase network installation cost to avoid the risk of provisioning shortage. More importantly, only when γ is larger than a threshold, it is economical (feasible) to dimension any capacity. More precisely, only when γ is larger than the marginal network cost (at bandwidth t), it is feasible to provide t units of capacity. We defer the rigorous substantiation of this claim to Appendix 8.5.1.

The Pareto-optimal solution can be obtained by minimizing the effective system cost, with a given per unit cost for unsatisfied traffic γ. That is

$$\begin{aligned} \min_{\{\text{tpl.}\},\{\text{r.a.}\},\Delta,t} \quad & C_{\text{n}}(N,\Delta,t) + E_x[C_p(x,t)] \\ \text{s.t.} \quad & 2 \leq \Delta \leq N-1, \\ & \Delta, t \in Z^+, N \text{ is given.} \end{aligned} \tag{8.3}$$

In this optimization formulation, the inputs are:

- The number of nodes (network size) N;
- The PDF $f(x)$ that models the traffic demand between a source-destination pair (note that we assume that the demands are uniform all-to-all and i.i.d);
- The type of optical switches and the corresponding parameters (cf. Section 5.3):
  - For OXC switching architecture, the inputs include the cost scaling function $F_i(K_{\text{o}})$, where K_{o} is the number of OXC ports, and the corresponding per port cost β_i (cf. Table 5.1);
  - For OEO switching architecture, the inputs include the port (interface rate) R, per wavelength data rate r, port utilization η, and per port cost β_{e};
- The cost per fiber connection α;
- The per unit cost for unsatisfied traffic γ.

The objective is to minimize the effective system cost over:

- The type of symmetric regular topology, denoted as "tpl." in (8.3);
- The type of routing algorithm, denoted as "r.a." in (8.3);
- The node degree of the symmetric regular topology Δ;
- The bandwidth to be provisioned t. For the convenience of analysis, we write t as $t = \bar{x} + q\sigma$, with q being a constant to be determined. In this thesis, q is called the *margin*.

In (8.3), the constraint $\Delta \leq N-1$ imposes an upper limit to the possible values of the optimal node degree Δ^* for a topology of N nodes; the constraint $\Delta \geq 2$ ensures that the optimal topology meets the reliability requirement of more than one connected.

8.2.2 Service Level Requirement Approach

In our second approach, instead of assigning a monetary penalty for the provisioning shortage, we use a fixed service level requirement as a constraint in the optimization model and then minimizing the network cost of meeting it. This approach is well suited for the situations, in which costs of shortage are difficult to quantify and are probably not simply proportional to the magnitude of the shortage. Under these scenarios identifying appropriate forms for the penalty functions and reasonable values for their parameters would be quite a challenge. In general, as the service level requirement (such as the probability that a demand is unsatisfied due to bandwidth shortage) becomes more stringent, more bandwidth needs to be provided – the network cost will increase as a consequence.

As discussed in Chapter 3, for a practical network provisioning under random traffic, it is often not necessary (or impossible) to achieve totally non-blocking operation – it suffices if the blocking is considerably low. For a random demand x and its associated probability density function $f(x)$, in Section 3.2 we have defined an overflow probability (or fraction of unserved traffic) p. If t unites of bandwidth are

provisioned, then p is define by (3.3),

$$\int_t^{\infty} f(x)dx = p. \tag{8.4}$$

By including service level requirement (8.4), we have the second formulation as follows:

$$\begin{aligned} \min_{\{\text{tpl.}\},\{\text{r.a}\},\Delta,t} \quad & C_{\text{n}}(N,\Delta,t) \\ \text{s.t.} \quad & \int_t^{\infty} f(x)dx \leq p, \\ & 2 \leq \Delta \leq N-1, \\ & \Delta, t \in Z^{+}, N \text{ is given.} \end{aligned} \tag{8.5}$$

In this optimization formulation, the inputs are:

- The number of nodes (network size) N;
- The PDF $f(x)$ that models the traffic demand between a source-destination pair (note that we assume demands are uniform all-to-all and i.i.d);
- The type of optical switches and the corresponding parameters (cf. Section 5.3):
  - For OXC switching architecture, the inputs include the cost scaling function $F_i(K_{\text{o}})$, where K_{o} is the number of OXC ports, and the corresponding per port cost β_i (cf. Table 5.1);
  - For OEO switching architecture, the inputs include the port (interface rate) R, per wavelength data rate r, port utilization η, and per port cost β_{e};
- The cost per fiber connection α;
- The fraction of unserved traffic (overflow probability) p.

The objective is to minimize the normalized effective system cost over:

- The type of symmetric regular topology, denoted as "tpl." in (8.5);

- The type of routing algorithm, denoted as "r.a." in (8.5);

- The node degree of the symmetric regular topology Δ;

- The bandwidth to be provisioned t. For the convenience of analysis, we write t as $t = \bar{x} + q\sigma$, with q being a constant to be determined. In this thesis, q is called the margin.

In (8.5), we further assume that the network serves the same type of customers, thus they have the same requirement on shortage probability.

8.3 Solving the Optimization Problems

8.3.1 Optimal Topology and Routing Algorithm

As a first step to solve (8.3) and (8.5), we need to identify the optimal topology and the optimal routing algorithm. We have shown in Chapter 6 that, under all-to-all uniform deterministic traffic (where t is a fixed given value), with minimum hop routing algorithm, Generalized Moore Graphs achieve the lower bound on network cost and are good reference topologies. In this section, we show that this result can be extended to the random traffic case – with minimum hop routing, Generalized Moore Graphs still provide the fundamental limit on the effective system (network and penalty) cost. To prove this claim we again rely on the "dominated function" technique, albeit we now compare functions of two variables (note that the optimization is in regard to both Δ and t). Equations (8.3) and (8.5) imply that for a given network size N and provisioned bandwidth t, the expected penalty cost is independent of the type of topology and the routing algorithm. Thus for finding the optimal topology and routing algorithm we can focus only on the network cost and show that Generalized Moore Graphs achieve the lower bound (on the network cost) via minimum hop routing. The rest of the proof follows the same line of development as that in Chapter 6, and is omitted here.

8.3.2 Optimal Bandwidth Provisioned, Node Degree, and Effective System Cost Obtained by Solving (8.3)

In this section, we solve the optimization problem (8.3) using the Δ-nearest Neighbors topology under uniform traffic distribution as an example. For the Δ-nearest Neighbors, 3-D switching fabrics (cf. Table 5.1 and set $\zeta = 0$), and uniform traffic distributions (with given mean $\bar{x}$ and σ), the optimization problem has the following form:

$$\begin{aligned} \min_{\Delta,t} \quad & \alpha\Delta + \beta_1 t(N-1)\left(\frac{3}{2} + \frac{N-1}{2\Delta}\right) + \gamma\frac{N-1}{2\sqrt{3}\sigma}\int_t^{\bar{x}+\sqrt{3}\sigma}(x-t)dx \\ s.t. \quad & 2 \le \Delta \le N-1, \\ & \Delta, t \in Z^+, \ N \text{ is given.} \end{aligned} \tag{8.6}$$

By relaxing Δ and t as continuous variables, using Karush-Kuhn-Tucker (KKT) condition, and considering the case when constraints are inactive, we have the following first-order conditions:

$$\alpha - \beta_1 t^* \frac{(N-1)^2}{2\Delta^{*2}} = 0, \tag{8.7}$$

$$\beta_1\left(\frac{3}{2} + \frac{N-1}{2\Delta^*}\right) - \frac{\gamma(N-1)(\bar{x}+\sqrt{3}\sigma - t^*)}{2\sqrt{3}\sigma} = 0. \tag{8.8}$$

Note that we also need the condition under which the effective system cost in (8.6) is jointly convex in Δ and t. The derivation of the convecity condition is provided in Appendix 8.5.2. Solving for optimal provisioned bandwidth t^* and optimal node degree Δ^*, we have

$$\begin{aligned} t^* = & \left\{2^{-\frac{1}{6}}3^{-\frac{1}{3}}\sigma^{\frac{1}{3}}\gamma^{-\frac{1}{3}}\left[-3\sqrt{3}(\alpha\beta_1)^{\frac{1}{2}} + (2^4 3^{\frac{1}{2}}B\frac{\sigma}{\gamma} - 3^3\alpha\beta)^{\frac{1}{2}}\right]^{\frac{1}{3}}\right. \\ & \left. + 2^{\frac{7}{6}}3^{-\frac{1}{6}}\sigma^{\frac{2}{3}}\gamma^{-\frac{2}{3}}B\left[-3\sqrt{3}(\alpha\beta_1)^{\frac{1}{2}} + (2^4 3^{\frac{1}{2}}B\frac{\sigma}{\gamma} - 3^3\alpha\beta)^{\frac{1}{2}}\right]^{-\frac{1}{3}}\right\}^2, \end{aligned} \tag{8.9}$$

$$\begin{aligned} \Delta^* = & \left(\frac{\beta_1}{2\alpha}\right)^{\frac{1}{2}}(N-1)\left\{2^{-\frac{1}{6}}3^{-\frac{1}{3}}\sigma^{\frac{1}{3}}\gamma^{-\frac{1}{3}}\left[-3\sqrt{3}(\alpha\beta_1)^{\frac{1}{2}} + (2^4 3^{\frac{1}{2}}B\frac{\sigma}{\gamma} - 3^3\alpha\beta)^{\frac{1}{2}}\right]^{\frac{1}{3}}\right. \\ & \left. + 2^{\frac{7}{6}}3^{-\frac{1}{6}}\sigma^{\frac{2}{3}}\gamma^{-\frac{2}{3}}B\left[-3\sqrt{3}(\alpha\beta_1)^{\frac{1}{2}} + (2^4 3^{\frac{1}{2}}B\frac{\sigma}{\gamma} - 3^3\alpha\beta)^{\frac{1}{2}}\right]^{-\frac{1}{3}}\right\}, \end{aligned} \tag{8.10}$$

where $B = \frac{3\beta_1}{2} - \frac{\gamma(\bar{x}+\sqrt{3}\sigma)}{2\sqrt{3}\sigma}$ to simplify the appearance of the expression.

The expression in (8.9) for the optimal bandwidth provisioned can be expressed in q^* via $t^* = \bar{x} + q^*\sigma$,

$$\begin{aligned} q^* &= \sigma^{-1}\Big\{2^{-\frac{1}{6}}3^{-\frac{1}{3}}\sigma^{\frac{1}{3}}\gamma^{-\frac{1}{3}}\left[-3\sqrt{3}(\alpha\beta_1)^{\frac{1}{2}} + (2^4 3^{\frac{1}{2}}B\frac{\sigma}{\gamma} - 3^3\alpha\beta)^{\frac{1}{2}}\right]^{\frac{1}{3}} \\ &+ 2^{\frac{7}{6}}3^{-\frac{1}{6}}\sigma^{\frac{2}{3}}\gamma^{-\frac{2}{3}}B\left[-3\sqrt{3}(\alpha\beta_1)^{\frac{1}{2}} + (2^4 3^{\frac{1}{2}}B\frac{\sigma}{\gamma} - 3^3\alpha\beta)^{\frac{1}{2}}\right]^{-\frac{1}{3}}\Big\}^2 - \sigma^{-1}\bar{x}. \end{aligned} \tag{8.11}$$

q^* is called the *optimal margin*, which gives the designer a reference on the extra margin to be provisioned.

When $\bar{x} \gg \sigma$, we can simplify (8.9) to

$$t^* = \frac{2\cdot 3^{\frac{1}{3}}\bar{x} + 2^{\frac{1}{3}}\left(-3^2B_1\sigma + \sqrt{3^4B_1^2\sigma^2 - 3\cdot 2^2\bar{x}^3}\right)^{\frac{2}{3}}}{2^{\frac{2}{3}}3^{\frac{2}{3}}\left(-3^2B_1\sigma + \sqrt{3^4B_1^2\sigma^2 - 3\cdot 2^2\bar{x}^3}\right)^{\frac{1}{3}}}, \tag{8.12}$$

where $B_1 = \sqrt{6\alpha\beta_1}/\gamma$. When $\gamma \gg \sigma$, we have $t^* \to \bar{x}$.

For a uniform distribution (of non-negative random variables) with a mean $\bar{x}$, the maximum possible variance is $\sigma = \bar{x}/\sqrt{3}$ (this corresponds to the case of $t_{\min} = 0$, as shown in equation (3.2)). Under this condition, the expression for t^* is

$$t^* = \frac{2\cdot 3^{\frac{1}{3}}B_2\sigma + 2^{\frac{1}{3}}\sigma^{\frac{2}{3}}\left(-3^2B_1 + \sqrt{3^4B_1^2 - 3\cdot 2^2B_1^2\sigma}\right)^{\frac{2}{3}}}{2^{\frac{2}{3}}3^{\frac{2}{3}}\sigma^{\frac{1}{3}}\left(-3^2B_1 + \sqrt{3^4B_1^2 - 3\cdot 2^2B_2^2\sigma}\right)^{\frac{1}{3}}}, \tag{8.13}$$

where $B_2 = \sqrt{3}(3\beta_1/\gamma - 2)$.

In the process of solving for Δ^* and t^*, we also note that as $\gamma \to \infty$, we have $t^* \to t_{\max}$ and $\Delta^* \to \sqrt{\beta_1 t_{\max}/2\alpha}(N-1)$, and the minimal effective system cost is given by

$$C_{\text{eff}}^* = \left(\sqrt{2\alpha\beta_1 t_{\max}} + \frac{3\beta_1 t_{\max}}{2}\right)(N-1). \tag{8.14}$$

This means, when the penalty for unsatisfied demand is extremely large, the design problem (8.6) reduces to an optimization for deterministic traffic for the maximum traffic. This result can be generalized to any demand PDF with a finite support. On the other hand, when $\gamma \to 0$, the constraint $t \geq 0$ is active, and we have $t^* \to 0$. This means, it is economical not to provision any bandwidth in this situation.

Next we investigate the impact of the mean $\bar{x}$ and the variance σ of a uniform distribution to the minimal effective system cost. For a given mean $\bar{x}$ and variance σ, the minimal effective system cost $C^*_{\text{eff}}(\bar{x}, \sigma)$, as a function of $\bar{x}$ and σ, is given by

$$\begin{aligned} C^*_{\text{eff}}(\bar{x}, \sigma) &= \min_{\Delta,t} C_n(N, \Delta t) + E_x[C_p(x,t)] \\ \text{s.t.} &\quad 2 \le \Delta \le N-1, t > 0. \end{aligned} \tag{8.15}$$

Using the sensitivity analysis [49], we have

$$\begin{aligned} \frac{\partial C_{\text{eff}}(\bar{x}, \sigma)}{\partial \sigma} &= \frac{\partial \{C_n(N, \Delta, t) + E_x[C_p(x,t)]\}}{\partial \sigma} |_{\Delta^*, t^*} \\ &= \frac{\left[(\bar{x} + \sqrt{3}\sigma) - t^*\right]\left[t^* - (\bar{x} - \sqrt{3}\sigma)\right]}{\sigma^2} \\ &= \frac{(t_{\max} - t^*)(t^* - t_{\min})}{\sigma^2} \ge 0, \end{aligned} \tag{8.16}$$

when $t^* \ge t_{\min}$. Thus as the uncertainty of the traffic demand increases, the optimal effective system cost increases too. following the same line of development, we have also

$$\frac{\partial C_{\text{eff}}(\bar{x}, \sigma)}{\partial \bar{x}} > 0. \tag{8.17}$$

That is, as the mean of the random traffic demand increases, the minimal effective system cost also increases. This is obvious.

For other types of topologies and traffic demand distribution, closed form solutions do not exist when solving (8.3). We will provide numerical solutions for these cases in Section 8.4.

8.3.3 Optimum Bandwidth Provisioned, Node Degree, and Network Cost Obtained by Solving (8.5)

In this section, we solve the optimization problem (8.5) using Δ-nearest Neighbors topology and uniform traffic distribution as an example. We also discuss the implications of some design parameters, such as fraction of unserved traffic p, to the optimal solutions. With Δ-nearest Neighbors, 3-D switching fabrics (cf. Table 5.1 and set $\eta = 0$), and uniform traffic distributions (for simplicity we assume that $t_{\min} = 0$ and

$t_{\max} = 2\sqrt{3}\sigma$), the optimization problem (8.5) takes into the following form:

$$\begin{aligned} \min_{\Delta,t} \quad & \alpha\Delta + \beta_1 t(N-1)\left(\frac{3}{2} + \frac{N-1}{2\Delta}\right) \\ \text{s.t.} \quad & \frac{1}{2\sqrt{3}\sigma}\int_t^{2\sqrt{3}\sigma} dx \le p, \\ & 2 \le \Delta \le N-1, \\ & \Delta, t \in Z^+, \ N \text{ is given.} \end{aligned} \tag{8.18}$$

To solve this problem, we first relax Δ and t as continuous variables. The fraction of unserved traffic constraint indicates that the feasible t would be in the range of $t \in (t^\circ, 2\sqrt{3}\sigma)$, where t° satisfies

$$\frac{1}{2\sqrt{3}\sigma}\int_{t^\circ}^{2\sqrt{3}\sigma} dx = (1 - \frac{t^\circ}{2\sqrt{3}\sigma}) = p. \tag{8.19}$$

We note that the objective function is linear and monotonically non-decreasing with t. Therefore to be optimal, the fraction of unserved traffic constraint must be active:

$$t^*(p) = t^\circ = 2\sqrt{3}\sigma(1-p). \tag{8.20}$$

After the optimal bandwidth provisioned t^* is solved, the problem (8.18) can be simplified to a convex optimization of node degree Δ only,

$$\begin{aligned} \min_{\Delta} \quad & \alpha\Delta + \beta_1 t^*(N-1)\left(\frac{3}{2} + \frac{N-1}{2\Delta}\right) \\ \text{s.t.} \quad & 2 \le \Delta \le N-1, \\ & N \text{ and } t^* \text{are given.} \end{aligned} \tag{8.21}$$

Solving for optimal node degree, we have

$$\begin{aligned} \Delta^* &= \left(\frac{\beta_1 t^*}{2\alpha}\right)^{1/2}(N-1) \\ &= \left(\frac{\sqrt{3}\beta_1\sigma(1-p)}{\alpha}\right)^{1/2}(N-1). \end{aligned} \tag{8.22}$$

Thus the minimal normalized network cost is given by

$$\begin{aligned} C_{\text{n}}^* &= \left(\sqrt{2\alpha\beta_1 t^*} + \frac{3\beta_1 t^*}{2}\right)(N-1) \\ &= \left[\sqrt{4\sqrt{3}\alpha\beta_1\sigma(1-p)} + 3\sqrt{3}\beta_1\sigma(1-p)\right](N-1). \end{aligned} \tag{8.23}$$

Table 8.1: Optimal margin q^* as a function of p for different PDFs of random demand.

Distribution	$q^*(p) = (t^*(p) - x)/\sigma$	$p \to 0$	$p \to 1$
Uniform	$\sqrt{3}(1-2p)$	$q^* \to \sqrt{3}$	$q^* \to -\sqrt{3}$
Exponential	-$[\ln p + 1]$	$q^* \to \infty$	$q^* \to -1$
Half Normal	$\sqrt{2\pi/(\pi-2)}\text{erf}^{-1}(1-p)$ $-\sqrt{2/(\pi-2)}$	$q^* \to \infty$	$q^* \to -\sqrt{2/(\pi-2)}$
Upper Bound	$\sqrt{\frac{1-p}{p}}$	$q^* \to \infty$	$q^* \to 0$

Table 8.2: Optimal node degree Δ^* and minimal normalized network cost C_{n}^* as functions of p for different topologies.

Topology	Optimal Node Degree Δ^*	Minimal Normalized Network Cost C_{n}^*
Δ – nearest Neighbors	$\frac{1}{\sqrt{2}}\left(\frac{\beta_1 t^*(p)}{\alpha}\right)^{\frac{1}{2}}(N-1)$	$\left(\sqrt{2\alpha\beta_1 t^*(p)} + \frac{3\beta_1 t^*(p)}{2}\right)(N-1)$
Moore Graphs	$\frac{1}{4}\left(\frac{\beta_1 t^*(p)}{\alpha}\right)\frac{(N-1)\ln N}{\left\{W\left(\frac{\sqrt{(\beta_1 t^*(p)/\alpha)(N-1)\ln N}}{2}\right)\right\}^2}$ $\sim \frac{\beta_1 t^*(p)}{\alpha}\frac{N}{\ln N}$	$\alpha\Delta^* + \beta_1 t^*(p)(N-1)\left(\frac{\ln N}{\ln \Delta^*}+1\right)$ $\sim t^*(p)N\left[1+\frac{1}{\ln(tN)}\right]$

In the process of solving for Δ^* and t^*, we also note that as $p \to 0$, we have $t^* \to t_{\max} = 2\sqrt{3}\sigma$ and $\Delta^* \to \sqrt{\beta_1\sqrt{3}\sigma/\alpha}(N-1)$, then the minimal normalized network cost is given by

$$\begin{aligned} C_{\text{n}}^* &= \left(\sqrt{2\alpha\beta_1 t_{\max}} + \frac{3\beta_1 t_{\max}}{2}\right)(N-1) \\ &= \left(\sqrt{4\sqrt{3}\alpha\beta_1\sigma} + 3\sqrt{3}\beta_1\sigma\right)(N-1), \end{aligned} \tag{8.24}$$

which is the same as (6.25). This means, when the requirement of the fraction of unserved traffic is extremely stringent, the design problem (8.18) reduces to an optimization of deterministic traffic for the maximum or minimum possible traffic. This result can be generalized to any demand PDF with a finite support. On the other hand, when $p \to 1$, we have $t^* \to 0$. This means that it is economical not to provision any bandwidth in this situation.

Following the same procedure, we can solve (8.5) for various types of topologies (such as Generalized Moore Graphs) and traffic distributions (cf. Table 3.1). The

results are summarized in Table 8.1 and 8.2 and are discussed in Section 8.4.

As mentioned in Section 3.2, in solving (8.4), among all PDFs with the same mean $\bar{x}$ and standard deviation σ, the "Upper Bound" distribution (3.4) requires the maximum (worst case) margin. Since network cost increases with the amount of bandwidth provisioned, the "Upper Bound" distribution can also be used to size the worst case network cost. The theoretical substantiation for "Upper Bound" distribution is left in Appendix 8.5.3.

8.4 Results and Discussion

As discussed previously, the optimal network architecture depends on network size, fiber-OXC cost ratio, PDF of the random demand, as well as network designer's risk aversion. Based on the models set up in Section 8.2 and the solutions obtained in Section 8.3, this section provides results to illustrate and interpret these dependencies. As examples, we consider a green field design of a network with 50-node ($N = 50$), which resembles typical size of metropolitan access networks. According to the estimation of the realistic cost ratio between fiber and OXC in metropolitan area networks, we set $\alpha/\beta_1 = 40$. For simplicity but not losing generality, we set $\beta_1 = 1$.

8.4.1 Results of Bi-Objective Optimization Approach

We start with the results of bi-objective optimization approach. In the process of solving (8.3) for different types of topologies and distributions, both the node degree Δ and provisioned bandwidth t are relaxed as positive real numbers. As such, Δ^* and t^*, obtained by solving the optimality equations may not be integers. When rounding non-integers Δ^* and t^*, we compare the effective system cost for ($\lceil\Delta^*\rceil$, $\lceil t^*\rceil$),($\lceil\Delta^*\rceil$, $\lfloor t^*\rfloor$),($\lfloor\Delta^*\rfloor$, $\lceil t^*\rceil$), and ($\lfloor\Delta^*\rfloor$, $\lfloor t^*\rfloor$) and choose the one with the least cost. To evaluate the accuracy of the results obtained by rounding, we compare them with the results of exhaustive searches – we look for the node degree and provisioned bandwidth (integers), for which the minimum effective system cost is achieved. The

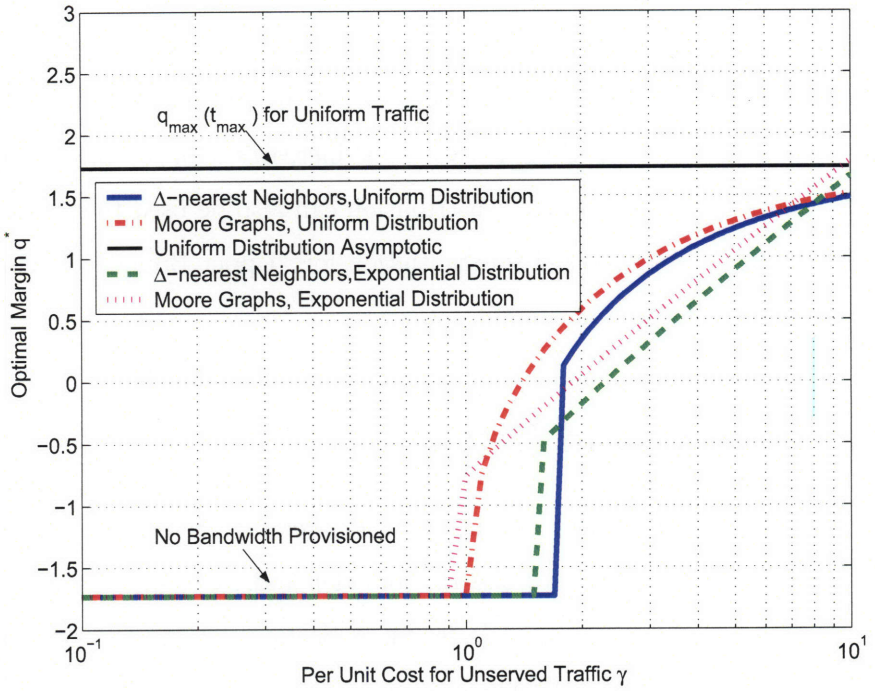

Figure 8-3: Optimal margin q^* vs. per unit cost of unserved traffic γ, with $N = 50$, $\alpha/\beta_1 = 40$, and $\beta_1 = 1$.

comparisons verify that the relaxation-rounding solutions fit well with the exhaustive search results. As discussed in 8.2, from the viewpoint of bi-objective optimization, γ represents the relative weight (importance) of the penalty cost for unserved traffic. From the perspective of network operation, γ can be interpreted as the revenue loss for per unit of unsatisfied traffic or as a risk index reflecting levels of risk aversion. Only when γ is above a threshold value, it is economical (feasible) to provision any capacity for the network. To illustrate how the optimal network architecture changes as a function of per unit cost of unsatisfied traffic γ, according to the results of bi-objective approach, Figure 8-3, Figure 8-4, and Figure 8-5 plot the γ dependencies of the optimal margin $q^*(q^* = (t^* - \bar{x})/\sigma)$, optimal node degree Δ^*, and minimal effective system cost C^*_{eff}, respectively. The per unit cost of unsatisfied traffic γ is normalized in terms of the minimal normalized network cost per unit traffic, with $\gamma = 1$ meaning that per unit penalty cost equals to the minimal normalized network cost (per node)

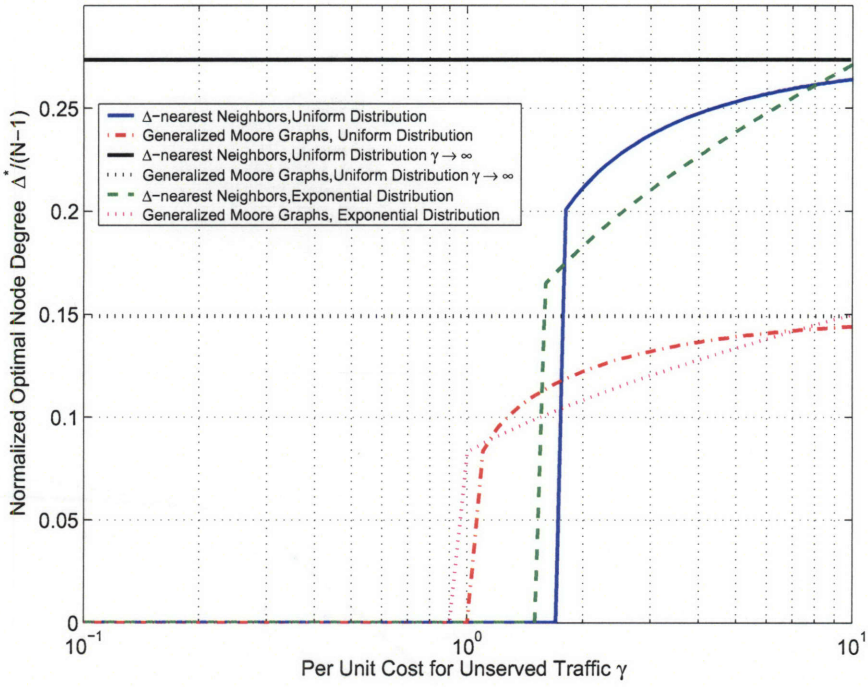

Figure 8-4: Normalized optimal node degree $\Delta^*/(N-1)$ vs. per unit cost of unserved traffic γ, with $N = 50$, $\alpha/\beta_1 = 40$, and $\beta_1 = 1$.

to support one unit of (static) traffic. For a 50-node network, the minimal normalized network cost per unit traffic is 4.8 at $\bar{x} = 3$, based on the calculations in Chapter 6 (cf.(6.26) and Table 6.3).

In these figures the γ dependencies are plotted for the combinations of two types of traffic distributions – uniform and exponential, both with $\bar{x} = 3$ and $\sigma = \sqrt{3}$ (as illustrated in Figure 8-2), and two types of topologies – Δ-nearest Neighbors and Generalized Moore Graphs. As shown in these figures, there are three distinct γ-regions of the dependencies and only for γ in certain range (e.g., $0.9 \sim 3$), are Δ^*, t^*, and minimal effective system cost C^*_{eff} sensitive to the change of γ. Next we discuss the behaviors of q^*, Δ^*, and C^*_{eff} in these γ-regions in detail:

- When γ is small enough, as shown in Figure 8-3, we have $t^* \to 0$ ($q^* \to -\sqrt{3}$), i.e., it is economical not to provision any bandwidth. The effective system cost is dominated by the penalty cost for unserved traffic.

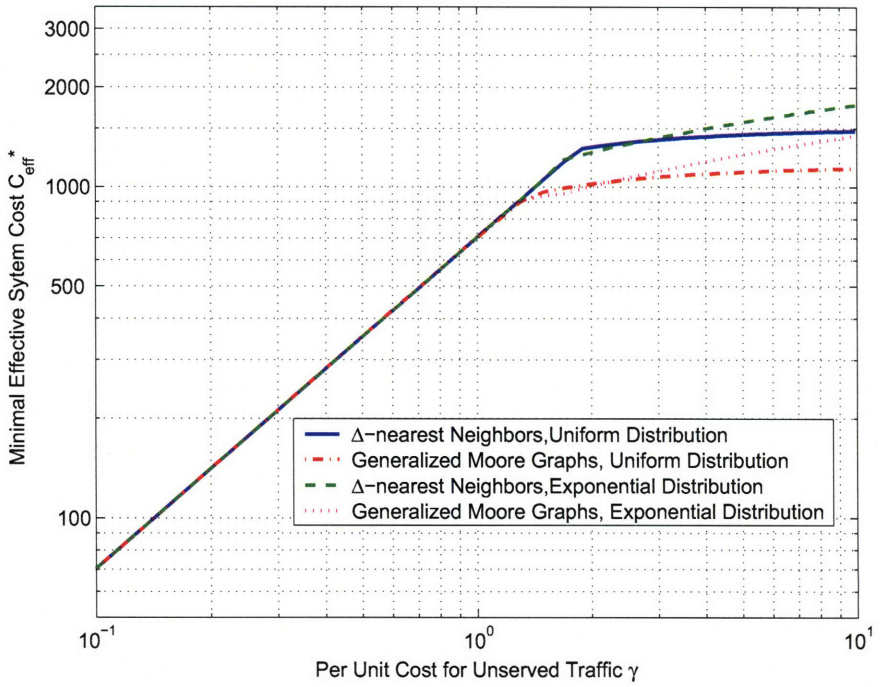

Figure 8-5: Minimal effective system cost C_{eff}^* vs. per unit cost of unserved traffic γ, with $N = 50$, $\alpha/\beta_1 = 40$, and $\beta_1 = 1$.

- When γ is large, it is economical to provide bandwidth, as discussed in Appendix 8.5.1. For this design example, as shown in Figure 8-3, the threshold γ (to dimension any bandwidth) are 1.8, 1.6, 1.0, and 0.9 for Δ-nearest Neighbors with uniform distribution, Δ-nearest Neighbors with exponential distribution, Generalized Moore Graphs with uniform distribution, and Generalized Moore Graphs with exponential distribution, respectively. For γ value above the threshold in the range of $0.9 \sim 3$, the tradeoff between the network cost and the penalty cost for unsatisfied traffic becomes notable. In this range, as γ increases, it is optimal to provision for more bandwidth. This leads to the increase of the optimal node degree for the network, so a good balance between the cost of fibers and OXCs can be achieved, as discussed in Chapter 6.

  In this range, for the uniform distribution, which has a finite support, the design problem (8.3) reduces to an optimization for the worst case uniform all-to-all traffic, with demand between each node pair equal to $t_{\max}$, as also shown in Figure 8-3. It is also worth pointing out that in this range the values of Δ^*, and t^*, and optimal effective system cost C^*_{eff}, as shown in Figures 8-3, 8-4, and 8-5, increase at a faster rate for exponential distributions than for the uniform distributions. This phenomenon can be explained by the fact that the exponential distribution has an infinite support.

- When γ is very large, in Figure 8-4 we observe that with the same γ and traffic distribution, a Δ-nearest Neighbors has a larger optimal node degree than a Generalized Moore Graph does. This trend is consistent with the results for the static (or quasi-static) traffic, as discussed in Chapter 6. At large γ, a key observation from Figure 8-5 is that with a given γ, the minimal effective system cost for a Generalized Moore Graph is less than that for a Δ-nearest Neighbors topology. This is consistent with our analysis in Section 8.3.1. This again demonstrates the importance of choosing a good physical architecture.

According to the results in section 8.3.2 for bi-objective approach, we further assess how the optimal network architecture changes as a function of the variance of the

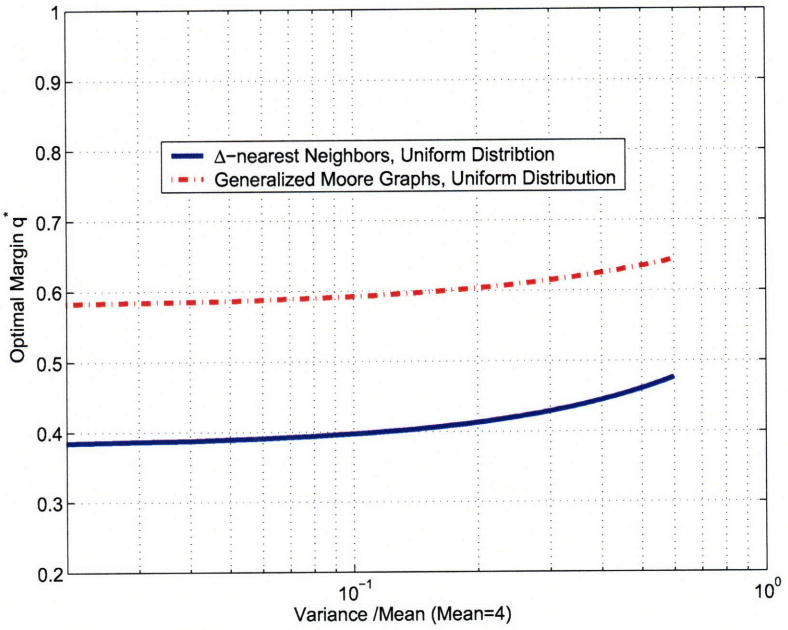

Figure 8-6: Optimal margin $q*$ vs. variance σ (normalized to mean $\bar{x}$), with $N = 50$, $\alpha/\beta_1 = 40$, $\beta_1 = 1$, $\bar{x} = 4$, and $\gamma = 2$.

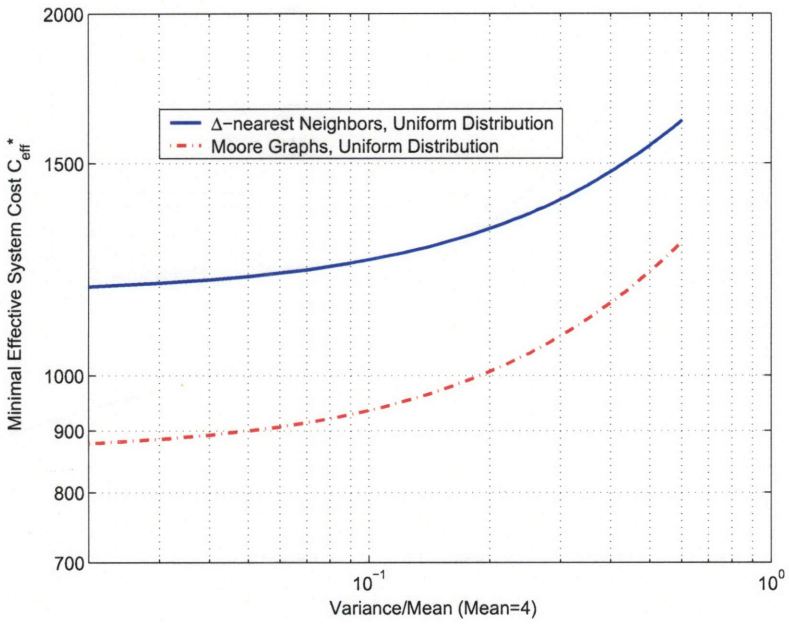

Figure 8-7: Minimal effective system cost C^*_{eff} vs. variance σ (normalized to mean $\bar{x}$), with $N = 50$, $\alpha/\beta_1 = 40$, $\beta_1 = 1$, $\bar{x} = 4$, and $\gamma = 2$.

distribution. In Figure 8-6, we plot the optimum provisioned bandwidth versus σ for two types of topologies – Δ-nearest Neighbors and Generalized Moore Graphs, both have 50 nodes and with uniform distribution; in Figure 8-7 we plot the minimal effective system cost versus σ for the same topologies and under the same conditions. In these plots, $\bar{x}$ is set to 4 and γ is set to 2. As illustrated in these figures, the optimal margin and the effective system cost all increase as the variance σ increases. The more detailed discussions are in the following:

- The case when σ is small corresponds to the scenario in which the designer has a fairly accurate prediction of the traffic demand. Thus it is optimal to provision for the mean value of the traffic forecast. Again the optimization problem (8.3) is reduced to a design for static (or quasi-static) traffic (6.1).

- The case when σ is large corresponds to the situation in which the uncertainty associated with the traffic prediction is large. Under this circumstance, it is optimal to provision more bandwidth to match the increasing σ. Therefore, the

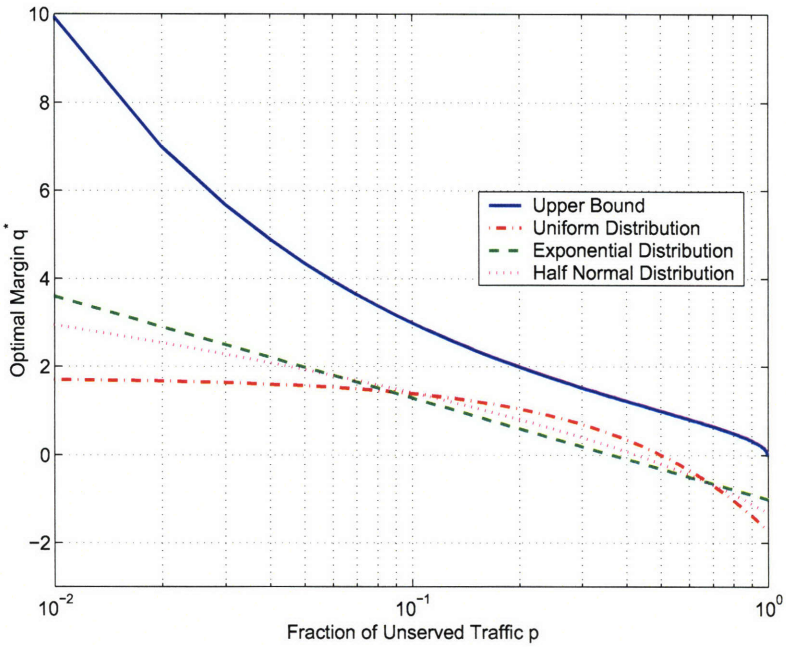

Figure 8-8: Optimal margin q^* vs. fraction of unserved traffic p.

effective system cost increases with a greater rate.

8.4.2 Results of Service Level Requirement Approach

Next we illustrate and discuss the results based on the optimization model (8.5) of service level requirement approach in Section 8.2.2. This model is well suited for the situations in which γ is hard to quantify. Then the Network designers can use these results to size the effect of demand uncertainties on the network installation cost. The results are presented in Tables 8.1 and 8.2 for the optimal margin q^*, optimal node degree Δ^*, and optimal network cost C_{n}^* for different random demand distributions and network topologies. Figure 8-8 and Figure 8-9 plot the optimal margin and minimal normalizd network cost as functions of the fraction of unserved traffic p, respectively. We note that p, like γ, can also be interpreted as a risk index – a lower p shows the designer's willingness to trade network cost over bandwidth shortage, and vise versa. Figure 8-8 shows that the optimal margin q^* decreases as the fraction

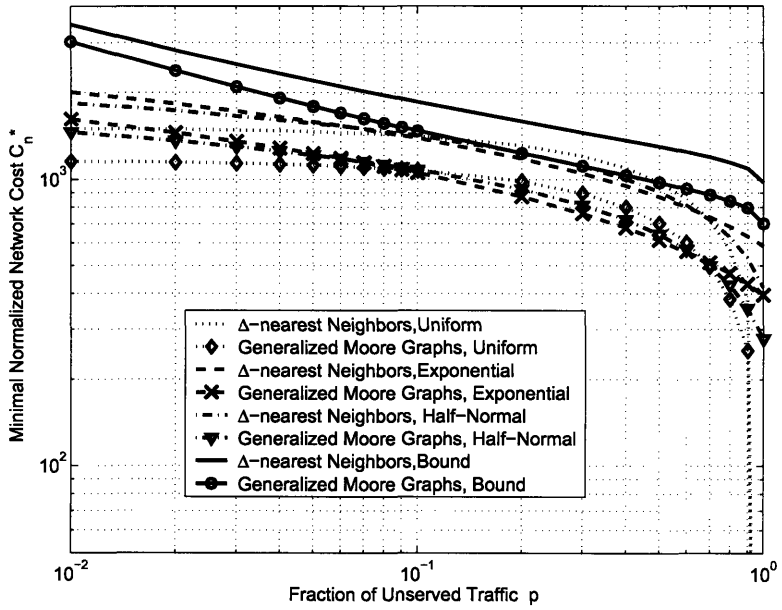

Figure 8-9: Minimal normalized network cost C_n^* vs. fraction of unserved traffic p.

of unserved traffic p increases. Figure 8-9 shows that the costs for networks with physical topologies of Generalized Moore Graphs are less than those for networks with physical topologies of Δ-nearest Neighbors, for the same demand distribution and fraction of unserved traffic. In other words, the trends displayed in Figures 8-8 and 8-9 are consistent with the results of bi-objective optimization approach. We also note that the "Upper Bound" distribution can be used to size the worst case (an upper bound) optimal margin q^* (Figure 8-8) and the worst case network cost (Figure 8-9) among all possible probability distributions with the same mean and variance, albeit the upper bound is quite pessimistic, especially when p is small.

8.5 Chapter Appendix

8.5.1 Derivation of the Feasibility Condition to Build a Network

In this appendix, we provide a derivation of the condition, under which it is feasible to build a network. Suppose the network installation cost for providing t units of bandwidth to a single user is $g(t)$, with the penalty cost for the unsatisfied traffic (for a single user), the effective system cost takes the form of

$$g(t) + \gamma \int_t^{\infty} (x - t) f(x) dx. \tag{8.25}$$

By setting the first derivative of the effective system cost to zero, we obtain

$$\frac{g'(t)}{\gamma} = \int_t^{\infty} f(x) dx. \tag{8.26}$$

This implies that to dimension any capacity $t > 0$, it requires that

$$\gamma > g'(t). \tag{8.27}$$

That is, the per unit cost for unsatisfied traffic needs to be larger than the marginal cost to provide t units of capacity. If $g(t) = ct$, we have $\gamma > c$.

8.5.2 Derivation of the Joint Convexity Conditions in (8.6)

In this section, we derive the condition under which the effective system cost in (8.6) is jointly convex in Δ and t.

As shown in (8.6), the effective system cost is

$$C_{\text{eff}}(N, \Delta, t) = \alpha\Delta + \beta_1 t(N-1)\left(\frac{3}{2} + \frac{N-1}{2\Delta}\right) + \gamma \frac{N-1}{2\sqrt{3}\sigma} \int_t^{\bar{x}+\sqrt{3}\sigma} (x - t) dx. \tag{8.28}$$

When the Hessian matrix of (8.28) is positive definite, the effective system cost is jointly convex in Δ and t. The Hessian matrix is

$$\begin{vmatrix} \frac{\partial^2 C_{\text{eff}}}{\partial \Delta^2} & \frac{\partial^2 C_{\text{eff}}}{\partial \Delta \partial t} \\ \frac{\partial^2 C_{\text{eff}}}{\partial t \partial \Delta} & \frac{\partial^2 C_{\text{eff}}}{\partial t^2} \end{vmatrix} = \begin{vmatrix} \frac{\beta t(N-1)^2}{\Delta^3} & -\frac{\beta(N-1)^2}{\Delta^2} \\ -\frac{\beta(N-1)^2}{\Delta^2} & \frac{\gamma(N-1)}{2\sqrt{3}\sigma} \end{vmatrix} \tag{8.29}$$

In order for the Hessian matrix to be positive definite, it must be true that the determinant of the Hessian matrix is positive, that is

$$\frac{\gamma t}{2\sqrt{3}\sigma} - \frac{\beta(N-1)}{\Delta} > 0. \tag{8.30}$$

8.5.3 Proof for "Upper Bound" Distribution

In this section, we provide a detailed description on how we obtain the PDF that requires the maximum (worst case) margin $q = (t - \bar{x})/\sigma$, among all distributions with the same mean $\bar{x}$ and standard deviation σ (variance σ^2).

For a given overflow probability p, the margin q is a function of both distribution function $f(x)$ and overflow probability p. we want to find a distribution $f(x)$ that has the mean $\bar{x}$ and the variance σ^2, and, at the same time, requires the maximal $q\sigma$. We can cast the finding of the maximal $q\sigma$ as an optimization problem:

$$\begin{aligned} \max_{f(x)} \quad & q\sigma \\ \text{s.t.} \quad & f(x) \geq 0; \\ & \int f(x)dx = 1; \\ & \int xf(x)dx = \bar{x}; \\ & \int x^2 f(x)dx = \bar{x}^2 + \sigma^2; \\ & \int_{\bar{x}+q\sigma}^{\infty} f(x)dx = p. \end{aligned} \tag{8.31}$$

For a given $q\sigma$, we are also interested in finding a distribution function $f(x)$ that has mean $\bar{x}$ and variance σ^2, and, at the same time, has the maximal overflow

probability p. This gives rise to the following optimization problem,

$$\begin{aligned} \max_{f(x)} \quad & p = \int_{\bar{x}+q\sigma}^{\infty} f(x)dx \\ \text{s.t.} \quad & f(x) \geq 0; \\ & \int f(x)dx = 1; \\ & \int xf(x)dx = \bar{x}; \\ & \int x^2 f(x)dx = \bar{x}^2 + \sigma^2; \\ & q \text{ is given.} \end{aligned} \tag{8.32}$$

The optimization problems as described in equations (8.31) and (8.32) are equivalent, in the sense that an optimal solution of one problem is also an optimal one of another. We next provide an intuitive argument of the equivalence of these two optimization problems. We first need the following lemma.

Lemma 2 *$f_1(x)$ and $f_2(x)$ are two continuous and monotonically decreasing functions, such that $f_1(x) \in [0, \infty)$ and $f_2(x) \in [0, \infty)$. If $f_1(x) \geq f_2(x)$ for all $x \in [0, \infty)$ and the inverse functions $f_1^{-1}(y)$ and $f_2^{-1}(y)$ exist for $y \in [0, \infty]$, then we have $f_1^{-1}(y) \geq f_2^{-1}(y)$ for $y \in [0, \infty)$.*

Proof: For any $y \in [0, \infty]$, there is a x_2 such that $y = f_2(x_2)$ and $f_1(x) \geq y$. $f_1(x)$ is monotonically decreasing, thus $f_1(x) \geq f_1(\infty)$. Since $f_1(x)$ is also continuous, there exists a $x_1 \in [x_2, \infty)$, such that $f_1(x_1) = y$ [57]. Therefore, we have $f_1^{-1}(y) = x_1 \geq x_2 = f_2^{-1}(y)$.

We now define $F(y)$ as $F(y) = \int_0^y f(x)dx$. With Lemma 2, we verify that the overflow probability of a given distribution, denoted as $1 - F(q\sigma)$, decreases monotonically as q increases. Assume that there are two distributions f^* and f', both with zero mean and σ^2 variance, and for any given q the overflow probability $1 - F(q\sigma + \bar{x})$ for distribution f^* is greater or equal to the overflow probability $1 - F'(q\sigma + \bar{x})$ for any other distribution f' (as shown in Figure 8-10). Let $q^*(p^\circ)$ and $q'(p^\circ)$ denote the margins for f^* and f' that achieve the overflow probability p°, respectively. Using Lemma 2, we reach the conclusion that $q^*(p^\circ) \geq q'(p^\circ)$. We thus prove that the optimization problems of (8.31) and (8.32) are indeed equivalent.

With the equivalence of the two formulations, we show that the following distributions are solutions to the optimization problems. That is, for a given $q\sigma$, the maximum overflow probability is $p = \frac{1}{1+q^2}$. The resulting distribution function that has the maximum overflow probability is

$$f(x) = \begin{cases} \frac{1}{1+q^2}, & x = \bar{x} + q\sigma; \\ \frac{q^2}{1+q^2}, & x = \bar{x} - \frac{\sigma}{q}. \end{cases} \tag{8.33}$$

Similarly, for a given overflow probability requirement p, the maximum margin obtained is $q = \sqrt{\frac{1-p}{p}}$. The resulting distribution function that requires the maximum margin is

$$f(x) = \begin{cases} p, & x = \bar{x} + \sqrt{\frac{1-p}{p}}\sigma; \\ 1-p, & x = \bar{x} - \sqrt{\frac{p}{1-p}}\sigma. \end{cases} \tag{8.34}$$

Next, we use the Chebyshev Inequality to verify that the distribution is asymptotically optimal. With the Chebyshev Inequality we have

$$\Pr[|x - \bar{x}| \leq q\sigma] \leq \frac{\sigma^2}{q^2\sigma^2} = \frac{1}{q^2}, \tag{8.35}$$

which is equivalent to

$$\Pr[x - \bar{x} \geq q\sigma] + \Pr[x - \bar{x} < -q\sigma] \leq \frac{1}{q^2}. \tag{8.36}$$

Clearly for any distribution, we have $\Pr[x - \bar{x} < -q\sigma] \geq 0$. Thus

$$\Pr[x - \bar{x} \geq q\sigma] \leq \frac{1}{q^2}. \tag{8.37}$$

That is, for any distribution function $f(l)$, the probability that $l > q\sigma$ is bounded by $\frac{1}{q^2}$. The PDF, given in (8.33), has a blocking probability $\Pr[x - \bar{x} \geq \sigma] = \frac{1}{1+q^2}$. As $q \to \infty$, we have $\frac{1}{1+q^2} \approx \frac{1}{q^2}$. Thus we show that the distribution in (8.33) is asymptotically optimal for large q.

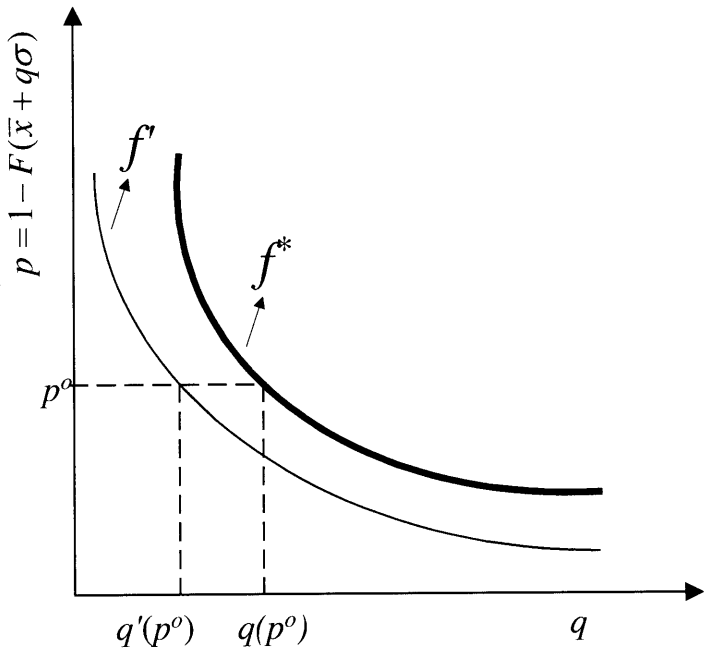

Figure 8-10: Fraction of unserved traffic $p = 1 - F(\bar{x} + q\sigma)$ as functions of q for possible distributions.

Chapter 9

Irregular Networks and Non-Uniform Traffic

Up until now, we have been analyzing the scalable network architecture by focusing on regular physical topologies and uniform traffic. In practice, network topologies are seldom regular or even regularizable. Also, the number of demands on node pairs are rarely equal. As such, it is often difficult to directly derive the analytical expressions or solutions. Normally the evaluation of irregular topologies under non-uniform traffic is carried out numerically. Despite these, we present in this chapter that, based on the framework of this thesis, we can extend the results derived for symmetric regular networks under uniform traffic to evaluate the cost efficiency of irregular networks under non-uniform traffic. In particular, we use results of Chapters 5, 6, and 7 to construct network cost lower and upper bounds and estimates. This chapter is organized as follows. In Section 9.1, we identify conditions under which minimum hop routing is still optimal. In Section 9.2, we focus on irregular networks under uniform traffic. We first show that the results for Generalized Moore Graphs and Δ-nearest Neighbors can be used to provide useful estimates for irregular networks. We next demonstrate how we use Generalized Moore Graphs as references to suggest possible improvements for irregular physical topologies. In Section 9.3, we study regular networks under non-uniform traffic. We first review the concept of minimum and maximum flow trees. Based on these concepts, we provide network cost lower

and upper bounds for regular networks under arbitrary (non-uniform) traffic. Finally in 9.4, by combining the results from 9.2 and 9.3, we construct network cost lower and upper bounds for irregular networks under arbitrary traffic.

9.1 Irregular Topologies, Arbitrary Traffic, and Minimum Hop Routing

As introduced in Section 4.4, an irregular topology, with Figure 9-1 as an example, is characterized by the following parameters:

- The number of nodes N;
- The maximum node degree $\Delta_{\max}$;
- The minimum node degree $\Delta_{\min}$;
- The average node degree $\bar{\Delta}$, which is defined as

$$\bar{\Delta} = \frac{1}{N}\sum_{i=1}^{N}\Delta_i, \tag{9.1}$$

  where Δ_i is the degree of node i.

For the convenience of discussion, we denote an irregular topology as $(N, \Delta_{\max}, \Delta_{\min}, \bar{\Delta})$. The average minimum hop distance $H_{\min}(N, \Delta_{\max}, \Delta_{\min}, \bar{\Delta})$ is then defined as

$$H_{\min}(N, \Delta_{\max}, \Delta_{\min}, \bar{\Delta}) = \frac{1}{N(N-1)}\sum_{i=1}^{N}\sum_{j=1}^{D_i} n_i(j), \tag{9.2}$$

where D_i denotes the network diameter from node i (the maximal hop distance from node i via minimum hop routing), and $n_i(j)$ denotes the number of nodes that are j hops away from node i.

Before analyzing the cost efficiency of an irregular network, we need to identify conditions under which minimum hop routing is still optimal. In Section 6.2.1, we proved that under uniform traffic, minimum hop routing is optimal for any given

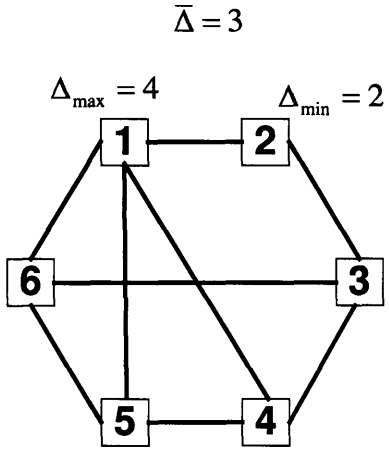

Figure 9-1: An irregular topology with $N = 6$, $\Delta_{\max} = 4$, $\Delta_{\min} = 2$, and $\bar{\Delta} = 3$.

regular network with a non-decreasing switching cost function. For an irregular network, without regularity and nodal symmetry, the relationship between the minimum hop routing and the network cost becomes much more complicated. To maintain the tractability of our analysis, we restrict our analysis to linear switching cost structuree (e.g., $F_1^i(K_o^i) = \beta_1 K_o^i$ for 3-D OXC, where K_o^i is the switch size at node i, cf. Table 5.1). Under this condition we can prove that minimum hop routing is still optimal, as summarized in the following result.

Theorem 14 *For a general (possibly irregular) network under arbitrary traffic, if the per node switching cost is a linear function of port count, minimum hop routing minimizes the switching cost.*

The linearity of the switching cost implies that minimizing the total switching cost is equivalent to minimizing the total network load. In other words, when switching cost is linear, the minimum network load solution is also the minimum network cost solution. The minimization of network load (also network cost) can only be achieved by routing traffic via minimum hop. A rigorous substantiation of this result is deferred to Appendix 9.5.1.

We note that if there are multiple minimum hop paths between a node pair, all the minimum hop routings minimize the switching cost, as long as the switching cost is linear with the number of ports. In other words, the minimization is indifferent to the detail of a routing algorithm. However, this is not the case if the switching cost is super-linear with the port count. As an example, Figure 9-2 shows two different minimum hop routing algorithms to support the same set of lightpath demands. The number near each node indicates the number of ports required (via the routing adopted). For a linear scaling of switching cost, both algorithms yield a total switching cost of $13\beta_1$. For a quadratic scaling, the routing in Figure 9-2 (a) incurs a total switching cost of $39\beta_3$; while the routing in Figure 9-2 (b) incurs a total switching cost of $47\beta_3$.

9.2 Irregular Networks Under Uniform Traffic

9.2.1 Lower and Upper Bounds on Network Cost

In light of Theorem 14, when analyzing the cost of an irregular network in this section, we restrict our attention first to uniform all-to-all traffic, minimum hop routing, and linear switching cost (e.g., $F_1^i(K_o^i) = \beta_1 K_o^i$). Our approach is to use the results of average minimum hop distances for Generalized Moore Graphs and Δ-nearest Neighbors to size the average minimum hop distance of an irregular topology $(N, \Delta_{\max}, \Delta_{\min}, \bar{\Delta})$. The results, already provided in section 4.4, are summarized here again for the convenience of discussion.

Theorem 15 *(Theorems 4 and 5) The average minimum hop distance of an irregular topology is lower bounded by the average minimum hop distance of a Generalized Moore Graph of N nodes and node degree $\Delta_{\max}$. That is,*

$$H_{\min}(N, \Delta_{\max}, \Delta_{\min}, \bar{\Delta}) \geq H^M_{\min}(N, \Delta_{\max}). \tag{9.3}$$

The average minimum hop distance of an irregular topology is upper bounded by the average minimum hop distance of a Δ-nearest Neighbors Topology of N nodes and

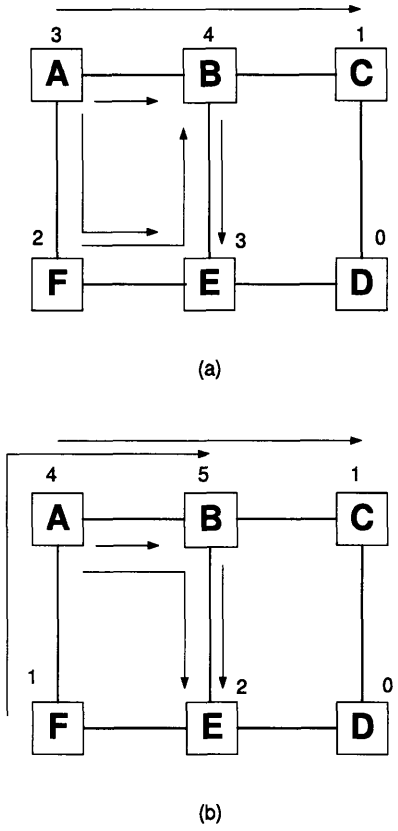

Figure 9-2: Two minimum hop routings to support demands A → B, A → C, A → E, F → B, and B → E. The switching cost is a quadratic function of number of ports. For a linear scaling of switching cost, both algorithms yield the same switching cost. For a quadratic scaling, two algorithms yield different total switching costs.

node degree $\Delta_{\min}$. *That is*

$$H_{\min}(N, \Delta_{\max}, \Delta_{\min}, \bar{\Delta}) \leq H^{N}_{\min}(N, \Delta_{\min}). \tag{9.4}$$

Since the switching cost is proportional to the average minimum hop distance, a direct application of Theorem 15 provides us with a cost lower bound and a cost upper bound for an irregular network.

Theorem 16 *For an irregular network of* $(N, \Delta_{\max}, \Delta_{\min}, \bar{\Delta})$, *the network cost under uniform traffic has a lower bound*

$$C(N, \Delta_{\max}, \Delta_{\min}, \bar{\Delta}) \geq \alpha N\bar{\Delta} + \beta_1 N(N-1)[H^{M}_{\min}(N, \Delta_{\max}) + 1], \tag{9.5}$$

and an upper bound

$$C(N, \Delta_{\max}, \Delta_{\min}, \bar{\Delta}) \leq \alpha N\bar{\Delta} + \beta_1 N(N-1)[H^{N}_{\min}(N, \Delta_{\min}) + 1], \tag{9.6}$$

The derivation for Theorem 16 is left in Appendix 9.5.2.

When $N \gg \bar{\Delta}$, $N \gg \Delta_{\max}$, and $N \gg \Delta_{\min}$, we approximate the ratio of the cost upper bound to the cost lower bound as

$$\frac{\alpha N\bar{\Delta} + \beta_1 N(N-1)H^{\mathrm{N}}_{\min}(N, \Delta_{\min})}{\alpha N\bar{\Delta} + \beta_1 N(N-1)H^{\mathrm{M}}_{\min}(N, \Delta_{\max})} \approx \frac{N}{\ln N}\frac{\ln \Delta_{\max}}{2\Delta_{\min}}. \tag{9.7}$$

Equation (9.7) indicates that the ratio scales as $\frac{N}{\ln N}$. In Appendix 9.5.3, we provide the derivations for this asymptotic result.

For an irregular networks with $\Delta_{\max} = 6$, $\Delta_{\min} = 3$, and $\bar{\Delta} = 4$, Figure 9-3 plots these two bounds in the form of normalized network cost per unit traffic $C(N, \Delta_{\max}, \Delta_{\min}, \bar{\Delta})/[N(N-1)]$ as a function of network size N. Based on the estimation of a realistic cost ratio between fiber and switching in metropolitan area networks, we set $\alpha/\beta_1 = 40$ and $\beta_1 = 1$. The plot indicates that as N increases, the gap between the upper and lower bounds increases with N (cf. 9.7). We also note that, as the size of the network increases, the lower bound of the normalized network cost per unit traffic decreases; while the upper bound of that first decreases and then increases. This can be explained as follows: the minimum node degree is set as a fixed value 3. This node degree (of 3) is optimal only for certain sizes of networks

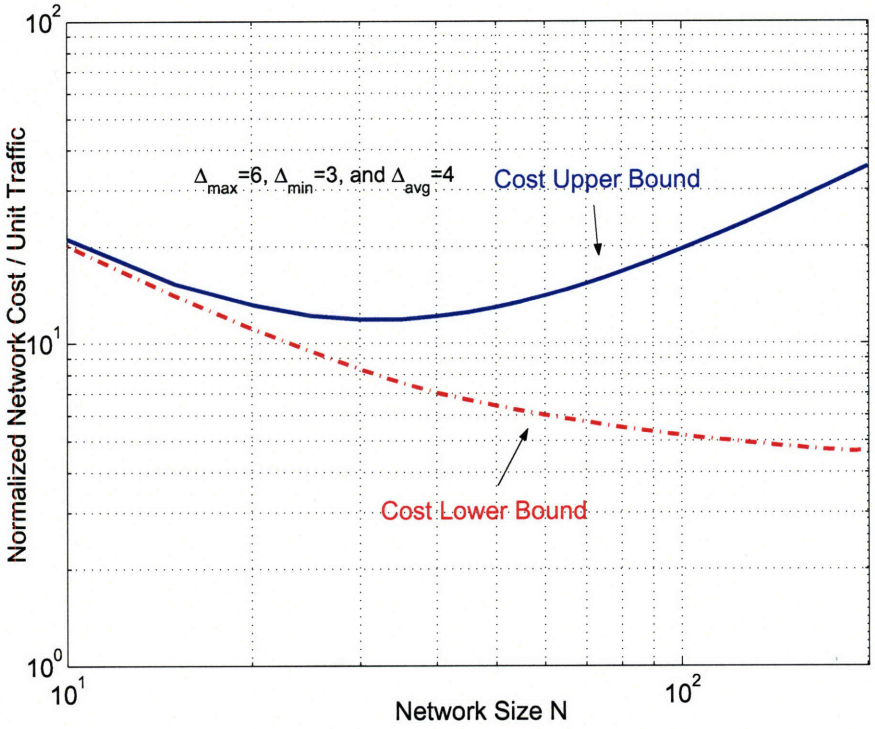

Figure 9-3: Network cost upper and lower bounds (in the form of normalized network cost per unit traffic) as functions of network size N. Fiber and switching cost parameters are: $\alpha/\beta_1 = 40$ and $\beta_1 = 1$.

($N = 10 \sim 30$). As the size of the network increases, this node degree (of 3) becomes less efficient, as discussed in Chapter 6 (cf. Figure. 6-8).

To have an idea on how close these two bounds match the actual cost of the irregular networks, we employ randomly generated networks. That is, for a given set of parameters (N, $\Delta_{\max}$, $\Delta_{\min}$, and $\bar{\Delta}$), we construct around 4000 instances of networks at random, compute the cost of each of them, and compare their cost distributions with the corresponding lower and upper bounds. We plot in Figure 9-4 and Figure 9-5 the cost histograms for random networks of size $N = 20$ and $N = 40$, respectively. The node degree parameters for each N are set as $\Delta_{\max} = 6$, $\Delta_{\min} = 3$, and $\bar{\Delta} = 4$. These histograms demonstrate that Generalized Moore Graphs can be used for effectively sizing the cost of an irregular network, especially when N is small (e.g., $N = 10 \sim 30$) and the network is densely connected (e.g., $\bar{\Delta}/N \geq 0.2$). On the contrary, the cost upper bounds generated by using Δ-nearest Neighbors are loose, especially when N is large (e.g., $N \leq 40$) and the network is sparsely connected (e.g., $\bar{\Delta}/N \leq 0.1$).

To look for a better estimates of network cost, we use $\bar{\Delta}$ to replace $\Delta_{\max}$ in (9.5) and $\Delta_{\min}$ in (9.6). Thus the new estimates are

$$\alpha N\bar{\Delta} + \beta_1 N(N-1)[H^{\mathrm{M}}_{\min}(N,\bar{\Delta}) + 1], \tag{9.8}$$

and

$$\alpha N\bar{\Delta} + \beta_1 N(N-1)[H^{\mathrm{N}}_{\min}(N,\bar{\Delta}) + 1]. \tag{9.9}$$

We also use the Symmetric Hamilton Graph to provide an alternative estimate of network cost as following:

$$\alpha N\bar{\Delta} + \beta_1 N(N-1)[H^{\mathrm{H}}_{\min}(N,\Delta_{\min}) + 1], \tag{9.10}$$

where $H^{\mathrm{H}}_{\min}(N,\Delta) = 3/4 + (N-2)/4(\Delta - 1)$, as derived in Section 4.5.6. Including these estimates to the corresponding Figures 9-4, 9-5, and **??**, we find that they do give better estimates. Note that we term (9.8) to (9.10) as "estimates", since we have not been able to prove that they are indeed tighter bounds for every irregular network $(N, \Delta_{\max}, \Delta_{\min}, \bar{\Delta})$.

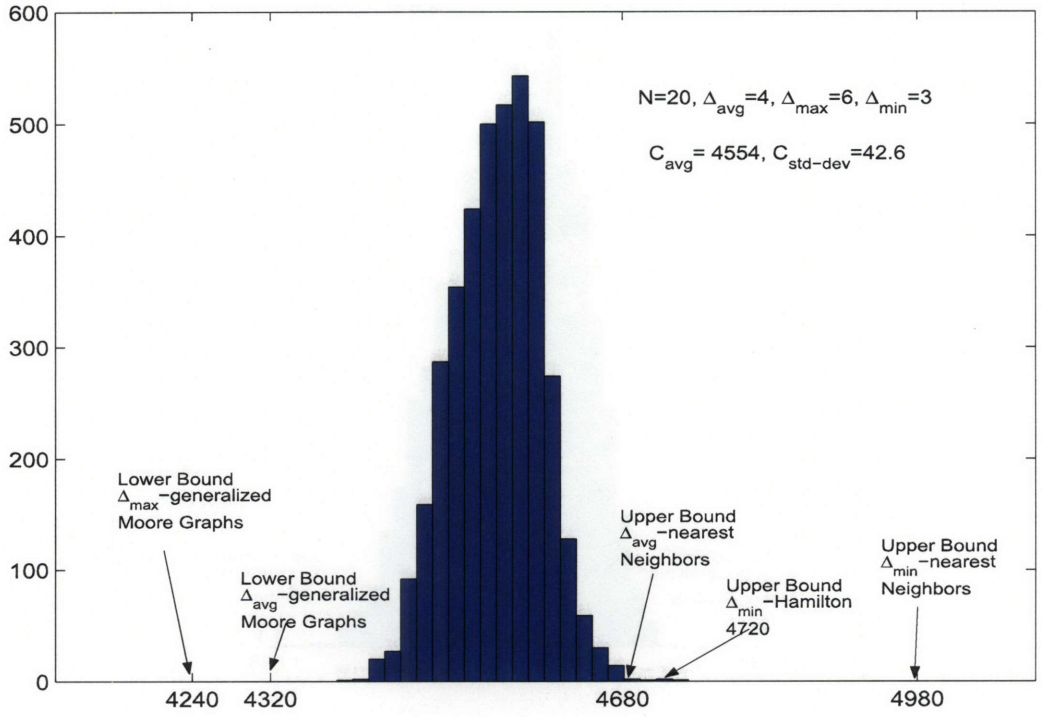

Figure 9-4: Network cost histogram for randomly generated networks, with $N = 20$, $\Delta_{\max} = 6$, $\Delta_{\min} = 3$, and $\bar{\Delta} = 4$. The fiber and switching cost parameters are: $\alpha/\beta_1 = 40$ and $\beta_1 = 1$.

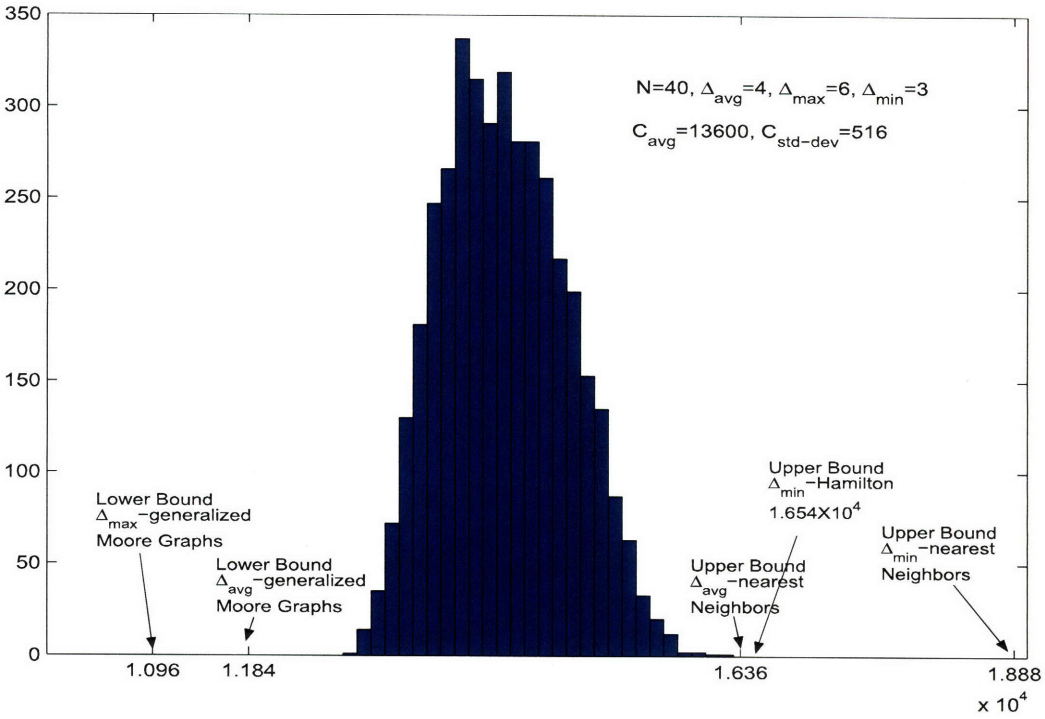

Figure 9-5: Network cost histogram for randomly generated networks, with $N = 40$, $\Delta_{\max} = 6$, $\Delta_{\min} = 3$, and $\bar{\Delta} = 4$. The fiber and switching cost parameters are: $\alpha/\beta_1 = 40$ and $\beta_1 = 1$.

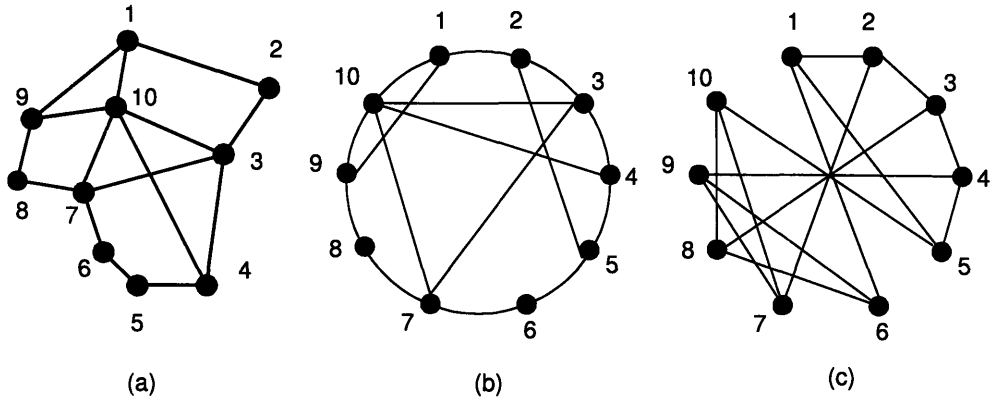

Figure 9-6: (a) Network 1 with $N = 10$, $\Delta_{\max} = 5$, $\Delta_{\min} = 2$, and $\bar{\Delta} = 3$; (b) Network 1 redrawn as a chordal ring; (c) The Petersen Graph (redrawn) with $N = 10$ and $\Delta = 3$.

9.2.2 Generalized Moore Graphs as References for Possible Improvements for an Irregular Physical Topology

In this section we use examples to demonstrate how we can use Generalized Moore Graphs as references to suggest possible improvement for irregular physical topologies. In particular, we consider three representative networks, which are labeled as Network 1, Network 2, and Network 3, with physical topologies illustrated in Figure 9-6(a), Figure 9-7(a), and Figure 9-8(a), respectively. The key network design parameters of them are summarized in Table 9.1. In our study, we assume that all fiber connections have approximately the same cost and all nodes are equipped with 3-D OXCs (cf. Table 5.1 with ζ set to 0). For clarity of discussion, we redraw the topologies of Network 1, Network 2, and Network 3 in the form of chordal rings in Figure 9-6(b), Figure 9-7(b), and Figure 9-8(b), respectively. For each of the networks, we look for the minimum number of switching ports required by solving (9.27) to (9.29) in Section 9.5.1 numerically. The results show that to support all-to-all uniform traffic, a total of 261, 636, and 1292 switching ports are required for Network 1, Network

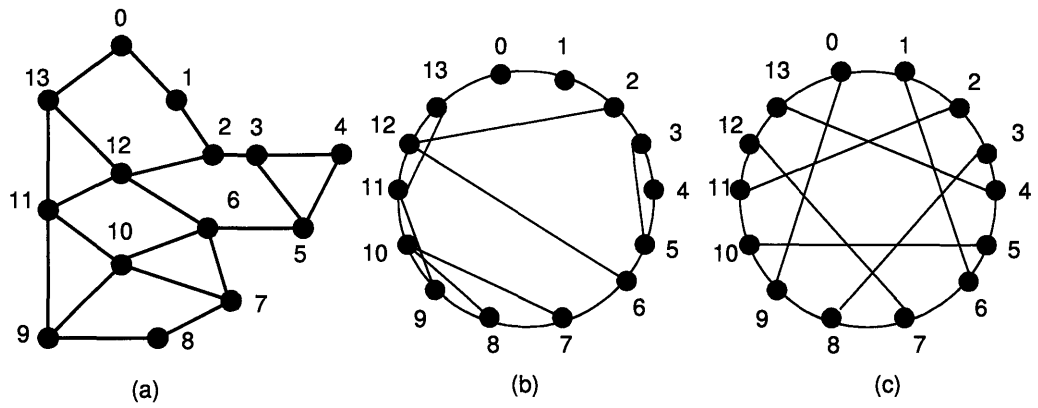

Figure 9-7: (a) Network 2 with $N = 14$, $\Delta_{\max} = 4$, $\Delta_{\min} = 2$, and $\bar{\Delta} = 3$; (b) Network 2 redrawn as a chordal ring; (c) The Heawood Graph with $N = 14$ and $\Delta = 3$.

2, and Network 3, respectively. We then connect the same set of nodes in the form of Generalized Moore Graphs and their close relatives (via fiber patched panels). In particular, we suggest that the nodes in Network 1 are connected via the Petersen Graph, the nodes in Network 2 are connected via the Headwood Graph, and the nodes in Network 3 are connected via a close relative of Generalized Moore Graphs, as shown in Figure 9-6(c), Figure 9-7(c), and Figure 9-8(c), respectively. For a fair comparison, here we let each suggested network uses the same number of fiber connection as its original one does. The parameters and results of the suggested networks are also listed in Table 9.1. It is seen that each of these suggested networks requires less ports. The reduction of costs ranges from 7% to 15%. We believe that the savings are likely to be more pronounced for larger networks. An interesting trend is observed in these figures. From the perspective of a chordal ring, the original topologies of Network 1, Network 2, and Network 3 tend to have more "local" connections – most of the nodes connect to their neighbors. In comparison, the improved topologies tend to have more "diagonal" connections – more nodes are linked across the ring.

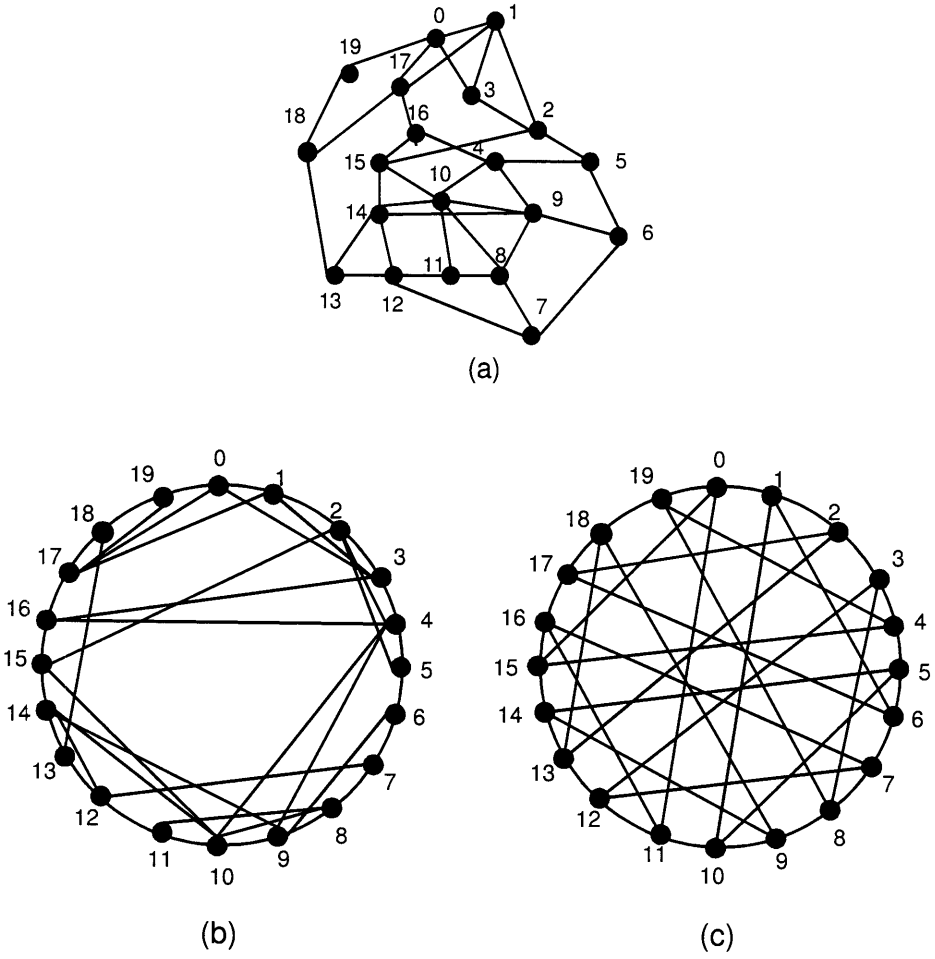

Figure 9-8: (a) Network 3 with $N = 20$, $\Delta_{\max} = 6$, $\Delta_{\min} = 3$, and $\bar{\Delta} = 4$; (b) Network 3 redrawn as a chordal ring; (c) A close relative of Generalized Moore Graph with $N = 20$ and $\Delta = 4$.

Table 9.1: Parameters for Network 1, Network 2, and Network 3.

	Network 1	Petersen Graph	Network 2	Heawood Graph	Network 3	Close Reltative
N	10	10	14	14	20	20
Δ_{max}	5	3	4	3	6	4
Δ_{min}	2	3	2	3	3	4
$\bar{\Delta}$	3	3	3	3	4	4
No. of fibers	30	30	52	52	80	80
No. of ports	261	240	636	560	1292	1140

9.3 Regular Networks Under Non-Uniform Traffic

In this section, we focus on evaluating cost efficiencies of regular networks under non-uniform traffic. In particular, we derive network cost lower and upper bounds for any regular networks of node number N, node degree Δ, and a traffic matrix $T = [t_{i,j}]$. As in the analysis in Section 9.2, we still assume that switching cost at each node is linear with number of ports. As such, minimum hop routing requires the least number of switching ports (cf. Theorem 14). For simplicity and clarity, we also make the assumption that all the fiber connections have the same cost.

9.3.1 Minimum and Maximum Flow Trees

The derivation of cost lower and upper bounds hinges on the concepts of minimum and maximum flow trees. The concept of minimum flow tree is developed as a tool to analyze network congestion [58] [59]. Following the rationale (of constructing a minimum flow tree), we introduce the concept of maximum flow tree for our work.

The construction of a minimum flow tree is based on the routing spanning tree of a Generalized Moore Graphs. That is, in a regular topology of node degree Δ, for each node there can be at most Δ destinations one hop away, Δ^2 destinations two hops away, etc. Moreover, for each source the Δ destinations with the largest traffic are connected by one hop paths, the next Δ^2 destinations in descending order of traffic are connected by two-hop paths, and so on. The intuition of minimum flow

tree is to minimize the propagation of larger traffic values. As such, the larger traffic $t_{i,j}$ is closer to node i. As an example, for the traffic matrix shown in Figure 9-9 (a), Figure 9-9 (b) illustrates the construction of a minimum flow tree from node A.

The construction of a maximum flow tree is based on the routing spanning tree of a Δ-nearest Neighbors. That is, in a regular topology of node degree Δ, for each node there are Δ destinations one hop away, Δ destinations two hops away, etc. That is, each (except probably the last) level is packed with only Δ nodes. Moreover, for each source the Δ destinations with the smallest traffic are connected by one hop paths, the next Δ destinations in ascending order of traffic are connected by two-hop paths, and so on. The intuition of maximum flow tree is to maximize the propagation of larger traffic values. As such, the smaller traffic $t_{i,j}$ is closer to node i. As an example, for the traffic matrix shown in Figure 9-9 (a), Figure 9-9 (c) illustrates the construction of a maximum flow tree from node A.

9.3.2 Network Cost Lower and Upper Bounds for Regular Networks Under Non-Uniform Traffic

With the concepts of minimum and maximum flow trees, we are ready to provide cost lower and upper bounds. To derive a lower bound, we first perform a permutation for traffic matrix $T = [t_{i,j}]$, such that the elements of each row are in a descending order. That is, for $1 \leq i \leq N$ and $1 \leq j \leq N$, let π_i be a permutation of $(1, 2, \cdots N)$ and $\pi_i(j)$ be the jth element of π_i, such that

$$t_{i,\pi_i(j)} \geq t_{i,\pi_i(j')} \text{ for } j \leq j'. \tag{9.11}$$

We also define D as the network diameter and m_k as the number of nodes packed in 1st to kth levels of the minimum flow tree. That is,

$$m_k = \begin{cases} \sum_{i=1}^{k} \Delta^i, & \text{if } 1 \leq k \leq D-1, \\ N-1, & \text{if } k = D. \end{cases} \tag{9.12}$$

As stated in Section 5.3.1, setting up a lightpath of k hops requires $k+1$ ports. A direct application of this fact gives us the lower bound on total switching cost for any

	A	B	C	D	E	F	G	H	I	J	K	L	M
A	0	6	5	1	2	4	3	2	1	2	1	1	2

(a)

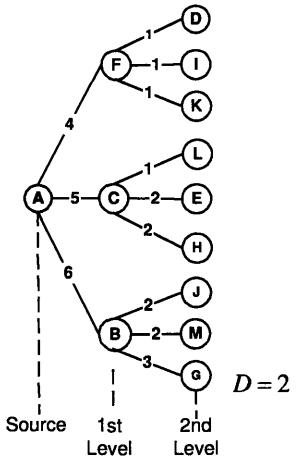

(b)

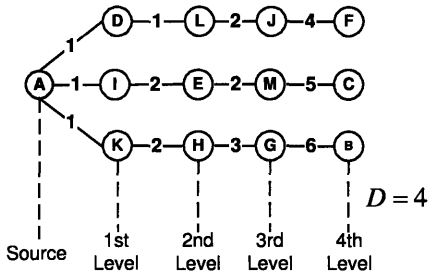

(c)

Figure 9-9: (a) Traffic demand from node A to other nodes; (b) Minimum flow tree from node A; (c) Maximum flow tree from node A.

regular network of node number N and node degree Δ, with a traffic matrix $T = [t_{i,j}]$. That is,

$$C_s \geq \beta_1 \sum_{i=1}^{N} \sum_{k=1}^{D} \sum_{j=m_k}^{N-1} t_{i,\pi_i(j)}(k+1). \tag{9.13}$$

Since the fiber cost is $C_f = \alpha N \bar{\Delta}$, we have a lower bound of network cost

$$C \geq \alpha N \bar{\Delta} + \beta_1 \sum_{i=1}^{N} \sum_{k=1}^{D} \sum_{j=m_k}^{N-1} t_{i,\pi_i(j)}(k+1). \tag{9.14}$$

To derive an upper bound, we first perform a permutation for traffic matrix $T = [t_{i,j}]$, such that the elements of each row are in an ascending order. That is, for $1 \leq i \leq N$ and and $1 \leq j \leq N$, let π'_i be a permutation of $(1, 2, \cdots N)$ and $\pi'_i(j)$ be the jth element of π'_i, such that

$$t_{i\pi'_i(j)} \leq t_{i\pi'_i(j')} \text{ for } j \leq j'. \tag{9.15}$$

We also define m'_k as the number of nodes packed in 1st to kth levels of the maximum flow tree. That is,

$$m'_k = \begin{cases} k\Delta, & \text{if } 1 \leq k \leq D-1, \\ N-1, & \text{if } k = D. \end{cases} \tag{9.16}$$

A direct application of the fact that a k-hop lightpath requires $k+1$ ports gives us the upper bound on total switching cost for any regular network of node number N and node degree Δ, with a traffic matrix $T = [t_{i,j}]$. That is,

$$C_s \leq \beta_1 \sum_{i=1}^{N} \sum_{k=1}^{D} \sum_{j=m'_k}^{N-1} t_{i\pi'_i(j)}(k+1). \tag{9.17}$$

Since the fiber cost is $C_f = \alpha N \Delta$, we have an upper bound of network cost

$$C \leq \alpha N \Delta + \beta_1 \sum_{i=1}^{N} \sum_{k=1}^{D} \sum_{j=m'_k}^{N-1} t_{i\pi'_i(j)}(k+1). \tag{9.18}$$

9.4 Irregular Networks Under Arbitrary Traffic

Combining the results of Sections 9.1 - 9.3, in this section we provide network cost lower and upper bounds for irregular networks under non-uniform traffic. As in the analysis in the previous section, we assume minimum hop routing and linear switching cost at every node.

To derive a lower bound, we first perform a permutation for traffic matrix T, such that the elements of each row are in a descending order. That is, for $1 \leq i \leq N$ and $1 \leq j \leq N$, let π_i be a permutation of $(1, 2, \cdots N)$ and $\pi_i(j)$ be the jth element of π_i, such that

$$t_{i,\pi_i(j)} \geq t_{i,\pi_i(j')} \text{ for} j \leq j'. \tag{9.19}$$

We also define m_k as the number of nodes packed in 1st to kth levels of the minimum flow tree. That is,

$$m_k = \begin{cases} \sum_{i=1}^{k} \Delta_{\max}^{i}, & \text{if } 1 \leq k \leq D-1, \\ N-1, & \text{if } k = D. \end{cases} \tag{9.20}$$

As stated in Section 5.3.1, setting up a lightpath of k hops requires $k+1$ ports. A direct application of the fact gives us the lower bound on total switching cost for any irregular network $(N, \Delta_{\max}, \Delta_{\min}, \bar{\Delta})$, with a traffic matrix $T = [t_{i,j}]$. That is,

$$C_{\mathrm{s}} \geq \beta_1 \sum_{i=1}^{N} \sum_{k=1}^{D} \sum_{j=m_k}^{N-1} t_{i\pi_i(j)}(k+1). \tag{9.21}$$

Since the fiber cost is $C_{\mathrm{f}} = \alpha N \bar{\Delta}$, we have a lower bound of network cost

$$C \geq \alpha N \bar{\Delta} + \beta_1 \sum_{i=1}^{N} \sum_{k=1}^{D} \sum_{j=m_k}^{N-1} t_{i\pi_i(j)}(k+1). \tag{9.22}$$

To derive an upper bound, we first perform a permutation for traffic matrix T, such that the elements of each row are in an ascending order. That is, for $1 \leq i \leq N$ and $1 \leq j \leq N$, let π_i' be a permutation of $(1, 2, \cdots N)$ and $\pi_i'(j)$ be the jth element of π_i', such that

$$t_{i\pi_i'(j)} \leq t_{i\pi_i'(j')} \text{ for} j \leq j'. \tag{9.23}$$

We also define m'_k as the number of nodes packed in 1st to kth levels of the maximum flow tree. That is,

$$m'_k = \begin{cases} k\Delta_{\min}, & \text{if } 1 \le k \le D-1, \\ N-1, & \text{if } k = D. \end{cases} \tag{9.24}$$

A direct application of the fact that a k-hop lightpath requires $k+1$ ports gives us the upper bound on total switching cost for an irregular network $(N, \Delta_{\max}, \Delta_{\min}, \bar{\Delta})$, with a traffic matrix $T = [t_{i,j}]$. That is,

$$C_{\mathrm{s}} \le \beta_1 \sum_{i=1}^{N} \sum_{k=1}^{D} \sum_{j=m'_k}^{N-1} t_{i\pi'_i(j)}(k+1). \tag{9.25}$$

Since the fiber cost is $C_{\mathrm{f}} = \alpha N \bar{\Delta}$, we have an upper bound of network cost

$$C \le \alpha N \bar{\Delta} + \beta_1 \sum_{i=1}^{N} \sum_{k=1}^{D} \sum_{j=m'_k}^{N-1} t_{i\pi'_i(j)}(k+1). \tag{9.26}$$

9.5 Chapter Appendix

9.5.1 Proof for Theorem 14

Proof: To prove this theorem, we first formulate a switching cost minimization problem for arbitrary topology, traffic, and switching cost function, using the framework of multi-commodity flow. We then show that when the switching cost is linear with port count, the formulation is equivalent to that of an (all-pairs) minimum hop routing problem.

For a given traffic matrix on a given network topology, finding the optimal routing that minimize the switching cost takes the following form:

$$\min \; C_{\mathrm{s}}(l_{i,j}^{s,d}) = \sum_i F_j^i(K_{\mathrm{o}}^i) \tag{9.27}$$

$$\text{s.t.} \sum_i l_{i,j}^{s,d} - \sum_j l_{i,j}^{s,d} = \begin{cases} t_{s,d}, & \text{if } s = i; \\ -t_{s,d}, & \text{if } d = i; \\ 0, & \text{otherwise;} \end{cases} \tag{9.28}$$

$$K_{\mathrm{o}}^{i} = \sum_{s \neq i,d} \sum_{j} l_{j,i}^{s,d} + \sum_{j} t_{i,j} + \sum_{j} t_{j,i}. \tag{9.29}$$

In this formulation, the parameters for topology, traffic, and switching cost are denoted as following:

- The integer parameter i, $i \in \{1, 2, \cdots, N\}$, denotes the nodes of the network;
- The integer ordered pair (i, j), $i \in \{1, 2, \cdots, N\}$ and $j \in \{1, 2, \cdots, N\}$, with $i \neq j$, denotes a fiber connection from node i to node j;
- The integer ordered pair (s, d), $s \in \{1, 2, \cdots, N\}$ and $d \in \{1, 2, \cdots, N\}$, with $s \neq d$, denotes a source-destination pair from s to d. Traffic demand between the corresponding node pair is denoted by integer valued $t_{s,d}$.
- The integer K_{o}^{i} represents the number of ports at node i. K_{o}^{i} equals to the sum of the number of pass-through, added, and dropped lightpaths at node i, which are of the value of $\sum_{s \neq i,d} \sum_{j} l_{j,i}^{s,d}$, $\sum_{j} t_{i,j}$, and $\sum_{j} t_{j,i}$, respectively.
- $F_{j}^{i}(K)$, with $j \in \{1, 2, 3\}$, is the OXC cost function of type j (cf. (5.10) and Table 5.1) at node i.

Also in this formulation, equation (9.28) is the conservation of flow constraint. Equation (9.29) relates all the flows that pass-through, initiated and dropped at a node i to the number of ports at node i. For a given irregular network topology and a set of (arbitrary) traffic demands, we want to solve for $l_{i,j}^{s,d}$ – the amount of traffic for the source-destination pair (s, d) to be routed on the fiber (i, j).

Under arbitrary traffic, for every node i we have

$$\sum_{j} t_{i,j} = \sum_{s=i.d} \sum_{j} l_{i,j}^{s,d}. \tag{9.30}$$

Thus the number of ports at node i is

$$K_{\mathrm{o}}^{i} = \sum_{s,d} \sum_{j} l_{j,i}^{s,d} + \sum_{j} t_{j,i}; \tag{9.31}$$

If the switching cost is a linear function of port count (e.g., $F_1^i(K_o^i) = \beta_1 K_o^i$ for 3-D OXC), the formulation (9.27) to (9.29) can be simplified as

$$\min \left\{ C_s(l_{i,j}^{s,d}) = \beta_1 \sum_{s,d} \sum_i \sum_j l_{i,j}^{s,d} + \sum_i \sum_j t_{j,i} \right\} \tag{9.32}$$

$$\text{s.t.} \sum_i l_{i,j}^{s,d} - \sum_j l_{i,j}^{s,d} = \begin{cases} t_{s,d}, & \text{if } s = i; \\ -t_{s,d}, & \text{if } d = i; \\ 0, & \text{otherwise.} \end{cases} \tag{9.33}$$

Note that the term $\sum_i \sum_j t_{j,i}$ in the objective function does not depend on $l_{i,j}^{s,d}$, thus (9.32) and (9.33) are equivalent to

$$\min \left\{ C_s(l_{i,j}^{s,d}) = \beta_1 \sum_{s,d} \sum_i \sum_j l_{i,j}^{s,d} \right\} \tag{9.34}$$

$$\text{s.t.} \sum_i l_{i,j}^{s,d} - \sum_j l_{i,j}^{s,d} = \begin{cases} t_{s,d}, & \text{if } s = i; \\ -t_{s,d}, & \text{if } d = i; \\ 0, & \text{otherwise.} \end{cases} \tag{9.35}$$

Note that (9.34) and (9.35) are the exact formulation for a (all-pairs) minimum hop routing problem [50], we thus prove that minimum hop routing minimizes the switching cost. We also note that the solution to this minimum hop routing problem may not be unique.

9.5.2 Derivations of Network Cost Upper and Lower Bounds

In this section, we provide the derivation for Theorem 16, which gives network cost lower bound (9.5) and upper bound (9.6). As stated in Chapter 5, the first-order network cost model consists of fiber cost and optical switch cost. The fiber cost is

proportional to the number of fibers used, that is

$$\begin{aligned} C_{\mathrm{f}} &= \alpha \sum_{i=1}^{N} \Delta_i \\ &= \alpha N \frac{\sum_{i=1}^{N} \Delta_i}{N} \\ &= \alpha N \bar{\Delta}. \end{aligned} \tag{9.36}$$

Next, we consider the optical switch cost. Since we assume that the switching cost is a linear function of port count, e.g., $F_1^i(K_{\mathrm{o}}^i) = \beta_1 K_{\mathrm{o}}^i$, the total switching cost is proportional to the total number of switching ports required. We again let D_i denote the diameter of node i and let $n_i(j)$ denote the number of nodes whose minimum hop path from node i consists of j hops, the switching cost is expressed as

$$\begin{aligned} C_{\mathrm{s}}(N, \Delta_{\max}, \Delta_{\min}, \bar{\Delta}) &= \beta_1 \sum_{i=1}^{N} K_o^i \\ &= \beta_1 \sum_{i=1}^{N} \sum_{j=1}^{D_i} (n_i(j) + 1) \\ &= \beta_1 \sum_{i=1}^{N} \sum_{j=1}^{D_i} n_i(j) + \beta_1 \sum_{i=1}^{N} \sum_{j=1}^{D_i} 1 \\ &= \beta_1 N(N-1) \left[\frac{\sum_{i=1}^{N} \sum_{j=1}^{D_i} n_i(j)}{N(N-1)} + 1 \right] \\ &= \beta_1 N(N-1)[H_{\min}(N, \Delta_{\max}, \Delta_{\min}, \bar{\Delta}) + 1]. \end{aligned} \tag{9.37}$$

Note that in the above derivation, we use the fact that

$$\beta_1 \sum_{i=1}^{N} \sum_{j=1}^{D_i} 1 = N(N-1). \tag{9.38}$$

Applying the inequalities in Theorem 15 to the above equation, we prove that an irregular network of $(N, \Delta_{\max}, \Delta_{\min}, \bar{\Delta})$ has a network cost lower bound and network cost upper bound, as expressed in (9.5) and (9.6), respectively.

9.5.3 Derivation of the Asymptotic Ratio Between Network Cost Upper and Lower Bound

In this section, we provide the derivation for the asymptotic ratio between network cost upper and lower bound, as stated in (9.7). Theorem 16 indicates that for an irregular network of $(N, \Delta_{\max}, \Delta_{\min}, \bar{\Delta})$, the network cost has a lower bound

$$C(N, \Delta_{\max}, \Delta_{\min}, \bar{\Delta}) \geq \alpha N\bar{\Delta} + \beta_1 N(N-1)[H^{\mathrm{M}}_{\min}(N, \Delta_{\max}) + 1], \tag{9.39}$$

and an upper bound

$$C(N, \Delta_{\max}, \Delta_{\min}, \bar{\Delta}) \leq \alpha N\bar{\Delta} + \beta_1 N(N-1)[H^{\mathrm{N}}_{\min}(N, \Delta_{\min}) + 1]. \tag{9.40}$$

The ratio of the upper bound to the lower bound is

$$\begin{aligned} &\frac{\alpha N\bar{\Delta} + \beta_1 N(N-1)[H^{\mathrm{N}}_{\min}(N, \Delta_{\min}) + 1]}{\alpha N\bar{\Delta} + \beta_1 N(N-1)[H^{\mathrm{M}}_{\min}(N, \Delta_{\max}) + 1]} \\ &= \frac{1 + \frac{\beta_1(N-1)}{\alpha\bar{\Delta}}[H^{\mathrm{N}}_{\min}(N, \Delta_{\min}) + 1]}{1 + \frac{\beta_1(N-1)}{\alpha\bar{\Delta}}[H^{\mathrm{M}}_{\min}(N, \Delta_{\max}) + 1]} \end{aligned} \tag{9.41}$$

When $N \gg \bar{\Delta}$, $N \gg \Delta_{\max}$, and $N \gg \Delta_{\min}$, we approximate the ratio of the upper bound to the lower bound as

$$\frac{\frac{\beta_1(N-1)}{\alpha\bar{\Delta}}[H^{\mathrm{N}}_{\min}(N, \Delta_{\min}) + 1]}{\frac{\beta_1(N-1)}{\alpha\bar{\Delta}}[H^{\mathrm{M}}_{\min}(N, \Delta_{\max}) + 1]} \approx \frac{H^{\mathrm{N}}_{\mathrm{asym}}(N, \Delta_{\min})}{H^{\mathrm{M}}_{\mathrm{asym}}(N, \Delta_{\max})}. \tag{9.42}$$

We have derived the asymptotic expressions for Generalized Moore Graphs in Section 4.5.3 and that for Δ-nearest Neighbors topologies in Section 4.5.4. That is, for Generalized Moore Graphs we have (4.11)

$$H^{\mathrm{M}}_{\mathrm{asym}}(\Delta, N) \to \log_{\Delta} N = \frac{\ln N}{\ln \Delta}. \tag{9.43}$$

For Δ-nearest Neighbors topologies we have (4.18)

$$H^{\mathrm{N}}_{\mathrm{asym}}(\Delta, N) \to \frac{1}{2} + \frac{N-1}{2\Delta}. \tag{9.44}$$

Substitute (9.43) and (9.44) into (9.42), we obtain the ratio of the upper bound to the lower bound as $\frac{N}{\ln N}\frac{\ln \Delta_{\max}}{2\Delta_{\min}}$.

Chapter 10

Summary and Comments

In this chapter, we conclude this thesis and comment on possible further extensions.

10.1 Thesis Summary

In current telecom environment, carriers have deployed huge capacity in the long-haul networks. At the meantime, end users' access to higher data rates is still costly. To bridge the gap between the bandwidth glut at the backbone and the high access cost for the end-users, the architecture of next generation optical MAN will be an important contributor to the reduction of access network cost. The objective is to design networks that not only require a low installation cost, but also have good scalability – a decreasing cost-per-node-per-unit-traffic as the number of users and transaction size increase. This architecture feature is essential for any commercially deployed network to attract serious providers and investors to commit to the venture as part of a sensible business.

The central theme of this thesis is to identify scalable network architectures over the possibilities of optical networks as allowed by the technology: fiber connection topologies, switching technology selection and dimensioning, as well as routing and wavelengths assignment, with emphasis on exploring the benefit of optimizing over fiber connection topologies. Due to the intrinsic complexity of such an optimization problem and because of our interest in gaining insights into how the cost structures

drive architectural tradeoffs, for the first part of this thesis, we take an analytical approach by concentrating on networks with regular topologies and (static and random) uniform all-to-all traffic. These assumptions are idealizations, nonetheless they keep the analysis tractable and provide us insights into more complex problems and they act as points of departures for the analysis of more realistic scenarios (such as irregular networks and non-uniform traffic) in the later part of this thesis.

The search for the scalable fiber connection architecture hinges on analyzing the tradeoffs among expensive network resources. In our parametric, first-order, and homogeneous cost model, the constituent parts, which are closely related to fiber topology, are fiber cost and switching cost. To build a network, one can support lightpaths by laying down direct fiber connections among all source-destination nodes. This design obviously requires minimal switching resources but maximal amount of fibers. Another way to establish lightpaths is by hopping through one or more nodes. Such a design requires less fiber connections but more switching resources. As such, the optimal connectivity of a fiber connection topology is determined by the fiber-to-switching cost ratio. Further, we show that the amount of switching resources used at nodes is proportional to the average minimum hop distance (for regular topologies and uniform traffic)[1]. To support the same set of (uniform) demands, we show that regular topologies with the smallest average minimum hop distances have lowest fraction of pass-through traffic and thus require less switching ports.

These provide guidelines for rigorous studies of cost-effective network architectures. For a few representative classes of regular networks (e.g., Δ-nearest Neighbors and Generalized Moore Graphs, whose constructions are detailed in Chapter 4), we first derive or approximate the closed-form expressions for important parameters, such as average minimum hop distance, switch size, and network cost. We then set up the corresponding optimization formulations. We have found that for regular networks and uniform traffic, the joint design problems of fiber connection topology, dimen-

[1]For example, in Chapter 5 we show that the size of an OXC, K_o, equals to $(H_{\min}+1)(N-1)t$, with $H_{\min}$, N, and t denoting the average minimum hop distance, network size, and unit of traffic between a node pair, respectively.

sioning, and routing can be solved optimally and analytically for a special class of regular graphs – Generalized Moore Graphs [2]. That is, we prove that with minimum hop routing, Generalized Moore Graphs, whose average minimum hop distances scale favorably as $\log_\Delta N$, achieve the lower bound on network cost and are good reference topologies. We also show that topologies with structures close to Generalized Moore Graphs can achieve close-to-minimum cost. The investigation of the cost scalability further demonstrates the advantage of the Generalized Moore Graphs and their close relatives as benchmark topologies: with linear switching cost, the minimal normalized cost per unit traffic decreases with increasing network size. In comparison, for less efficient fiber topologies (e.g., Δ-nearest Neighbors) and switching cost structures (e.g., quadratic cost), the minimal normalized cost per unit traffic plateaus or even increases with increasing network size. Our study has also revealed other attractive properties of Generalized Moore Graphs in conjunction with minimum hop routing. When minimum hop routing is employed for uniform traffic in Generalized Moore Graphs, the aggregate network load is evenly distributed over each fiber. Further, to support a given uniform traffic demand, Generalized Moore Graphs require the minimum (or close to the minimum) number of wavelengths, which directly affects the complexity and the cost of dispersive elements and filters in the network. This is the first time that Generalized Moore Graphs are identified as optimum architectures in the context of network cost efficiency. These architectures are very different from the currently used ones in MANs, such as rings, interconnected rings, or non-optimized mesh networks.

With the parametric network cost structure, closed-form solutions of the optimal degree and cost as functions of various network design parameters (such as network sizes and wavelengths of traffic between node pairs) are obtained. These results show that for a MAN of moderate size (a few tens to a few hundred nodes), under certain cost structures, neither rings nor fully connected mesh networks are optimal topolo-

[2] As elaborated in Chapter 4, 6, and 7, the assumptions of uniform traffic and symmetric topology, as well as the special construction of Moore Graphs make this joint problem solvable. For non-uniform traffic and other classes of graphs, the joint problem remains difficult to solve.

gies. The optimal network connectivity is in the range of $0.03N$ to $0.1N$ (when the fiber-to-switch cost ratio $\alpha/\beta_1 = 40$, α and β_1 denote the cost per fiber connection and the cost per port for linear switching cost structure, respectively). The advantage of analytical approaches is self-evident: they provide valuable references on how the optimal network connectivity scales as the design parameters change. More importantly, the results demonstrate that switching technologies have a tremendous impact on the final topological architectures. The optimal topologies connecting the same set of nodes can differ significantly when different switching fabrics are used, even when these topologies are designed to serve the same traffic demand. Among all-optical technologies currently available, for smaller networks (a few to a dozen nodes) and light traffic, quadratic switching cost structures (e.g., 2-D switching fabrics) have cost advantage. However, as the size of the network and the demand among node pairs increase, linear switching cost structure (e.g., 3-D switching fabrics) have the best scalability. Thus, the cost benefit of deploying 3-D switching technology for the future network is apparent. Moreover, a comparison of the cost benefit between OXC and OEO switches shows that at low data rate (e.g., below 1Gb/s for every source-destination pair for a 50-node network, as shown in Figure 6-16), it is economical to use OEO switches; at high data rate (e.g., above 1Gb/s for every source-destination pair for a 50-node network, as shown in Figure 6-16), it is more cost-advantageous to use OXC switches.

We also take steps to broaden the scope of this work to address more realistic design scenarios from two facets.

- We look into irregular network topologies and (static) non-uniform traffic, which represent most existing networks. We show that if the switching cost is linear with port counts, minimum hop routing is still optimum [3]. The results of Generalized Moore Graphs can be used to provide useful estimates for the cost of irregular networks – a Generalized Moore Graph with a node degree that equals to the minimal node degree of an irregular network provides lower bound

[3]The implications of topology regularity, traffic uniformity, and switching cost structure are summarized in Table 10.1 and Table 10.2 in Section 10.2.2.

on network cost. Also Generalized Moore Graphs can be exploited to suggest improvements for irregular fiber connection topologies. We show examples that connecting the same set of nodes via a Generalized Moore Graph results in savings on the number of switching ports [4].

For irregular topology under arbitrary traffic, we provide the lower bound on network cost using the concept of minimum flow tree, which is based on the unique construction of Generalized Moore Graphs (each of its nodes has a full (or almost full) Δ-ary routing spanning tree) and an (idealized, not always realizable) permutation of traffic matrix (the Δ destinations with the largest traffic are connected by one hop paths, the next Δ^2 destinations in descending order of traffic are connected by two-hop paths, and so on). More importantly, the construction of the minimum flow tree, though idealized, yields a general yet crucial design guideline: a cost-effective physical topology should minimize the propagation of large traffic values.

- We also investigate designing networks that are robust to demand uncertainties, which are caused by diversification of services, changing of usage patterns, and data-dominated traffic in the metro environment, etc. We present a framework to assist network designers to dimension optical MAN, incorporating uncertainties in demands. In this framework the interplay among topology design, resource provisioning, and routing are analyzed based on two stochastic optimization models that use probability distributions of demands as inputs. In one model, the weighted sum of network installation cost and expected penalty cost for unsatisfied traffic is minimized. In another model, the network installation cost is minimized subject to certain service level requirements. The optimization results enable us: (1) to identify the Generalized Moore Graphs as the physical architectures that are most robust (in cost) to demand uncertainties among rich classes of regular topologies, assuming the (random) uniform all-to-

[4]In these examples, every improved network uses the same number of fiber connections as the original one does, as illustrated in Section 9.2.2

all traffic, and (2) to provide analytical references on how optimal dimensioning, network connectivity, and network costs change as functions of the designer's level of risk aversion, service level requirements, and probability distributions of the demand.

To summarize, in setting up the topology, traffic, and network cost models, we seek a balance between the analytical tractability and a good representation of today's network. As such, the results presented in this thesis mainly serve to explore the landscape of options, to illustrate the trends, and to provide references for more realistic design scenarios. For solving a real world problem, more detailed and more accurate models need to be established, albeit at the cost of more intensive computation and the loss of analytical tractability. We will provide comments on the possible extensions in next section.

10.2 Comments

10.2.1 Comments on the Design of Wide Area Networks (WANs)

The complexity of designing WANs is still dominated by the size of the set of candidate edges, which grows approximately with 2^{N^2} (cf. Section 1.2.2). Thus finding a perfect solution via exhaustive search or solving ILP is unrealistic. (It is only practical for small size networks, $N \leq 10$). Besides the network size factor, compared with MAN or LAN, in a WAN a fiber connection spans a much longer distance, e.g., a few hundred to a thousand kilometers. With such a long distance, the optical signal must be amplified and reconditioned periodically. Because either amplifiers or regenerators are required for every 50 to 100 kilometers (cf. Section 2.1.4), establishing fiber connections may dominate the network cost. Moreover, the distances between node pairs vary significantly. For example, a fiber between Seattle and Salt Lake City spans a much longer distance than that between Boston and New York City, thus requires more amplifiers and regenerators. As such, we can no longer assume that all

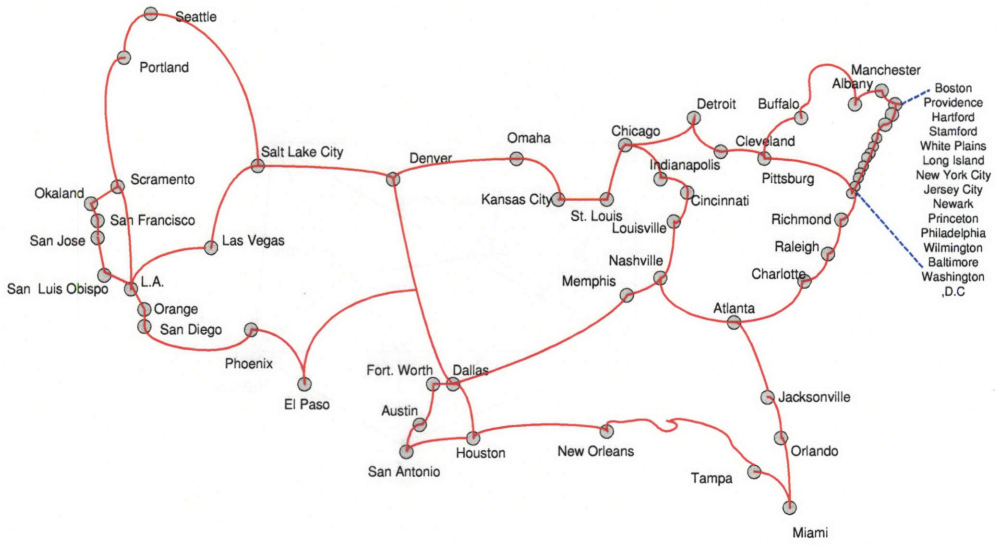

Figure 10-1: The fiber topology of Level 3.

the fiber connections have approximately the same cost. In other word, the fiber cost needs to be modeled as length-dependent. Due to this dependency, it is often difficult to directly set up analytical models let alone obtain the solutions. Nonetheless, the methodology established in this thesis and the results obtained from studying symmetric regular topologies and uniform traffics can be applied to the design of WAN in the following directions.

First, the analysis of the tradeoff between the fiber and switching resources can help us evaluate the cost efficiency and suggest possible changes of existing WAN topologies as technologies evolve. As an example, Figure 10-1 shows the physical topology of Level 3's national backbone network [60]. The network consists of 56 nodes and 63 (bidirectional) edges. The network is sparsely connected, with the maximum node degree of $\Delta_{\max} = 4$, the minimum node degree of $\Delta_{\min} = 2$, and an average node degree of $\bar{\Delta} = 2.25$. Such a connectivity is economical if the costs of establishing fiber connections are considerably higher compared with those of switching lightpaths. If in the future, the cost reduction rate of fiber is faster than that of switching, adding

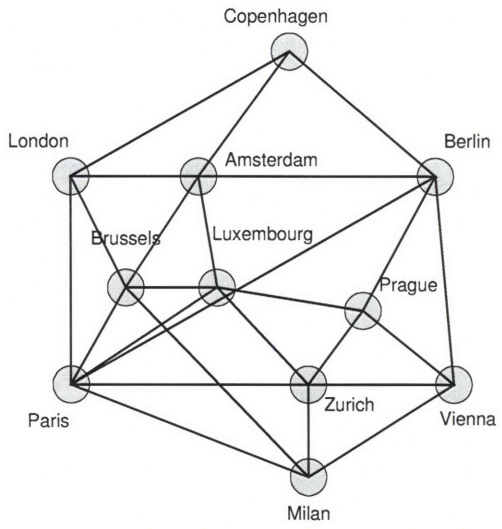

Figure 10-2: The fiber topology of COST 239 network.

new fiber spans will maintain or increase the cost efficiency (provided that there are enough dark fibers available). As another example, Figure 10-2 shows the physical topology of COST 239 network [61] in Europe. The network consists of 11 nodes and 26 (bidirectional) edges. Compared with Level 3's network, this network is densely connected, with the maximum node degree of $\Delta_{\max} = 5$, the minimum node degree of $\Delta_{\min} = 3$, and an average node degree of $\bar{\Delta} = 4.7$. Such a connectivity makes sense if the costs of fibers are considerably lower compared with those of switching. If in the future, the cost reduction rate of fiber is slower than that of switching, selling off or leasing some of the fiber spans will maintain or increase the cost efficiency of the network.

In a green field design scenario, the analysis of the tradeoff between the fiber and switching costs can also inform us the nodal characteristics of a good physical topology, as illustrated in Figure 10-3. We can establish a region of plausible solutions, which is bracketed by a minimum node degree $\Delta_{\min}$ and a maximum node degree $\Delta_{\max}$. The establishment of such a region significantly reduces the solution space, allowing a more sophisticated topology construction that yields minimum or near-to-

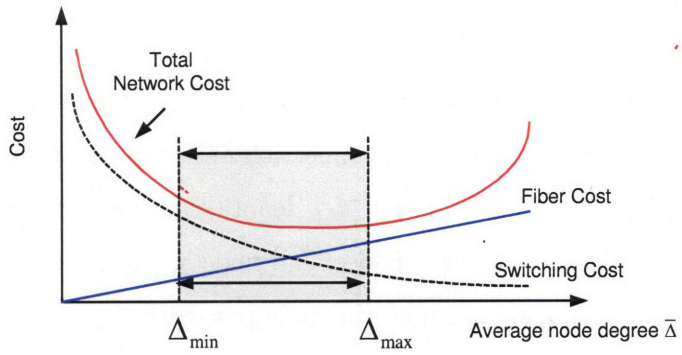

Figure 10-3: The analysis of the tradeoff between the fiber and switching costs can inform us the nodal characteristics of a good physical topology.

minimum cost.

Moreover, the insights gained from the study of symmetric network can help us construct efficient topology design algorithms. As previously mentioned, the construction of minimum flow tree provides us an important guideline in topology designs – a good network topology should minimize the propagation of large traffic. As an example of applying this guideline, We consider a design scenario in which the nodal connectivity requirement is given [62]. That is, the design requires that 50% of the nodes are degree-2 nodes, 35% degree-3 nodes and 15% degree-4 nodes (if needed, up to 3% of the nodes can be changed to degree-5 or degree-6 nodes). We propose an intuitive and efficient algorithm, which consists of two parts – *node degree assignment* and *connecting the nodes*, as detailed in the following:

- *Node degree assignment*: for a given traffic matrix $T = [t_{i,j}]$, calculate the aggregated traffic originated from each node $\sum_{j=1}^{N} t_{i,j}$ and rank them in the descending order. The node with the maximum aggregated traffic is assigned with the highest node degree; the node with the minimum aggregated traffic is assigned with the lowest node degree, and so on. These steps, combined with the steps in "connecting the nodes", **limit the travels of large traffic volume to as few number of hops as possible.**

- *Connecting the nodes*: given a set of locations, we can first connect the nodes via a minimum spanning tree or "two tree" [4] to ensure that the network is one or two connected, respectively. Then as long as the nodal degree requirement is not violated, we add a fiber connection one at a time to increase the network connectivity. Let $t_{i,j}$, $h_{i,j}$, and $d_{i,j}$ denote the demand, number of hops, and Euclidian distance between node i and node j, respectively. Each time we add a new fiber span, we use it to the node pair with the largest $\frac{t_{i,j}h_{i,j}}{d_{i,j}}$. We repeat the same process as long as the network connectivity constrain is satisfied. By doing so, **we not only let large traffic travel as few number of hops as possible (illustrated in Figure 10-4 (a)), but also make effective use of fiber (illustrated in Figure 10-4 (b)).**

As preliminary testing, we apply this algorithm to small networks ($N = 6$ or $N = 7$)[5]. The results show that the networks designed by this algorithm have costs close to the minimum (obtained by exhaustive searches).

In summary, the length-dependency of fiber cost adds another layer of difficulty in designing WANs. Owing to the intrinsic complexity associated with the design problem, strict optimal solutions can be obtained only for networks of small sizes. For networks of large size, we have to rely on heuristics. The insights and guidelines obtained from this thesis, in combination with sophisticated search mechanisms (such as "Tabu" search [63] and genetic algorithm [64]) are likely to provide near-optimal solution in a computationally efficient manner.

10.2.2 Comments on Minimum Hop Routing

In Chapter 6, we show that, minimum hop routing minimizes the switching cost, under the following conditions:

- The network is regular;
- The traffic is all-to-all uniform;

[5]We limit the testing cases to small networks, since finding the optimal solutions via exhaustive searches is computationally prohibitive for networks with $N \geq 8$.

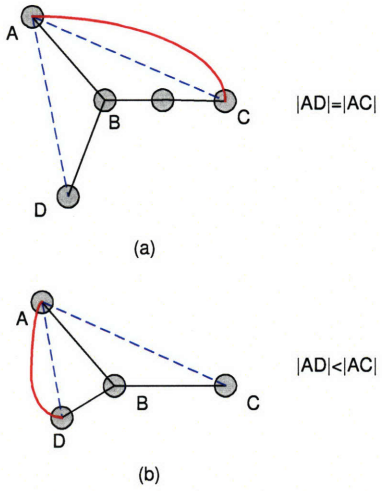

Figure 10-4: A topology design algorithm: each time a fiber span is added, the node pair with the largest $\frac{t_{i,j}h_{i,j}}{d_{i,j}}$ is connected, where $t_{i,j}$, $h_{i,j}$, and $d_{i,j}$ denote the demand, number of hops, and Euclidian distance between node i and node j, respectively. In (a) we have $d_{\mathrm{A,\,D}} = d_{\mathrm{A,\,C}}$ and $t_{\mathrm{A,\,D}} = t_{\mathrm{A,\,C}}$. Since $h_{\mathrm{A,C}} > h_{\mathrm{A,\,D}}$, a fiber span is added between nodes A and C. In (b) we have $h_{\mathrm{A,\,D}} = h_{\mathrm{A,\,C}}$ and $t_{\mathrm{A,\,D}} = t_{\mathrm{A,\,C}}$. Since $d_{A,D} < d_{A,C}$, a fiber span is added between nodes A and D. The algorithm limits the travel of large traffic to as few number of hops as possible and makes effective use of fiber at the same time.

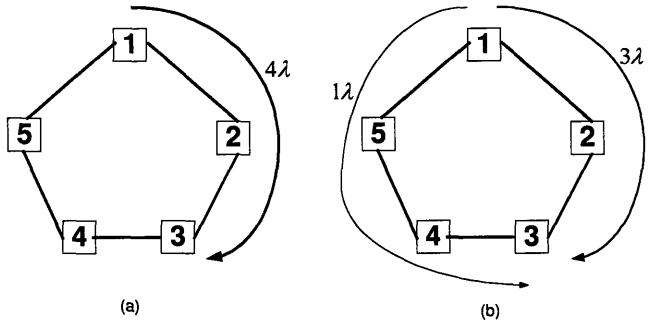

Figure 10-5: Routing algorithms for arbitrary traffic and super-linear switching cost.

- The switching cost is an increasing function of the number of ports (this is obvious, nonetheless we need this assumption for mathematical rigor);
- The routing is offline (the entire matrix is given upfront and routing decisions are made in "one shot") and symmetric [6].

In Chapter 9, we prove that, minimum hop routing also minimizes the switching cost, under the conditions:

- The network is arbitrary;
- The traffic is arbitrary;
- The switching cost at a node is linear with the number of ports;
- The routing is offline.

In this section, we consider the situations that a part of above conditions is not satisfied and minimum hop routing is not optimal. We provide examples and comments for both offline and online cases. We first look into the offline case. As an example, Figure 10-5 shows two different routings to send 4 wavelengths of traffic from node 1 to node 3 in a 5-node ring network. In Figure 10-5 (a), every wavelength

[6]When the routing is non-symmetric, in order for minimum hop routing to be optimal, the switching cost has to be increasing and *convex* function of the number of ports.

Table 10.1: Minimum hop routing for linear increasing switching cost.

Topology / Traffic	Uniform All-to-all	Non-uniform
Regular Topology	Optimal	Optimal
Irregular Topology	Optimal	Optimal

Table 10.2: Minimum hop routing for super-linear increasing switching cost.

Topology / Traffic	Uniform All-to-all	Non-uniform
Regular Topology	Optimal	Not necessarily optimal
Irregular Topology	Optimal	Not necessarily optimal

of traffic is routed via the minimum hop path; while in Figure 10-5 (b), 3 wavelength of traffic is routed via the minimum hop path and 1 wavelength of traffic is routed via the maximum hop path. If the switching cost is quadratic with the port counts ($F_3(K_o) = \beta_3 K_o^2$, with K_o denoting the switch size and β_3 denoting the cost per port, cf. Table 5.1), the routing algorithm in Figure 10-5 (a) incurs a cost of $48\beta_3$, yet the algorithm in Figure 10-5 (b) incurs a cost of $43\beta_3$. This simple example shows that under arbitrary traffic and super-linear switching cost, minimum hop routing does not always generate the minimal switching cost – cost efficient routings may include a combination of minimum and non-minimum hop routing algorithms. The results of the implications of topology regularity, traffic uniformity, and switching cost scaling on the minimum hop routing are summarized in Table 10.1 and Table 10.2.

We next look into the online case, in which the connection requests arrive at random and the holding times of a connection are finite. In this case, routes need to be determined one-by-one as they occur, without a prior knowledge of future demand. For online routing, a common objective is to minimize the blocking probability. Under certain circumstances, routing the demands through longer hops may enhance the network blocking performance. Figure 10-6 shows such an example. Suppose that lightpath requests from node A to node B and from node C to node F have occupied

all the wavelength resources on link DE. When node G requests one wavelength of demand to node K, the minimum hop routing would select the route G → D → E → K. Because of insufficient resources on the link DE, this request would be blocked. However, if we take a "greedy" approach to route the demand via a longer path G → H → I → J → K (suppose there are no other demands occupying the wavelengths on this path), the request can be granted. This example shows that non-minimum hop routing may be beneficial in setting up a single lightpath. At the meantime, we should be cautious that such a "greedy" approach tends to choose longer and longer paths in an attempt to satisfy the current request without cosidering any possible future requests. Depending on the arrivals and the durations of lightpath requests, the overall blocking performance may suffer. Figure 10-6 (b) gives an example. Similar to Figure 10-6 (a), the link DE is occupied at the time when node G requests one wavelength of demand to node K. Routing via a longer hop G → H → I → J → K can satisfy this request. However, this longer path may interfere with potential future traffic demands between other source destination pairs, such as (future) demands between node L and node O, node M and node N. These demands, in turn, seek longer routes. The long-term blocking performance degrades as a consequence. From this example, it is reasonable to expect that whether routing via longer hops can improve network blocking performance depends on the burstiness of the traffic between a node pair, which is normally characterized by the ratio between the average holding time and the average inter-arrival time [32]. When the ratio is small, the greedy approach of using longer paths would lower the long-term blocking. As the ratio increases, the benefit (in terms of blocking) of routing via longer path is likely to diminish.

In general, constructing optimal routing schemes becomes much more complicated for online cases. A sophisticated routing algorithm needs to consider not only minimizing the usage of network resources, but also other factors such as network blocking probability and load balancing, etc. A good online algorithm will strike a balance between the solution quality and execution complexity.

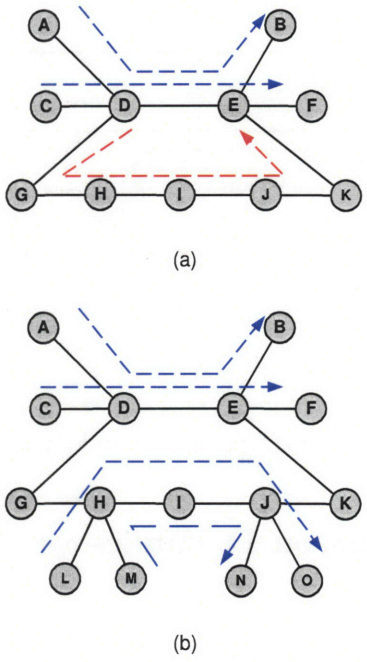

Figure 10-6: Online routing algorithms: (a) shows an example that routing the demands through longer hops may enhance the network blocking performance; (b) shows that a "greedy" approach tends to choose longer and longer paths in an attempt to satisfy the current request without cosidering any possible future requests. Depending on the arrivals and the durations of lightpath requests, the overall blocking performance may suffer.

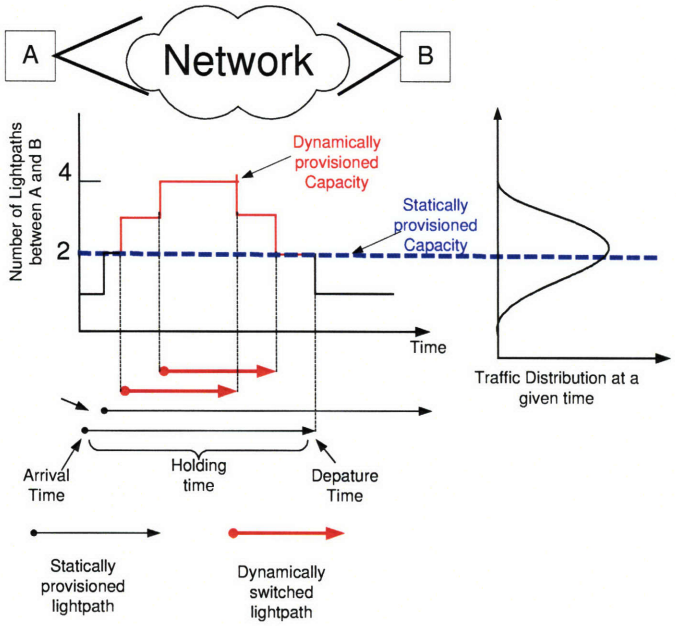

Figure 10-7: Dynamic traffic, static and dynamic lightpath provisioning.

10.2.3 Comments on Dynamics vs. Static Lightpath Provisioning

As mentioned in Chapter 1 and Chapter 5, the switching cost model used in this thesis includes both patch panel and dynamic switching. That is, we assign different per port cost for different type of switching – β_p for static switching (via patch panel) and β_i ($i = 1, 2,$ and 3, β_1, β_2, and β_3 are cost per port for linear, multi-stage, and quadratic cost scaling, respectively) for different types of dynamic switching. The case of mixed (cost per port) "β"s – β_p for static switching and β_i for dynamic switching – is an obvious extensions of this thesis. In this section, we provide comments on the advantage of static and dynamic switching and lightpath provisioning and research directions in hybrid network provisioning.

The main advantages of dynamic optical switching include:

- *Protection and restoration*: active switching elements are required for the successful executions of various protection schemes, such as 1:N protection [33].

We also note that even static traffic requires dynamic switching for network reliability.

- *Reconfigurability and efficient use of network resources*: dynamic switching enables lightpath to be set up at the moment when extra capacity is needed and to be taken down when this extra capacity is no longer needed, thus enhances a network's capability to adapt to traffic fluctuation (as shown in Figure 10-7) and pattern change. More importantly, with dynamic switching wavelength resources are no longer reserved permanently as in the case for static provisioning, where wavelengths are reserved even in the situation of no traffic flowing through them. In other words, via careful design, dynamic switching allows efficient sharing of network resources among user pairs. As an example, Figure 10-8 shows the cost saving enabled by the sharing of network resources – to support traffic A-B and E-F, static provisioning requires 2 wavelengths (shown in Figure 10-8 (b), while dynamic provisioning requires 1 wavelength (shown in Figure 10-8 (c)).

Depending on the characteristic of the traffic, it may not be necessary to switch every wavelength dynamically. For example, when the network traffic is constant (e.g., the traffic has a very small variance to mean ratio), the lightpaths can be provisioned statically – they can be setup via "hard-wiring" using fixed routing and wavelength assignment. The main advantage of the static provisioning is that the cost (per port) of the equipment required (such as fiber-patched panels) is much lower, compared with active switching equipment. The downside of the static provisioning is the inefficient use of the network resources, especially for dynamic traffic. In static provisioning, the wavelength used by a lightpath is reserved quasi-permanently for a user pair. It can not be used by others pairs, even there is no traffic between this user pair (cf. Figure. 10-8).

For dynamic traffic, it is practical to take a hybrid approach in network dimensioning [65]. That is, low-cost switching equipments, such as fiber-patched panels, handle the static or quasi-static portions of the traffic, while more expensive dynamic

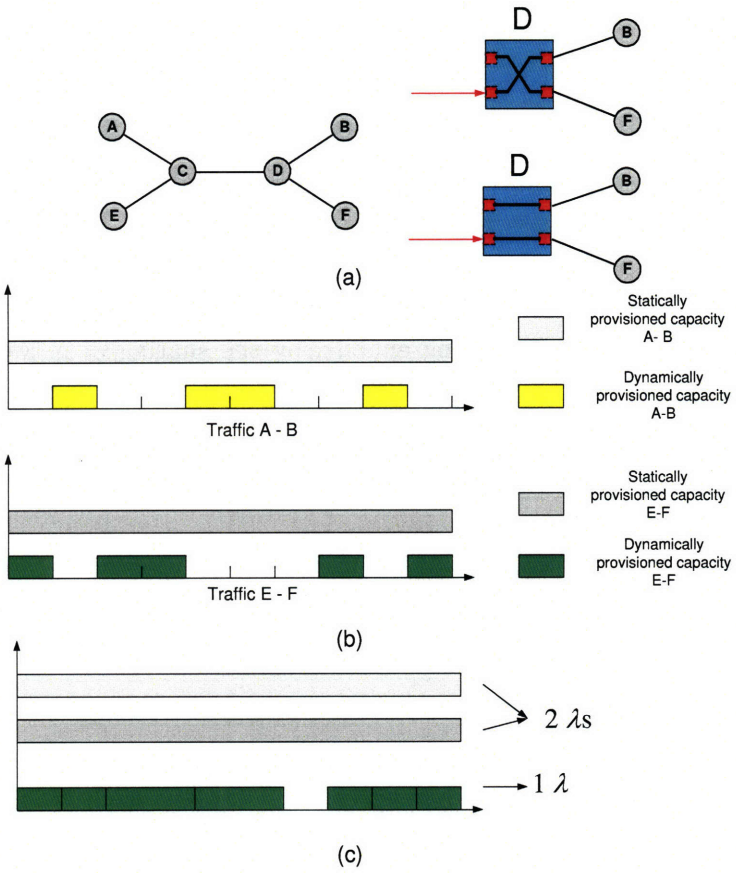

Figure 10-8: (a) A network of 6 nodes; (b) static provisioning to support traffic A-B and E-F; (c) dynamic provisioning to support A-B and E-F.

switching equipments accommodate the fluctuating portions (as illustrated in Figure 10-7). For hybrid network dimensioning, in addition to network cost, other design objectives, such as network blocking probability, network resource utilization, and the number of users supported, are also to be included [65]. It is reasonable to expect that the optimal amount of static and dynamic provisioning is likely to be determined by the factors such as characteristics of traffic, the relative (per port) cost ratio between static and dynamic provisioning, fiber topology, and routing algorithm, etc. However, correctly formulating and efficiently solving such an optimization problem with multi-objectives remain difficult. A sensible first step is to focus on more manageable tasks (that study the dependency of one design objective as functions of one or two design parameters). In addition, simplified and idealized network and traffic models can be used to obtain quantitative insights. For example, as illustrated in Figure 10-9, a "shared link (fiber)" topology, in which a single fiber (link) (colored in red) supports the (dynamic) traffic flowing from the nodes on the left side to the nodes on the right side of the fiber (link), is a good starting point to study the hybrid capacity provisioning. As for traffic models, both stochastic model [7] and random model [8] are fair approximations of the network operations. Moreover, a known framework for hybrid dimensioning (as illustrated in Figure 10-10) [65], together with the aforementioned network and traffic models, allow us to analyze the intrinsic tradeoff in hybrid capacity provisioning. In this framework, the traffic load of each user pair is first offered to the statically provisioned capacity, which is reserved for a specific node pair, thus can not be accessed by other user pairs even the capacity is not currently used. If all the statically provisioned capacity is not enough to handle the traffic load, the overflowing traffic is then offered to the dynamically provisioned capacity, which can be shared by many user pairs. Some of the research directions, as addressed by recent works [65] [66] [67], include:

[7] In the stochastic model, in the arrivals and departures of lightpaths (illustrated in Figure 10-7) are modeled as stochastic process, as discussed in Section 3.2.

[8] The random model takes a "snapshot" view of network traffic. The demand between a node pair at some instant is characterized by a random variable, as discussed in Section 3.3.

- Optimal static and dynamic provisioning as a function traffic statistics and blocking requirement. For example, using a random traffic model, [67] shows that if the demand between a user pair has a Gaussian distribution with a mean of $\bar{x}$ and variance of σ, a minimum $\bar{x}$ wavelengths should be statically provisioned. In [66], given a blocking probability requirement, an upper bound (worst case) on required dynamic switching resources is obtained among the sets of all possible random distributions.

- Optimal static and dynamic provisioning as a function of (average) traffic load and relative cost ratio between static and dynamic bandwidth provisioning. For example, with a simple cost structure (the cost is linear combination of the statically and dynamically provisioned capacities), [65] shows that two factors, which determine if and how much dynamically switched capacity is used, are the offered load of a user pair (denoted as A in [65], in the units of Erlangs) and the relative cost ratio between static and dynamic bandwidth provisioning (denoted as CR in [65]). A plot of of A vs. CR prescribes the regions where all-static, all-dynamic, and hybrid static-dynamic provisioning are used.

- Network utilization as a function of number of user supported and traffic statistics, under given blocking probability requirement. Dynamic switching has the potential of allowing efficient sharing of network resources among user pairs. To what extent dynamic switching can reap the benefit of statistical multiplexing of the aggregated traffic of user pairs is likely to depend on the number of users and their traffic statics, thus needs to be analyzed.

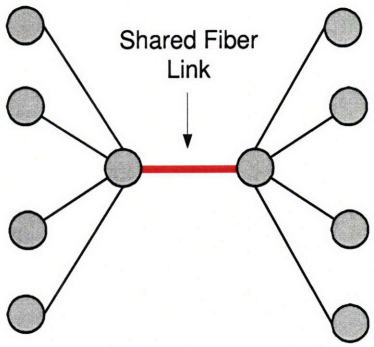

Figure 10-9: A shared fiber topology model.

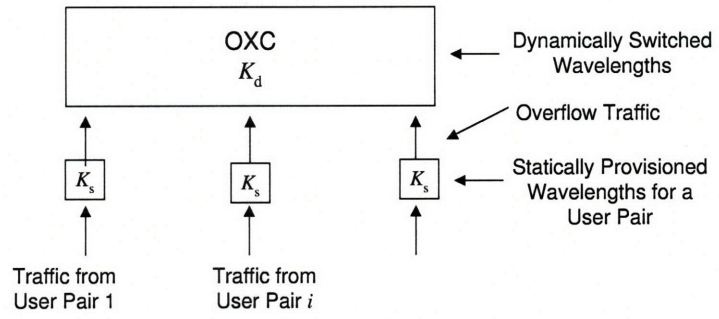

Figure 10-10: A model for stochastic traffic and hybrid static-dynamic dimensioning.

Bibliography

[1] A. Saleh and J. Simmons, "Evolution Towards the Next Generation Optical Network," *J. Lightwave Technol.*, vol.17, pp. 3303-3321, September 2006.

[2] V. W. S. Chan, Guest Editorial: Optical Communications and Networking Series, *IEEE J. Select. Areas Commun.*, vol.23, pp. 1441-1443, August 2005.

[3] S. Korotky, "Network global expectation model: a statistical formalism for quickly quantifying network needs and costs," *J. Lightwave Technol.*, vol.22, pp. 703-722, March 2004.

[4] W. Grover, *Mesh-Based Survivable Networks*, Prentice Hall, 2004.

[5] A. Saleh and J. Simmons, "Architectural principles of optical regional and metropolitan access networks," *J. Lightwave Technol.*, vol.17, pp. 2431-2448, December 1999.

[6] S. V. Kartalopoulos, *DWDM: Networks, Devices, and Technology*, IEEE Press, 2003.

[7] B. Ganguly and V. W. S. Chan, "A scheduled approach to optical flow switching in the ONRAMP optical access network testbed," *Optical Fiber Communication Conference Exposition 2002 (OFC 2002)*, March 2002.

[8] I. Chlamtac, A. Ganz, and G. Karmi,"Lightpath communications: an approach to high bandwidth optical WANs," *IEEE. Trans. Commun.*, vol.40, pp. 1171-1182, July 1992.

[9] R. Ramaswami and K. Sivarajan, "Routing and wavelength assignment in all-optical networks," *IEEE/ACM Trans. Networking*, vol.3, pp. 489-500, October 1995.

[10] H. Zang, J. P. Jue, and B. Mukherjee. "A review of routing and wavelength assignment approaches for wavelength-routed optical WDM networks," *SPIE Optical Networks Magazine*, vol.1, pp. 24-32, January 2000.

[11] J. Labourdette, E. Bouillet, R. Ramamurthy, and A. Akyamac, "Fast approximate dimensioning and performance analysis of mesh optical networks," *IEEE/ACM Trans. Networking*, vol.13, pp. 906-917, August 2005.

[12] B. A. Caenegem, W. V. Parys, F. D. Turck, and P. M. Demeester, "Dimensioning of survivable WDM networks," *IEEE J. Select. Areas Commun.*, vol.16, pp. 1146-1157, September 1998.

[13] F. Bentivogilio, E. Iannone,"The opaque optical network", *SPIE Optical Network Magazine*, vol.1, pp. 24-31, October 2000.

[14] S. Sengupta, V. Kumar, and D. Saha, "Switched optical backbone for cost-effective scalable core IP networks," *IEEE Communication Magazine*, pp. 60-70, June 2003.

[15] B. Melian, M. Laguna, and J. Moreno-perez," Minimizing the cost of placing and sizing wavelength division multiplexing and optical cross-connect equipment in a telecommunications network," *Networks*, vol.45, pp. 199-209, August 2005.

[16] M Saad and Z. Luo, "Design of WDM networks under economy of scale pricing and shortest path routing," *IEEE J. Select. Areas Commun.*, vol.24, pp. 26-36, April 2006.

[17] R. A. Barry and P. A. Humblet," Models of blocking probability in all-optical networks with and without wavelength changers," *IEEE J. Select. Areas Commun.*, vol.14, pp. 858-867, June 1996.

[18] S. Baroni and P. Bayvel, "Wavelength requirement in arbitrarily connected wavelength-routed optical networks," *J. Lightwave Technol.*, vol.15, pp. 242-251, February 1997.

[19] A. Narula-Tam, P. J. Lin, and E. Modiano, "Efficient routing and wavelength assignment for reconfigurable WDM networks," *IEEE J. Select. Areas Commun.*, vol.20, pp. 75-88, January 2002.

[20] P. Saengudomlert, E. Modiano, and R. G. Gallager, "On-line routing and wavelength assignment for dynamic traffic in WDM ring and torus networks," *Proc. IEEE Infocom*, April 2003.

[21] J. A. Bannister and L. Fratta, "Topological design of the wavelength-division optical network," *Proc. IEEE Infocom*, pp. 1005-1013, June 1990.

[22] S. Binetti and A. Bragheri,"Mesh and mutli-ring optical networks for long-haul applications," *J. Lightwave Technol.*, vol.18, pp. 1677-1684, December 2000.

[23] T. Carpenter, D. Heyman, and I. Saniee, "Studies of random demands on network costs," *Telecommunication Systems*, vol.10, pp. 409-421, 1998.

[24] A. Lisser, A. Ourou, J.-Ph Vial, and J. Gondzio. "Capacity planning under uncertain demand in telecommunications networks," *Hautes Etudes Commercials -Geneve*, October 1999.

[25] C. Mauz, "Dimensioning of a transport network being robust to changes of the traffic pattern," *Proc. ICTON*, pp. 62-65, June 2002.

[26] N. Geary, A. Antonopoulos, and J. Mitchell. "Networks and business modeling under traffic forecast uncertainties: a case study," *Proc. DRCN*, pp. 304-310, October 2003.

[27] D. Leung and W. Grover, "Capacity planning of survivable mesh-based transport networks under demand uncertainty," *Photonic Network Communications*, vol.10, pp. 123-140, 2005.

[28] B. E. A. Saleh and M. C. Teich, *Fundamentals of Photonics*, John Wiley Sons, 1991.

[29] T. E. Stern and K. Bala, *Multiwavelength Optical Networks: A Layered Approach*, Prentice Hall, 2000.

[30] M. Kuznetstov, etc., "A next-generation optical regional access network," *IEEE Communication Magazine*, pp. 66-72, January 2000.

[31] J. Buus and E. J. Murphy, "Tunable lasers in optical networks," *J. Lightwave Technol.*, vol.24, pp. 5-10, January 2006.

[32] M. Schwartz, *Broadband Integrated Networks*, Prentice Hall, New Jersey, 1996.

[33] R. Ramaswami and K. N. Sivrajan, *Optical Networks: a Practical Perspective*, Morgan Kauffman, 1998.

[34] D. Mitra and Q. Wang, "Stochastic traffic engineering for demand uncertainty and risk-aware network revenue management," *IEEE/ACM Trans. Networking*, vol. 13, no. 2, pp. 221-233, April 2005

[35] H. Liu, B. K. Chen, and F. A. Tobagi, "Power-law tradeoffs between optical and clectronic switching," *Proc. IEEE Infocom*, Barcelona, Spain, April 2006.

[36] S. Subramaniam, A. K. Somani, M. Azizoglu, and R. A. Barry,"A performance model for wavelength conversion with non-Poisson traffic," *Proc. IEEE Infocom*, pp. 500-597, Kobe, Japan, April 1997.

[37] L. Caccetta and W. F. Symyth, "Graphs of maixmum diameter," *Discrete Mathematicss*, vol.102, pp. 121–144, 1992.

[38] W. G. Bridges and S. Toueg, "On the impossibility of directed Moore Graphs," *Journal of Combinatorial Theory*, Series B, vol. 29, pp. 339-341, 1980.

[39] A. J. Hoffman and R. R. Singleton, "On Moore Graphs with diameter 2 and 3," *IBM J. Res. Dev.*, vol.4, pp. 497-504, 1960.

[40] M. Samples,"Vertex-symmetric Generalized Moore Graphs," *Discrete Applied Mathematics*, vol. 138, no. 1-2, pp. 195-202, 2004.

[41] M. Samples, *http://www.cs.uni-essen.de/samples/mean-distance.html*, 2006.

[42] M. G. Hluchyj and M. J. Karol, "ShuffleNet: an application of Generalized Perfect Shuffles to multihop lightwave networks," *J. Lightwave Technol.*, vol.9, no.10, pp. 1386-1396, October 1991.

[43] K. Sivarajan and R. Ramaswami, "Lightwave networks based on de Bruijn graphs," *IEEE/ACM Trans. Networking,* vol.2, no.1, pp. 70–79, February 1994.

[44] G. Panchapakesan and A. Sengupta, "On a lightwave network topology using Kautz Digraphs," *IEEE Trans. Computers*, vol.48, no.10, pp. 1131–1138 October 1999.

[45] B. Mukherjee, *Optical WDM Networks*, Springer, 2006.

[46] Y. Saad and M. Schultz, "Topological properties of hypercubes," *IEEE Trans. Computers*, vol.37, no.7, pp. 867–872, July, 1988.

[47] J. Akiyama, H. Era, and F. Harary, "Regular graphs containing a given graph," Elem. Math. , vol. 83, pp. 15-17, 1983.

[48] EURESCOM P615 Deliverable 2 - "Evolution Towards an Optical Network Layer," ftp.eurescom.de/ pub-deliberables/p700-seriers/p709/D3/Vol7/p709d3vol7.pdf.

[49] S. Boyd and L. Vandenberghe, *Convex Optimization*, Cambridge Univeristy Press, 2004.

[50] D. P. Bertsekas, *Nonlinear Programming*, 2nd Edition, Athena Scientific, 2003.

[51] B. Bollobas, *Modern Graph Theory*, Springer, 1998.

[52] R. P. Gupta, "The Chromatic index and the degree of a graph," *Not. Amer. Math. Soc.* vol. 13, pp. 719, 1966.

[53] I. Holyer, "The NP-Completeness of edge coloring," *SIAM J. Comput.* vol. 10, pp.718-720, 1981.

[54] M. Freire and J. Rodrigues, "The role of network topologies in the optical core of IP-over-WDM networks with static wavelength routing," *Telecommunication Systems*, vol.24, pp. 111-122, 2003.

[55] Y. Xin, G. N. Rouskas, and H. Perros, "On the physical and logical topology design of large-scale optical networks," *J. Lightwave Technol.*, vol.21, pp. 904-915, February 1997.

[56] M. Vaughn and R. Wagner, "Metropolitan network traffic demand study," *Proc. 13th Annual Meeting of the Lasers and Electro-Optics Society (LEOS 2000)*, vol. 1, pp. 102-103, Nov. 2000.

[57] R. Rudin, *Principles of Mathematical Analysis*, McGraw-Hill, 1976.

[58] R. Ramaswami and K. N. Sivarajan, "Design of logical topologies for wavelength-routed optical networks," *IEEE J. Select. Areas Commun.*, vol.14, pp. 840-851, June 1996.

[59] B. Yener and T. Boult, "Flow trees: a lower bound computation tool for network optimizaton," *Technical Report CUCS-006-94, Computer Science Department, Columbia University*, 1994.

[60] http://www.level3.com/673.html, December 2006.

[61] D. A. Schupke, C. Gruber, and A. Autenrieth, "Optimal configuration of p-cycles in WDM networks," *IEEE International Conference on Communications (ICC)*, New York, April 2002.

[62] BAA06-29 Proposer Information Pamphlet –"Dynamic multi-terabit core optical networks: architecture, protocols, control and management (CORONET)," Defense Advanced Research Projects Agency (DARPA),

http://www.fbo.gov/spg/ODA/DARPA/CMO/BAA06-29/Attachments.html, 2006.

[63] F. Glover and M. Laguna, *Tabu Search*, Kluwer Academic Press, 1997.

[64] J. H. Holland, *Adaptation in Natrual and Artificial Systems*, University of Michigan Press, 1975.

[65] R. Skoog, A. V. Lehmen, G. Clapp, J. W. Gannett, H. Kobrinski, and V. Poudyal, "Metro network design methodologies that build a next-generation network infrastructure based on this generation's services and demands," *J. Lightwave Technol.*, vol.22, pp. 2680-2692, December 1999.

[66] C. Guan and V. W. S. Chan, "Topology Design of OXC-Switched WDM Networks", *IEEE Journal for Selected Area in Communication*, vol. 23, no. 8, pp.1670-1686, August 2005

[67] L.-W. Chen, *Dynamic resource allocation in WDM networks with optical bypass and waveband switching*, PhD thesis, MIT, September 2005.